UNIVERSITY OF SOUTHAMTPON

DYNAMICAL STUDIES OF MOLECULAR DISSOCIATION ON Mo(100)

A thesis submitted to the University of Southampton in support of candidature for the degree of Doctor of Philosophy

By Benjamin Wilkinson

School of Chemistry
February 2008

UNIVERSITY OF SOUTHAMPTON

ABSTRACT

FACULTY OF SCIENCE

DEPARTMENT OF CHEMISTRY

Doctor of philosophy

DYNAMICAL STUDIES OF MOLECULAR DISSOCIATION ON MO(100)

By Benjamin Wilkinson

The dynamics of the dissociative chemisorption of H_2 on clean, hydrogen covered and nitrogen covered Mo(100), and of N_2 on clean and nitrogen covered Mo(100), has been studied under UHV conditions using a supersonic molecular beam. H_2 and N_2 dissociative adsorption on the clean Mo(100) surface are found to proceed via both a direct and classical accommodated indirect channel. Additionally a dynamic channel is identified specific to the H_2/Mo(100) adsorption system. The dynamic channel allows dissociative adsorption to take place at incident energies greater than can be accounted for in terms of a fully accommodated molecular precursor, the channel extending to incident energies of around 70meV, and has very little, or no, surface temperature dependence ($dS_0/dT_S \leq -1.4\times10^{-4}$ K^{-1}). Two possible mechanisms are suggested to account for the dynamic channel, both consistent with the experimental observations. One mechanism is that of "dynamic steering", where incident molecules' are very strongly steered into particularly favourable dissociation geometries on particular surface sites. The other suggested mechanism is that of a "dynamic precursor", where, rather than trapping taking place via accommodation of the molecules' incident energy to the surface (as is the case for a typical accommodated precursor), steering forces instead allow the transfer of energy from momentum normal to the surface to other molecular degrees of freedom.

The creation of an Mo(100)-c(2×2)N surface causes a considerable increase in the barrier to direct dissociative adsorption encountered by the H_2 molecule, the minimum barrier being shifted to >70meV. This change is also accompanied by the loss of the dynamic channel, although a concurrent increase in the contribution of the fully accommodated precursor channel is thought to somewhat mask this loss.

No evidence of a dynamic channel is found when examining the dynamics of dissociative adsorption of N_2 on the Mo(100) surface, all data pertaining to the system being accounted for within the confines of a combination of direct and classical accommodated indirect channels. The apparent lack of a dynamic channel is explained by a combination of the larger mass of the N_2 molecule with respect to the lighter H_2 (the steering forces having a greater impact on lighter molecules), and their differing electronic structures (this difference defining the depth of the dynamic well into which the molecule might trap).

A relatively large amount of research has, in the past, been directed at comparing the surface structure and adsorption kinetics of hydrogen adsorption upon Mo(100) and W(100). This thesis adds to this a comparison of the adsorption dynamics. In addition a comparison is drawn between N_2 adsorption on Mo(100) and W(100) with the molybdenum surface seen to mirror the tungsten surface in many ways.

Table Of Contents

To my mother and father

&

To the memory of Jim Pollock

Acknowledgements

Thanks go to the EPSRC for the financial support which has allowed me to carry out this research and to Professor Brian Hayden for providing me with the chance to undertake this thesis and for supporting me throughout.

Special thanks to Claire Mormiche and Tim Nunney for their patience when introducing me to the UHV beam system and to both for taking the time to answer my many questions. Thanks also to the rest of the Hayden group, Chris, Peter Suchsland, Peter Stone, Laura, Raf and Faisel for all the little bits of assistance and advice they've given me over the years, Narou, Scott and Oli also for many interesting tea time conversations, and for solving any computer related problems thanks to mike and more recently to Duncan and Chris.

A big thank you goes to the team at the workshop for their help on the many occasions when the UVH rig encountered mechanical problems or required alterations and to the glassblowers for the frequent use of their spot-welding equipment.

Moving away from university I would like to thank Peter Wells and Dave Quin for helping keep me involved in various sports, Laura for so many things and perhaps most of all for putting up with me when I was at my most stressed, and Ruth for giving me a place to stay when I was close to completing my research but running out of finances.

Last, but by no means least, thanks to Kate for always being there and keeping me smiling, and to my parents for their financial support, their belief in me, their advice, and their love.

Acronyms and Symbols

Acronyms

UHV	Ultra-High Vacuum
LEED	Low Energy Electron Diffraction
XPS	X-ray Photoelectron Spectroscopy
TPD	Temperature Programmed Desorption
K&W	King and Wells
PES	Potential Energy Surface
LDA	Local Density Approximation
EMT	Effective-Medium Theory
DFT	Density Functional Theory
FWHM	Full Width Half Maximum
TSP	Titanium Sublimation Pump
QMS	Quadrupole Mass Spectrometer
CV	Control Volume
TOF	Time Of Flight
EB	Electron Bombardment
SIRS	Surface Infra-Red Spectroscopy
EELS	Electron Energy Loss Spectroscopy
IR	Infra-Red
HREELS	High Resolution Electron Energy Loss Spectroscopy
GGA	Generalised Gradient Approximation

Symbols

E_i	Incident energy
φ	Angle of incidence
T_S	Surface temperature
T_n	Nozzle temperature
U	Potential well depth / Internal energy
erf	Error function
v	Velocity of a molecule
M_{eff}	Effective surface mass
m	Molecular mass
μ	Relative mass $\left(\mu = \frac{m}{M_{eff}} \right)$
S	Sticking probability
S_0	Initial sticking probability
S_{max}	Maximum sticking probability
θ	Coverage
R	Rate (of desorption or dissociation)
υ_{des}	Frequency factor for desorption
υ_{diss}	Frequency factor for dissociation
E_{des}	Activation energy of desorption
E_{diss}	Activation energy of dissociation

ζ	Trapping probability
E(A-B)	Metal-adsorbate bond energy
χ	Electronegativity
P	Pressure
P_n	Nozzle pressure
P_{1st}	Background pressure of 1st chamber
P_{2nd}	Background pressure of 2nd chamber
M	Mach number
D	Diameter
χ_M	Position of mach disk
H	Enthaply
E_K	Kinetic energy
t	Time
υ_{col}	Collision frequency
ς	Number of collisions required for rotational relaxation
σ	Cross section
Q	Heat
W	Work
E	Energy
V	Volume / Voltage
C_P	Molar specific heat capacity of gas at constant pressure
R	Rydberg/gas constant
k_B	Boltzmann constant
x_i	Molar fraction
N_A	Avogadro constant
$\overline{V}$	Molar volume
h	Planck constant
υ	Frequency
ϕ	Workfunction
E_B	Binding energy of an electron
λ	Inelastic mean free path length of an electron / de Broglie wavelength
I	Intensity
p	Momentum
e	Charge on an electron ($e \approx 1.6\times10^{-19}C$)
ω	Accelerating voltage
α	Angle of incidence
τ	Surface residence time of adsorbed species
Φ	Period of vibration of a bond
F_d	Fraction of molecules from the beam not directly incident upon the crystal surface
E^0_{vib}	Vibrational ground state energy
ΔE	Difference between the barriers to desorption and dissociation of an adosorbed precursor species ($\Delta E=E_{des}-E_{diss}$)
k_{des}	Rate of desorption
k_{diss}	Rate of dissociation
υ_{freq}	Vibrational frequency
c	Speed of light

Chapter I: Introduction

I.1 The history of gas – solid boundary surface science

Surface science has a long history, with the discovery of the platinum-surface-catalysed reaction of H_2 and O_2 being made as early as 1823 (by Döbereiner). However, investigations into atomic and molecular adsorption at the gas – solid boundary only really began early in the 20th century when in 1915 Langmuir began to study atomic and molecular adsorption.

By the late 1950's economical ultrahigh vacuum (UHV) systems had become available (largely thanks to the huge interest in space sciences at the time), and the study of clean well defined single crystal surfaces became possible. This in turn led to the development of a wide range of surface analysis techniques including, among others, LEED, XPS, TPD and K&W (all of which have been used extensively to obtain the data upon which this thesis is based) allowing surface properties to be examined on an atomic level. There followed a growth in surface chemistry research which has continued through to the present time. Using various surface analysis techniques, processes such as adsorption, desorption, catalysis and bonding, which were previously only investigated as macroscopic surface phenomena, could be re-examined on a molecular level (as opposed to merely observing the kinetics of the overall reaction). For example, ammonia synthesis catalysis is of huge industrial importance, with ~1% of the total global energy consumption used for ammonia production [1], but before the development of UHV the process could only be observed in terms of the changes in product and reactant concentrations. The advent of UHV and various surface analysis techniques allowed the detailed analysis of the mechanisms by which a particular catalytic reaction might proceed.

I.2 Heterogeneous Catalysis

A heterogeneous catalyst tends to be in the form of a metal surface which facilitates a reaction but remains unchanged by it. Molecules adsorb on to the catalytic surface, undergo bond breaking/forming and molecular rearrangements, and finally, desorb from the surface as products. The adsorption of the reactant on a catalyst acts to reduce the potential energy barrier to product formation.

Even if a reaction may result in the lowering of the overall potential energy of the system, there is often a large potential energy barrier to be overcome in order for gas phase reactants to form products, with the molecules experiencing a strong repulsive interaction as they approach each other. To get the reactants close enough to react, the barrier must be overcome by providing the reactants with energy, usually in the form of increased temperature. A catalyst provides a route to dissociation with a much lower barrier or sometimes with no barrier at all.

The following diagram (figure 1) shows examples of the 1D potential energy surface (PES) experienced by a gas molecule as it approaches a catalyst surface.

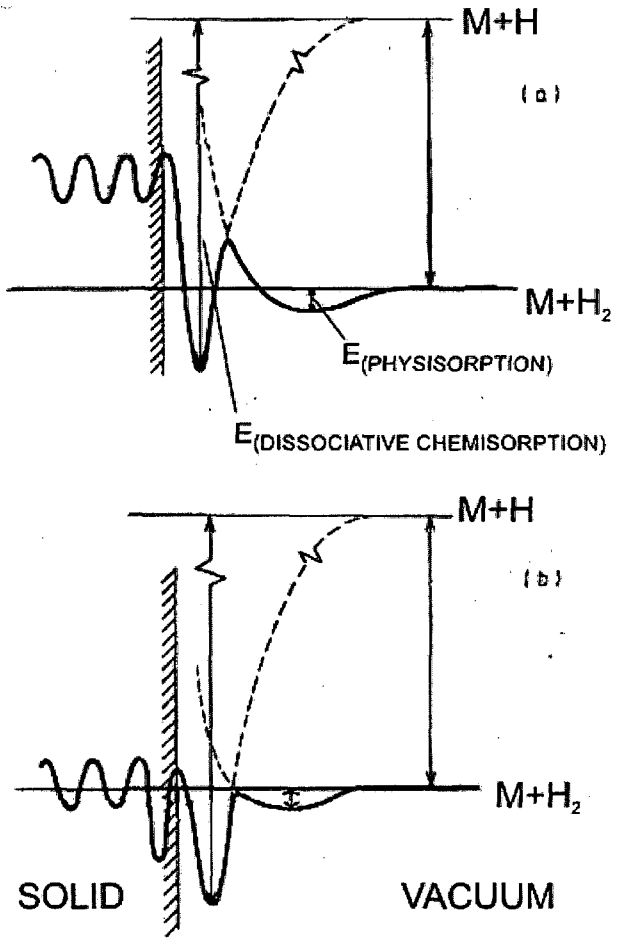

Figure 1: *One dimensional potential energy surfaces showing the potential that might be experienced by an adsorbate (in this example hydrogen) as it approaches two different metal surfaces, with the y-axis describing the potential energy of the system and the x-axis the position of the hydrogen with respect to the surface. The two plots show the potential of the atomic species (M+H) and molecular species ($M+H_2$) as they approach the metal surface, with* ***a)*** *being an example of activated dissociation, and* ***b)*** *non-activated dissociation. Figures* ***a)*** *and* ***b)*** *are also examples of when sorption (the adsorbate molecule penetrating into the bulk) is unfavourable and favourable (respectively). [2]*

I.3 Adsorption

I.3.1 Physisorption

It can be seen that as the molecule approaches the surface it first encounters a shallow molecular well where weak physical forces between the metal surface and the gas molecule act to reduce the potential energy of the system. This is known as physisorption and is due to Van der Waals type forces, where the polarisation of molecules into dipoles causes an attraction between molecule and surface, either via the free rotation of a molecular dipole (Debye forces) or an induced dipole formed via a shift in electron cloud distribution (London forces). When the molecule – surface distance becomes small the molecules will experience a repulsive force which will

begin to dominate the attractive forces. These repulsive interactions arise largely as a consequence of the Pauli Exclusion Principle.

In the case of physisorption adsorbate–absorbate interactions tend to be comparable in strength to absorbate–substrate interactions and the Van der Waals distance usually determines the densest overlayer packing. Because of this, low temperature physisorption of a gas like N_2 can be useful in determining the total surface area of a solid.

I.3.2 Chemisorption (molecular and dissociative)

As the molecule approaches the surface it may also begin to encounter chemical forces between itself and the surface that may result in the formation of chemical bonds. This process is labelled chemisorption.

As noted in figure.1, a barrier to chemisorption may or may not exist. Where a barrier does exist (figure.1a) the chemisorption is described as activated, whereas where it does not (figure.1b) it is described as non-activated. Figure.1 also illustrates how, after chemisorbing, the adatom may go one step further and penetrate into the metal's bulk atomic lattice. Below the metal surface a reactant atom might encounter a series of potential peaks and wells as it moves through the bulk lattice. If the peaks are relatively low the reactant atom may be able to move into the bulk. This process is known as absorption.

The depth of an adsorption potential well is related to bond strength and the relative shallowness of the physisorption well illustrates the weakness of the physisorption bond between molecule and surface. A chemisorption bond between metal and reactant atom will be much stronger and the potential energy well therefore considerably deeper. In the simplistic 1D PES of depicted in figure.1 only chemisorption between the gas atom and surface has been illustrated. When the molecule splits to form this bond between the individual atom and metal substrate, dissociative chemisorption is said to take place. However it is also possible for a molecule to form a chemical bond

with a surface (molecular chemisorption) and this case can be illustrated more clearly using a 2D PES.

The 2D PES below takes into account not just the surface to reactant separation, but also the separation distance of the reactant atoms. It shows more clearly how the translational and vibrational energies of the incoming molecule may affect the probability that the molecule will stick to the surface.

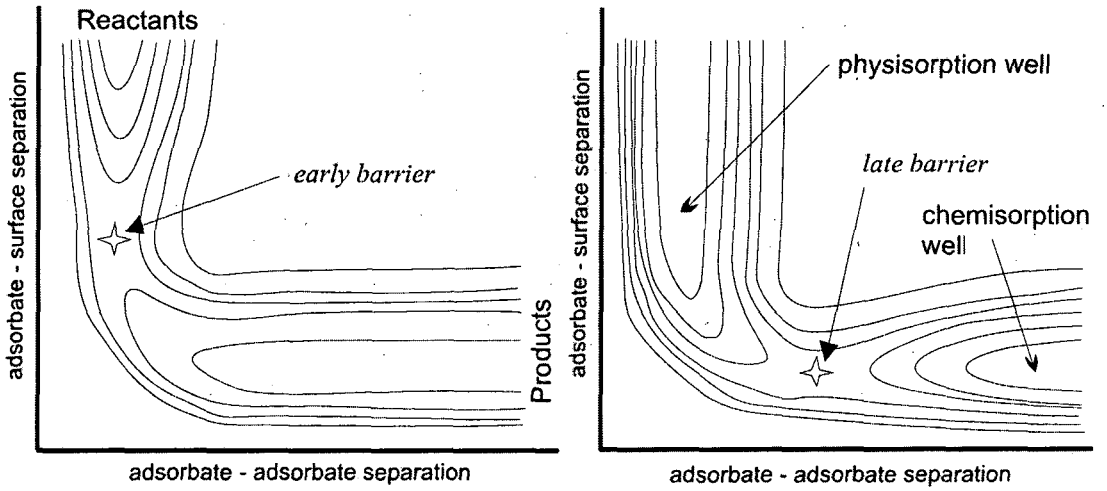

Figure 2: *Two dimensional potential energy surface showing the path of a diatomic adsorbate dissociating on two different metal surfaces as a function of adsorbate-surface separation (y-axis) and the separation of the two atoms that make up the diatomic reactant molecule (x-axis).* ***a)*** *Represents a metal surface where there is an early barrier to dissociation.* ***b)*** *Represents a late barrier to dissociation. The position of the centre of this barrier is usually referred to as the "saddle point", and its position is labelled here with a star. Diagram taken from [3].*

Figure.2 is labelled with a "saddle point", at which the transition from molecular state to atomically adsorbed state occurs. The position of this saddle point gives an indication of the relative importance of the translational and vibrational energy of the incoming molecule. An early saddle point, occurring at an adsorbate-surface separation value considerably higher than the dissociation well, would require a larger translational energy contribution in order to overcome this initial barrier. A late saddle point, where the molecular bond is being stretched considerably with regards to the molecules equilibrium interatomic separation, would result in the vibrational energy of

the molecule coupling well with the barrier and aiding dissociation. In fact too much translational energy here might result in the molecule leaving the entrance channel potential energy well before it has had the opportunity to dissociate and stick. In order to stick an incoming molecule often must lose some of it kinetic energy to the surface either by excitation of surface phonons, the creation of electron–hole pairs, or possibly the transfer of normal momentum to another molecular degree of freedom.

The energy losses due to the excitation of phonons have been described theoretically using the "hard cube model" [4]. The model is based on the following four assumptions:

a) The interaction of a gas atom with a surface atom is represented by an impulsive force of repulsion, meaning that both the incident gas particle and the surface atom may be considered as rigid elastic particles.

b) The gas-surface intermolecular potential is uniform in the plane of the surface (i.e. the surface is perfectly smooth), hence the interaction does not change the tangential velocity of the gas particle, thus there are no forces acting parallel to the surface.

c) The surface atoms are represented by independent particles (cubes) confined by square-well potentials (i.e. rigid boxes). A gas particle interacts with a single surface atom by entering the "box", colliding with the surface particle, and then departing. Although it would be more realistic to consider the surface atoms as harmonic oscillators.

d) A temperature-dependent velocity distribution is assigned to the surface atoms. A one-dimensional Maxwellian distribution is chosen for the component of velocity of the cubes in the direction normal to the surface. This may not be an appropriate distribution for surface atoms but it does satisfy certain equilibrium conditions.

The theory has been developed to give the trapping probability (ζ) as a function of the incident energy (E_i), angle of incidence (φ), and surface temperature (T_s) for a given well depth (U), surface atom mass (M) and molecular mass (m) [5,6].

$$\zeta(E_i,\varphi,T_s)_{U,M,m} = \frac{1}{2} + \frac{1}{2} erf(a v_{\lim}) + \frac{e^{(-a v_{\lim})^2}}{2\sqrt{\pi} a v_{well}} \qquad \text{(I.1)}$$

Where:-

erf = the error function

v_{well} = the velocity of the molecule after being accelerated by a well of depth U

$$v_{\lim} = \frac{\mu+1}{2}\sqrt{\frac{2U}{m}} + \frac{\mu-1}{2}\sqrt{\frac{2}{m}\left(E_i \cos^2\varphi + U\right)} \qquad \text{(I.2)}$$

= the cube velocity above which the molecule cannot trap

$$a = \sqrt{\frac{M_{eff}}{2kT_s}} \qquad \text{(I.3)}$$

With M_{eff} being the effective surface mass, and μ the relative mass $\left(\mu = \frac{m}{M_{eff}}\right)$.

The trapping probability can be seen to fall off rapidly with decreasing relative mass of the molecule with respect to that of the surface atom and with the increasing of the molecules incident energy, however the surface temperature dependence may be either positive or negative depending on the incident energy.

See appendix A for the full derivation and description of the hard cube model.

I.4 The Precursor State

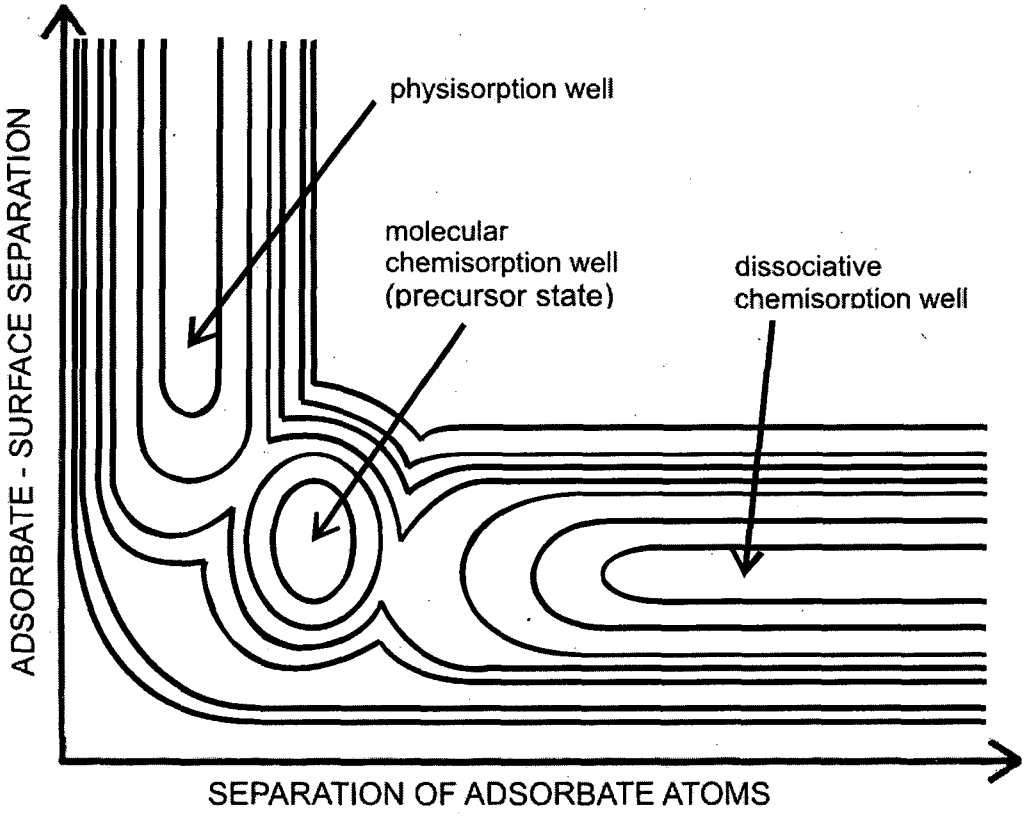

Figure 3: *A simplistic representation of the 2D PES of a diatomic molecule adsorbing on a surface via a precursor state*

Figure.3 indicates a situation where 2 saddle points are present and molecular chemisorption may occur. The molecule can approach the surface via the physisorption potential well and from here access the molecular chemisorption well (where a chemical bond is formed between molecule and surface, e.g. NO on Ni(100) [7], from which it might desorb and vacate the surface or, alternatively, go on to dissociate.

Molecularly adsorbed states which the adsorbate occupies before dissociation are known as precursor states. The existence of a precursor state was first proposed by Kisliuk in 1957 [8], who suggested a mobile precursor state that may visit several surface sites.

When the molecule cannot immediately dissociate but is first trapped in a physisorbed or chemisorbed precursor state, before proceeding to eventually dissociate, the process is known as indirect dissociation. Conversely, if a molecule is able to immediately access the dissociation well without the need for a precursor, direct dissociation is said to occur.

I.5 Dissociative Adsorption

I.5.1 Direct Dissociation

Direct dissociative adsorption may occur when, either the process is non-activated, or when, in the activated case, the incident kinetic energy of the molecule is higher than the PE barrier to dissociation.

Direct dissociation is often characterised by an increase in the initial dissociative sticking probability (S_0) of the incident molecule with increasing incident energy (E_i). This is because an increase in the E_i allows access to non optimised trajectories (there will be a range of barriers to dissociation present for different impact sites and molecular orientations).

Direct dissociation requires the incident molecule to impact around a vacant surface site for direct dissociation to be successful. Originally it was assumed [9] that, at least in the case of a simple diatomic molecule, 2 adjacent vacant sites would be required.

If this assumption were correct it would result in the sticking having a coverage dependence of:-

$$S = a(1-\theta)^2 \qquad \textbf{(I.4)}$$

Where S is the sticking probability of an incoming gas molecule and θ is the fraction of adsorbate sites occupied with respect to the saturation coverage (therefore 1-θ being the proportion of vacant sites).

Although this model does account reasonably well for some systems under conditions where direct dissociation is dominant (e.g. hydrogen on Pt(533) at high incident energies [10]), deviations may occur due to adsorbate induced surface reconstructions occurring as the coverage (θ) changes (e.g. oxygen on W(100) [11]), interactions between adsorbates (e.g. CO and NO on Pt(100) [12]), or even the ability of one of the adsorbate atoms to migrate (e.g. H_2 on Ni(100) [13]). In this later case, the coverage dependence is very different. With only one vacant site being required for dissociation (since the other adsorbate atom may migrate to find a vacant site for itself) the coverage dependence of the sticking would instead be proportional to number of free sites, rather than the square of this value (as the Langmuir model proposes).

$$S \propto (1-\theta) \qquad \textbf{(I.5)}$$

When undergoing direct dissociation the molecule has a very short time of residence at the surface, and will not have the opportunity to reach thermal equilibrium. Consequently there is no dependence of initial sticking (S_0) on surface temperature (T_s) (although an exception to this may occur when dissociation happens via quantum mechanical tunnelling through the activation barrier [14]).

I.5.2 Indirect Dissociation

Indirect dissociation involves, as previously mentioned, the trapping of the adsorbate molecule into a precursor state before the molecule sticks dissociatively.

When a molecule has insufficient energy to access the direct channel it may still undergo dissociative sticking via first trapping in a molecular precursor state from which dissociation may go on to take place after molecular vibrations. A molecule in a precursor state will not necessarily go on to dissociate. A partition will exist between the molecule dissociating and desorbing [15]. Since the balance of this partition is, to some extent, determined by the temperature of the surface, the indirect sticking probability can be strongly surface temperature dependent.

The rate of dissociation or desorption of the precursor state can be described by the following equation:-

$$R = \upsilon \, e^{-\frac{E}{kT_S}} \qquad \text{(I.6)}$$

Where R is the rate of dissociation or of desorption, E the barrier between the precursor and the dissociated atomic state (in the case of dissociation), or the barrier between the precursor and the free molecular state (in the case of desorption). υ will depend on the availability of suitable sites and the mobility of the precursor [16,17].

Combining the two forms (dissociation and desorption) of this equation gives an expression relating relative sticking probability to the surface temperature. To determine dissociative sticking probability (S) a further term, ζ, must be added to describe the initial trapping probability of the molecule into the precursor well (this term may usually be taken to be T_S independent):-

$$S = \zeta \left[1 + \left(\frac{\upsilon_{des}}{\upsilon_{diss}} \right) e^{\left(\frac{-E_{des} + E_{diss}}{kT_S} \right)} \right]^{-1} \qquad \text{(I.7)}$$

The relationship between sticking probability and surface temperature, as shown by this equation, is not a simple one. There are a number of limits that can be picked out from the equation. If the energy barrier to desorption of the molecule is much larger than the barrier to dissociation, then the term within the square brackets will tend to 1 and $S \approx \zeta$. Also, if the barrier to desorption is only slightly greater than the barrier to dissociation ($E_{des} > E_{diss}$) then S will still be equal to ζ if $\upsilon_{diss} >> \upsilon_{des}$ (for example if there were a large number of available sites for dissociation to occur). However, providing these limits don't apply the dissociative sticking probability will increase with surface temperature if $E_{diss} > E_{des}$, but fall if $E_{des} > E_{diss}$.

In order for this partition function to apply the molecule must first, of course, trap into the precursor state. The initial trapping probability into the precursor state depends

upon the incident energy of the adsorbate molecule. However, unlike for direct dissociation where there is often a large potential energy barrier to overcome, access to the precursor state tends to be non-activated or the barrier very small. This leads to a relationship where there is a strong decrease in the sticking probability with increasing kinetic energy of the molecule. This is because the trapping of a molecule into a shallow precursor well is heavily dependent on the molecules ability to dissipate its energy. The greater the kinetic energy of the molecule the more energy it will need to dissipate through the collision with the surface. Molecules that are unsuccessful in dissipating sufficient energy will scatter back from the potential barrier, returning to the gas phase.

I.5.3 Extrinsic and Intrinsic Precursors

Precursor states are labelled as either extrinsic or intrinsic. When a molecule reaches the precursor state via a collision over an empty surface site it is described as intrinsic. The extrinsic precursor, on the other hand, will accommodate over a region of the surface pre-covered with adsorbates. After accommodating into the precursor state, the extrinsic precursor must find a "hole" to dissociate (by moving to a new surface geometry or via changing rotational position). This difference in precursor species type leads to differences in the coverage dependence of the indirect sticking, depending on which precursor route is dominant.

Since the intrinsic precursor requires a vacant surface site over which to accommodate its sticking will exhibit similar coverage dependence to that which a direct channel might. For example, an intrinsic precursor limited by trapping into a single vacant site might exhibit approximately $(1-\theta)$ dependence (with possible variations due to adsorbate–adsorbate interactions or coverage dependent surface restructuring).

The sticking of an extrinsic precursor should show an insensitivity to coverage until the surface begins to saturate and finding vacant sites for dissociation becomes limiting. In fact, if a much better mass match for the incoming adsorbate sticking via the extrinsic channel results in the relative efficiency of the extrinsic precursor over the intrinsic

precursor, there may be an initial rise in sticking with increasing coverage as the increase in adatoms allows greater access of the incoming molecules into the extrinsic channel. Such an assumption has been made to explain the initial increase in the sticking probability with coverage for the adsorption of nitrogen on W(100) [18].

The influence of adsorbates on an incoming molecule's probability of dissociation is of crucial importance to industrial catalysis where synthesis will often occur with a high coverage of reactants. The effectiveness of a catalyst may be heavily influenced by which precursor channel the reactant can access most efficiently.

Before leaving the subject of precursors it should be noted that though, in general for indirect sticking, an increase in E_i tends to lead to a decrease in S_0 an exception may exist for a particular variety of intrinsic precursor. If access to the intrinsic well is activated it may give rise to a system where S_0 increases with increasing E_i and only the strong T_s dependence will distinguish it from the direct channel (e.g. O_2 on Pt(111) [19], N_2 on Fe(111) [20]) .

I.6 Theoretical Investigations

Various theoretical investigations into the substrate adsorbate system have been undertaken and these shall occasionally be referred to. It is therefore useful at this point to trace through a brief history of this work and the development of the theory to its present form.

The most simplistic method of considering an adsorbate substrate interaction is Pauling's equation where the metal-adsorbate bond energy, E(A-B), is equivalent to the combination of the metal-metal bond energy, E(B-B), and the adsorbate-adsorbate bond energy, E(A-A), and the difference in the electronegativity, χ, of the two:-

$$|\chi_A - \chi_B| = 0.102\sqrt{\left(\Delta / kJmol^{-1}\right)} \qquad \text{(I.7)}$$

With Δ representing the excess energy of an A-B bond over the average energy of A-A and B-B bonds, which can be attributed to the presence of an ionic contribution to the covalent bonds.

$$\Delta = E(A-B) - \frac{1}{2}\{E(A-A) + E(B-B)\} \qquad \textbf{(I.8)}$$

However, such a basic theory neglects many aspects to the substrate-adsorbate interaction and this is borne out by the inaccuracy of the results achieved using the equation. This method of analysis tends to show a peak in the bond energy mid-row along the d-band metals, whereas in reality it has been shown that the energy tends to decrease from left to right across a row [21].

The Hartree-Fock approximation (also known as self consistent field method) provided a quantum mechanical approach. The Schrodinger equation for the complicated many body system of an adsorbate bonding to a substrate is unsolvable, but Hartree-Fock provided an approximate method for the determination of the ground state wavefunction and energy.

Hartree utilised the Born-Oppenheimer approximation (that due to the nuclei's size relative to the electrons, the nuclei may be considered as static) and proposed that an electron could be considered as moving in the potential of the average electric field of the other electrons and other nuclei. Fock added to this the principle of antisymmetry approximations (i.e. the exchange effect – the potential due to the effect described by the Pauli exclusion principle). However this theory still neglects the electron correlation effect (due to repulsive interactions between electrons they tend to avoid each other and therefore their motion is correlated).

The advancement from the Hartree-Fock theory was made by introducing something called the local density approximation (LDA). This proposed that the embedding energy of an atom is equivalent to the energy of embedding in a homogeneous electron gas, with corrections added to account for the inhomogeneous reality.

Such a model is reminiscent of the Somerfeld free electron model, where valence electrons are modelled as an 'electron gas' completely detached from their ions and moving in a constant potential. The jellium model often referred to in the LDA describes a system where ions of the solid are 'smeared out' into a uniform positive background for the homogeneous electron gas.

These models completely ignore the structure of the material and the jellium picture was improved by using pseudopotentials to model the effects of the substrate's ionic lattice.

Two theoretical approaches to take advantage of the LDA were the effective-medium theory (EMT) and density functional theory (DFT).

These are the main theories currently in use, utilizing the LDA to replace complex many body electronic wavefunctions with an effective potential that is a function of the electron density.

The framework of EMT has been used to extract hydrogen binding properties of adsorbates on a metal surface with a good degree of accuracy [22]. The efficiency of the theory in comparison to the previous many body electronic wavefunction models means EMT calculations can be performed fast enough to allow them to be used to simulate dynamic processes such as adsorption [23].

DFT was essentially created (or at least put on a sound theoretical footing) in 1964 by Hohenberg and Kohn [24], and its primary method of implementation uncovered by Kohn and Sham [25] who provided the framework within which the many-body picture of interacting electrons in a static external potential was reduced to a problem of non-interacting electrons in an effective potential (which included the coulombic exchange and correlation interactions between the electrons as well as the static external potential).

The basic premise of DFT is that the electron density (the probability of finding an electron at a certain point in space) totally specifies a system, i.e. all properties of a system are expressible in terms of its electron density.

DFT successfully modelled adsorption systems using slabs, usually of between 5 and 11 metal layers and semi-infinite geometry. An example of the use of this model is the work done in successfully reproducing the experimentally observed adsorbed states of N_2 on Fe(111) [26].

An example of how these theoretical calculations might currently be used to assist experimental investigations is the analysis of the chemical behaviour of alloy surfaces with mixed metal sites for ammonia synthesis using DFT [27]. Predictions are made as to which alloys might prove to be good ammonia synthesis catalysts.

In a catalytic reaction an important function of transition metals is to atomise diatomic molecules (in the case of ammonia synthesis N_2 and H_2) and then supply the atoms to other reactants or reaction intermediates. The thermodynamic driving force for the atomisation is from the strength of bonding of these atoms to the surface. However, if the surface bonds are too strong, the reaction intermediates block the adsorption of new reactant molecules because of their long surface residence times. The Bronsted-Evans-Polanyi relation, that states that for dissociative chemisorption the activation energy depends linearly on the reaction (adsorption) energy, has been shown to hold for surface reactions [28], and by the use of DFT calculations such relations have been firmly established for a number of systems [29]. Because of this a balance must be struck since should the adsorbate–surface bond be too weak, the necessary bond-scission process may be absent. This is demonstrated by the volcano-like shape of the plot produced when calculating activities of various transition metals for the dissociative chemisorption of reactant molecules [30]. The shape is due to the steadily decreasing heat of adsorption associated with a transition metal from left to right across a row. Figure.4 shows how DFT calculations have been used to predict an alloy that might prove to be a better ammonia synthesis catalyst than the promoted iron catalyst currently in use.

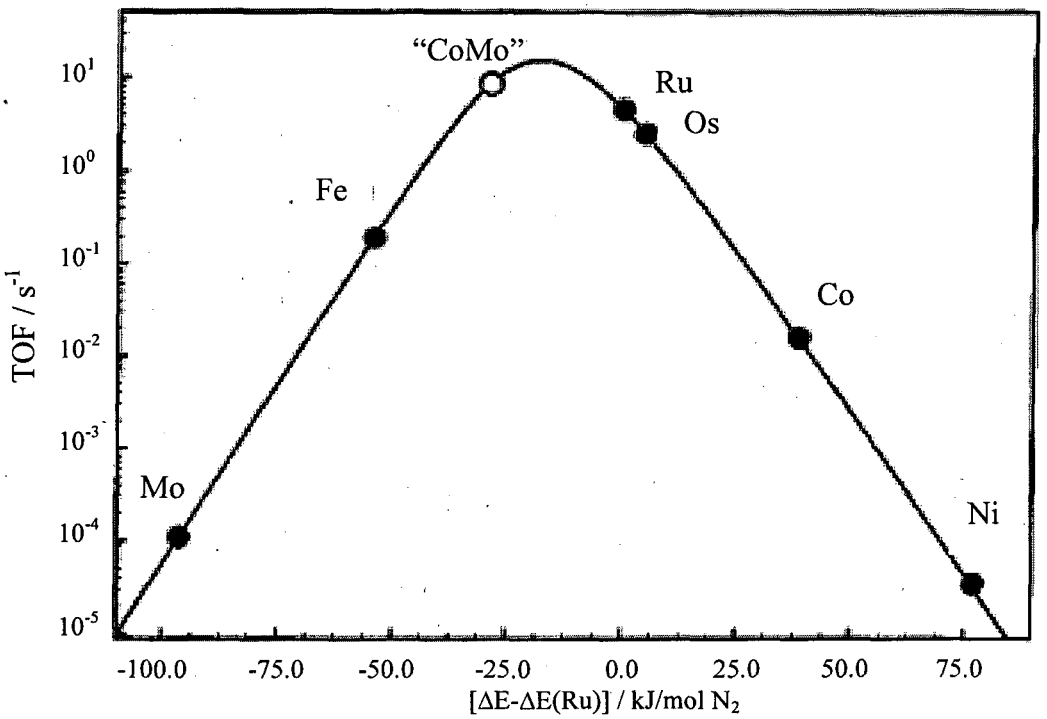

Figure 4: *An example of a volcano plot, showing turnover frequencies for ammonia synthesis as a function of adsorption energy of nitrogen using a micro kinetic model and the linear relation existing between the potential energy and the activation energy for N_2 dissociation [27].*

I.7 Aims/Applications of the Thesis

The aim of this thesis is to study the adsorption of H_2 and N_2 upon the molybdenum (100) surface. It is hoped that by analysing changes in the dissociative adsorption probability with varying incident energy of the molecules, surface temperature of the molybdenum sample and pre-coverage of the surface with either hydrogen or nitrogen, it will be possible to draw conclusions regarding the specifics of the reaction mechanism, for example, whether, under a particular set of conditions, the route to the dissociative adsorption of the molecule is direct or indirect and, if direct whether activated or non-activated, or if indirect whether accommodated or dynamic. Careful analysis of such data should also give some indication of the potential barriers encountered during the process.

Although the study of the dynamics of the adsorption of H_2 and N_2 on Mo(100) is an area yet to be examined within the currently published literature, and therefore of considerable interest in itself in terms of providing new data regarding the dynamical behaviour of two commonly encountered species of molecule, there are two particular areas to which the results gleaned within this study are likely to be of particular interest.

The first of these is in terms of a comparison of the N_2/H_2 on Mo(100) adsorption systems with the equivalent W(100) systems. The kinetics and surface structures resulting from N_2 and H_2 adsorption have already been the subject of numerous studies comparing the two [31-36], and have shown the two systems to be largely similar, making any differences easy to isolate from other factors and therefore of considerable interest to study. Also a large body of data has been produced examining the adsorption dynamics of the tungsten system [15, 37-41], making a dynamic study of the equivalent molybdenum systems for N_2 and H_2 the missing piece of the puzzle in terms of providing a full comparison of the interaction of these diatomic molecules with the two surfaces.

The second is in the advancement of ammonia synthesis catalysis. The iron-based ammonia synthesis catalyst was discovered by testing over 2500 different catalysts in 6500 experiments, however, recently a rational catalyst development strategy was suggested which would avoid the need for this type of trial and error experimentation. A volcano type relation between the NH_3 synthesis activity of different catalysts and their nitrogen adsorption energy has been shown to exist, as has been described above, with the dependence of the catalytic activity on the nitrogen adsorption energy shown to be a consequence of a linear (Bronstead-Evans-Polanyi) relationship between the activation energy for the rate-limiting step, which is the N_2 dissociation, and the stability of absorbed N on the surface [28]. The volcano shape implies there to be an optimum nitrogen adsorption energy due to the two mutually opposing ways in which a high activity might be achieved (either with a small dissociation barrier to N_2 dissociation, or with low coverage of adsorbed atomic nitrogen during ammonia synthesis), and the rational approach was to attempt to construct a surface with the desired intermediate nitrogen interaction energy by combining two metals, one with too high an adsorption energy and one with too low an adsorption energy.

Norskov et al. used DFT slab calculations to study the chemical behaviour of alloy surfaces with mixed metal sites in terms of their ammonia synthesis catalytic activity [27]. In particular it was shown using DFT calculations that a CoMo alloy would have a higher activity than iron (see figure 4).

This was confirmed experimentally by C.J.H. Jacobsen [42], who observed the addition of a small amount of Cs to CoMoN to result in a catalyst with higher activity than that of the commercial multi promoted iron catalyst (see figure 5). FeMo and NiMo alloys were also shown to be ammonia synthesis catalysts with a high activity [42].

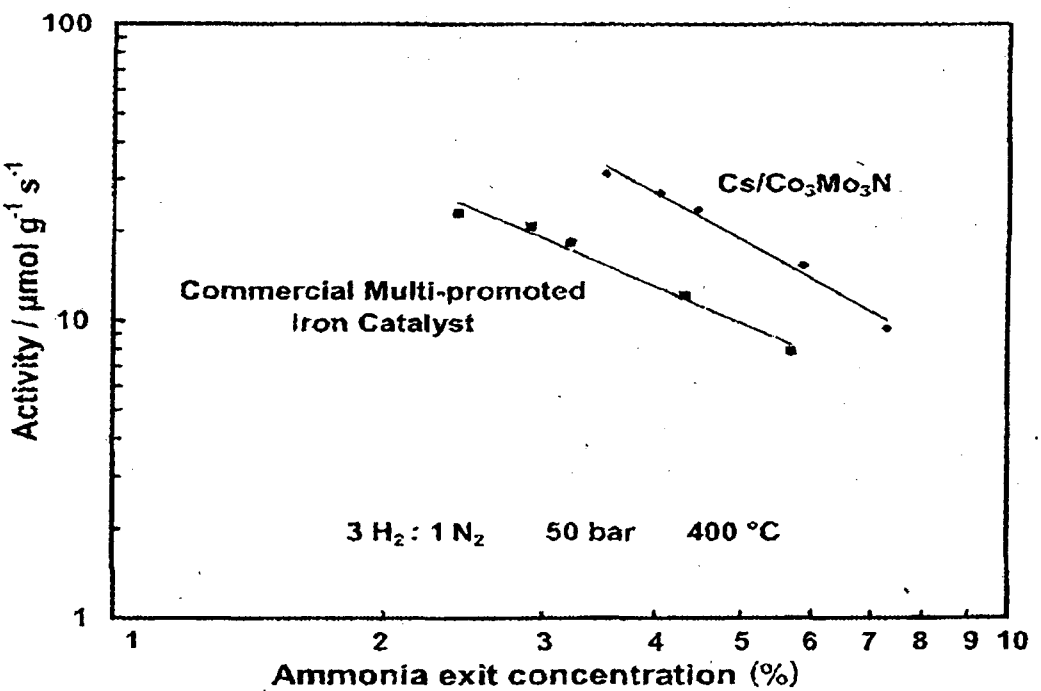

Figure 5: *The catalytic activities of Cs promoted CoMo and a commercial multi-promoted Fe catalyst. Taken from [42]*

Studying the dynamics of N_2 and H_2 (the constituents of NH_3) dissociative adsorption on the Mo(100) surface should provide a good base for the study of these potential ammonia synthesis catalysts.

I.8 References

[1] Jacobsen C. J. H., Chem. Commun., 12(2000)1057

[2] Davenport J. W., Estrup P. J., "The chemical physics of solid surfaces and heterogeneous catalysis", Elsevier Science Publishers B. V., chap.1, p.2, 1990

[3] Darling G. R., Holloway S., "The chemical physics of solid surfaces", Elsevier B. V., chap.2, p.29, 2003

[4] Logan R. M., Stickney R. E., J. Chem. Phys., 44(1966)195

[5] Kuipers E. W., Tenner M. G., Spruit M. E. M., Kleyn A. W., Surf. Sci., 205(1988)241

[6] Arumainayagam C. R., McMaster M. C., Schoofs G. R., Madix R. J., Surf. Sci., 222(1989)213

[7] Vattuone L., Yeo Y. Y., King D. A., Cat. Lett., 41(1996)119

[8] Kisliuk P.,J. Phys. Chem. Solids, 3(1957)95

[9] Langmuir I., Am. Chem. Soc., 40(1918)1361

[10] Gee A. T., Hayden B. E., Mormiche C., Nunney T. S., J. Chem. Phys., 112(2000)7660

[11] Moslemzadeh N., Barret S. D., Surf. Sci., 600(2006)2299

[12] Yeo Y. Y., Vattuone L., King D. A., J. Chem. Phys., 104(1996)3810

[13] Baer R., Zieri Y., Kosloff R., Surf. Sci., 411(1998)L783

[14] Luntz A.C., Bethune D. S., J. Chem. Phys., 90(1989)1274

[15] Butler D. A., Hayden B. E., Surf. Sci., 337(1995)67

[16] Poelsema B., Verheij L. K., Comsa G., Surf. Sci., 152/153(1985)496

[17] Persson M., Wilzen L., Andersson S., Phys. Rev. B., 42(1990)5331

[18] Rettner C. T., Schweizer E. K., Stein H, Auerbach D J, J. Vac. Sci. Technol., A7(1989)1863

[19] Luntz A.C., Williams M. W., Bethune D. S., J. Chem. Phys., 89(1988)4318

[20] Rettner C. T., Stein H., Phys. Rev. Lett., 59(1987)2768

[21] Bligaard T, Norskov J K, Dahl S, Matthiesen J, Christensen C H, Sehested J, J. Catalysis, 224(2004)206

[22] P. Nordlander, S. Holloway, and J.K. Norskov, Surf. Sci., 136 (1984) 59

[23] McMullen T, Plumer M L, Stott M J, Zaremba E, Phys. Rev. B, 38(1988)1077

[24] Hohenberg P, Kohn W, Phys. Rev., 136(1964)B864

[25] Kohn P, Sham L J, Phys. Rev., 140(1965)1133

[26] Mortensen J. J., Hansen L. B., Hammer B., Norskov J. K., J. Catalysis, 182(1999)479

[27] Jacobsen C J H, Dahl S, Bjerne S, Clausen S B, Logadottir A, Norskov J K, J. Am. Chem. Soc., 123(2001)8404

[28] Barteau M. A., Catal. Lett. 8(1991)175

[29] Norskov J. K., Bligaard T., Logadottir A., Bahn S., Bollinger M., Hansen L. B., Bengaard H., Hammer B., Sljivancanin Z., Mavrikakis M., Xu Y., Dahl S., Jacobsen C. J. H., J. Catal. 209(2002)275

[30] Bligaard T., Norskov J. K., Dahl S., Matthiesen J., Christensen C. H., Sehested J., J. Catal. 224(2004)206

[31] Reutte J. E., Chabal Y. J., Christman S. B., J Electron Spec. Rel. Phenom., 44(1987)325

[32] Prybyla J. A., Estrup P. J., Ying S. C., Chabal Y. J., Christman S. B., Phys. Rev. Lett., 58(1987)1877

[33] Zaera F., Kollin E. B., Gland J. L., Surf. Sci., 166(1986)L149

[34] Felter J.E., Barker R.A., Estrup P.J., Phys. Rev. Lett. 38(1977)1138

[35] Han H. R., Schmidt L. D., J. Phys. Chem. 75(1971)227

[36] Chabal Y. J., Christman S. B., Arrecis J. J., Prybyla J. A., Estrup P. J., J. Electron Spec.and Rel. Phenom., 44(1987)17

[37] Butler D. A., PhD . Thesis, University of Southampton, 1994

[38] Butler D. A., Hayden B. E., Jones J. D., Chem. Phys. Lett., 217(1993)423

[39] Butler D. A., Hayden B. E., Topics in Catal., 1(1994)343

[40] Butler D. A., Hayden B. E., Chem. Phys. Lett., 232(1995)542

[41] Berger H. F., Resch Ch., Grosslinger G., Eilmsteiner G., Winkler A., Rendulic K. D., Surf. Sci. Lett., 275(1992)L627

[42] C.J.H. Jacobsen, Chem. Commun. (2000) 1057

Chapter II: Instrumentation and Equipment

II.1 UHV System Set Up

The experiments reported in this thesis were carried out using an ultra-high vacuum (UHV) chamber. The base operating pressure for this chamber was typically between 4×10^{-11}mbar and 1×10^{-10}mbar (as measured via an ion gauge).

The main chamber pumping is via two turbo-molecular pumps (Leybold water cooled 1000 ls^{-1}, Leybold water cooled 151 ls^{-1}) backed by a diffusion pump (Edwards E04 water cooled 600 ls^{-1}), which is in turn pumped by a rotary pump (Edwards E2M18 5 ls^{-1}). A titanium sublimation pump (TSP) was also used in short bursts to improve the pumping of oxygen from the chamber. The TSP works by evaporating a thin layer of reactive titanium that will react with the oxygen in the chamber before sticking to the chamber walls, hence trapping the oxygen.

The main chamber was equipped with the facilities to perform low energy electron diffraction (LEED from Omicron), X-Ray Photoelectron Spectroscopy (XPS from Vacuum Generators), ion bombardment, and also included a gas doser (set up to dose both nitrogen and oxygen) and a quadrupole mass spectrometer (QMS from Vacuum Generators, QXK300).

The chamber was also equipped with a differentially pumped (via the main chambers backing rotary pump) xyzθ rotatable manipulator upon which samples could be mounted. The manipulator (and therefore also the sample) could be cooled via a liquid nitrogen reservoir.

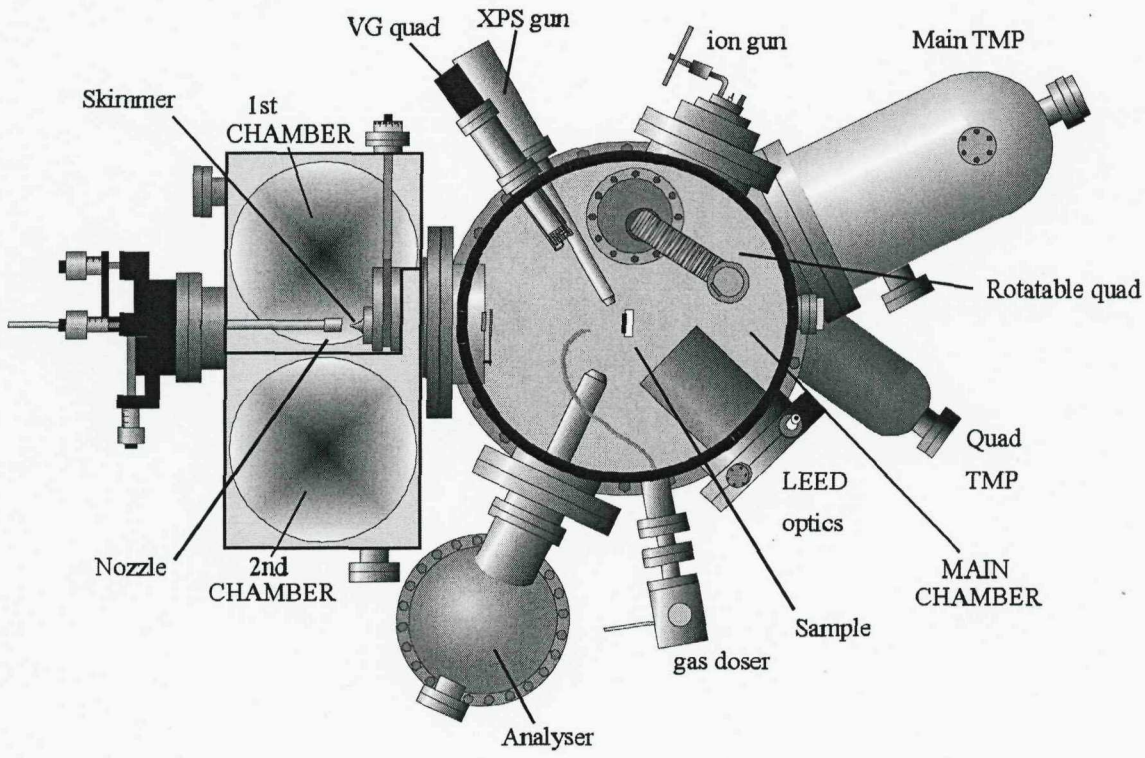

Figure 1: *UHV chamber diagram*

To aid the pumping of water from the chamber it is possible to heat the chamber to up to 140°C. A baking period of between 14 and 24 hours, followed by a further day's pumping, produces a chamber pressure of around 1×10^{-10}mbar.

Most experiments were performed using a supersonic molecular beam and this required two further vacuum chambers, each individually pumped. The 1st and 2nd chambers (as labelled in figure.1) were each pumped by a 6" oil diffusion pump (Edwards E06 1000 ls^{-1}) and backed by, in the case of the 1st chamber, an Edwards E2M40 rotary pump (12.5 ls^{-1}), and, in the case of the 2nd chamber, a smaller Edwards E2M18 (5 ls^{-1}) rotary. The base operating pressures of these two chambers were $<1\times10^{-7}$mbar for the 1st chamber (measured using a penning gauge), and 2×10^{-8}mbar for the 2nd chamber (measured using an ion gauge).

II.2 The Supersonic Molecular Beam

The concept of the effusive molecular beam was developed by Stern and Gerlach in 1919 [1]. Their design produced a beam of molecules with a large energy distribution and this was improved upon by the supersonic molecular beam designed in 1951 by Kantrowitz and Grey [2] which was able to produce a much narrower energy distribution.

A supersonic molecular beam is formed when gas at a relatively high pressure, behind a nozzle, P_n, expands into a region of low pressure, P_{1st}. In this case a gas mixture of usually between 0.5 and 2 bar (as measured by a barometer) is put into the gas line behind a 30μm quartz nozzle and expanded into the 1st chamber (P_{1st}). This nozzle can be resistively heated via a tungsten filament (0.38mm diameter) coiled around it with a thin layer of carbon film between the nozzle and the filament protecting the quartz tube. The nozzle temperature (T_n) is monitored by three K-type thermo couples (Ni/Cr–Ni/Al), one located inside the nozzle, and two between the carbon film and the quartz, one at the exit of the nozzle and another approximately one centimetre back along the nozzle. The temperature of each of these thermocouples was recorded as a function of the current passed through the filament so as to provide calibrated back ups from which the temperature could be accurately determined should the primary thermocouple fail. The thermocouple within the nozzle was taken to be the most accurate temperature measure of the gas mixture. The position of the nozzle is adjustable and may be tilted on the x and y axis (the axis perpendicular to the beam, x horizontally and z vertically) by $\pm 2.5°$ and moved along this axis by ± 12.5 mm. A dust filter was positioned directly behind the nozzle to prevent blockages.

The shape of the nozzle will to some extent determine the motion of the gas molecules. The shape is designed to create a nozzle jet avoiding motion perpendicular to the beam axis as opposed to a free jet which would occur if the "nozzle" was merely a hole in a flat wall.

A free jet would cause there to be a larger beam divergence though even this problem can be minimised by keeping P_n relatively high. $P_n >> P_{1st}$ allows the gas to be

considered to be expanding isentropically, with negligible heat conduction or viscous (internal resistance to flow) effects. The gas density will decrease along the beam axis and will, at some point, change from continuum flow (high density flow with very short molecular mean free paths) to free molecular flow (where the mean free paths are long and virtually no molecular collisions will occur).

As the area of the nozzle decreases the pressure difference accelerates the gas towards the sample. As this expansion occurs the temperature of the gas drops drastically. The distribution of molecular speeds of the gas molecules is approximately Maxwellian, with the distribution being described by equation II.1.

$$P(v_i) = 4\pi v_i^2 \left(\frac{m}{2k_B \pi T} \right)^{3/2} e^{\left(-\frac{m v_i^2}{2k_B T} \right)} \qquad \textbf{(II.1)}$$

Where $P(v_i)$ gives the distribution of molecular speeds, v_i the speed of the molecule, T the temperature of the gas, and m the mass of the gas molecule. As the temperature of the gas drops the distribution of speeds becomes narrower. This narrow energy distribution allows for the accurate examination of the interaction between the sample and molecules of a specific energy.

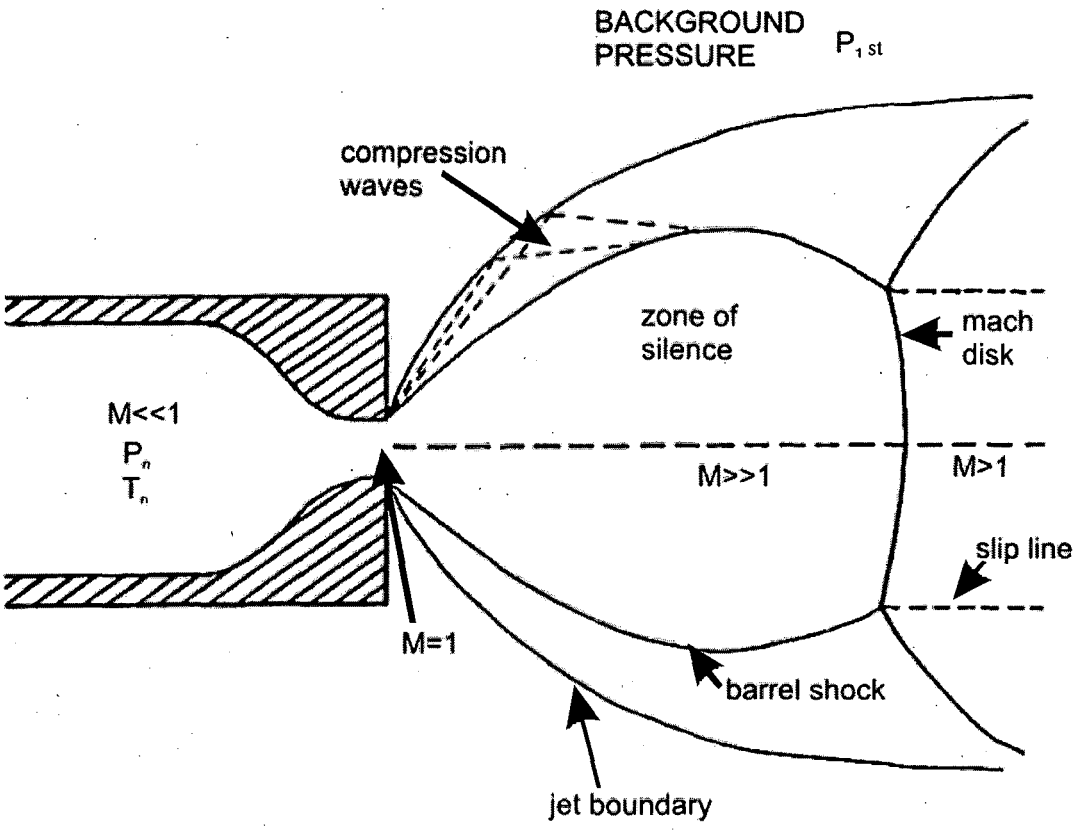

Figure 2: *supersonic molecular beam generation. Taken from [3]*

Figure 2 illustrates the expansion taking place. The area labelled the "zone of silence" is characterised by molecules moving at supersonic speeds. Within this zone the expansion is isentropic, i.e. the molecular flow is independent of the boundary conditions.

Moving away from the nozzle exit the velocity of the molecules continues to increase until the expansion reaches a boundary where the pressure becomes comparable to the background pressure of the chamber and overexpansion occurs.

At this boundary the beam becomes compressed by a series of shockwaves (very thin non-isentropic regions of large density, pressure, temperature and velocity gradients). The shockwaves act to rapidly slow down the molecules and reduce the Mach number to subsonic values (M<1)

$$M = \frac{speed\ of\ molecule}{speed\ of\ sound} \qquad \textbf{(II.2)}$$

The point at which the molecules are decelerated to the speed of sound (M=1) is known as the Mach disk. The position of the disk relative to the nozzle exit (χ_M) is described by a function containing the ratio of the nozzle pressure (P_n), background pressure (P_{1st}), and nozzle diameter (d)

$$\chi_M = 0.6\left(\frac{P_n}{P_1}\right)^{1/2} d \qquad \textbf{(II.3)}$$

In order for the supersonic beam to reach the sample without passing the Mach disk a skimmer must be incorporated into the design to extract the centre of the beam. The nozzle may be moved back and forth along the axis of the beam (z-axis) and this allows the positioning of the skimmer within the zone of silence at ~100d from the nozzle exit. The skimmer is made from stainless steel, has a 300μm opening, and is conically shaped with walls angled to deflect scattered molecules away from the beam axis avoiding the creation of shockwaves in front of the skimmer.

This deflection of molecules causes the background pressure in the 1st chamber to rise. Typically initiating the beam was seen to cause a rise in pressure from $<1\times10^{-7}$ to $\sim1\times10^{-4}$mbar. Those molecules extracted by the skimmer pass into the 2nd chamber and may then pass through a collimating aperture and into the main chamber. In order to align with this aperture the skimmer's position may be moved along the x and y axis, however, once aligned there should be no need to further alter the skimmer position. This aperture is variable and consists of a steel plate which may be moved up or down to reveal and align apertures with diameters of 0.5, 1.3 and 3mm. The sample is located a further 16.2cm from the aperture, within the main chamber and these varying aperture sizes result in beam diameters at the crystal surface of 1.25, 3.25 and 7.5mm, respectively.

The 2nd chamber is another high vacuum region with base pressure, $P_{2nd}\sim1\times10^{-8}$mbar, with high mean free path lengths ensuring that molecules moving along the central

beam axis can progress without disruption. When the nozzle and skimmer are aligned the pressure rises as molecules not passing through the aperture are deflected back into the 2nd chamber. However, the pressure still remains low, typically rising to only 1×10^{-7}mbar.

The element of the beam that makes it into the main chamber consists of 2 components whose respective contributions to the main chamber pressure are labelled as $P_{effusive}$ and P_{beam}. $P_{effusive}$ accounts for the diffuse element of the beam that contributes to the increase in the pressure of the main chamber but is not directly incident upon the sample surface. P_{beam} describes the element of the beam colliding directly with the sample.

A mica flag within the main chamber, close to the aperture, may be moved to either allow the beam to be incident upon the sample, or to block the path of the beam. The mica flag has a very low adsorption cross section ensuring that almost all molecules incident upon it are reflected and contribute to the pressure within the main chamber.

The main chamber is maintained at ultra-high vacuum and typically operates at $<1\times10^{-10}$mbar. Introduction of the beam into the chamber causes a rise in pressure dependent upon the constitution of the beam and the aperture size. Typically the pressure is observed to rise to between 4×10^{-9} and 7×10^{-8}mbar.

If the initial enthalpy of the gas is converted into kinetic energy of the gas molecules during the expansion it may be written that:-

$$H_1 + E_{K(H_1)} = H_n \qquad \textbf{(II.4)}$$

$$E_K = \frac{1}{2}mv^2 \qquad \textbf{(II.5)}$$

Taking H to be the enthalpy per unit mass:-

$$H_1 + \frac{1}{2}v^2 = H_n \qquad \textbf{(II.6)}$$

$$v^2 = 2(H_n - H_1) \qquad \textbf{(II.7)}$$

During the expansion the temperature of the gas will drop rapidly along with the increase in velocity, this allows for rotational and vibrational relaxation to begin taking place. The extent to which relaxation occurs will depend very much on the molecule in question. The equation describing rotational relaxation (cooling), dT_r/dt, is as follows:-

$$\frac{dT_r}{dt} = \frac{(T - T_r)}{\tau} \qquad \textbf{(II.8)}$$

With τ being the ratio of required collisions (ς) to the collision frequency (υ)

$$\tau = \frac{\varsigma}{\upsilon} \qquad \textbf{(II.9)}$$

$$\upsilon = n v \sigma \qquad \textbf{(II.10)}$$

σ being the effective molecular cross section, n the number of molecules, and v the uniform molecular velocity.

The number of collisions required for rotational relaxation to occur is specific to the particular molecule. For hydrogen a large number are required and $\tau \approx 5/3$ whereas N_2 requires fewer collisions and $\tau \approx 7/5$.

Typically a molecule undergoing the expansion will experience between 100 and 1000 collisions. To undergo vibrational relaxation a small diatomic molecule (such as H_2 or N_2) has a relaxation period of $\sim 10^4$ collisions, therefore the degree of vibrational cooling will be small. This is due to the vibrational energy level spacing being large for small diatomics. If the quantum harmonic oscillator approximation is made, the quantum vibrational energy level spacings are inversely proportional to the square root of the reduced mass of the atoms composing the diatomic molecule. Therefore small diatomics will have larger energy level spacing and heavier diatomics much finer quantum vibrational energy level spacing.

The first law of thermodynamics predicts that the internal energy of an isolated system is constant. The energy might change form but there is no gain or loss. Therefore any change in the internal energy (U) of the system is due to heat absorbed by (Q) or work done (W) on the system.

$$dU = \delta Q + \delta W \tag{II.11}$$

With $$\frac{dU}{dt} = \frac{\delta Q}{dt} + \frac{\delta W}{dt} \tag{II.12}$$

If a control volume is considered equation II.12 becomes equation II.13, the CV subscript denoting the internal energy of a control volume, and E_0 and E_1 being the energy of the system in the initial stagnation state and a later state (respectively). Therefore m_0E_0 is the rate of flow of energy into the control volume and m_1E_1 the rate of energy flow out.

$$\frac{dU_{CV}}{dt} = \frac{\delta Q}{dt} + \frac{\delta W}{dt} + m_0 E_0 - m_1 E_1 \tag{II.13}$$

With

$$Q = \lim_{dt \to 0} \frac{\delta Q}{dt} \tag{II.14}$$

and

$$W = \lim_{dt \to 0} \frac{\delta W}{dt} \tag{II.15}$$

If this system is considered to be steady state (i.e. overall there is conservation of mass and energy), then $\frac{dU_{CV}}{dt} = 0$. Also, this would allow m_0 and m_1 to be replaced simply by m since the value of mass flowing in will be equal to that flowing out.

This leaves:-

$$Q + W = m(E_1 - E_0) \tag{II.16}$$

The total energy (E) will be the sum of the kinetic (E_K) and internal (U) energies of the gas.

$$Q + W = m\left[\left(E_{K1} + U_1\right) - \left(E_{K0} - U_0\right)\right] \tag{II.17}$$

The kinetic energies are replaced with $\frac{1}{2}mv^2$ and the velocity of the gas in the initial stagnation state is considered to be zero (i.e. v_0=0) with v_1 being the speed of the gas molecules as the expansion is taking place. Furthermore the system is considered to be adiabatic (i.e. overall no heat gained or lost), resulting in:-

$$Q = 0 \tag{II.18}$$

&

$$W = -(P_1V_1 - P_0V_0) \tag{II.19}$$

Combining these values of heat and work with equation II.17

$$-P_1V_1 + P_0V_0 = \frac{1}{2}mv_1^{\,2} + U_1 - U_0 \tag{II.20}$$

The term enthalpy has already been mentioned, and here it is defined as

$$H = U + PV \tag{II.21}$$

$$dH = dU + d(PV) \tag{II.22}$$

Substituting in equation II.11 to replace dU

$$dH = dQ + dW + PdV + VdP \tag{II.23}$$

When a gas expands it must do work on the surrounding atmosphere to push it back as it takes up a greater volume. The work done by or to a system can be described by the change in the volume of the system multiplied by the pressure.

$$dW = -PdV \tag{II.24}$$

Substituting this into equation II.23

$$dH = dQ - PdV + PdV + VdP \tag{II.25}$$

$$dH = dQ + VdP \tag{II.26}$$

In the case of an isobaric system $dP = 0$, and therefore:-

$$dH = dQ \tag{II.27}$$

With

$$C_P = \frac{dQ}{dT}\Big)_P = \frac{dH}{dT}\Big)_P \tag{II.28}$$

C_P is the molar specific heat capacity of the gas at constant pressure.

As the gas expands the number of collisions and the temperature of the gas quickly decreases. The change in temperature from the stagnation state to the state in which it exists after the expansion is related to the molar enthalpy.

$$dH = C_P dT \tag{II.29}$$

Equation II.6 is rearranged and substituted into the above equation

$$-\frac{1}{2}mv_1^2 = C_P dT \tag{II.30}$$

Substantial cooling occurs during the expansion, with the temperature of the stagnation state (T_n) being substantially greater than that of the gas after the expansion (T_1), i.e. $T_n >> T_1$. Therefore,

$$dT = T_1 - T_n \tag{II.31}$$

can be approximated to

$$dT = -T_n \tag{II.32}$$

Substituting into equation II.30 and rearranging

$$v_1 = \sqrt{\frac{2}{m} C_P T_n} \tag{II.33}$$

In the case of an ideal gas

$$C_P = \left(\frac{\gamma}{\gamma - 1} \right) R \tag{II.34}$$

With

$$\gamma = \frac{C_P}{C_V} \tag{II.35}$$

The assumption is made that the gas mixture can be considered as a monoatomic ideal gas provided that the seed gas is monoatomic and ideal and that the reactant gas only makes up a very small percentage of the total gas mixture.
Complicated calculations using the heat capacities of the gases can be ignored since in the case of a monoatomic ideal gas,

$$C_P = \frac{5}{2} R \tag{II.36}$$

If the gas mixture used is an ideal gas seeded with only a very small fraction of the reactant gas it may be assumed that the expansion will exhibit ideal behaviour. Therefore the terminal velocity of the molecules in the expanding gas may be expressed as

$$v = \sqrt{\frac{5RT}{m}} \qquad \textbf{(II.37)}$$

It may be necessary to consider a mixture of i ideally behaving gases with mole fractions x_i and masses m_i. In the case of a seed gas where only a small fraction (<4%) of the total gas is made up of the reactant gas, particularly when the reactant gas molecule is a small diatomic such as H_2 or N_2, it may be assumed that this also behaves as an ideal gas within the mixture.

$$v = \sqrt{5RT\frac{1}{\sum x_i m_i}} \qquad \textbf{(II.38)}$$

To obtain the velocity of an individual gas particle rather than the molar value it is necessary to divide by $\tilde{N}_A$. Noting that $R/N_A = k_B$, the following equation is produced, describing the velocity of a gas particle within the molecular beam:-

$$v = \sqrt{5k_B T\frac{1}{\sum x_i m_i}} \qquad \textbf{(II.39)}$$

II.3 Calculating E_K Of Reactant Particles In The Beam

Typically the velocity, and hence the kinetic energy, E_i (the i subscript denoting kinetic energy when incident upon the sample surface), of the particles produced from a supersonic molecular beam are calculated using time of flight (TOF) measurements [4,5].

The facilities required for TOF measurements were not available. However, TOF measurements have previously been carried out using this UHV system [5], with the results found to be in reasonable agreement with estimations using the following theoretical calculations. In cases where a large difference in mass exists between seed and reactant particles a correction may however be required for the drift of the TOF value from the calculated E_i value. These corrections are shown in appendix B.

The kinetic energy of the reactant gas molecules will depend on the following:

a) the seed gas
b) the reactant gas
c) the amount of reactant gas in the seed gas
d) the nozzle temperature

The continuum flow of gas behind the nozzle allows for the use of a technique called seeding where a heavy inert seeding gas decelerates lighter reactant gas molecules or vice-versa. The gas mixture is altered via flow controllers positioned at the beginning of the beam line. Figure 3 is a diagram illustrating the flow controller set up.

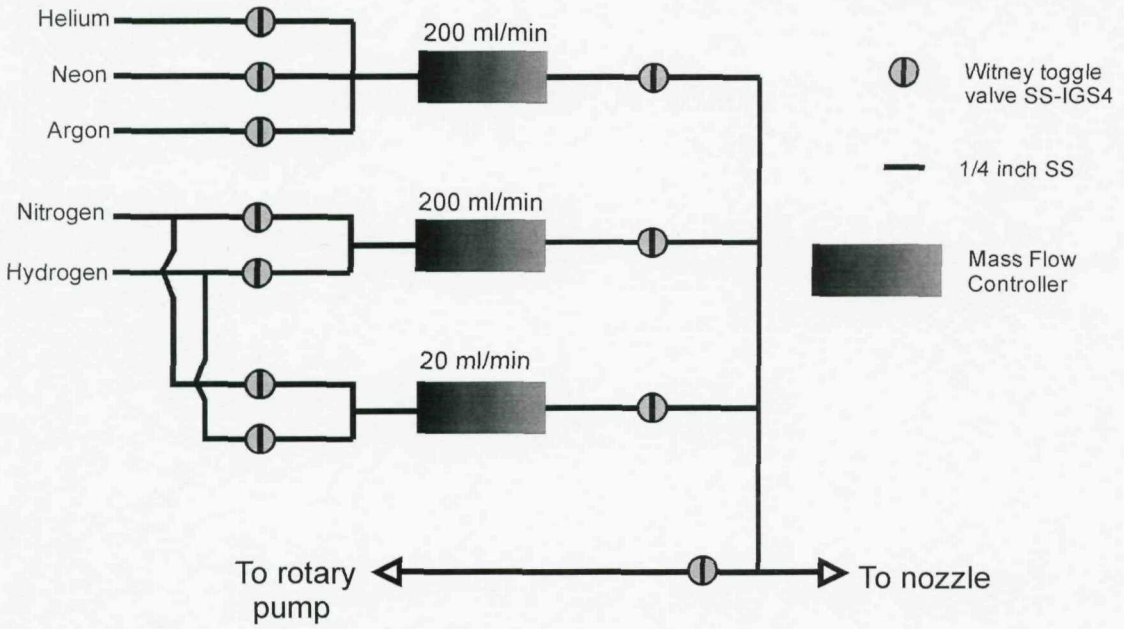

Figure 3: *Flow controller configuration*

The beam line can be pumped via an Edwards E2M18 rotary pump (5 ls^{-1}) to allow a quick changeover between gases without contamination.

The kinetic energy of the seed gas particles in the beam line is

$$E_{K(n)(seed)} = \frac{1}{2} m_{(seed)} v^2_{(n)(seed)} \qquad \textbf{(II.40)}$$

Kinetic theory also allows for the expression of the kinetic energy of the gas in terms of its temperature.

Using basic kinetic theory a relation between the root mean square velocity of the particles and the temperature of the gas can be determined

$$v_{RMS} = \sqrt{\frac{3RT}{M}} \qquad \textbf{(II.41)}$$

A single molecule within the gas will have its speed altered when it collides with other molecules, but its average translational kinetic energy over time will be:-

$$\overline{E_{K(n)(seed)}} = \frac{1}{2} m v_{RMS}^2 \qquad \textbf{(II.42)}$$

Substituting equation II.41 into equation II.42,

$$\overline{E_{K(n)(seed)}} = \frac{1}{2} m \left(\frac{3RT_n}{M} \right) \qquad \textbf{(II.43)}$$

The molar mass (M) may be replaced by Avogadro's number (N_A) multiplied by the mass (m). If R/N_A is then replaced by the Boltzmann constant:-

$$\overline{E_{K(n)(seed)}} = \frac{3}{2} k_B T_n \qquad \textbf{(II.44)}$$

Therefore by measuring the temperature of the gas the average translational kinetic energy is also being measured.
The internal energy of the molecule depends not on the translational kinetic energy but also on contributions from the rotational and vibrational kinetic energies of the molecule

$$U = E_{K(trans)} + E_{K(vibr)} + E_{K(rot)} \qquad \textbf{(II.45)}$$

However, in the case of a monoatomic ideal gas there will be no vibrational or rotational energy contribution.

Therefore

$$U = \frac{3}{2} k_B T_n \qquad \textbf{(II.46)}$$

The molar enthalpy of the monoatomic ideal gas (H) differs from the internal energy in that it does not take into account the work done by the system in expanding into the surrounding atmosphere. H is therefore larger than U by PV

Using the ideal gas law

$$P\overline{V} = k_B T \tag{II.47}$$

$\overline{V}$ is the molar volume, hence

$$H = \frac{3}{2}k_B T_n + k_B T_n \tag{II.48}$$

The enthalpy represents the reserve of energy of the gas molecule which, in the case of the ideal monoatomic gas forming a supersonic molecular beam, is transferred to the kinetic energy of the gas.

$$H = E_{i(seed)} \tag{II.49}$$

$$\frac{5}{2}k_B T_n = \frac{1}{2}m_{(seed)}v^2_{(seed)} \tag{II.50}$$

Producing the same result as derived in equation II.39

$$v^2_{(seed)} = \frac{5k_B T_n}{m_{(seed)}} \tag{II.51}$$

If a reactant gas is being seeded within a carrier gas, the energy of the reactant gas can be calculated by assuming the velocity of the reactant gas to be equal to the velocity calculated for the pure seed gas. This approximation assumes the gas mixture to be mainly made up of the seed gas with <4% reactant gas present in the mixture.

$$E_{i(react)} = \frac{1}{2}m_{(react)}v^2_{(react)} \tag{II.52}$$

Making the assumption that $v_{(react)} = v_{(seed)}$,

$$E_{i(react)} = \frac{1}{2} m_{(react)} v_{(seed)}^2 \qquad \textbf{(II.53)}$$

The experiments performed have always used He, Ne or Ar (all monoatomic gases that are assumed to behave as ideal gases) as the seed, therefore substituting the calculated value for $v_{(seed)}^2$ and using equation II.53

$$E_{i(react)} = \frac{5}{2} \frac{m_{(react)}}{\sum x_i m_i} k_B T_n = \frac{5}{2} \frac{m_{(react)}}{x_{(seed)} m_{(seed)} + x_{(react)} m_{(react)}} k_B T_n \qquad \textbf{(II.54)}$$

This formula is shown, by comparison with TOF measurements [7], to give a reasonable approximation of the incident energy for H_2/He beams, with the values falling within the predicted error margins attached to the results. The errors associated with this calculation for a helium seeded beam are taken to be the same as those calculated previously using TOF measurements on this system. However, when considering a reactant-seed mixture with a greater mass difference there is seen to be a significant drift from the value predicted by equation II.54. For example, in the case of a 1%H_2/Ar beam (with T_n=312K), equation II.54 predicts $E_{i(react)}$ to be 3.2meV, a considerable drift from the TOF calculations which record a value of 13 ±1meV [8].

II.4 Kinetic energy calculation for small diatomics

The above calculations all assume the gas to be ideal and monoatomic. However the calculations must be altered slightly when the gas under consideration is not monoatomic, for example, in the case of a diatomic seed, or of an unseeded beam made up purely of the reactant gas.

The translational kinetic energy of the gas particle in a specific direction is given by $\frac{1}{2} k_B T_n$, with a multiple of 3 accounting for the 3 degrees of freedom associated with

translational motion (in x, y, and z), assuming the molecule has no preferred direction of travel.

If the gas is not monoatomic, then as well as these 3 translational degrees of freedom the vibrational and rotational motion of the molecule must also be taken into account.

In the case of small diatomics such as H_2 and N_2 there are a further vibrational and rotational degrees of freedom to be taken into consideration when calculating the internal energy of the gas and hence the velocity of the molecules within the beam.

As the temperature increases the rotational, and eventually the vibrational, motions of the molecules will become activated, although in the typical temperature range experienced by the gas within the nozzle it may be that, for small diatomics, only the rotational degrees of freedom are activated. The below plot of specific heat capacity as a function of temperature for H_2 shows that although the rotational degrees of freedom are activated well below room temperature the vibrational degrees of freedom tend to be frozen out until relatively high temperatures are reached.

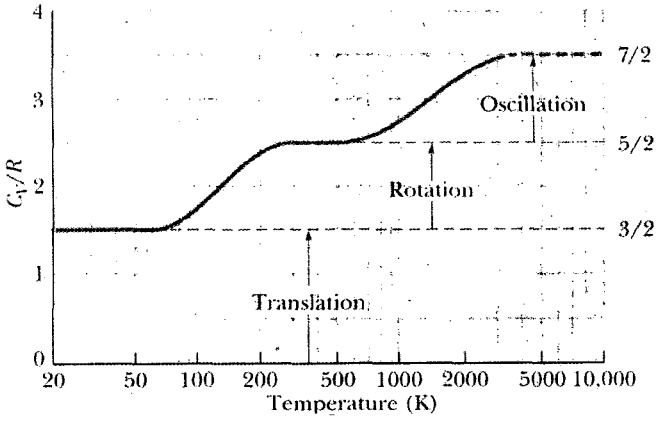

Figure 4: *For H_2 at very low temperatures only translation motion is possible. Rotational and vibrational motions begin to contribute as the temperature increases. Although rotational motion is already active at room temperature the temperature must approach close to 1000K before the same can be said for molecular vibrations (Reproduced from [9]).*

The late onset of this vibrational motion can be understood in terms of the vibrational energy level spacing of the molecule. As has been previously mentioned, the quantum harmonic oscillator approximation relates the energy level spacing to the square root of

the reduced mass of the atoms composing the diatomic, if, as is the case for N_2 and H_2, the atoms are small, then the vibrational energy level spacing will be large and a substantial energy input will be required in order to reach the 1st vibrational excitation energy.

According to the equipartition theorem, any input of energy into a closed system of molecules is evenly divided among the degrees of freedom available to each molecule. Assuming that the molecules tend to remain in their lowest possible vibrational state, because the energy level spacings are so large, the incident energy is re-written as,

$$E_i = (3.6)k_B T_n \qquad \textbf{(II.55)}$$

This exact value may, in reality, vary slightly depending upon the specific diatomic, and the temperature of the gas, with the value tending to become larger as the size of the diatomic and the temperature of the gas is increased.

II.5 The Molybdenum Sample

The sample used in these studies was a molybdenum single crystal. Molybdenum is a body centred cubic, with a melting point of 2890K. The molybdenum single crystal used in these studies had its front face cut and polished to within 0.5° of the (100) plane by Metal Crystals and Oxides (Cambridge). The dimensions of the crystal were at first 10 × 10 × 1.2 mm and then later changed to a circular crystal with a diameter of 9 mm and depth of 1 mm. The switch to a crystal of smaller size was made to aid the heating of the crystal since the power supply used for heating was limited and it was often difficult to consistently bring the larger crystal to the required temperatures.

Grooves of 0.4 mm were cut into the top and bottom of the crystal and the crystal was mounted on two 0.38 mm diameter tungsten wires fitted into these grooves and spot-welded to 2 stainless steel support bars. These stainless steel bars were screwed to an oxygen free copper support. The bars were electrically insulated from the copper support via two thin sheets of mica and ceramic spacers on the screws. The thin mica

sheets ensured good electrical insulation while still retaining thermal conduction, allowing the sample to be cooled via the liquid nitrogen reservoir within the manipulator.

The sample was heated by means of electron bombardment (EB). A 0.25mm diameter spiral filament of thoriated tungsten positioned directly behind the crystal was heated resistively causing electrons to be emitted from the wire surface. A large positive voltage was placed on the crystal accelerating the electrons into the back of the sample. This electron bombardment allowed large and rapid temperature increases. A sufficient current must first be passed through the spiral filament to obtain electron emission from the wire. Once emission is achieved the heat transferred to the sample is determined by the quantity of electrons emitted and the energy of the electrons that collide with the sample, the quantity being controlled by the current put through the filament and the energy of the electrons being controlled by the accelerating voltage placed on the sample.

The voltage that could be placed upon the sample was limited by the power supply unit to 1000V, therefore the voltage was kept constant and the temperature varied by increasing the current on the filament. The temperature of the sample was measured using a W3 type (W3%Rh/W25%Rh) thermocouple. This was calibrated against a K type (Ni/Cr – Ni/Al) thermocouple for temperatures below 273K (see Appendix C).

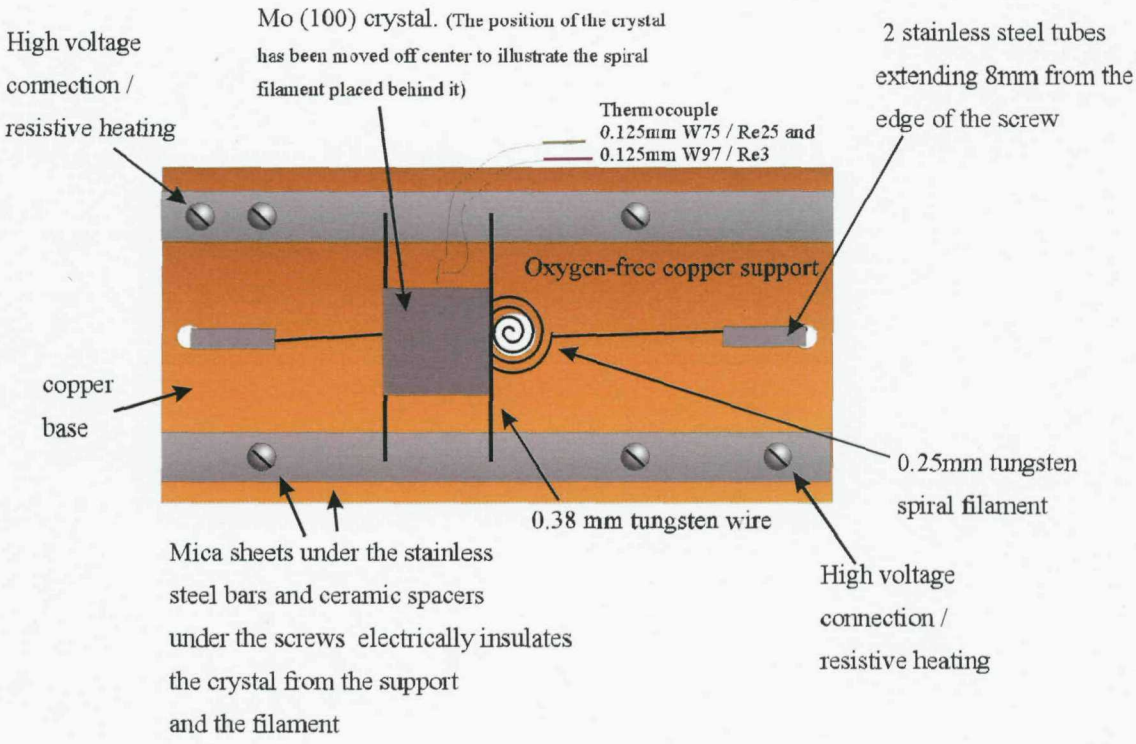

Figure 5: *Sample mount configuration*

II.6 References

[1] Stern O., Gerlach W., Z. Phys., 8(1921)110

[2] Kantrowitz A., Grey J., Rev. Sci. Instr., 22(1951)328

[3] Miller D. R., Atomic and Molecular Beam Methods, ed. G. Scoles, Oxford Uni. Press NY (1998) vol.1, chap.2

[4] Gee A. T., Hayden B. E., J. Chem. Phys., 113(2000)10333

[5] Gee A. T., Hayden B. E., Mormiche C., Nunney T. S., J. Chem. Phys. 93(1990)5240

[6] Mormiche C., PhD. Thesis, University of Southampton, 2002

[7] Gee. A., PhD. Thesis, University of Southampton, 2000

[8] Butler D. A., PhD . Thesis, University of Southampton, 1994

[9] Halliday D., Resnick R., Walker J., Fundamentals of Physics Extended, Wiley (1997) p.498

Chapter III: Experimental Methods And Techniques

III.1 Cleaning The Molybdenum Sample

Before carrying out experiments it was necessary to obtain a Mo(100) surface clean of contaminants. The main contaminants reported to commonly be present on this surface are oxygen, carbon, sulphur and nitrogen [1-4]. Nitrogen and sulphur were found to be easy to remove simply by heating the sample, however the removal of carbon and oxygen was found to be significantly more complicated. Various techniques for cleaning this surface have been suggested within the literature [5-9].

Attempts were made to clean the sample by means of ion sputtering, annealing, oxygen treatments and high temperature flashes.

III.1.1 Ion Sputtering

An ion gun was used to sputter the sample with argon ions. The particular ion gun used was a saddle-field ion source type, a cold cathode device. The argon atoms are ionized by means of electron bombardment and the electrostatic saddle-field configuration induces these ionizing electrons to describe long oscillatory paths without recourse to a magnetic field. The source anode was enclosed by the cathode and therefore extraction electrodes were not required.

During the sputtering process a sample is bombarded with a beam of energetic argon ions which sputters off the top layers, removing both metal and contaminant atoms. After sputtering the sample is annealed to restore order to the surface.

III.1.2 Annealing and High Temperature flashes

Heating a sample may provide contaminant molecules with enough energy to overcome the barrier to desorption, allowing them to be removed from the sample surface. Oxygen was found to be strongly bound to the molybdenum surface and this required the sample to be heated to >2000K in order for its removal. Because such a high temperature was required the cleaning was limited to short flashes since significant evaporation of the metal may begin to occur close to these temperatures (see appendix D). After cycles of high temperature anneals a metallic coating was noticed to have formed on ceramic insulation positioned near the crystal. Using a scanning electron microscope the coating was identified as molybdenum. This metalisation caused significant problems, shorting the high voltage supply necessary for the EB heating, and possibly creating a metallic surface behind the crystal upon which the molecular beam, if not properly aligned with the crystal, could be incident, and from which "false" results might be produced. This problem of "false" data shall be examined later in this chapter.

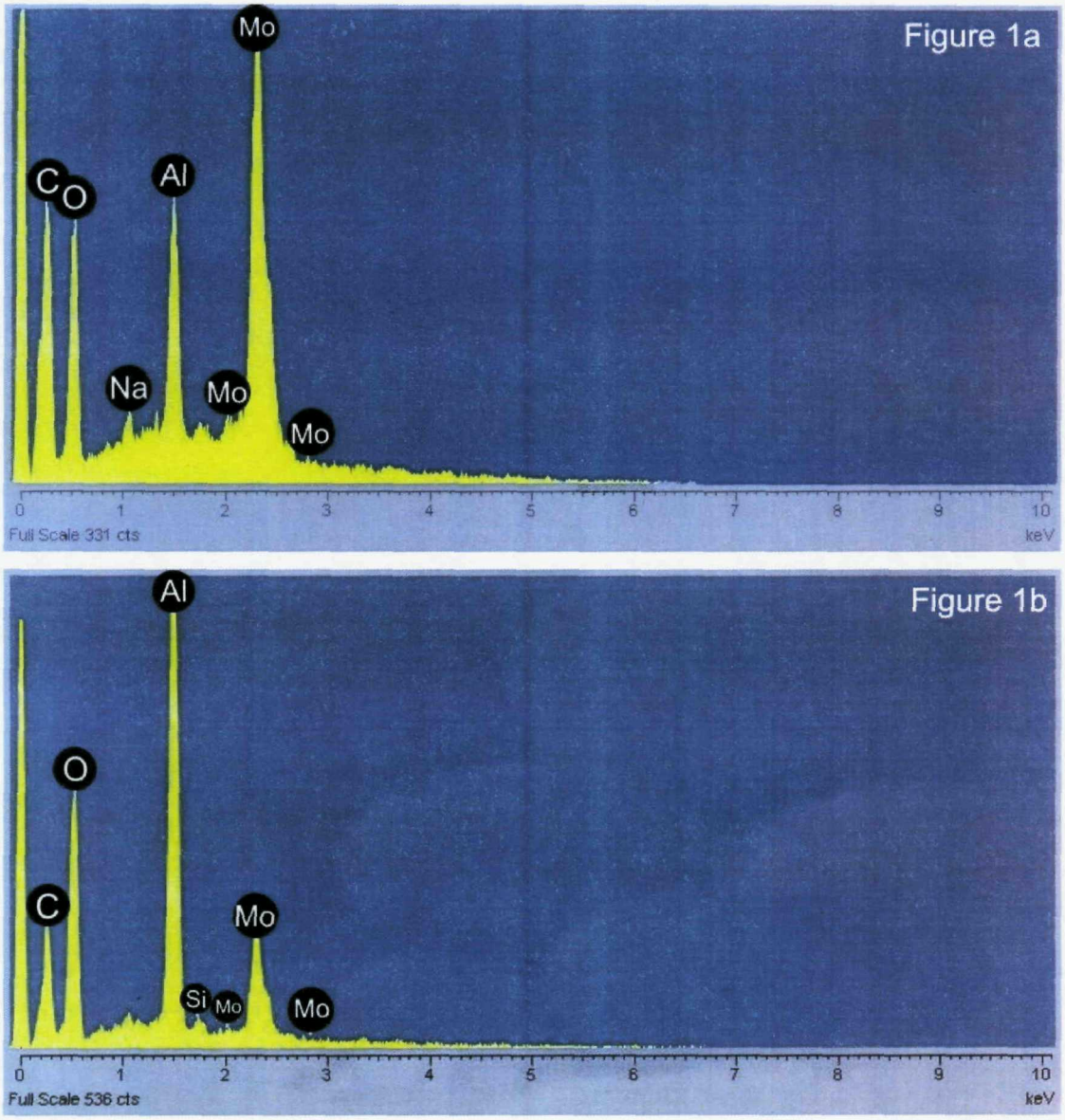

Figure1: a) *Scanning microscope plot taken from the metal coated area of a ceramic spacer insulating a screw close to the crystal.* ***b)*** *Plot taken from the same ceramic on an area with little metallisation. The large reduction in the Mo peak on plot b indicates that the metal coating present on this ceramic is molybdenum. (Al is a constituent component of the ceramic)*

III.1.3 Oxygen Treatments

The presence of a reactant gas while heating may aid the removal of certain contaminants. The process is applied by dosing small amounts of gas into a UHV chamber while maintaining the sample which requires cleaning at elevated temperatures. The dosed gas molecules react with contaminant molecules on the

surface. The resultant molecules then desorb from the surface when the sample is annealed. In the case of molybdenum it is reported that annealing the sample in an oxygen atmosphere will aid the removal of carbon from the crystal surface [5-9]. Carbon present at the surface reacts with the oxygen and, upon further annealing, is removed in the form of CO or CO_2.

III.1.4 The Cleaning Process Used to Obtain The Clean Mo(100) Surface

The technique found here to be most effective in producing a clean well ordered Mo(100) surface began by annealing the surface to ~1300 K in 1×10^{-6} mbar of oxygen in order to remove carbon from the surface. This oxygen treatment could be required to last for 12 hours or more as more carbon is pulled from the bulk crystal to the surface during heating. An insufficient oxygen treatment would see carbon migrating to the surface during future heating cycles, re-contaminating the surface. Initially upon receiving the crystal, and also when the crystal had been exposed to atmosphere for a prolonged period (>2 days), the oxygen treatment required a running time of approximately 12 hours to completely remove the carbon contamination, both that on the surface and that travelling up to the surface from the bulk. For shorter periods of exposure to atmosphere a surface that remained clean of carbon could be reproduced after short oxygen treatments of 1 hour or less, or sometimes without the need for any oxygen treatment.

Oxygen was then removed from the surface by flashing the crystal to ~2073 K for <1 second. A high level of oxygen contamination (for example directly after an oxygen treatment) might require 5 or 6 repeat flashes. This technique was found not to require the use of ion sputtering, and avoids the risk of damage to the surface structure that sputtering may cause.

The absence of contaminants from the surface was determined by a combination of x-ray photoelectron spectroscopy (XPS) and low energy electron diffraction (LEED) measurements. These techniques will be described in detail shortly.

Once a clean surface was obtained a King and Wells type experiment [10] using a specific reactant molecule, gas mixture, beam energy and crystal temperature, was performed and repeated until a model clean surface result was obtained. As work progressed it was possible to repeat the King and Wells experiment under specific conditions and, by comparison with the model result, determine whether a clean surface had been obtained and whether the beam was functioning correctly. The King and Wells technique will also be described in detail shortly.

III.2 Surface Analysis Techniques

III.2.1 X-Ray Photoelectron Spectroscopy

Photoelectron spectroscopy is a process which involves the excitation of electrons in an atom at the surface of a sample by means of monoelectronic x-rays, with an energy of >100eV. It was first developed by the Nobel prize winner K. Siegbahn [11], and is a technique that allows one to determine the species present at the surface of a sample. For example it may be used to monitor the quantity of contaminant (such as oxygen) present in comparison with clean molybdenum metal surface present. The progress of the cleaning may in this way be monitored using XPS. It is sensitive to surface contaminants down to levels of just 1% of a monolayer and therefore a good indicator of a clean surface.

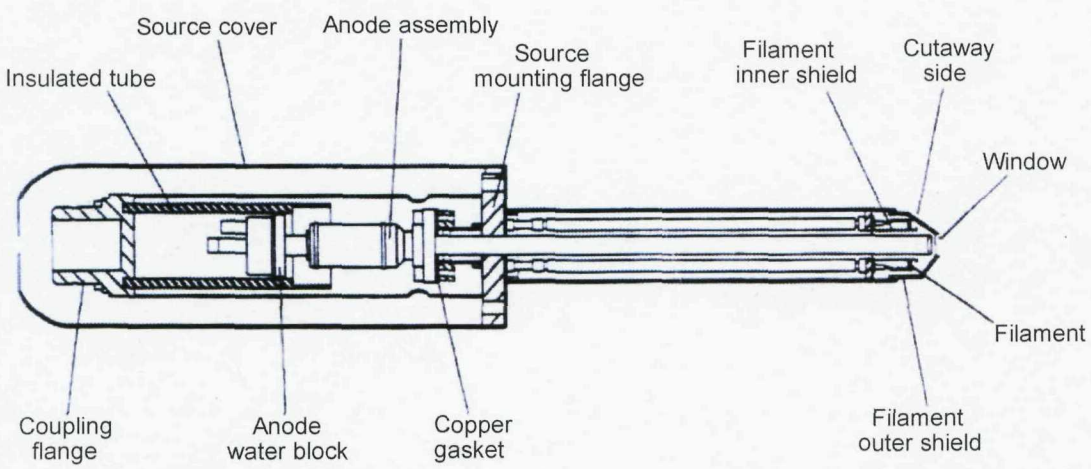

Figure 2: *A reproduction of the dual anode x-ray gun (VG Microtech).*

The x-rays used for this procedure are produced by an x-ray gun. In the gun, filaments are heated in order to emit electrons. The filament used here is a 1% thoria coated tungsten ribbon, heated via a 5A current, producing an emission current of 20mA. The thoriated tungsten produces an electron emission many times greater than that of pure tungsten at the same temperature. A difference in potential then attracts the electrons to the anode. The accelerating voltage placed on the anode was set to 15 kV (with the filament being at near earth potential). When colliding with the anode the electrons may knock out a core electron from the anode. An electron from an outer shell then fills the core hole. In order to drop from a loosely bound outer shell into a more tightly bound inner shell the electron must lose energy. This energy may be lost by emission of a photon of radiation.

The energy of the photon is only dependent upon the difference in energy between the two energy levels. Hence the energy of the x-ray photon is independent of the energy of the initial incoming electron and only dependent upon the metal used as the anode. In this case a dual anode is used with an Al coating on one face and Mg on the other. Alternating between these anodes allows x-rays of different energies to be emitted. The ability to alternate between two different anodes is important in that it allows the identification of auger electrons emitted from the Mo sample.

The emission from the target anode consists of narrow emission lines associated with the filling of core holes created by the incident electron beam. The principal line emitted for both the Mg and Al targets is due to the $2p_{1/2 \text{ and } 3/2} \rightarrow 1s$ decays, an unresolved doublet corresponding to 1253.6eV for Mg (with a full width at half maximum, FWHM, of 0.7eV) and 1253.6eV for Al (with FWHM of 0.85eV). There is a broad Bremsstrahlung background (Bremsstralung radiation being that emitted by a charged particle undergoing deceleration), however a thin Al window is used as a partial filter for any unwanted x-ray lines ensuring the photon source is nearly monochromatic. The window also acts to isolate the anode field, preventing stray electrons from interfering with experiments.

The heat generated during this process is sufficient to evaporate the anode and it has therefore been provided with a water cooling system.

The x-rays incident upon the sample may knock out a core electron providing it with kinetic energy (E_K). The kinetic energy of this photoelectron may be calculated using Einstein's photoelectric equation. This uses the concept of conservation of energy to produce an equation relating the energy of the incident photon ($h\upsilon$) to the binding energy of the electron (E_B) and the emitted electrons kinetic energy (E_K). If the condition of conservation of energy is applied and it is assumed that the photoelectron escapes the surface without undergoing any inelastic collisions, then the kinetic energy of the photoelectron emitted will be equal to the energy of the incident photon minus the energy required to release the electron from its bound state within the atom into the vacuum level. It should be noted that for a solid the binding energy is given relative to the Fermi level (the highest occupied electronic state), and therefore a small additional energy input known as the workfunction (ϕ) is required to move the electron from the Fermi level into the vacuum level.

$$E_K = h\upsilon - E_B - \phi \qquad \textbf{(III.1)}$$

If a core electron has been knocked out an electron from an outer shell will then drop to fill the core hole. The energy lost by the electron in dropping to the core state is removed in one of 2 ways....

i) Fluorescence. A photon of radiation is emitted with energy equal to the difference in energy between the core energy level and the energy level of the electron that drops into the hole.

ii) Auger process. An auger electron is emitted with kinetic energy dependent on the difference of these energy levels.

Auger electrons are independent of the initial photon energy. If x-rays are produced from a different anode the $h\upsilon$ value of the x-ray photon will be altered, in turn changing the kinetic energy of the emitted photoelectrons but having no effect on the energy of the auger electrons. Switching anodes, as previously mentioned, will allow the identification and separation of these auger electrons from the photoelectrons.

The emitted electrons' intensity is plotted as a function of binding energy with:-

$$E_B = h\nu - E_K - \phi \qquad \textbf{(III.2)}$$

Because the auger peak position will remain constant when the energy of the incident photon is changed it is easy to separate contributions to the spectrum from the auger relaxation from those due to photoelectron emissions.

The kinetic energy of the auger electron is simply the binding energy of the auger electron and the work function of the metal deducted from the difference between the initial and final energy states of the electron that drops to fill the core hole.

The x-rays can penetrate far into the bulk (10^3 to 10^4Å) to produce an auger or photoelectron far from the sample surface, however XPS takes advantage of the short mean free path length of electrons in the solid, i.e. the electrons cannot escape without inelastic collisions except from within a few nanometres of the surface (0.3 to 3nm depending on the kinetic energy of the electrons). By using a grazing angle for incident radiation and electron emission collection the surface selectivity of XPS can be enhanced.

The average distance that an electron can travel without being scattered inelastically is defined as the inelastic mean free path length, λ. Hence the relation between λ and the intensity of the photoelectric signal unaffected by an inelastic collision is defined as

$$I = I_0 e^{\left(\frac{-d}{\lambda \cos \varphi_e}\right)} \qquad \textbf{(III.3)}$$

Where,

I = the intensity at the surface

I_0 = the intensity of photoelectrons from distance, d, below the surface

φ_e = the angle of the emission relative to the surface normal

As φ_e increases, the photoelectrons received by the analyser become more likely to have been generated at the surface of the sample. The electron energy analyser collects electrons emitted from the sample and determines their kinetic energy.
Because the electrons occupy discrete energy levels, the resulting spectrum will show distinct and separate peaks corresponding to these levels. XPS relies upon the approximation that core ionisation energies are insensitive to the bonds between atoms, to produce XPS lines that are characteristic of the elements present. However, although the approximation does work well to allow the identification of the elements present, it is not entirely true. The charge redistribution of the valence electrons that does occur during bonding does induce small changes in the binding energies of the core electrons. Shifts in the spectrum due to bonding are small, of a magnitude of no more than a few electron volts. A slightly shifted XPS peak may, for example, be an indication of an oxide being present. A polycrystalline Uranium sample upon which extensive experiments had already been carried out using this UHV system [12] was used for some initial experiments in order to test the UHV system and to be able to calibrate various instruments within the system against values previously obtained. The XPS spectrum for this exhibits two peaks within a few electron volts of each other where only one should exist, clearly indicative of an oxide induced shift in the binding energy of the U $4f_{7/2}$ electron. The ratio of the area of these peaks is an excellent indication of the level of oxygen contamination of the surface (figure 3).

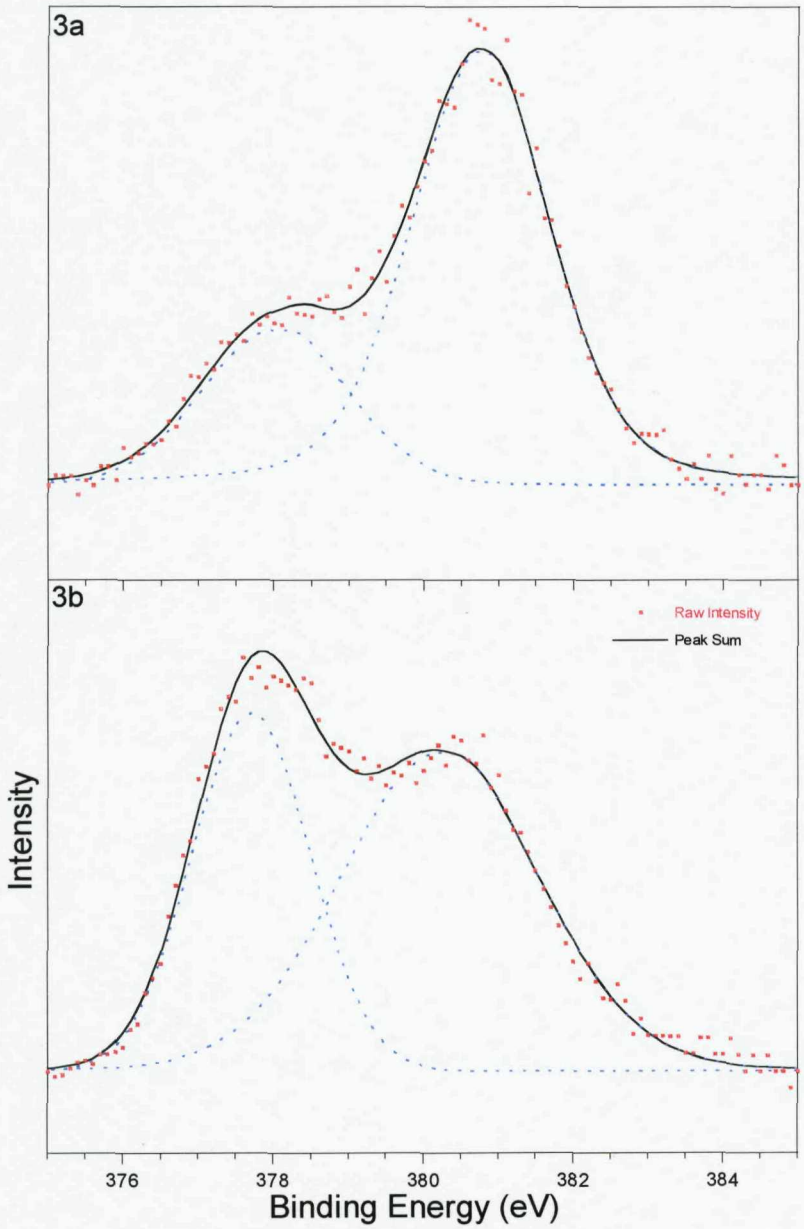

Figure 3: *Plot of the $U4f_{7/2}$ peak. Two peaks are clearly present and a curve fit has been used to identify them. The peak with higher binding energy relates to the photoemission from the uranium oxide and the peak of lower binding energy relates to photoemission from pure uranium. The plots are taken before (a) and after (b) a sputter and anneal cleaning cycle. There is a clear shift in the peak ratios, with the size of the uranium oxide peak reducing with respect to the size of the pure uranium peak, indicating that oxygen is being successfully removed from the surface.*

The widths of the peaks of the XPS spectrum depends on a variety of factors, the inherent width of the exciting radiation, the lifetime of the core hole being probed, and the resolution of the analyser [13]. Fluorescence occurring at depths below the surface

produces photoelectrons which undergo inelastic collisions before leaving the sample. These secondary electrons contribute to the XPS spectrum creating a large background to the photoelectron peaks.

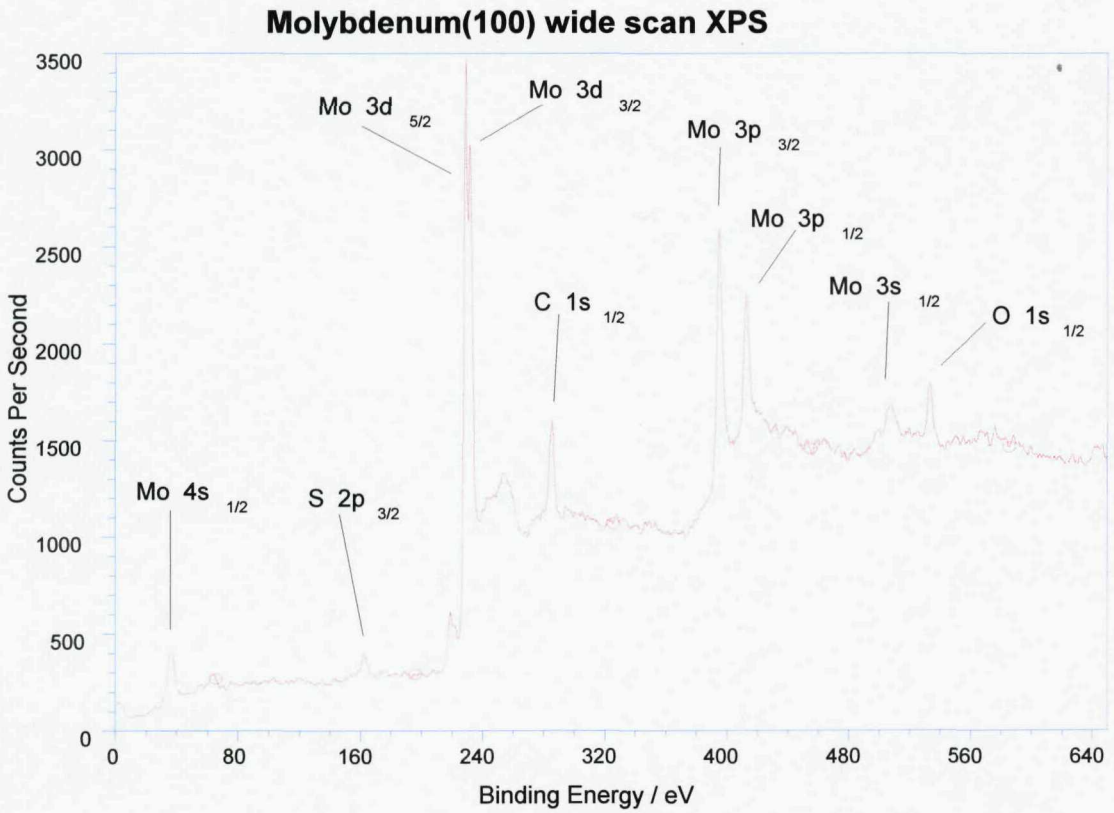

Figure 4: *A widescan plot of the molybdenum (100) sample before cleaning. As well as the peaks due to photoemission from various molybdenum orbitals, there are also clear peaks corresponding to photoemission from oxygen, carbon and sulphur.*

Although the Mo(100) single crystal that this thesis investigates does not exhibit any clearly identifiable oxide peaks in its XPS spectrum, comparison of the relative heights of the photoelectron peaks originating from emission of a core electron from a molybdenum atom and from a contaminant atom (in this case carbon, oxygen or sulphur) gives a good indication of how the cleaning of the surface is progressing.

The photoelectron peaks chosen for comparison are those with highest intensities so as to be most clearly separated from the background, these are the peaks originating from photoelectrons ejected from the Mo3d orbitals, and the $C1s_{1/2}$ and $O1s_{1/2}$ orbitals.

Sulphur was ignored since it was quickly removed from the surface by a simple anneal cycle, and did not return to the surface once removed.

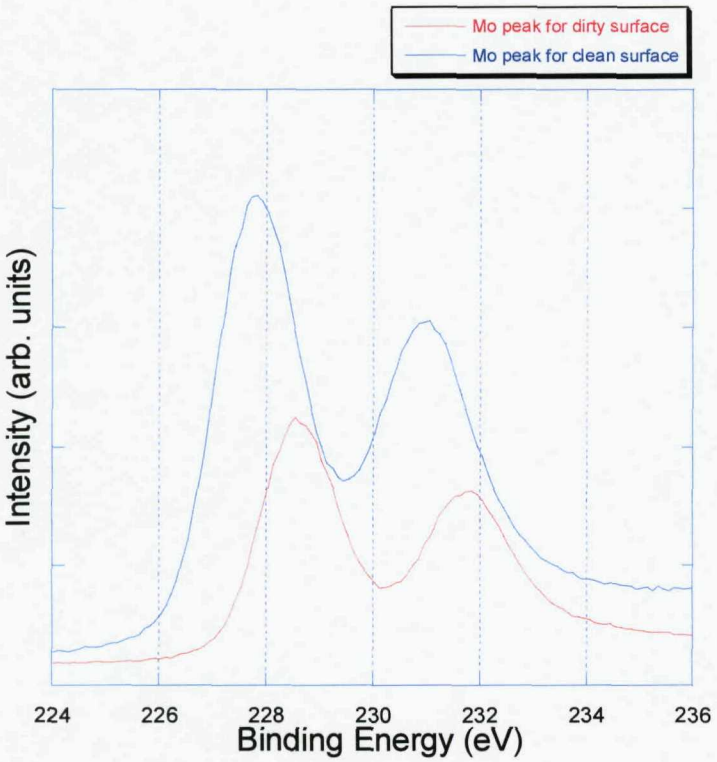

Figure 5: *These XPS peaks correspond to photoemission from the $Mo3d_{5/2}$ and $Mo3d_{3/2}$ orbitals. As the surface becomes clean the molybdenum peaks grow in intensity and shift to lower binding energies (blue line).*

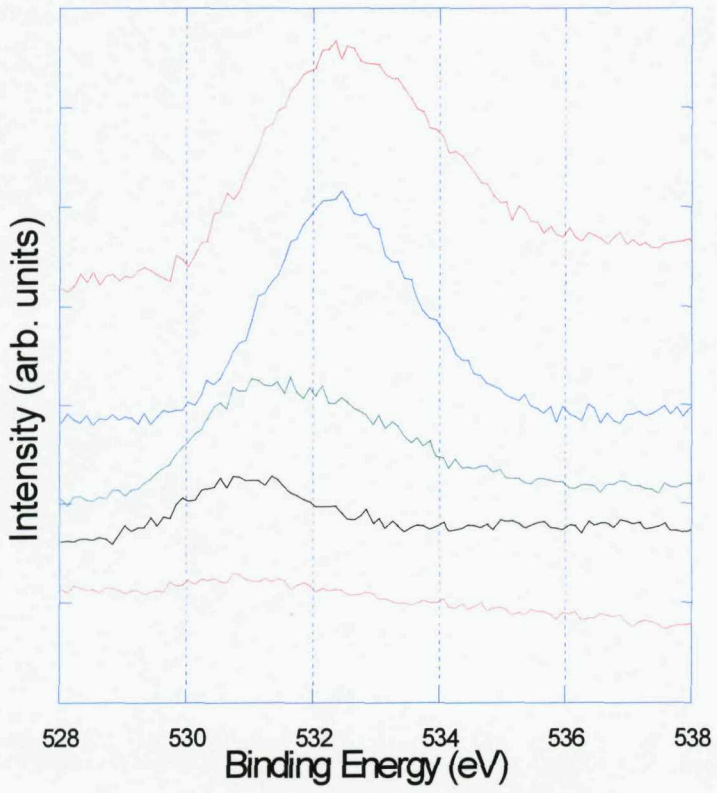

Figure 6: *This XPS peak corresponds to photoemission from the $O1s_{1/2}$ orbital. The various plots represent the level of oxygen contamination at the surface during the cleaning process. As the concentration of oxygen reduces there is a noticeable shift in the peak position to lower binding energy*

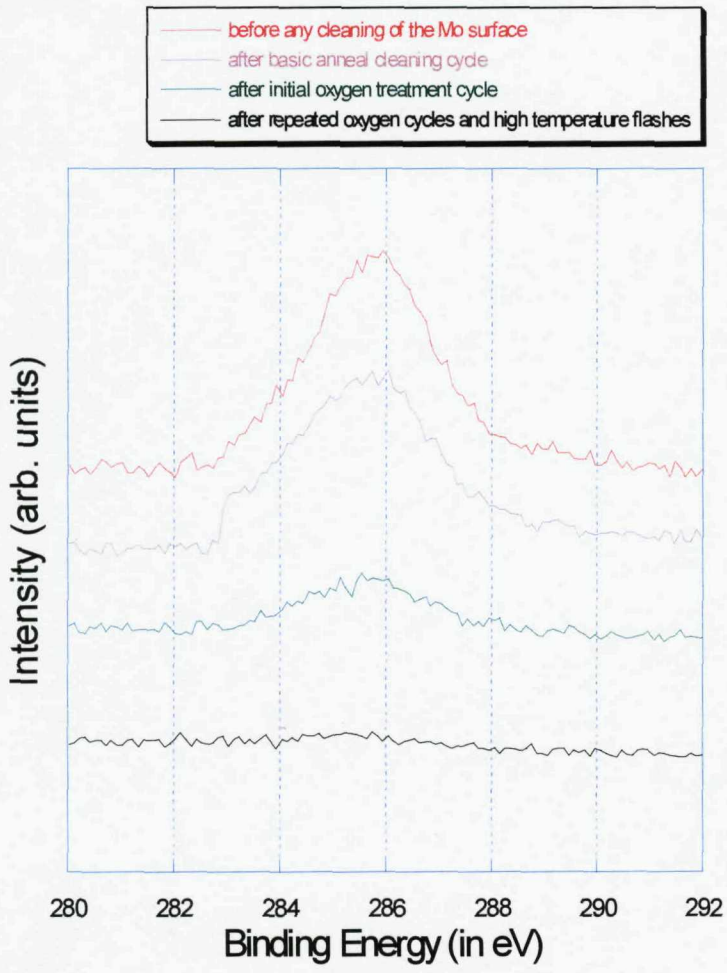

Figure 7: *This XPS peak corresponds to photoemission from the $C1s_{1/2}$ orbital. These plots demonstrate how the carbon contamination of the surface was reduced as the cleaning process progressed. The basic anneal cycle involved heating the crystal to approximately 1250 K for anything between 5 and 60 minutes, the oxygen treatments involved heating the sample to 1250 K in between 5×10^{-8} and 1×10^{-6} mbar of oxygen. Initially oxygen treatments were kept to between 20 minutes and 2 hours. The lowest peak was produced after much longer oxygen treatments (~6hours) followed by 1second flashes to approximately 2100 K in UHV.*

As oxygen was removed from the surface the Mo3d peaks were seen to increase in size in relation to the $O1s_{1/2}$ peak, and to shift to a lower binding energy. This shift is thought to be indicative of a molybdenum oxide being formed. The formation of a molybdenum oxide on a Mo(100) single crystal surface has been observed previously after exposure to oxygen at 700-900 K [6,14], and the $3d_{5/2}$ and $3d_{3/2}$ peaks observed here for the clean and dirty Mo(100) surface are in excellent agreement with those observed by Werfel and Minni for molybdenum metal and molybdenum oxide respectively [15]. They observe a $3d_{5/2}$ peak at 227.8 eV and a $3d_{3/2}$ peak at 231.0 eV for the molybdenum metal, and at 228.7 eV and 231.8 eV for MoO_2 on the Mo(100) single crystal surface, in excellent agreement with the $Mo3d_{5/2}$ and $Mo3d_{3/2}$ peaks observed for this sample at 227.80eV and 231.01eV (respectively) for the clean surface, and 228.60eV and 231.85eV (respectively) for the contaminated surface.

The shift in the molybdenum peak is explained as the presence of molybdenum oxide, the oxide provides the Mo3d electrons with less nuclear shielding as charge is transferred to the electronegative oxygen. The reduction in shielding of the attractive positive molybdenum nucleus acts to increase the binding energy of these electrons.

III.2.2 Low Energy Electron Diffraction (LEED)

This research used LEED only in a fairly limited fashion as a tool to check surface cleanliness and to make some observations of surface structure after nitrogen deposition. What follows is therefore only a brief discussion of the basics of the technique and its use in determining if a clean Mo(100) surface is present. A more extensive description and discussion of the technique can be found elsewhere [16].

LEED is used for determining the arrangement of atoms close to the surface. The LEED pattern portrays the 2D structure of the surface with diffuse patterns indicating either a poorly ordered surface or the presence of unordered impurities.

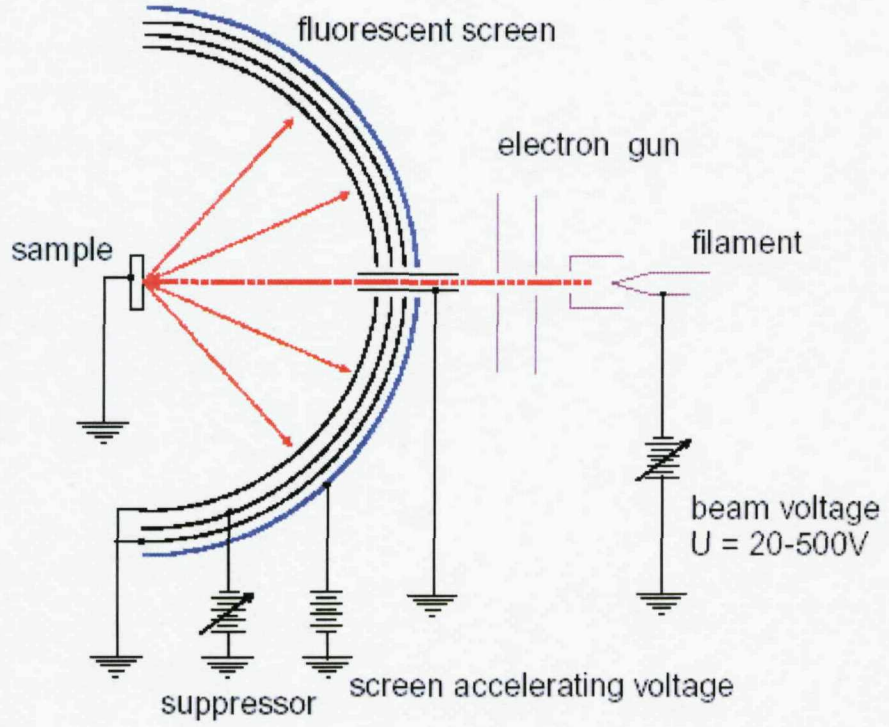

Figure 8: The typical LEED system:

Electrons are produced by passing a current through a thoriated tungsten filament. A current of 2.5 – 3A was sufficient to produce emission in the apparatus used for these experiments. A variable accelerating voltage propels a monoenergetic beam of electrons towards the sample. Electrons reflected from the sample surface will travel back towards the grids and screen. In order to reach the screen the electrons must first negotiate the series of grids. The first grid is set to earth so electrons travel though a field free region. The second grid is negatively bias to allow through electron with the primary beam energy while removing any inelastically scattered electrons. The 3rd grid is set at earth potential to reduce the effect of the field caused by the screen voltage on the second grid, and the screen is set to positive bias to attract the electrons making it through the array of grids.

LEED is a diffraction method using elastic scattering of beams of low energy electrons. The effect arises from the phenomena of wave particle duality. The diffraction features of the technique are due to the wave-like properties of the electrons. The behaviour can be explained using the de Broglie equation (equation III.4) relating the wavelength of a particle to its mass and velocity.

$$\lambda = \frac{h}{mv} = \frac{h}{p} \qquad \textbf{(III.4)}$$

Here h represents Planck's constant and p the electron's momentum.

The charge of the electron is known (e≈1.6×10c) and this allows the calculation of the effective wavelength of the electrons (λ) using the voltage through which the electrons are accelerated in the electron gun (ω).

$$E_K = \frac{1}{2}mv^2 = e\omega \qquad \textbf{(III.5)}$$

Where e is the charge of the electron and ω the accelerating voltage.

$$\lambda = \frac{h}{\sqrt{2me\omega}} \approx \left(\frac{150}{\omega}\right)^{\frac{1}{2}} \qquad \textbf{(III.6)}$$

The incident beam is scattered off the array of metal ion cores. The scattered beams can interfere constructively or destructively where the path difference between electrons scattered from adjacent atoms (with a spacing of d) is either nλ or nλ/2 respectively.
This is Bragg scattering therefore the Bragg equation can be applied:-

$$n\lambda = d\sin\varphi \qquad \textbf{(III.7)}$$

where n=0,1,2,3 etc for constructive interference.

The following equation is the modified expression for when the beam isn't perpendicular to the surface with α accounting for the incident angle of the beam:-

$$n\lambda = d(\sin\varphi - \sin\alpha) \qquad \textbf{(III.8)}$$

The electrons diffracted by the surface that undergo constructive interference are detected by the fluorescence they cause on the phosphor screen.

To get reasonable diffraction the λ of the electron, as controlled by the voltage V, must be less, but of approximately the same order of magnitude, as the spacing of the ion cores. Electrons with energies in the range of 20-500eV satisfy this condition and are of sufficiently low energy so as to be surface sensitive (do not penetrate too far into the metal).

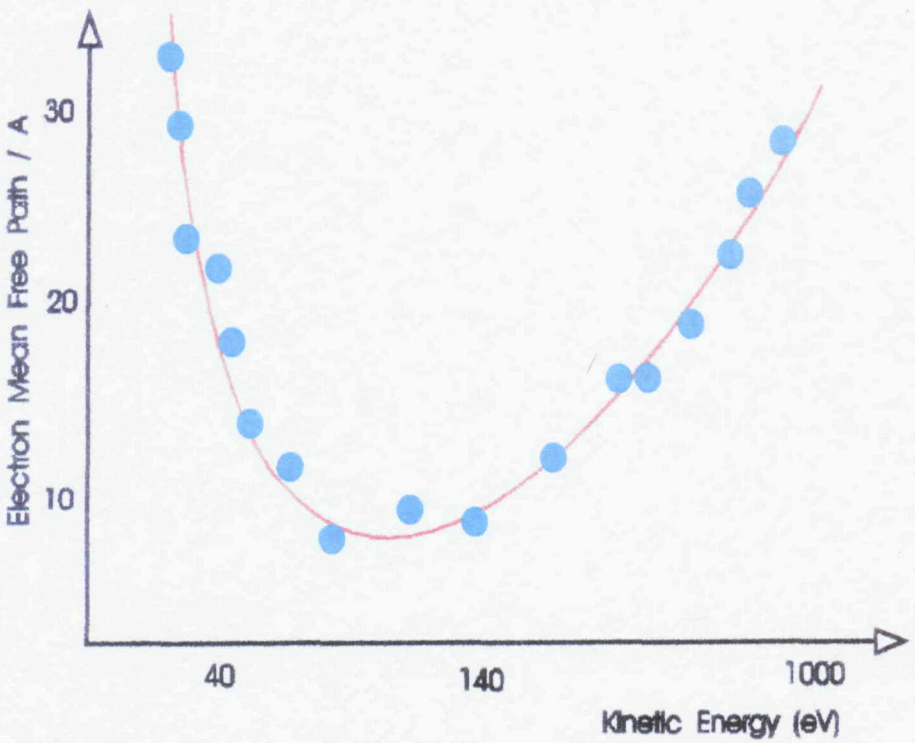

Figure 9: *It can be seen from the above plot that electrons in the energy region* $40<E_{KE}(eV)<500$ *are particularly surface specific [17].*

An inverse image of the atomic arrangement on the surface will be produced on the phosphor screen due to the relationship between the angle of diffraction and the atomic spacing, i.e. $\sin\varphi \propto \frac{1}{d}$.

Changes in the diffraction pattern are labelled according to the Wood notation [18] relative to the unreconstructed unit cell with lattice vectors h,k. This is defined as the p(1×1) structure, where p decribes the 'primitive' unit cell. As an example consider an overlayer or surface reconstruction of dimensions h,2k. Using the Wood notation this

would be described as a p(1×2) structure and would show LEED spots, corresponding to electron diffraction peaks, at ½ order positions along the k vectors.

The commonly observed structures on the clean Mo(100) surface are a p(1×1) structure that reconstructs (reversibly) to what at first appeared to be a form of c(2×2) structure at T<220 K [19]. The c notation indicates that the cell is not a 'primitive' cell, but contains an additional 'centred' lattice point within the cell. This cell structure may alternatively be described as a $p\left(\sqrt{2}\times\sqrt{2}\right)R45°$, where the lattice vectors are $\sqrt{2}$ times h,k and the entire structure is rotated by $45°$ since this cell is exactly equivalent to the c(2×2).

In fact this low temperature Mo(100) reconstruction is slightly more complex and was at first thought to have an incommensurate structure which appeared to manifest itself in the form of a quartet of extra spots around the (½,½) positions as seen in figure 10. The full label for this structure was determined to be $c\left(7\sqrt{2}\times\sqrt{2}\right)R45°$ [20]. The diffraction pattern this describes is thought to be caused by the presence of two domains rotated $90°$ with respect to each other [8].

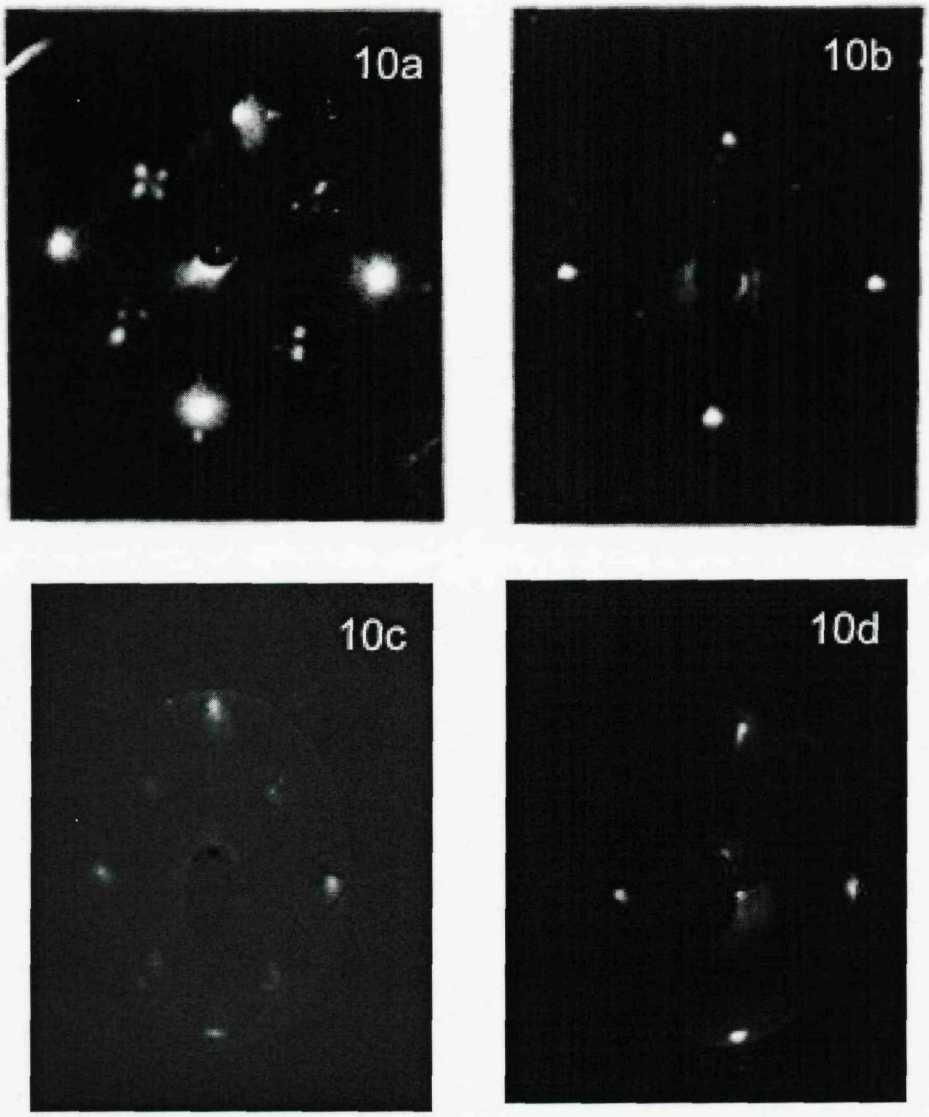

Figure10: a) *LEED pattern from the clean Mo(100) surface of Felter et. al. at 160K and a beam voltage at 42eV.* ***b)*** *LEED pattern from the same crystal and beam voltage at >293K. Both (a) and (b) are taken from [19].* ***c)*** *LEED pattern from the clean Mo(100) used in this thesis at ~125K. Beam voltage 38.5eV. The pattern shows spots in the normal (1,1) positions, and faint spots in the (½,½) positions.* ***d)*** *The same crystal at ~ 293K. Beam voltage 45.1eV. The pattern shows clear spots in the (1,1) positions*

The LEED photograph shown in figure.10c was taken directly after a high temperature flash. The spots were at first brighter and more visible but already began to fade in the minutes it took to activate the LEED assembly and align the camera. A LEED photograph taken 10 minutes after the flash showed the ½ order spots still to be present although very faint, but after 20 minutes a further photograph revealed that the ½ order spots had completely disappeared leaving only the (1×1) pattern (see figure 10d). I have struggled to observe the quartet of spots previously reported [8,19,21], although I

have at times observed a faint indication of a quartet of small spots in the ½ order positions. Generally I can at best only identify faint large blurred spots in these positions. Possibly this is because it often proved difficult to obtain surface temperatures much below 160 K. Felter reports the ½ order spots undergo a large increase in intensity only at <150 K (see figure 11) and become larger, more diffuse and streaky as temperature increases [22]. This temperature dependency combined with the rapid quenching of the reconstruction with the presence of even very small amounts of surface contaminants may account for the difficulties experienced in observing the clean surface reconstruction.

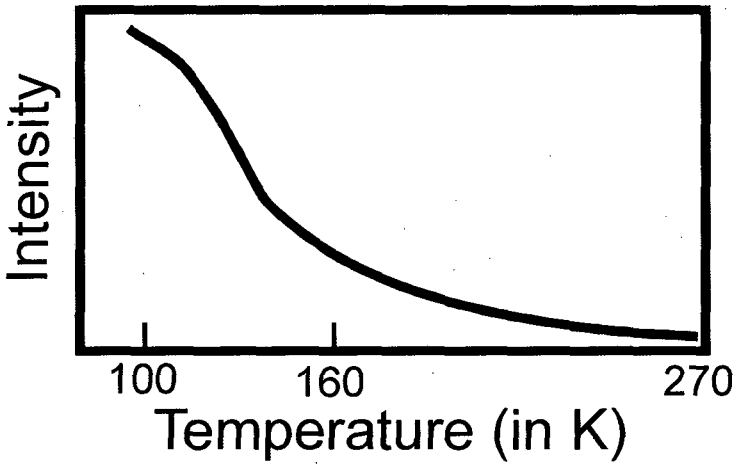

Figure 11: *Plot of intensity of the extra spots observed in the (½,½) for the clean Mo(100) surface as observed by Felter. Figure taken from [22].*

III.2.3 Temperature Programmed Desorption (TPD)

When an adsorbate covered surface is heated the adsorbed species may desorb. This occurs because the surface residence time of an adsorbed species (τ) will depend (exponentially) on temperature.

$$\frac{-d\theta}{dt} = \theta^x e^{\frac{-E_d}{RT}} \qquad \textbf{(III.9)}$$

Where θ is the surface concentration, E_d the barrier to desorption experienced by the deosrbing surface species and x = 1, 2 for a 1st or 2nd order desorption process, respectively. The main difference between 1st and 2nd order processes is the sensitivity of the 2nd order process to surface coverage. This displays itself as a shift in T_{max} (the temperature at which the pressure of desorbing gas is at it greatest) to lower temperature with higher coverage.

TPD is used to probe the strength of the adsorbate–surface bonds. By careful analysis it is possible to use the TPD technique to determine the state of the adsorbate (whether physisorbed, molecularly chemisorbed, or dissociatively chemisorbed), the bonding site on the surface and corresponding information about the surface structure, as well as giving indications of how these factors vary as the surface coverage and temperature changes.

A TPD is carried out by heating the surface relatively slowly so as to ensure that the desorption rate is much smaller than the pumping speed. Provided this condition is met, the pressure in the chamber is proportional to the desorption rate. If the pumping speed is too low or the heating rate too high there will be a loss of clarity with the peaks becoming less sharp.

Ideally a TPD will be carried out using a linear temperature ramp. Because the heating was controlled manually (rather than computer controlled), and the sample was heated via an electron bombardment technique (which can tend to give sharp increases in sample temperature if not very carefully controlled), a perfectly constant heating rate and linear temperature rise was not possible. However care has been taken to ensure the temperature rise was kept as close to linear as possible.

Figure 12 is an example of a TPD monitoring the desorption of nitrogen from the Mo(100) surface. The TPD is taken after nitrogen was dosed onto the clean molybdenum surface. This TPD appears to exhibit 3 clear peaks labelled γ, β_1 and β_2. This indicates two atomic chemisorption (β) peaks as well as one low temperature peak, assigned here as a molecular physisorption peak (γ). Identifying a γ peak can be difficult, a peak at low sample temperature may be due to physisorbed or molecularly chemisorbed species desorbing from the crystal surface, but it may also be due to

desorption from the spiral heating filament taking place when current is initially passed through it to begin the heating process.

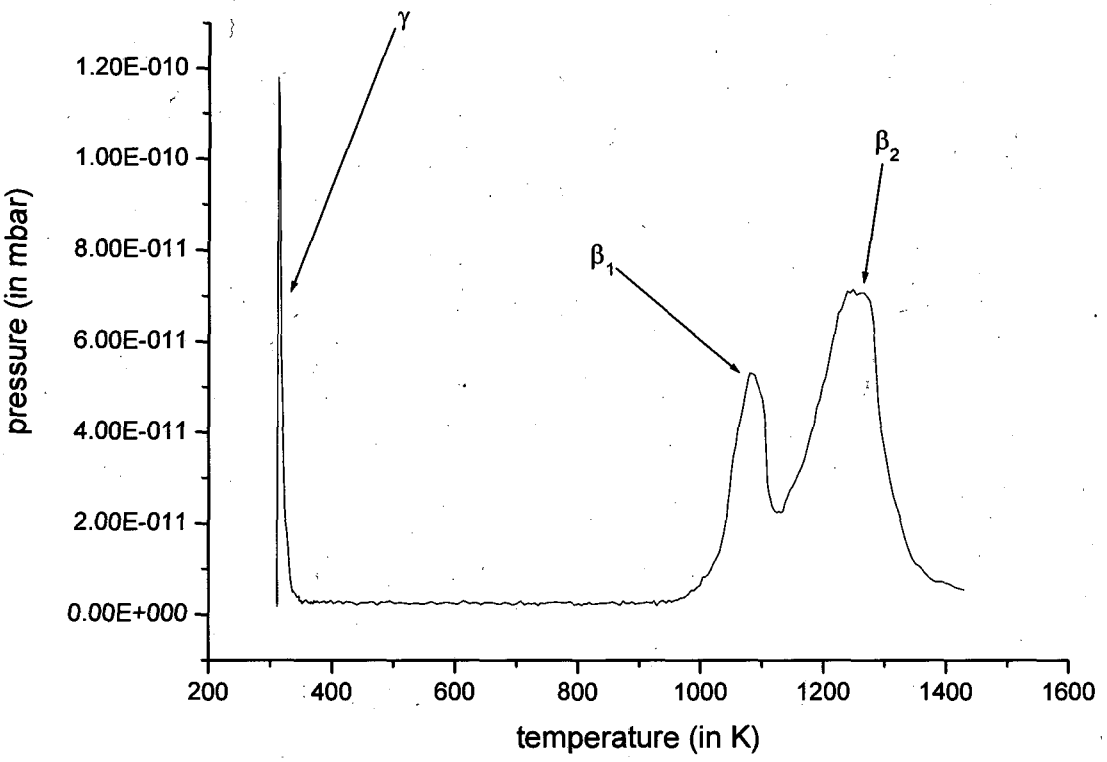

Figure 12: *Temperature Programmed Desorption (TPD) showing nitrogen desorbing from a cleaned Mo(100) surface that had exposed to 5×10^{-8} mbar of nitrogen for 180 seconds.*

III.2.4 King and Wells Experiments

The method of King and Wells allows the measurement of the sticking probability as a continuous function of time [24]. The experiments which have been performed concentrate on using the King and Wells (K&W) technique to measure the initial sticking probability as a function of surface temperature and beam energy, as well as providing a record of sticking probability as a function of coverage for each K&W experiment carried out.

The King and Wells technique works as follows: The crystal surface is cleaned or a well characterised adsorbate covered surface produced. The desired gas mixture is set

using the flow controllers, seeding the gas (in conjunction with varying the temperature of the nozzle) allows the energy of the reactant gas in the beam to be controlled, and a supersonic molecular beam is produced as described in section II.2. The aperture is opened and the nozzle positioned in line with the aperture. The beam is now directed at the mica flag within the main chamber which is positioned in front of the aperture. The mica flag has a very low adsorption cross-section. Its purpose is to stop the molecular beam reaching the sample directly, without adsorbing the gas molecules. The flag is then moved to allow the beam to be incident upon the sample surface. The opening of the flag contributes to the sticking of the molecules to the sample surface. Finally the changes of pressures in the main chamber produced during this process are monitored by the fixed quadrupole mass spectrometer and using this measurement the sticking probability is calculated.

The K&W technique is relatively simple in operation and gives a high degree of accuracy. It possesses 4 major advantages [24] applicable to the experiments performed.

a) Only the centre section of the target is sampled, avoiding crystal edge effects.
b) The technique is more accurate for fast adsorption processes than the uptake flash filament technique.
c) The randomized gas density component of the adsorbing gas in the crystal chamber remains low and the experiment runs for only short lengths of time (typically <60 seconds), reducing the amount of contaminants produced at the chamber walls by the impinging gas.
d) The technique can be used to examine the adsorption and desorption kinetics.

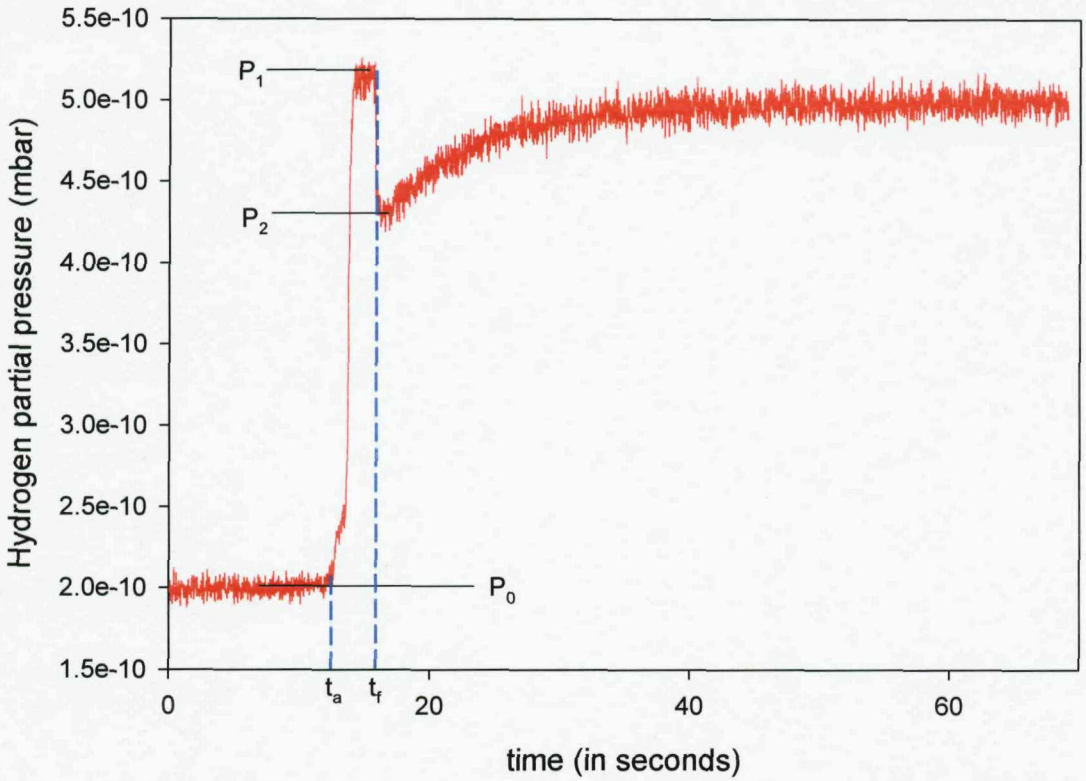

Figure 13: *This shows the pressure changes that typically take place during a K&W type experiment. The initial pressure recorded, P_0, is the background pressure of the main chamber, the pressure before the aperture is opened and the beam aligned. Upon opening the aperture there may be a small rise in pressure due to the pressure differential between the 2nd and main chambers. Upon aligning the beam (at t_a) the pressure in the main chamber rises rapidly, reaching equilibrium at P_1. Removing the flag and allowing the beam to be incident on the crystal surface (at t_f) causes a drop in pressure to P_2. This drop is due to the reactant gas molecules adsorbing onto the crystal surface. Typically this pressure might then be expected to rise back to ~P_1 as the crystal surface becomes saturated, with adsorbates and reactant molecules in the beam no longer find adsorption sites and being instead reflected back into the main chamber, thereby contributing to the main chamber pressure.*

The initial sticking probability is calculated as being the pressure drop due to gas adsorbed by the crystal surface, P_1-P_2, divided by the total pressure of gas from the supersonic molecular beam incident upon the crystal surface, $(P_1-P_0)\times(1-F_d)$. The term $1-F_d$ is included to account for the fact that not all of the pressure increase observed is due to gas molecules which will directly strike the crystal surface when the beam is aligned and the flag opened.

The two further elements that may contribute to the rise in main chamber pressure (P_1-P_0) are as follows:

a) When the beam is not aligned it should not affect the main chamber pressure. However, upon opening the aperture between the main and second chambers (before the beam is brought into alignment), a slight rise is observed in the pressure of the reactant gas measured in the main chamber. The pressure differential between the 1st and 2nd, and 2nd and main chambers, once the flow is initiated, results in a small amount of gas from the beam finding its way into the main chamber.

b) There is a noticeable effusive component of the beam which, although narrowed by the skimmer and consecutively by the aperture, will still contribute to the beam entering the main chamber, providing an element of the beam which is not directly incident upon the small crystal target.

These two components are described by the term F_d, the fraction of the beam not directly incident upon the crystal surface.

F_d was estimated by comparison of sticking probability measurements of nitrogen on W(100) at 300K obtained with this system [25], and those of Rettner et al. [26]. The value obtained for F_d for this system was 0.21.

The initial sticking probability is written as:-

$$S_0 = \frac{(P_1 - P_2)}{(P_1 - P_0)(1 - F_d)} \qquad \textbf{(III.10)}$$

Substituting in the value for F_d:-

$$S_0 = \frac{(P_1 - P_2)}{(P_1 - P_0)0.79} \qquad \textbf{(III.11)}$$

This calculation can be made from each K&W experiment to observe how the initial sticking probability varies as variables such as the surface temperature and the incident energy of the reactant molecules are varied. Furthermore, the sticking probability varies with surface coverage. Hence at a time, t, the sticking probability becomes:-

$$S_0 = \frac{(P_1 - P_t)}{(P_1 - P_0)0.79} \qquad \textbf{(III.12)}$$

For a particular time the coverage of the surface may also be calculated since the coverage, θ, is proportional to the area under the uptake curve.

$$\frac{\theta}{\theta_{sat}} = \frac{\int_{t1}^{t}(P_1 - P_t)dt}{\int_{t1}^{\infty}(P_1 - P_t)dt} \qquad \textbf{(III.13)}$$

Dividing the area enclosed between the curve and P_1 at a given point in time, by the total area encompassed by the complete curve, gives the fraction of available adsorption sites that are filled.

III.3 Aligning The Crystal and Beam

As has previously been mentioned the molybdenum sample is mounted on a manipulator which allows the crystal to be moved in x, y, z and θ. Rotating the crystal to face the beam was a simple matter, however aligning the crystal in the y (horizontal) and z (vertical) was found to be more complicated.

Initially the crystal was aligned using a laser. The laser was directed at the beam aperture from a window positioned directly opposite on the UHV rig, using a spirit level to check the laser was horizontal. The crystal was then moved into a position where the centre of the crystal was aligned with the laser.

However, using this method in order to align the crystal was found to be unreliable. Two possible reasons for this lack of accuracy are:

i) The difficulty of supporting the laser so as to maintain its exact orientation and position between alignment with the aperture and alignment with the crystal

ii) The relatively large distance between the window and the beam aperture, which results in any small errors in the angle of orientation of the crystal creating relatively large errors in y and z alignment.

Another method of alignment is to take repeated K&W sticking measurements (each taken after cleaning the molybdenum surface), keeping the energy of the reactant molecules in the beam (E_i) and the surface temperature of the molybdenum single crystal (T_s) constant, but moving the crystal gradually along the axis perpendicular to the direction of the beam.

This should produce a set of data where sticking is observed when the beam is incident on the sample surface and disappears as the crystal moves out of alignment with the beam. When beam and crystal are a small distance out of alignment the beam will be incident on the copper support. This support remains cool when the crystal is heated and therefore should provide a 'dirty', adsorbate covered, surface upon which no, or very little, sticking should occur.

Figure 14 illustrates how the sticking did in fact vary as the crystal position in y and z was varied. There are some interesting features demonstrated by this data. Firstly that the initial sticking probability at no point approaches a value close to zero despite the readings being taken over a range considerably greater than the length of the single crystal sample. This shows that the beam exhibits a significant initial sticking probability when incident upon the copper support.

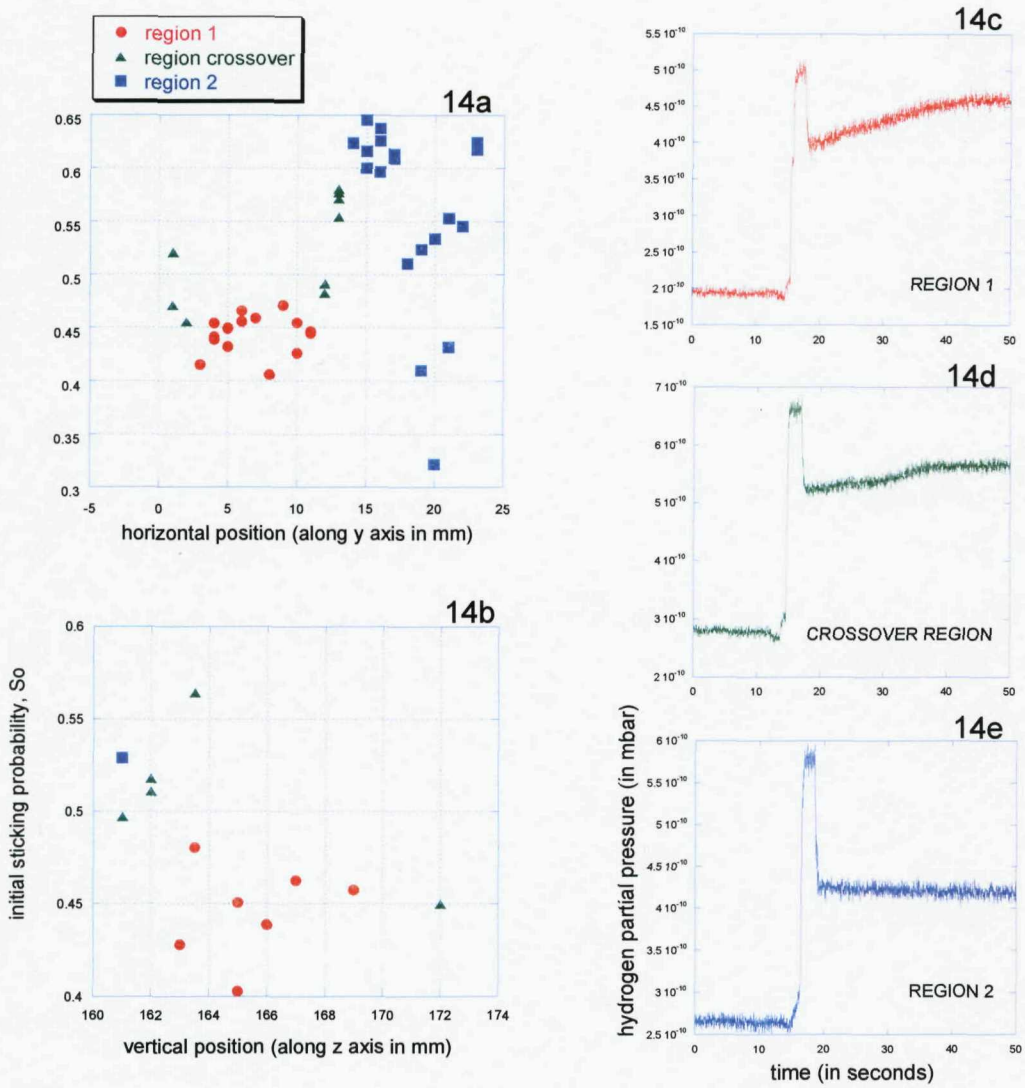

Figure 14: *(a) and (b) are plots of initial sticking probability as a function of crystal position. S_0 is determined using the K&W method. (c), (d) and (e) show the type of K&W plot being produced by data points labelled as region 1, crossover region (where elements of both types of plot are present), and region 2 (respectively).*

Another interesting feature is the changing shape of the K&W plot produced at different y and z positions. Two specific regions are apparent, each exhibiting specific plot shape. These differences are illustrated in figure.14(c, d and e).

Within region 1 the K&W sticking behaves in the manner commonly observed for sticking on a single crystal surface, with a sharp drop in pressure as the flag is opened followed by a gradual increase in pressure as the surface becomes saturated. However

in the other region the surface upon which the beam is incident appears not to saturate. After the initial drop in pressure when the flag is opened there is no gradual increase in pressure, the pressure, and therefore the sticking probability, remains constant.

Region 1 represents the case of the beam being incident upon the crystal surface. The explanation offered to account for the behaviour within region 2 is that sticking is taking place on a molybdenum film which coats the copper mount and support bars, this film being evaporated from the crystal during high temperature flashes (as observed in section III.3)

This can be accounted for by noting the gas pressure associated with heating the molybdenum sample to the 2073K, as required for the removal of contaminants from the sample surface (see appendix D). If each flash deposits a fresh layer of molybdenum on the support structure surrounding the crystal it provides a new surface, free of contaminants, upon which sticking may occur. The copper support and stainless steel support bars are not cut or polished and therefore provide a very rough surface with a much greater number of adsorption sites for a given area than that provided by the Mo(100) single crystal surface. This difference in adsorption sites available per unit area might result in K&W type plots where the surface appears not to show any signs of saturation during the period over which the K&W is taken.

By keeping the crystal in line with the beam but rotating it to face away from the beam aperture, it is possible to expose a part of the copper support that will have been shielded from metallisation. Doing this was seen to produce a K&W plot where no sticking is evident (i.e. there is no drop in pressure upon opening the flag) as would be expected for a beam incident upon such an adsorbate covered surface.

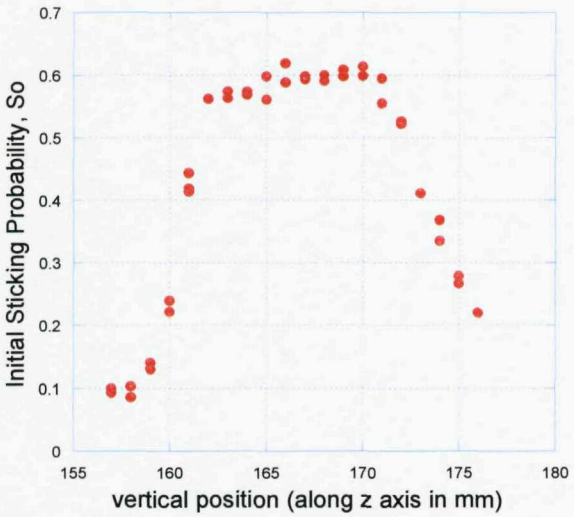

Figure 15: *Plot of S_0 as a function of vertical position. The beam is moved just out of alignment with the crystal along the horizontal axis. S_0 is determined using the K&W method and all data points exhibited region 2 type behaviour.*

With the crystal moved just out of alignment (into region 2) in the y axis the crystal position is moved along the z axis and a K&W plot of sticking taken after each millimetre of movement. S_0 is high while the beam is incident at points adjacent to the length of the crystal ($S_0 = 0.59 \pm 0.03$) and falls off rapidly when moved further away from the region parallel with the crystal. This corresponds well with the proposal that the sticking takes place on the molybdenum coating evaporated from the crystal since the colour change in the copper support surface along with common sense suggests that this metallisation is concentrated on areas that are in close proximity to the crystal.

III.4 References

[1] Lecante J., Riwan R., Guillot C., Surf. Sci., 35(1973)271

[2] Kenneth H. M., Lee A. E., Surf. Sci., 48(1975)591, 606

[3] Tabor D., Wilson J. M., J. Crystal Growth, 9(1971)60

[4] Bauer E., Poppa H., Surf. Sci., 88(1979)31

[5] Musket R.G., McLean W., Colmenares C.A., Makowiecki D.M., Siekhams W.J., Applications of Surf. Sci. 10(1982)143

[6] Zhang C., Van Hove M.A., Somorjai G.A., Surf. Sci., 149(1985)326

[7] Ko E. I., Madix R. J., Surf. Sci., 109(1981)221

[8] Prybyla J. A., Estrup P. J., Chabal Y. J., J. Chem. Phys. 94(1991)6274

[9] Zaera F., Kollin E. B., Gland J. L., Surf. Sci., 166(1986)L149

[10] King D. A., Wells M. G., Surf. Sci., 29(1972)454

[11] Siegbahn K., Nordberg R., Nording C.N., Fahlman A., Harmin K., Hedman J., "ESCA Molecular And Solid State Structure Studied By Means Of Electron Spectroscopy", Aimqvist and Wiksells, Uppsala, 1967

[12] Mormiche C., PhD. Thesis, University of Southampton, 2002

[13] Ebert H. D., PhD. Thesis, University of Southampton

[14] Smudde g., Stair P., Surf. Sci., 317(1994)65) (Zhang C., Van Hove M., Somorjai G., Surf. Sci., 149(1985)326

[15] Werfel F., Minni E., J. Phys. C, Solid State Phys., 16(1983)6091

[16] Ed. Woodruff D. P., Delchar T. A., 'Modern Techniques of Surface Science', Cambridge Univ. Press., (1986)

[17] McCash M. E., "Surface Chemistry", Oxford Uni. Press, (2001) chap.2, p.29

[18] Wood E., J. Appl. Phys., 35(1964)1306)

[19] Felter J.E., Barker R.A., Estrup P.J., Phys. Rev. Lett. 38(1977)1138

[20] Hildner M. L., Daley R. S., Felter T. E., Estrup P. J., J. Vac. Sci. Technol., A9(1991)1604

[21] Daley et al., Phys. Rev. Lett., 70(1993)1295

[22] Felter T. E., J. Vac. Sci. Technol., A2(1984)1008

[23] Somorjai G. A., "Introduction to surface chemistry and catalysis", Wiley-Interscience Publication, 1994, p.347

[24] Jones J. D., PhD. Thesis, University of Southampton, 1994

[25] Butler D. A., PhD. Thesis, University of Southampton, 1994

[26] Rettner C. T., DeLouise L. A., Auerbach D. J., J. Chem. Phys. 85(1986)1131

Chapter IV: Hydrogen adsorption on Mo(100)

IV.1 Introduction

The H/Mo(100) system has been the subject of many previous studies. These studies have investigated the structure and kinetics of the adsorption system, and therefore there exists a relative abundance of information describing the adsorption site, coverage/temperature dependent surface structures and adsorption/desorption kinetics. However, as yet no experimental studies have been published describing the dynamics of the system. This chapter examines the adsorption dynamics, investigating how the energy of an incoming H_2 molecule affects its behaviour as it approaches the surface, as well as how the hydrogen coverage and surface temperature influence the interaction of the surface with the incoming molecule.

IV.2 Literature Review

IV.2.1 Chemisorption of Hydrogen on the Mo(100) Surface

A TPD of the saturated H/Mo(100) surface tends to exhibit 3 β desorption peaks [1-3]. However these peaks are not thought to relate to a variety of adsorption sites. Surface infrared spectroscopy (SIRS) and electron energy loss spectroscopy (EELS) data indicate only one binding site, and indicate this site to be the bridge. EELS data taken from the H/Mo(100) system has been observed to exhibit 2 parallel vibrational modes [4]. Were the adsorption site to be the on top or the four-fold hollow the parallel modes would be degenerate, this therefore provides further indication that the bridge is indeed the site at which hydrogen adsorbs. Furthermore, the symmetric stretch mode of H on various transition metals has been observed to be within the range of 525-750cm^{-1} when adsorbing on the four-fold hollow sites, and >1300cm^{-1} when on top [5], whereas on Mo(100) it has been observed to vary between 1016cm^{-1} and 1270cm^{-1} (depending on hydrogen coverage, θ_H) [4], indicating the H is bridge bonded at any given coverage.

The picture of bridge bonded hydrogen agrees well with the 2 H per substrate atom commonly observed at saturation coverage [2,3,4,6,7,8], i.e. a saturation coverage of 2ML of hydrogen, and with the degree of blocking observed in a sulphur co-adsorption study [2]. In the study sulphur dosed onto Mo(100) adsorbed in the four-fold hollows and blocked hydrogen adsorption in the local vicinity. Hydrogen adsorption was observed for $\theta_S \leq 0.5$ML with adsorption completely blocked above this coverage. This characteristic is only reasonably explained within the bridge bonding adsorption picture. Were the hydrogen to bond at the four-fold hollows adsorption should still take place right up to a sulphur coverage of 1.0ML, whereas all on top sites should already be blocked at $\theta_S = 0.25$ML.

The LEED picture of the H/Mo(100) system is a complicated one (see figure 1) displaying a huge variety of LEED patterns with varying surface temperature (T_S) and coverage (θ). Hydrogen provides only a very weak scatter of electrons and the observed LEED patterns are identified as varying substrate reconstructions [9], the substrate reconstructing with changing hydrogen coverage and surface temperature. These surface structure phase transitions are generally first order (each phase bordered by regions of two structurally distinct coexisting phases), with islands of pure phase bordered by independent areas of co-existing phases.

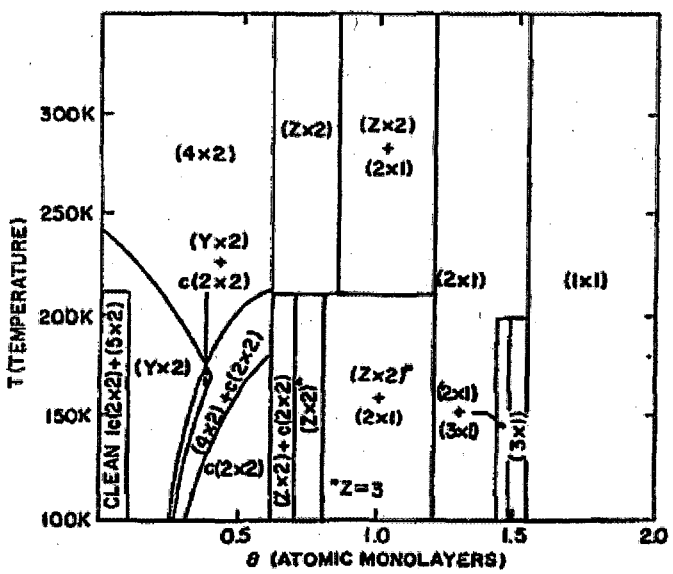

Figure 1: Phase diagram of the H/Mo(100) surface. The value of Y varies continuously from 4 to 5. Z varies from 2.75 to 3 at low temperatures and between 3 and 4 in the higher temperature region. Taken from [4].

IV.2.2 Mo(100) and W(100) Comparison

The many similarities between tungsten and molybdenum make an examination of these two hydrogen adsorption (100) systems of considerable interest. This is particularly so since, despite the lack of data relating to the dynamics of the H/Mo(100) system studied here, the dynamics of the H/W(100) system has been studied extensively [10-14].

Molybdenum is very similar to tungsten in many ways. Both exhibit bcc structure, with an almost identical lattice spacing (3.16Å for W and 3.15Å for Mo) and a similar electronic structure dominated by unfilled d-orbitals ($[Xe]4f^{14}5d^{4}6s^{2}$ for W and $[Kr]4d^{5}5s^{1}$ for Mo). Both Mo(100) and W(100) also exhibit a low temperature surface reconstruction developing over a similar temperature range.

In terms of hydrogen adsorption bonding takes places purely onto the bridge site on both surfaces, the presence of H causing the bridge site to reconstruct and producing a saturation coverage of 2ML on each surface. A number of papers have already made comparisons of the kinetics and structures of these two adsorption systems [1,6,7,15], and despite the many similarities identified, there are also noted to be some important differences, these manifesting themselves in the manner in which the hydrogen induced surface reconstructions progress. Whereas on Mo(100) the adsorption of H generally induces island structures with first order phase transitions [4,6,7,9], the W(100) surface behaves very differently, with the surface undergoing a gradual uniform second order phase transition (i.e. a single homogeneous structure made up of two superimposed distortion waves) as a c(2×2) structure is formed at ~0.3ML, thereafter gradually relaxing back to the unreconstructed surface structure as saturation coverage is approached [16]. As was the case for the H/Mo(100) system (described in chapter IV.2.1), the path taken by the surface reconstructions of the H/W(100) system was also traced using a combination of LEED and IR techniques [6,7,16]. The IR data for H/W(100) was seen to exhibit a gradual shift in the IR peak frequencies as the coverage increased. This differs from what was observed for the H/Mo(100) system, where the peaks that appeared in general remained at a relatively fixed frequency, with

new peaks appearing in tandem with the old and gradually coming to prominence as is characteristic of a 1st order phase transition.

The difference in the behaviour of the two systems has been attributed to differences in the adsorbate-adsorbate (A-A) interactions occurring on the two surfaces. At low coverage H-H interactions appear to be dominated by purely long range interactions on W(100), while on the Mo(100) there appears to be an additional attractive component leading to the island formation observed (although a repulsive element is still in evidence, with the islands still showing only a very small local density). The small dipole moment and atomic radius associated with adsorbed H render the direct A-A interactions (such as dipole-dipole, Van der Waals, and orbital overlap) negligible. The interactions are instead thought to be indirect, mediated by substrate phonons [6]. This is supported by the appearance of the strong adsorbate-substrate interactions manifested in the large adatom induced substrate reconstructions. In essence the differences are put down to differences in the coupling between substrate distortions induced by individual adatoms, with a stronger coupling in W allowing H to induce a distortion throughout the surface even when very few adatoms are present, whereas in Mo the distortion of the substrate is limited to the proximity of the adatom [7].

Having compared the kinetic features of the two systems and noted the many similarities, it is important to make some comment on the features of the dynamics of the H_2/W(100) adsorption system, the expectation being that it may hold many features in common with that of the equivalent molybdenum system. The behaviour of the initial sticking probability, S_0, as a function of incident energy is non-monotonous. A large and possibly non-activated direct channel has been identified, this channel being accompanied by a low energy channel stretching well beyond those energies predicted for a classical, fully accommodated, precursor channel to dissociation [11,12]. The low energy channel has been attributed to a dynamic adsorption mechanism this being sometimes identified as dynamic steering and other times as a dynamic precursor, both of which are described below.

IV.2.3 Dissociation Dynamics:- Dynamic Steering

During the 90's improvements in computing power made it possible to combine high dimensional quantum dynamical calculations of the dissociative adsorption of molecular beams with reliable ab initio PES calculations (calculated within the DFT slab model). During recent years these advancements have been put to use in the performance of quantum as well as classical simulations of the adsorption dynamics of hydrogen as it approaches a wide range of model potentials [17 and references therein,18]. The H_2/W(100) system has been amongst those to be considered. What was revealed was a PES with no barrier to dissociation over much of the surface [19]. This led to it being postulated that dissociation proceeded via a purely direct dissociation event with the low energy channel being explained as an enhancement of molecular steering into the favoured un-activated dissociation potential energy wells.

The concept of steering is that incident molecules are very strongly steered into particularly favourable dissociation geometries on particular surface sites. At low translational energies it is believed that the forces experienced by the molecule as it approaches the surface are strong enough to allow the slow moving adsorbate to re-orientate and translate across the surface (particularly in the case of molecules of low mass such as H_2) in order to find the optimum dissociation position, and that as this steering becomes less effective with increasing E_i the dissociation probability decreases. In essence, according to the steering theory, S_0 will initially fall with increasing energy because the steering forces have less time to operate as the energy and consequently the velocity of the molecule increase, making these forces less effective in steering the molecules into the favourable sites and geometries.

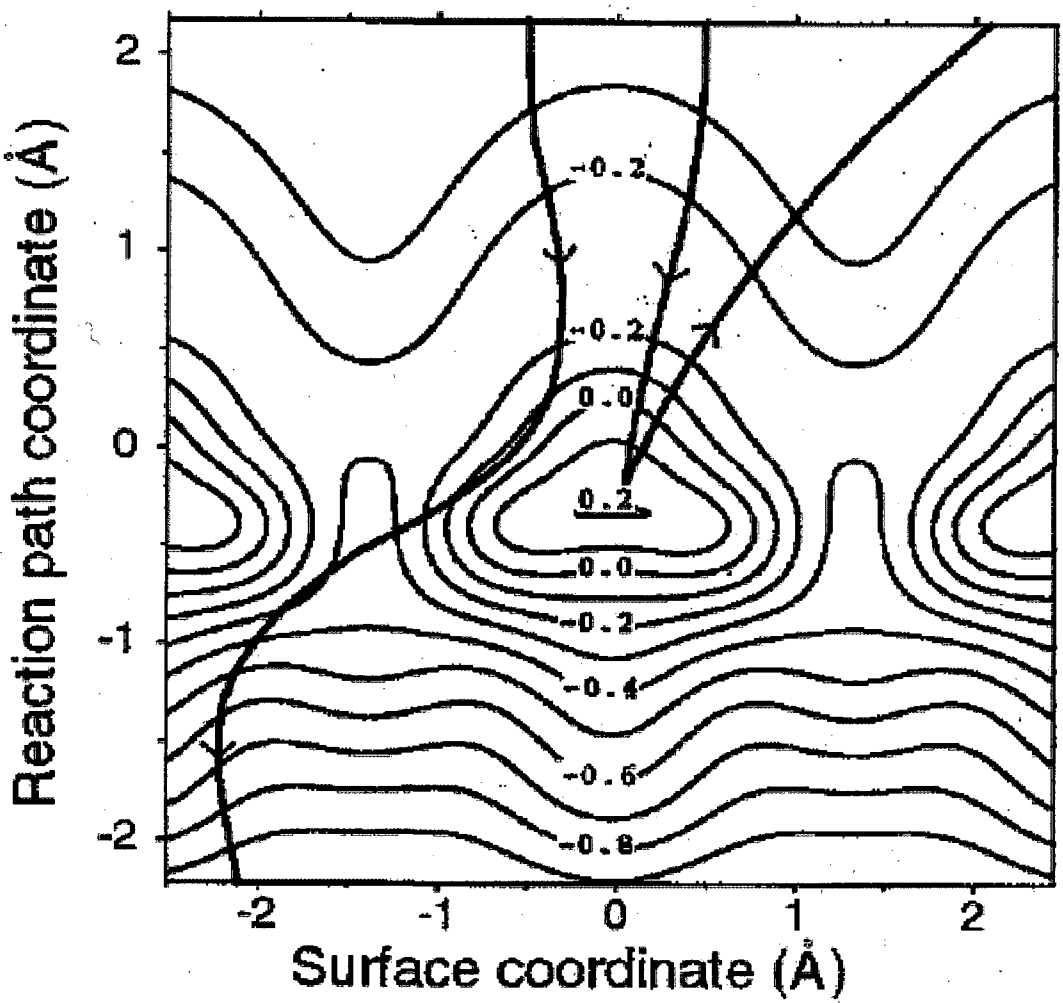

Figure 2: Classical illustration of the steering effect taken from [18]. Contour lines show the potential energy in eV along a 2D cut through the 6D configuration space of a hydrogen molecule with the molecular axis parallel to a transition metal surface. The left trajectory corresponds to a slow molecule where the steering forces have the chance to alter the molecules trajectory sufficiently to allow it to take a non-activated path to adsorption, and the right trajectory to a more energetic molecule which is too fast for the forces to divert it significantly and is reflected back into the gas phase.

In addition to the theoretical predictions, the lack of a strong surface temperature dependence displayed by the low energy channel was offered as experimental evidence supporting molecular steering model as being the model responsible for the reach of the low energy channel (up to E_i=150meV) on W(100). The steering theory offers some testable predictions:

1) It predicts that rotationally excited molecules (with j>2) will produce lower dissociation probabilities than molecules of the same total energy but occupying lower rotational states. This is because a particular orientation is required to be able access a particular potential dissociation well. Rotational excitation would suppress sticking because a range of barrier heights would be sampled at the different molecular orientations, rather than allowing the molecule the chance to just encounter the optimum barrier [17,18]. For example, at the on top site on a W(100) surface where dissociation is known to preferentially occur into the neighbouring bridge sites, a molecule orientated parallel to the surface will see no barrier to dissociation, whereas when orientated perpendicular to the surface a large barrier to dissociation will be encountered [19]. At low rotational energies the molecule can be steered into the favourable orientation, but at higher rotational energies this may not be possible. This is known as rotational hindering.

2) The prediction was also made that if steering were responsible for the low energy channel there could be the lack of a cosine component in the scatter due there being no requirement for molecular trapping. This lack of isotropic (cosine) scatter was indeed what was observed for a 20meV beam of hydrogen incident upon a Pd(111) surface (a beam energy well within the low energy channel observed for this surface) [20].

In the case of W(100), the large overlap of the direct channel with this low energy channel made attempts to prove or disprove these predictions, and hence determine the origins of the process creating the low energy channel, somewhat difficult.

IV.2.4 Dissociation Dynamics:- Dynamic Precursor Trapping

An alternative explanation to the typical physisorbed/chemisorbed fully accommodated precursor, and to dynamic steering, has been offered in the form of a "dynamically trapped" precursor to H_2 dissociative adsorption. This dynamic precursor is based on trapping into a potential well formed due to the drop in the vibrational ground state

energy (E^0_{vib}) occurring as a molecule approaches a surface and the intramolecular bond softens [18]. This can be understood in terms of the electron charge from the molecule accumulating between the H nuclei and the surface as the two approach each other in order to reduce the repulsion between them. Because the H_2 molecule only has two electrons this will necessarily be at the expense of the internal bonding of the molecule. Such behaviour tends to create a relaxation of the bond length of the molecule. At the bond length normal for an isolated molecule there would be little interaction between the surface and the first unoccupied antibonding orbital, since it lies far above the energy of the bonding orbital (~17eV), however, as the bond lengthens there is a shift upwards in the occupied $1\sigma_g$ bonding orbital and downwards in the first unoccupied antibonding $1\sigma_u$, this downward shift moving the $1\sigma_u$ to below the vacuum level where it is able to contribute to the surface bond.

Muller's modelling of the potential energy of the H_2 molecule as it approaches the bridge site of a Pt(111) surface [22] predicts E^0_{vib} to drop by ~50%, from its free molecule value of 270meV, over a distance of 1.1 to 1.6 Å in the vicinity of the surface (see figure 3). At low incident kinetic energies, E_i<200meV, the vibrational motion has been shown to adjust adiabatically to the softening of the H-H bond [22], this energy then being converted to other degrees of freedom, predominantly molecular (although recently a degree of energy exchange with surface phonons has been suggested, and this will be examined shortly). If enough energy is removed from the normal translational energy of the molecule then it may be left with insufficient normal energy to be able to climb out of the dynamic potential well back to the vacuum.

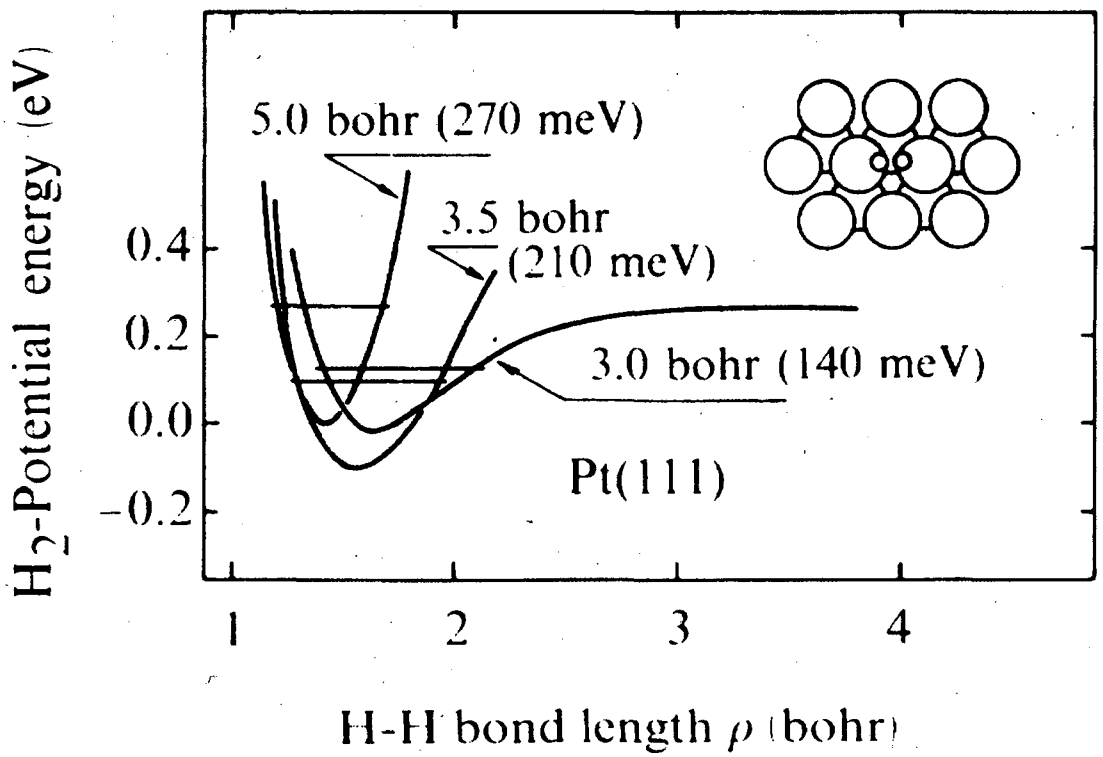

Figure 3: A model of the potential energy of a H_2 molecule as a function of the H-H bond length for 3 values of the perpendicular distance from a transition metal surface (from [22]) with energies in parenthesis referring to the vibrational ground states (E^0_{vib}).

Various mechanisms have been suggested to account for this energy loss, a normal to lateral coupling of the translational energy of the molecule being one [23]. Another being access to the bound levels of the vibrationally excited state dynamic wells (the vibrational excited energy levels having also experienced a drop in energy corresponding to the intramolecular bond softening) via a resonance with E_i within the realms of a non-adiabatic channel. Such an explanation has in the past been used to explain the resonant behaviour of $F+H_2$ gas phase collisions [24], and was put forward by Halstead and Holloway in their theoretical study of a H_2-metal adsorption system, with an activation barrier deep in the exit channel, as the means by which trapping could occur without invoking substrate degrees of freedom [23,25].

The currently favoured picture is that rotational excitation is the principal degree of molecular freedom to which the energy is transferred. In their calculation of the H/Pd(111) PES Crespo et al. [26] demonstrated that the energy released from the υ_0 softening can contribute to molecular rotation as well as accelerating the molecule

towards the surface. This mechanism of energy transfer to rotation implies that dynamic trapping necessarily functions in opposition to the concept of steering, inhibiting the ability of the PES to steer the molecule into orientations favourable to dissociation (parallel to the surface), causing it instead to encounter repulsive barriers as it rotates into unfavourable orientations during its approach towards the surface.

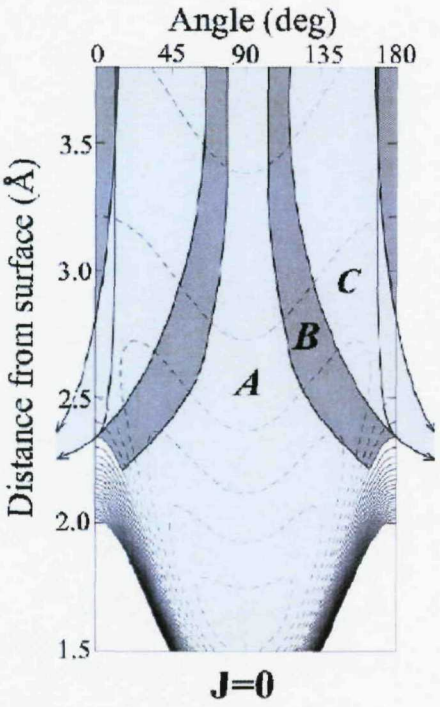

Figure 4: A 2D cut of the PES of a 160meV H_2 molecule approaching a transition metal surface, as a function of molecule-surface distance and angle (0^o=molecular axis perpendicular to the surface). Potential energy contours are indicated by the dashed lines. Trajectories in group A follow a direct route to dissociation, those in group B are reflected back towards the vacuum, whereas those in group C are driven, by momentum transfer to rotation, to the next potential channels. If the energy transfer is large enough to prevent the molecule from climbing the slope back to the vacuum then it is possible for dynamic trapping to take place. The width of the reaction window determines the relative importance of dynamic trapping, the broader the window, the less important the relative trapping contribution. Taken from [26].

This redistribution of energy to other molecular degrees of freedom allows the trapped molecule to still posses a high degree of translational excitation lateral to the surface while finding itself unable to regain the E^0_{vib} of the free H_2 molecular state required in order for it to leave the surface. A dynamically trapped molecule is not confined to a local potential well; it rotates, re-bounces and wanders over the surface (hence the name dynamic precursor). A molecule subject to dynamic trapping is not steered directly towards configurations favourable for dissociation, rather it undergoes aimless motion over a long time near the surface, until it finds its way towards dissociation (or desorbs).

To this point only the redistribution of energy to other molecular degrees of freedom has been discussed as a means to remove sufficient energy from the normal translational to trap the molecule in the dynamic well. Most studies have used a rigid surface model to examine the interaction, within which energy exchange with the surface phonons is not possible [26-29]. Recently the use of a simplistic surface oscillator model has been used to investigate the predicted effect of energy exchange with surface phonons within the dynamic precursor model [30,31]. In essence this model describes the T_S dependence based on the energy exchange during the initial collision, with a loss of energy to the surface making it harder for the molecule to climb back up the potential of the dynamic well towards the vacuum, and, once trapped, the ability of the relatively hot/cold surface to aid the molecule in returning to the vacuum or to quench desorption from the dynamic precursor state (particularly since the multiple encounters with the surface occurring within the dynamic trapping mechanism allow an enhanced interaction time between the trapped molecule and surface).

Furthermore it has been suggested that the reactivity of a surface may define whether or not H_2 is likely to experience dynamic trapping, with surfaces displaying only activated routes to direct dissociation being more likely to see dynamic trapping than surfaces upon which many non-activated paths exist, where it is suggested that dynamic steering is instead more likely to account for any increase in S_0 with decreasing E_i. Steering and dynamic trapping has been calculated as taking place on Pd(100) and Pd(111) respectively, in agreement with this principle [28].

Calculations revealed the T_S effect to be larger on a less reactive surface such as Pd(110) than a more reactive surface such as Pd(111) where a greater number of routes to direct sticking are non-activated and the precursor route to dissociation tends to account for less of the total dissociative sticking [28]. Little or no dependence of S_0 on T_S was observed recently for H_2 sticking on the relatively reactive W(100) surface [11] compared to the W(100)-c(2×2)Cu surface, the W(100)-c(2×2)Cu surface displaying a considerably higher barrier to direct dissociation, resulting in dissociation occurring almost exclusively via trapping at low energies and in a considerable drop in S_0 with increasing T_S [13] (the literature describing this surface will be considered in detail in chapter V). Earlier work on the H/W(100) system indicated a more substantial T_S

dependence [10], and this corresponded with the observation of a much larger indirect channel than was observed in more recent investigations [11].

It should be noted that the relative proximity of the T_S dependent trapping values measured by experiment to the trapping calculated using the rigid surface model [30,31] implies that trapping into the dynamic precursor remains mainly due to energy loss to other molecular degrees of freedom rather than to the surface. However, the relative importance of the surface temperature to the dynamic trapping channel of H_2 remains an area of considerable uncertainty and interest and will be investigated further within chapters IV and V.

Existence of a T_S dependence of S_0 is difficult to explain in terms of molecular steering within a direct channel framework and acts as one of a few possible indicators that suggest a dynamic precursor route to dissociative adsorption of H_2.

The presence of a dynamic precursor should leave a fingerprint within experimental data. Within the low energy regime in which it functions the dynamic precursor should produce a reduction of S_0 with increasing T_S and E_i, although this behaviour can be accounted for also within other models (such as a classical physisorbed or chemisorbed precursor, or molecular steering). The dynamic precursor should however also produce the following markers:

i) large molecular displacements parallel to the surface
ii) long residence times of the trapped molecule
iii) a total (as opposedd to normal) energy scaling [29]
iv) the loss of memory of initial conditions

In reference to the loss of memory, it has been noted by Cesare et al. [28] that a specularly peaked scatter pattern, with little or no cosine scatter component, may not necessarily indicate the absence of a dynamic precursor, rather it may simply indicate that virtually all molecules that have trapped go on to dissociatively adsorb. Using 6D PES DFT calculations Barredo et al. [32] calculated that upon the highly reactive Pd(111) surface most trapped H_2 molecules go on to dissociate. However, the presence of a $\cos\varphi$ component within the scatter (after taking into account time of flight

measurements to eliminate associative desorption) remains a good indicator of a precursor trapping channel being in operation [29].

IV.3 Results

IV.3.1 Summary

After obtaining a clean Mo(100) surface (as described in chapter III), a range of K&W type experiments (also described in chapter III) were performed examining the sticking of H_2 on Mo(100) for a range of H_2 incident energies, E_i, and Mo(100) surface temperatures, T_S. The initial sticking probability, S_0, has been recorded for a range of T_S at both a low and high E_i, and for a range of E_i at both a low and high T_S. In addition to these, plots have been produced to examine in detail how the sticking, S, varies with hydrogen coverage, θ_H, over the range of conditions. TPD plots have been produced after hydrogen has been dosed onto the surface via a K&W type sticking, and are in good agreement with those previously observed. Some interesting trends are seen within the K&W sticking plots, with the chamber pressure failing to return to the initial flag closed value (indicating the surface fails to saturate) within the expected time scale. The phenomena and how it changes over the full range of conditions is examined in detail using different aperture sizes and comparing the gas desorbed during a TPD with that apparently adsorbed during the corresponding K&W.

IV.3.2 H/Mo(100) Temperature Programmed Desorption

The TPD plots are taken after typical K&W sticking experiments, performed at $T_S \approx 150K$, and over a time scale during which the pressure plateaus. There are 3 peaks corresponding to dissociatively adsorbed hydrogen on the Mo(100) surface labelled on figure 5 as β_1, β_2 and β_3 observed at ~295K, ~320K and ~400K respectively. These results are in good agreement with those presented by Zaera et al. [2] who also observe 3 β peaks, putting β_1 at ~285K, β_2 at ~325 and β_3 at 400K. There is some disagreement within the literature with peak positions also having been reported as being somewhat

higher, at 325K, 375K and 450K [1,3]. The peaks appear to be shifted, each by ~50K, suggesting some systematic error in the temperature recording is most likely responsible.

It should be noted that the thermocouple used in the present study was a W3-type (W3%Rh/W25%Rh) and that this thermocouple is designed specifically to monitor accurately the high temperatures required during the cleaning process, and brings with it considerable errors when measuring the low temperatures at which the hydrogen TPD is taken. At <273 K the thermocouple was calibrated against a K-type (Ni/Cr – Ni/Al) thermocouple (see appendix C), this resulted in an error of ±8 K on each reading. Further inaccuracies are added through the temperature being manually controlled and recorded, this allowing for only a slow and fluctuating heating rate (of between 1.5 and 3.5 K/sec), the use of electron bombardment (required to produce the high T_S required to clean the surface) rather than resistive heating making maintaining a consistent heating rate at low temperatures more difficult still.

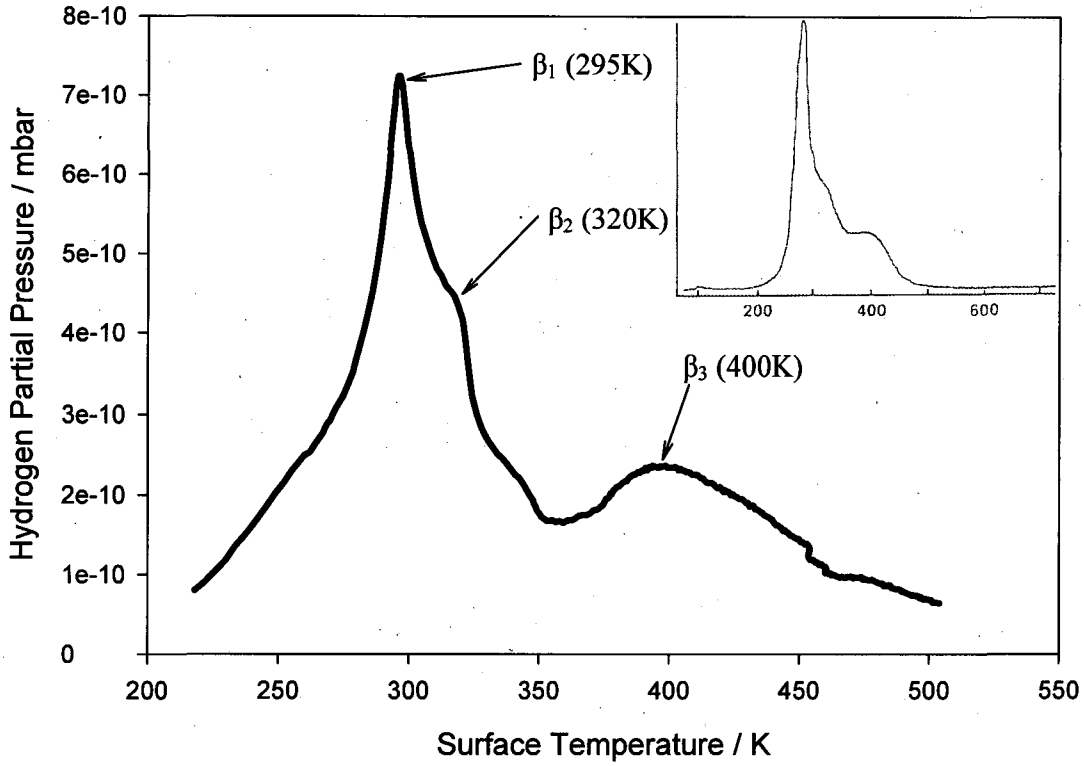

Figure 5: Temperature programmed desorption curve examining the desorption of H_2 from an Mo(100) surface saturated with hydrogen. The TPD was taken following a 5 minute K&W type sticking experiment using the largest aperture size where the behaviour of the K&W plot was monitored to ensure saturation of the surface was achieved. Inset shows the comparable data taken by Zaera et al. [2]

The β_2 and β_3 desorption peaks have been shown to obey 2nd order kinetics and β_1 1st order kinetics [1]. This suggests β_2 and β_3 are associated with adsorption into the reconstructing surface and β_1 into the static unreconstructed surface. Adsorption of hydrogen into all 3 β states has been shown not to be associated with hydrogen bonding into different adsorption sites, but to correspond to bonding purely into bridge sites at various degrees of reconstruction [2,4,6, 7,9], the evidence for this bridge bonding having already been examined in considerable detail (see chapter IV.2.1).

The saturation hydrogen coverage has been calculated by integration of the area encompassed during K&W sticking (as illustrated in the inset of figure 6). The hydrogen coverage is seen to exhibit what appears to be an exponential decay as a function of T_S at temperatures above that at which desorption of β hydrogen is first

observed to take place. That this drop is smooth rather than stepped is in good agreement with the picture that has been painted for H_2 adsorption onto the Mo(100) surface, that of adsorption into a single site on a reconstructing substrate. A variety of different adsorption sites would be expected to produce a plot more step-like in nature since desorption from differing sites would be expected to take place at different temperatures.

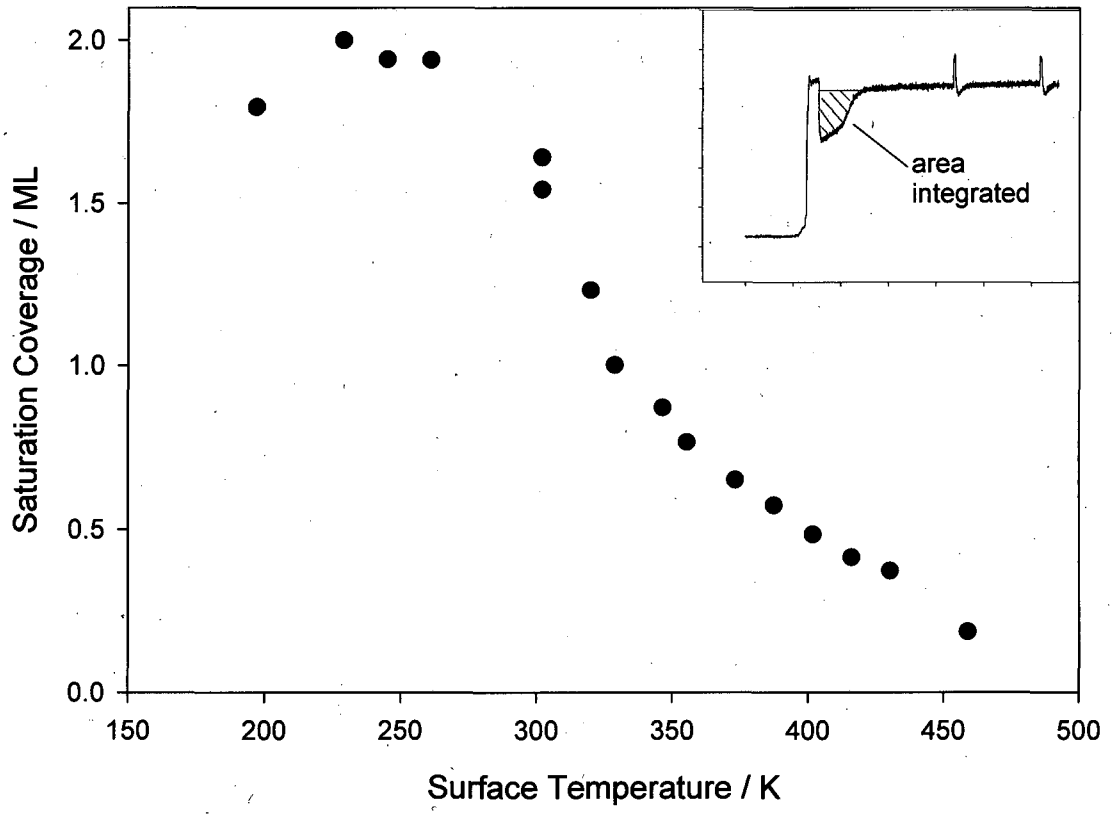

Figure 6: The saturation coverage (in monolayers) of hydrogen, adsorbed during a K&W type sticking, as a function of the surface temperature at which the sample is maintained. The relative saturation coverage of each data point was calculated by integrating the area traced out by the appropriate K&W. Inset is an example K&W with this area indicated.

IV.3.3 Indications of Hydrogen Migration Across The Surface

Figures 7a and 7b are typical of the K&W plots obtained here when a H_2 beam was directed at the clean Mo(100) sample surface. During these experiments the surface temperature of the molybdenum was held at ~181K, well below the temperature at which hydrogen is observed to desorb from the atomically bound state, ensuring that there is no unusual effect taking place associated with a steady state being reached between hydrogen adsorption and desorption from the surface. Typically the pressure of a K&W type plot like this would be expected to return to the flag closed value as the crystal surface gradually saturates, the surface then reflecting all further hydrogen incident upon it thus allowing all hydrogen from the beam to contribute to the chamber pressure, as is the case when the beam is incident upon the mica flag. What is instead observed is that, after the initial drop in pressure associated with the opening of the flag and the beam being incident upon the clean crystal surface, the chamber pressure increases (as expected with the adsorbed hydrogen beginning to reduce the number of free sites for subsequent hydrogen adsorption) but then plateaus at a pressure considerably below that of the flag closed value. This plateau is reached within less than a minute, and the pressure does not rise far from this value even after a further 3 minutes (see figure 7a).

of the support provide ample adsorption sites for the hydrogen in comparison to the flat molybdenum crystal. Were the beam to be partly incident upon the metallised areas of the support and part incident upon the crystal this might have caused the K&W plot to appear as it does in figure 7a (compare this with figure 14c of chapter III). However, particular care was taken to ensure the beam was incident only upon the very centre of the crystal and the smallest aperture size was used to ensure the beam diameter was considerably smaller than that of the crystal. In fact, upon using a larger sized aperture with a resultant beam diameter closer to that of the crystal (where it would be considerably more difficult to position the beam so as to be incident upon only the crystal and not upon any of the metallised surroundings) the plateau effect was actually seen to be reduced (figure 7b), with the pressure returning to close to the flag closed value and indicating that the hydrogen sticking did, in this case, saturate the surface upon which the beam was incident. Furthermore by performing a K&W sticking with the crystal temperature elevated (T_S=683K) well above the point at which all atomically bound hydrogen is seen to desorb (see figures 6 and 7) it was noted that no variation in pressure was observed during the K&W, with the flag open pressure being equal to the flag closed value (figure 7c). This provided a clear indication that the beam was indeed incident upon the sample and that this plateau effect is associated with the crystal itself and not any metallised areas of the sample support which are not significantly heated and would be expected to have continued to display sticking independently of the increase in crystal temperature.

By integrating the area covered by the pressure drop during the K&W and comparing this with a calculation of the integrated area of the TPD a comparison could be made between the pressure of gas adsorbed and the pressure desorbed. During the TPD only the crystal is heated (with the support remaining cooled via the liquid nitrogen reservoir) and therefore any hydrogen stuck on the metallised support surfaces will not be expected to contribute to the desorbing gas pressure. In the case of the larger sized apertures, where the K&W plot appears normal, the two values are in very good agreement (table 1), the value for gas adsorbed being almost equal to the value for gas desorbed. However, for the smaller beam diameter the two values are far apart. Were the beam adsorbing on the metallised support the quantity of gas adsorbed would be expected to be considerably larger than the quantity desorbed. However, the calculations revealed the opposite to be true.

Beam diameter (mm)	Area	Adsorption from K&W (in langmuirs)	Desorption from TPD (in langmuirs)
Large (7.5)	A*	0.0212	0.0206
Medium (3.25)	A*	0.0269	0.0268
Small (1.25)	A	0.0006	0.0118
Small (1.25)	B	0.0048	0.0118

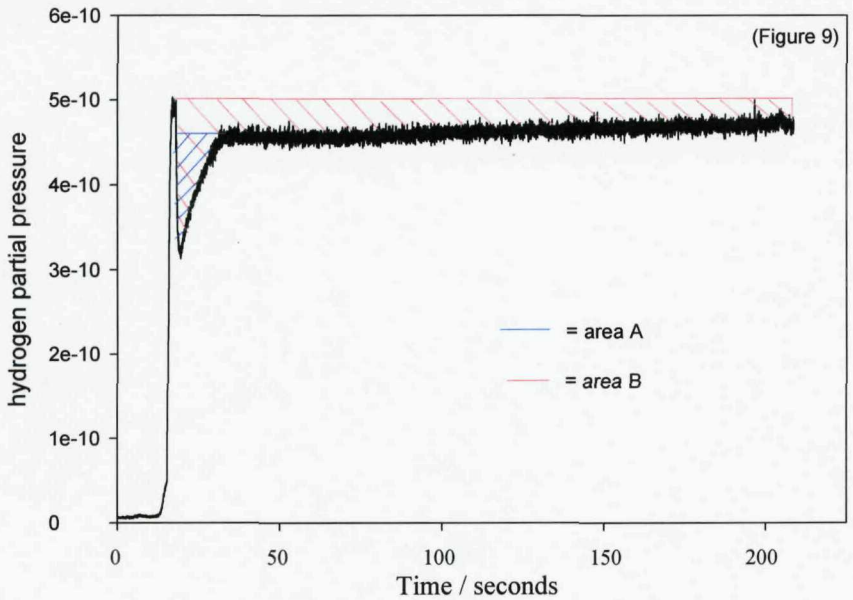

Table 1 & Figure 8: Comparison of the H_2 adsorbed onto the Mo(100) during a K&W sticking with the H_2 desorbed during a subsequent TPD. Area's A and B are illustrated in figure 8 by the blue and red shaded areas respectively. The A referred to the medium and large aperture sizes denotes the case where A≈B.*

Another alternative explanation to consider is that sticking upon the clean crystal surface may take place from the background hydrogen, present as part of the 21% diffuse scatter not directly incident upon the crystal (see chapter III.3), or from hydrogen that is initially reflected from the crystal surface. It appears that background hydrogen adsorption does indeed take place, since the value calculated for the gas desorbed is greater than even the total pressure adsorbed from the beam incident upon the crystal, measured as area B on figure 8. However, such sticking from background hydrogen could not cause the early plateau in pressure observed in figure 7a since, when the flag is closed, 100% of the hydrogen entering the chamber does so in the form of "background gas" (gas not part of the beam column incident directly upon the crystal surface), so any sticking due to background pressure would also manifest itself in a lower flag closed pressure value.

One further alternative to be considered is that the plateau is caused by adsorbed hydrogen migrating across the crystal surface. Hydrogen diffusion from areas upon which the beam is incident to areas of clean surface could account for the plateau. The diffusion would effectively make room for new hydrogen adsorption within the area upon which the beam is incident, provided there remains free Mo(100) surface for the hydrogen to diffuse onto. This would eventually create a steady state type situation with the rate of hydrogen adsorption becoming balanced by the rate at which migration produces new vacant adsorption sites. For this reason the larger aperture sizes, where the beams incident diameter is closer to that of the crystal itself, would exhibit this phenomena only to a much lesser degree, as is indeed observed to be the case (see table 1). This would also explain why the quantities of hydrogen adsorbed and desorbed are approximately equal for the larger apertures but the gas adsorbed within region A (figure 8) falls short of the desorbed value calculated from the corresponding TPD. The measure of hydrogen adsorbed within region B (figure 8) also fell considerably short, possibly implying that adsorption of "background" hydrogen, hydrogen sticking taking place on areas of the sample where the beam was not incident, also contributed significantly.

A significant plateau effect was observed at both high and low E_i. That the effect is present at high E_i, where a H_2 molecule is no longer likely to gain access to a molecular precursor state on the surface, implies that if diffusion is responsible for the plateau it cannot be restricted only to diffusion of a mobile precursor but must also apply to dissociated, atomically chemisorbed, hydrogen. Hydrogen atoms, with large thermal velocities by virtue of their light masses, diffuse particularly efficiently, with the adatoms believed to make frequent jumps from site to site [33]. Hydrogen has been observed to encounter only a very low barrier to diffusion on a variety of transition metal surfaces [33-35] including tungsten where hydrogen diffusion across the surface is calculated to occur readily as both activated diffusion at high temperatures, and also less effectively, but still to a significant degree, via tunnelling at low temperatures (T_S<140K) [36], with the mean square displacement of a hydrogen atom from its starting point calculated to increase with surface temperature within the activated region [37], although Daniels and Gomer observe the temperature dependence of hydrogen diffusion on the W(001) surface to be somewhat more complex [36].

IV.3.4 Dependence of S_0 on Incidence Energy

The dissociative sticking probability of molecular hydrogen on the Mo(100) surface was calculated using the K&W technique described in chapter III.2.4 summarised here by equation IV.1.

$$S_0 = \frac{(P_1 - P_2)}{(P_1 - P_0)0.79} \qquad \text{(IV.1)}$$

Where P_0 is the background pressure, P_1 the flag closed pressure, and P_2 the initial flag open pressure. These are all illustrated in chapter III.3 figure 13.

From previous work using this molecular beam system which has the benefit of TOF measurements [38] the error on the incident energy measurements are given as,
E_i +/- 1meV for the 1% H_2/Ar
E_i +/- 3meV for the 1% H_2/He

Assuming there are no problems in reproducing a good beam, errors for S_0 of H_2 on the Mo(100) depend predominantly upon how clean the surface is of contaminants, with the presence of contaminants tending to reduce S_0. The error values were estimated by taking 6 readings of S_0 for a given E_i and T_S (32meV and 165K respectively), removing the highest and lowest value, and calculating half of the range: S_0 +/- 0.01 for H_2 on Mo(100)

Figure 9 shows the results of K&W type S_0 calculations for a range of E_i on a Mo(100) surface held at low temperature (T_S=165K). $S_0(E_i)$ exhibits non-monotonous behaviour with S_0 initially dropping as E_i increases, then entering a 2nd regime at higher E_i where S_0 increases as the incident energy of the molecules is increased. Such behaviour is indicative of both a low and high energy channel to dissociation being present, and is most commonly associated with a direct channel predominantly determining the sticking probability at higher energies and an indirect channel (either via a fully accommodated or accommodated and dynamic precursor) dominating at lower energies where the energy of the incident molecules may be insufficient to surmount

the barrier to dissociation directly (e.g. N_2 adsorption on W(100) [39-42]). On a surface displaying non-activated paths to dissociation the concept of molecular steering has also been suggested to explain this non-monotonous behaviour (see chapter IV.2.3).

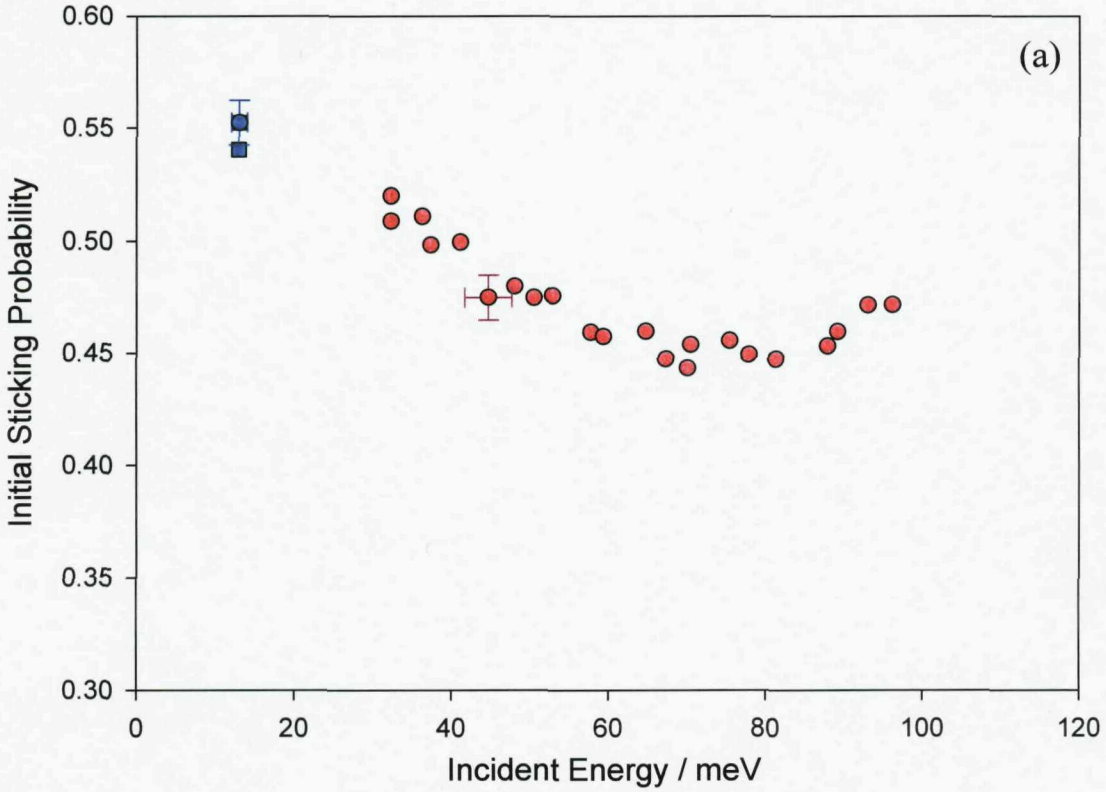

Figure 9: a) Initial sticking probability of hydrogen on Mo(100) as a function of incident energy. T_S=165K. Beam directed perpendicular to the surface ($\varphi=0^0$). Squares represent data taken using an argon seeded beam, circles represent data taken using a helium seeded beam. And b) the hard cube trapping fit for a 30meV potential well and an effective surface mass of 1Mo (black line).

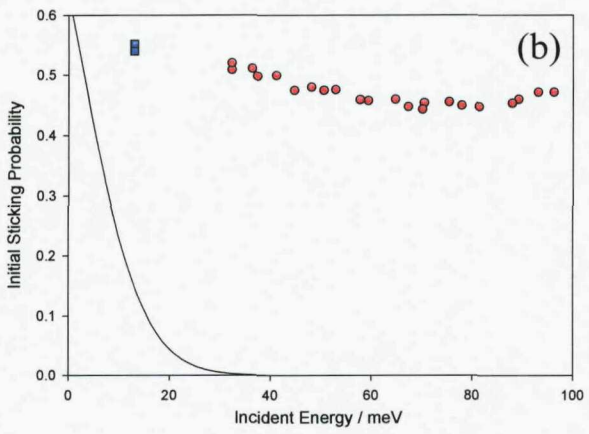

There is considerable overlap between the direct and the low energy channels. The hard cube model calculations shown in figure 9b suggest that the low energy channel extends considerably above what would be expected for a classical fully accommodated precursor, a typical physisorption well for hydrogen on a metal surface being only ~30meV (as recorded on various different crystal faces of Cu and Al [43],

the depth of the physisorption gas-surface potential tending to depend largely on the polarizability of the gas molecule and to only a small extent on the composition of the surface [44])

and there being no evidence of a chemisorbed precursor state being present on this surface (detailed calculations for H_2/W(100) in fact appearing to clearly rule out the presence of a molecular chemisorption state [19]).

The hard cube model is based on a repulsive force being experienced by the gas particle and surface atom upon collision, with both being considered as elastic and, therefore, the force impulsive. It depicts the surface as being made up of cubes with a face parallel to the plane of the surface and moving only normal to the surface. This entails that the assumption is made that the surface is completely flat, however, since this work only deals with collisions normal to the plane of the surface this assumption can be expected to hold reasonably well.

Each impinging gas molecule enters a square well attractive potential (U) created by the surface atom, and the trapping probability is determined by whether, after undergoing a collision based on Newton's laws for the collision of rigid elastic bodies, it has retained enough energy to be able to escape the well. The square well accelerates the molecule towards the surface, increasing its velocity by $\sqrt{\frac{2U}{m}}$ (m being the mass of the incident particle) and adding to the velocity with which it moved within the vacuum phase (V_{vac}).

The trapping probability is modelled as the fraction of molecules for which sufficient incident energy is lost during the collision with the surface to prevent escape from the square well potential and thus enable trapping. The hard cube model calculates the trapping probability as a function of the incident energy (E_i), angle of incidence (θ), and surface temperature (T_s) for a given well depth (U), molecular mass (m) and effective surface mass (M_{eff}), using the following equation:

$$\zeta(E_i,\theta,T_s)_{U,M,m} = \frac{1}{2} + \frac{1}{2}erf(av_{\lim}) + \frac{e^{(-av_{\lim})^2}}{2\sqrt{\pi}av_{well}} \qquad \textbf{(IV.2)}$$

Where $$v_{\lim} = \frac{\mu+1}{2}\sqrt{\frac{2U}{m}} + \frac{\mu-1}{2}\sqrt{\frac{2}{m}\left(E_i \cos^2\theta + U\right)} \quad \textbf{(IV.3)}$$

$$a = \sqrt{\frac{M_{eff}}{2kT_s}} \quad \textbf{(IV.4)}$$

$$\mu = \frac{m}{M_{eff}} \quad \textbf{(IV.5)}$$

With υ_{lim} being the impact velocity of the surface cube below which trapping is enabled, υ_{well} being the velocity of the molecule on impact with the surface, after it has been accelerated by the square well potential, erf being the error function, and μ the relative mass.

The variables (effective surface mass and potential well depth) have been chosen to produce the largest possible sticking probabilities from the cube model, with the true effective surface mass (i.e. the mass with which the hydrogen atom interacts during a collision) expected to be somewhat larger than the one Mo atom of this calculation, and the potential well depth being at the highest end of the anticipated range predicted for a physisobing H_2 molecule. That this maximum limit of the hard cube model for a typical physisorbing accommodated precursor still greatly underestimates the size of the low energy channel, with respect to the data, gives the first indication that a dynamic channel (either trapping or steering) might be responsible for the reach of this low energy adsorption channel of hydrogen on Mo(100).

The picture of the direct channel is somewhat clouded by the overlap with this substantial low energy channel, however the initial indications appear to be that a large direct channel exists for this surface, stretching well into the low energy regime and suggesting either a very low minimum barrier height to direct dissociation, or a non-activated surface. Typically, a direct channel results in S_0 increasing with increasing E_i once molecules are sufficiently energetic to overcome any minimum barrier to dissociation, an increase in the E_i will allow access to non-optimised trajectories (there being a range of barriers to dissociation present for different impact sites and molecular orientations). The shallow gradient of the initial drop in S_0 with increasing E_i

(occurring for E_i<60meV) may well be indicative of the reach of the direct channel down to even the lowest energies, the gradual drop in the size of direct channel with decreasing E_i possibly acting to balance, to some extent, the corresponding exponential rise of the indirect channel contribution to sticking. Were the direct channel only to become active at around the energies at which the indirect channel disappears then the low energy channel might be expected to exhibit a much sharper decline (as is the case for hydrogen adsorption onto the W(100)-c(2×2)Cu surface where the direct channel is inaccessible below ~150meV [13,14]).

IV.3.5 Dependence of S_0 on Surface Temperature

Comparing $S_0(E_i)$ taken at low and high T_S it is evident that the low energy channel to dissociation is T_S dependent, but that the high energy channel is T_S independent. Figure 10 shows how the magnitude of the low energy channel is diminished when the surface is maintained at a higher temperature and how this reduction in the indirect channel is not accompanied by a similar reduction in the direct channel, the data points instead tending to merge when the incidence energy rises above ~50meV.

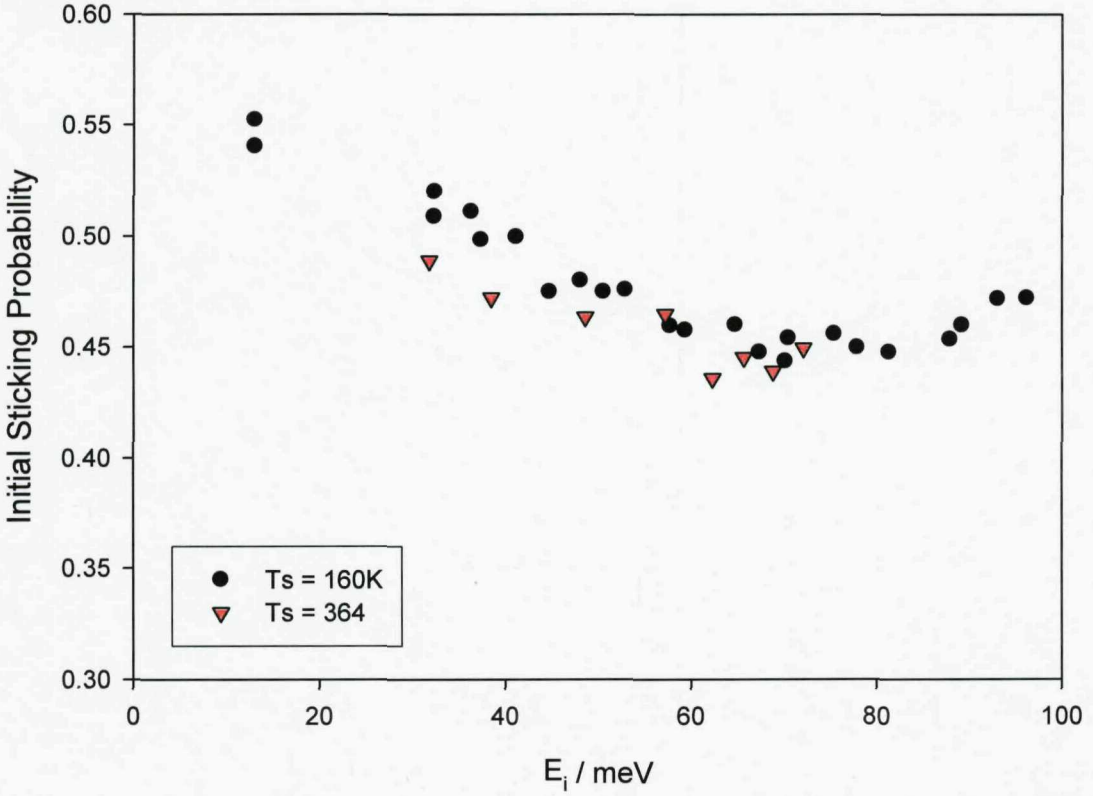

Figure 10: Initial sticking probability of hydrogen on Mo(100) as a function of incident energy. T_S=160 (black circles), T_S=364 (red triangles). φ=0

This behaviour is consistent with a direct channel dominating sticking at high energies. However at first glance it would appear to rule out dynamic steering, which is essentially a direct type channel, from being entirely responsible for the low energy channel, it being hard to conceive how a purely direct type channel might incorporate a T_S dependence (although this does not rule out steering function in tandem with an indirect channel). It might be possible to conceive of the potential energy surface presented by differing T_S dependent surface structures being responsible for different sticking probabilities within a direct channel, but such a model would then struggle to account for the direct channel no longer exhibiting a structural sensitivity at the higher beam energies.

.

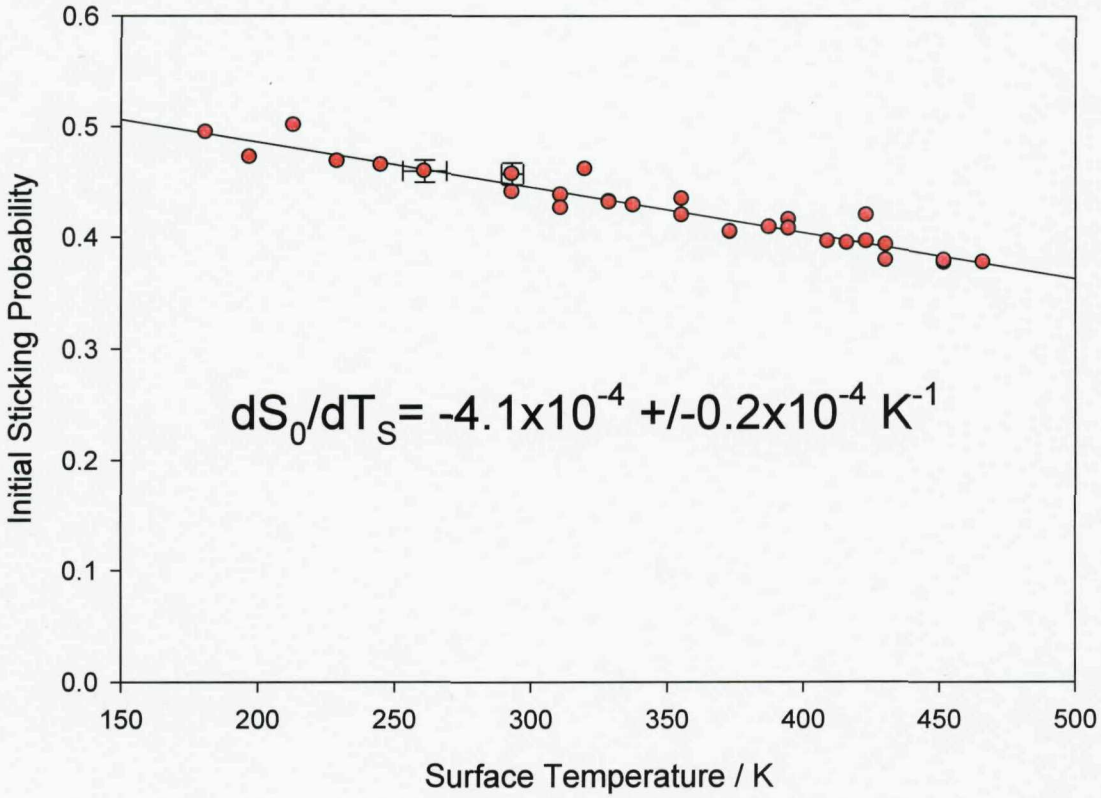

Figure 11: Initial sticking probability of H_2 on Mo(100) as a function of surface temperature, φ=0, E_i=16meV. The thermocouple recorded values in mV with the smallest measure recorded being 0.1mV. The errors on the T_S measure were taken as being half of this value. This results in the following error values: T_S +/- 8K when <293K, T_S +/- 4K when ≥293K. It should be noted that the variation of S_0 with T_S is not predicted to be a linear relationship (see figure 10) and therefore a straight line fit is not strictly valid. However this fit is performed to allow better comparison with previous data where a linear regression has also been carried out over a similar T_S range [e.g. 47,48]

The plot of $S_0(T_S)$ at very low E_i (figure 11) reveals a channel that presents a considerable T_S dependence. This T_S dependence is far too large to be accounted for only in terms of a variation in the trapping probability of a physisorbed precursor, the hard cube model, which describes the trapping as a function of surface temperature, requiring an unrealistically large well depth of >300meV to account for the gradient of -4.12×10^{-4} K^{-1} over the range $150<T_S(K)<500$ observed here for a beam of E_i=16meV

There are two temperature dependent steps that are encountered within the indirect route to dissociation: the initial trapping of the molecule and the subsequent partition

of the dissociation/desorption channels of this trapped molecule. Since it is clear that the temperature dependence is too large to reasonably relate to the initial trapping, where an unrealistically large potential well would be required to account for the behaviour, it must be assumed that the T_S dependence is being predominantly determined by the partition function.

It is assumed that the relative rates of desorption and dissociation of the precursor are each described by an Arrhenius type equation,

$$k = \upsilon e^{\left(-\frac{E}{k_B T_S}\right)} \qquad \textbf{(IV.6)}$$

The pre-exponential, υ, is the frequency factor (a measure of how frequently attempts are made by the precursor to desorb or dissociate). In a simplistic model υ_{des} could be envisaged as being determined by the vibrational frequency of the bond being broken between molecule and surface during desorption and υ_{diss} the vibrational frequency of the intramolecular bond of the trapped H_2 molecule which must be broken in order for dissociative adsorption to take place.

The initial dissociative sticking probability can be described in terms of the rates of desorption and dissociation (k_{des} and k_{diss} respectively) and the initial trapping probability (ζ),

$$S_0 = \frac{\zeta k_{diss}}{k_{diss} + k_{des}} \qquad \textbf{(IV.7)}$$

It can be rearranged and be expressed in terms of υ, E, and T_S:

$$\frac{\zeta}{S_0} = 1 + \frac{k_{des}}{k_{diss}} \qquad \textbf{(IV.8)}$$

Substituting in equation IV.6,

$$\frac{\zeta}{S_0} = 1 + \frac{\upsilon_{des}}{\upsilon_{diss}} e^{\left(\frac{-E_{des}+E_{diss}}{RT_S}\right)} \qquad \textbf{(IV.9)}$$

Where $\Delta E = E_{des} - E_{diss}$,

$$\frac{S_0}{\zeta} = \left(1 + \frac{\upsilon_{des}}{\upsilon_{diss}} e^{\left(-\frac{\Delta E}{RT_S}\right)}\right)^{-1} \qquad \textbf{(IV.10)}$$

$$S_0 = \zeta\left(1 + \frac{\upsilon_{des}}{\upsilon_{diss}} e^{\left(-\frac{\Delta E}{RT_S}\right)}\right)^{-1} \qquad \textbf{(IV.11)}$$

According to equation IV.11, and assuming that $\upsilon_{des}/\upsilon_{diss}$ remains independent of temperature, the negative gradient of dS_0/dT_S implies that $E_{des} > E_{diss}$ as illustrated by figure 12.

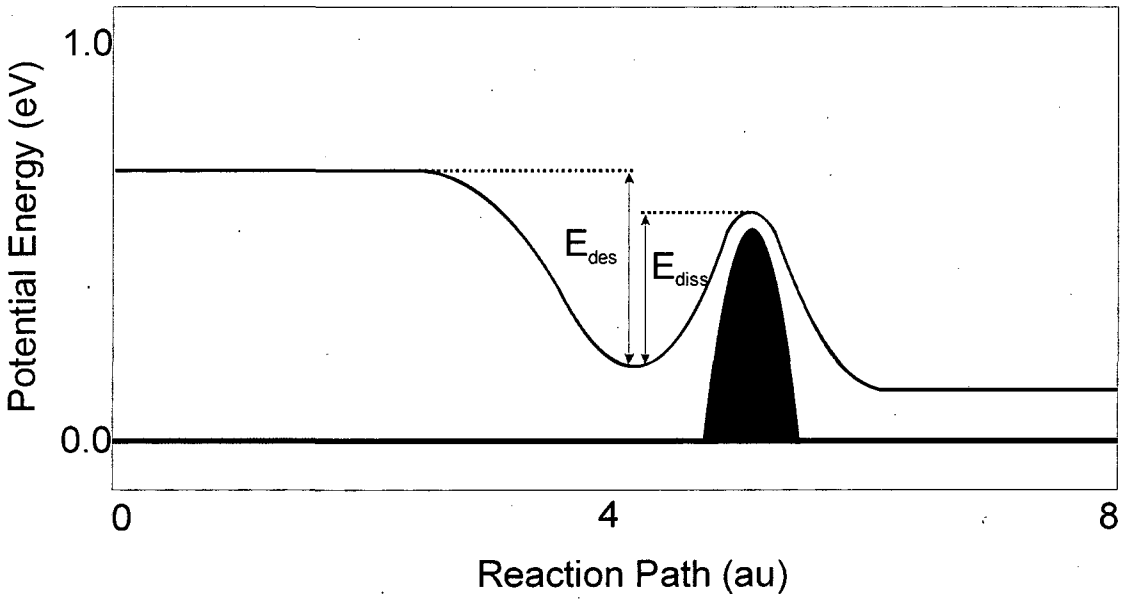

Figure 12: In the case of an accommodated or dynamic precursor no barrier to the trapping well would be expected to be present, therefore E_{des} can be estimated as being equal to the molecular well depth. E_{diss}-E_{des} will therefore be the overall activation energy along the reaction path.

At an incident energy of 32meV this temperature dependence is seen to diminish somewhat. Figure 13 showing a drop in the gradient to -1.4×10^{-4} +/- 0.2 K^{-1}. This may be caused in part by the increased contribution to the sticking of the temperature independent direct channel and a lowering of the trapping mediated contribution to S_0, but the drop in gradient is considerable, and cannot be accounted for by the small increase in contribution made by the direct channel (predicted to be ~15% greater at 32meV), an incidence energy of 32meV still falling well within the range where the indirect channel dominates sticking. The alternative explanation to consider is that a dynamic channel with little or no temperature dependence is making a significant contribution to S_0 at E_i=32meV.

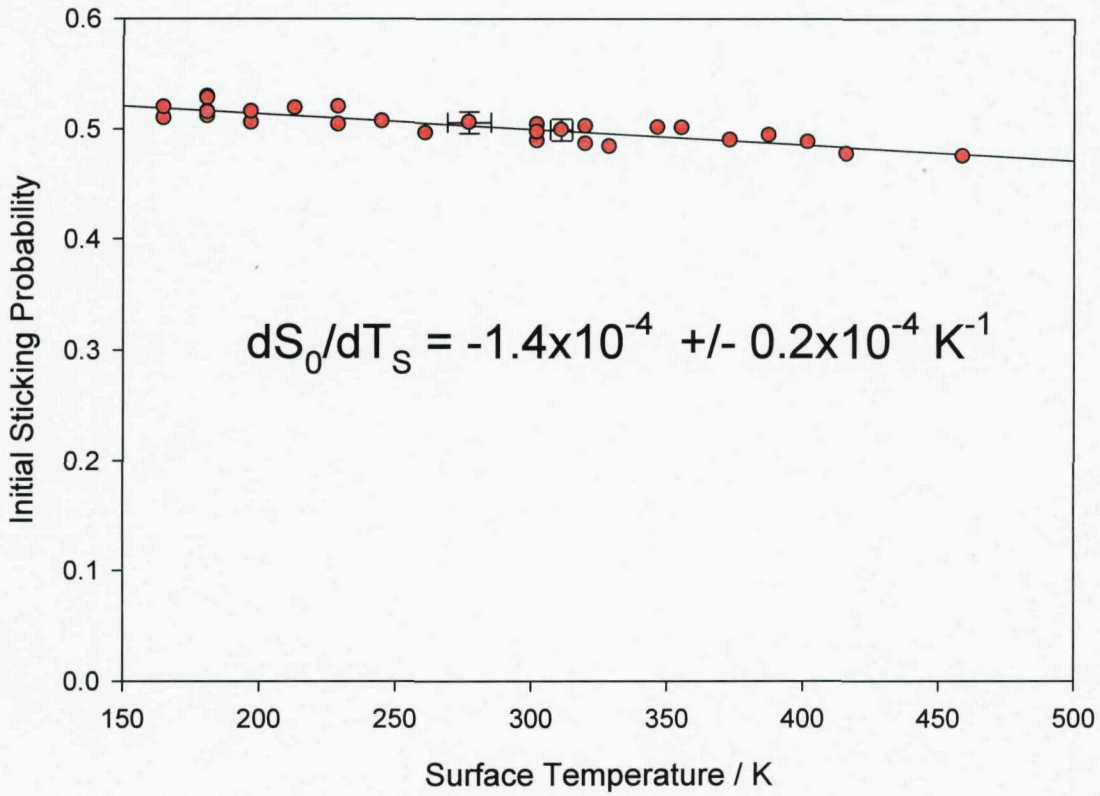

Figure 13: Initial sticking probability of H_2 onMo(100) as a function of surface temperature, φ=0, E_i=32meV. T_S +/- 8K when <293K, T_S +/- 4K when ≥293K

At E_i = 72meV the T_S dependence is seem to become almost negligible, displaying only a very slight and positive gradient. This is consistent with a direct channel dominating, and only a negligible indirect contribution to the sticking. The slight positive gradient can be accounted for if one pictures the surface as a single oscillator where an increase in T_S can be envisaged in terms of a 'kick' from the surface cube, aiding the molecule in surmounting the direct barrier to dissociation.

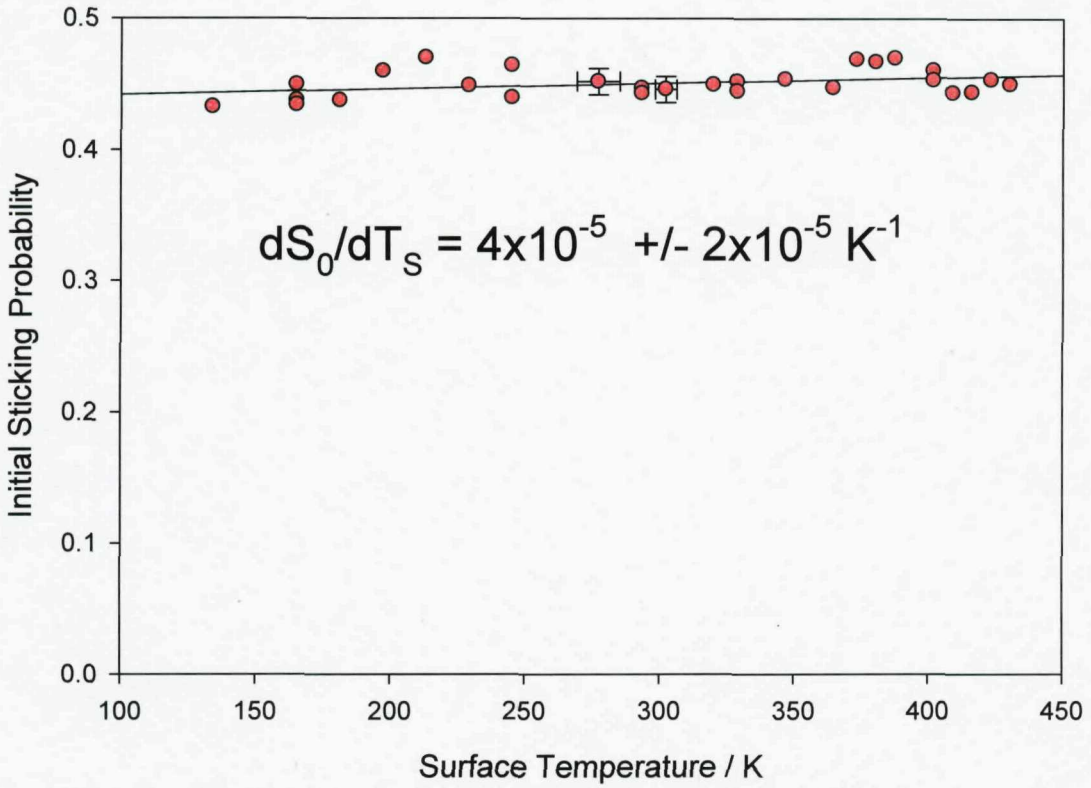

Figure 14: Initial sticking probability of H_2 onMo(100) as a function of surface temperature, φ=0, E_i=72meV. T_S +/- 8K when <293K, T_S +/- 4K when ≥293K

IV.3.6 Dependence of Sticking Probability on Hydrogen Coverage

The sticking probability of hydrogen on Mo(100) has been measured as a function of hydrogen coverage, θ_H, for a range of incident energies stretching from E_i=13meV to E_i=74meV, for a variety of surface temperatures and using both large and small beam apertures (where the beam is incident upon the majority of the area of the front face of the crystal or only a small fraction of the surface, respectively). Saturation coverage for hydrogen adsorbing atomically on this surface at low temperatures has been shown to take place at 2ML [2-4, 6-8], although, as shown by figure 6, the saturation coverage of hydrogen on the Mo(100) surface varies with increasing T_S.

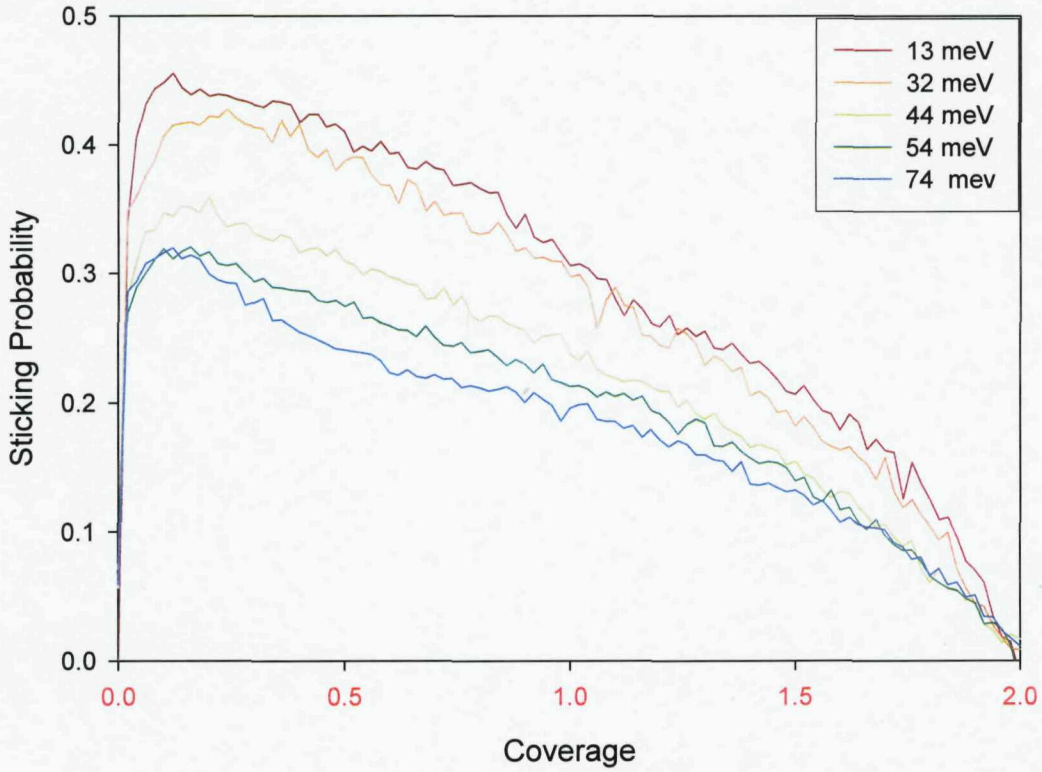

Figure 15: Sticking probability of H_2 as a function of hydrogen coverage on Mo(100) for a range of incident energies. Beam diameter=7 mm, $\varphi=0^0$, T_S=165 K and saturation coverage is 2ML. *The coverage values given here are based on the assumption that all adsorbed hydrogen remains within the beam diameter and does not migrate to area of the surface upon which the beam was not incident. Because there is good evidence that hydrogen migration does take place the coverage values recorded may be slightly larger than the true values, and for this reason are printed in red to highlight this potential inaccuracy (see also figures 16 and 17).*

Figure 15 shows a set of $S(\theta_H)$ plots taken at a low surface temperature (T_S=165K), where atomic hydrogen fully saturates the surface ($\theta_{H(sat)}$=2ML), over a range of E_i. At low energies (13-32meV) $S(\theta_H)$ displays complex behaviour, the sticking probability being largest at low coverage and $S(\theta_H)$ exhibiting an increasingly large negative gradient, $\delta S/\delta\theta_H$, with increasing coverage. This behaviour is often associated with an indirect extrinsic channel to dissociation, where the molecule being incident upon a vacant surface site is not integral to dissociative adsorption taking place, trapping also being able to take place upon already occupied sites, with the trapped molecule then able to move across the surface in search of vacant sites at which to dissociate. In the instance of an extrinsic channel at low E_i (the energy region in which an extrinsic channel will tend to be dominant) the sticking probability will tend to be almost

independent of θ_H at low coverages, with the dependence then tending to increase as the surface begins to saturate and finding vacant sites for dissociation becomes limiting.

Other possible causes of the complex coverage dependence are the migration of adsorbed hydrogen, indications of hydrogen migration across the surface having already been identified (chapter IV.3.3), and the formation of hydrogen induced surface reconstructions, these having also been previously identified and detailed (see figure 1) [4]. It is conceivable that the formation of different surface structures might act to either inhibit or promote further hydrogen adsorption, and that, if these surface reconstructions were to influence the direct sticking probability in a different manner to the indirect, they could even be envisaged to be responsible for the variation of the $S(\theta)$ plot as a function of E_i.(an increase in E_i shifting the balance of adsorption path from indirect towards direct dissociative adsorption). However, it is noted that the complex behaviour, particularly at higher coverage, is also strongly influenced by beam size (see figure 16). It is difficult to picture how these variations in coverage with changing beam diameter might be linked to surface structure reconstructions. An explanation for this dependence of the $S(\theta)$ plot shape on beam diameter could, however, be offered within the realms of the migrating hydrogen model.

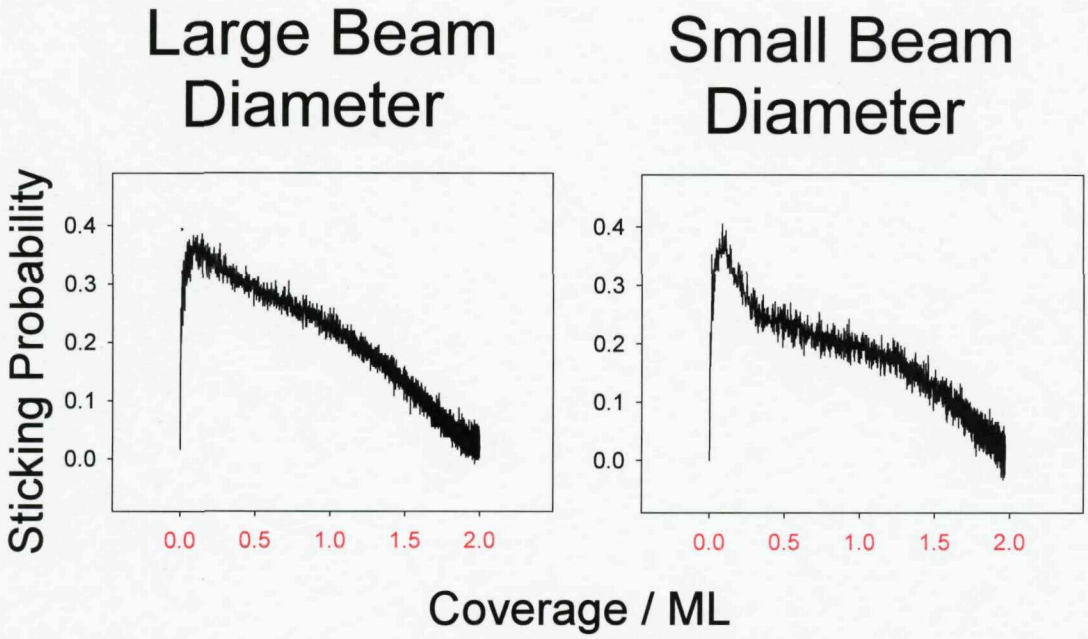

Figure 16: Plots of $S(\theta_H)$ using both a large and small beam diameter. Large beam diameter=7.5mm, small beam diameter=1.25mm. These result in the beams being incident upon ~70% and ~2% of the surface respectively. T_S=165K, $\varphi=0^0$ and E_i= 54meV

As has already been noted, hydrogen migration would be expected to have little effect at low coverage where the surface is mostly free of adsorbates, but to become more prominent as θ_H increases, with hydrogen atoms migrating to clean surface areas (upon which the beam is not incident) creating vacant sites within the surface area upon which the beam is incident. Such behaviour could be expected to maintain the sticking probability value as the coverage appeared to increase. This is because the coverage calculation makes the assumption that any hydrogen adsorbed by the Mo(100) surface remains within the area of the surface upon which the molecular beam is incident. Were the hydrogen to migrate to areas of the surface upon which the beam is not incident then the actual θ_H experienced by incoming H_2 molecules incident upon the surface would be lower than the recorded value (as noted in figure 15). If the beam diameter is small there will be plenty of clean Mo(100) surface surrounding the area upon which the beam is incident, whereas a larger beam diameter will encompass more of the sample surface. The larger beam diameter would therefore leave a smaller area of clean surface onto which adsorbed hydrogen could migrate and would thereby be expected to limit the effect (as is seen to be the case in figure 16).

The effect on the S(θ) plot associated with migration would be expected to exert greater influence at higher coverage. Migration of hydrogen will not affect the sticking probability upon the clean surface and can be expected to be most prominent when the area upon which the beam is incident nears saturation, with the availability of vacant surface sites for adsorption being entirely dependent upon the rate at which hydrogen diffusion takes place. Bearing this in mind it would seem that the identification of either extrinsic or direct type behaviour might best be identified by examining the low coverage region.

Concentrating on the low coverage region, the increase in E_i appears to correspond to the S(θ) plot exhibiting a steeper gradient. This fits well with the picture, suggested already during analysis of the S_0 as a function of E_i and T_S, in which an initially indirect extrinsic channel at low E_i is superseded by a direct channel as E_i increases. An extrinsic indirect channel would be expected to cause a significant drop in sticking probability of the extrinsic channel, whereas the direct channel would be expected to exhibit either an $S \alpha (1-\theta)$ or $S \alpha (1-\theta)^2$ relationship (depending upon whether a single, or two adjacent atomic adsorption sites, are required in order for a H_2 molecule to undergo direct dissociative adsorption).

As well as examining the $S(\theta_H)$ for a range E_i it was also examined for a range of T_S. When varying T_S it was necessary to take into account, when calculating the respective coverage values, that varying T_S could cause a variation in the saturation coverage of the surface. Using figure 6 to determine the saturation coverage at a given T_S and assuming the maximum saturation coverage of atomically adsorbed hydrogen to be 2ML, figure 17 has been produced tracing the $S(\theta_H)$ curves for $245<T_S(K)<416$.

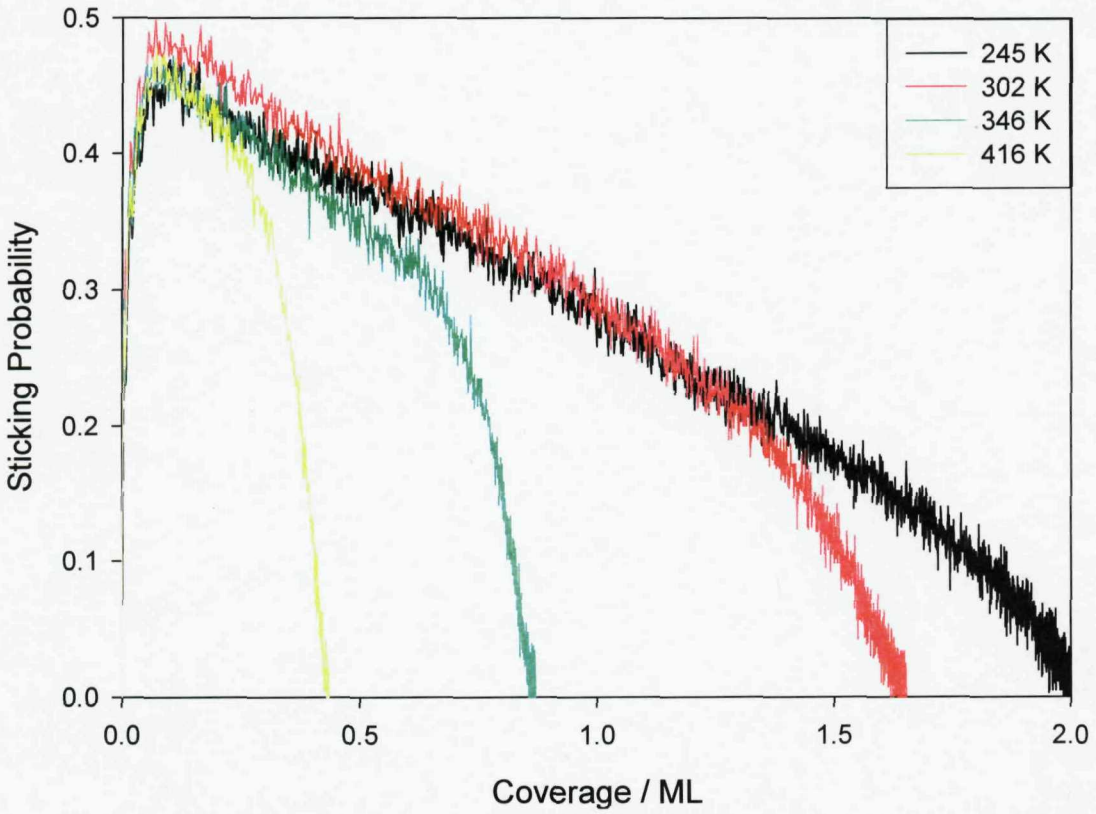

Figure 17: Sticking probability of H_2 as a function of hydrogen coverage on Mo(100) for a range of surface temperatures. $\varphi=0^0$, $E_i=32meV$, saturation coverage is surface temperature dependent and calculated using figure 6 and assuming a saturation coverage of 2ML at 245K.

At 32meV varying T_S appears to have little discernable effect on the shape of the $S(\theta_H)$ curve, suggesting that, if trapping takes place at this E_i, then increasing the surface temperature of the crystal does not reduce the ability of the hydrogen molecules to trap or of the trapped precursor to go on to dissociate.

IV.4 Analysis

IV.4.1 Dependence of S_0 on Incidence Energy

The implications of the non-monotonous behaviour of S_0 as a function of E_i for H_2 adsorption on the Mo(100) surface were discussed in the results section. The picture suggested was that of 3 dissociation channels, a typical fully accommodated physisorbing precursor at low E_i, a direct dissociation channel at high E_i, and a dynamic channel (either dynamic steering or a dynamic precursor) dominating the dissociative adsorption at intermediate E_i.

The large low energy channel of H_2 dissociative adsorption on Mo(100) (see figure 9), was seen to extend to incident energies well above that expected for a typical fully accommodated precursor channel for a H_2 molecule incident upon a transition metal surface, where only little energy transfer to surface phonons can take place due to the large mass mismatch, and where the broadening of electronic levels of H_2 molecules in front of metal surfaces [45] results in electronic excitations being very effectively quenched. This extended low energy channel is also seen on various other H_2/metal systems [46 and references therein] including the W(100) [10-12], Pt(533) [47,48], W(100)-c(2×2)N [12] and W(100)-c(2×2)Cu [13,14], and this behaviour is commonly attributed to a "dynamic adsorption channel".

The dynamic channel has been attributed to both dynamic steering and a dynamic precursor depending upon the surface. For example, ab-initio PES calculations for the H_2/W(100) system suggested steering as being responsible for the tendency of S_0 to continue to decrease as E_i increases beyond the range of the accommodated physisorbing precursor [19], with the presence of non-activated routes to direct dissociation on W(100) thought to help encourage a strong dynamic steering channel where molecules are often steered towards these favoured trajectories for dissociation. However, plenty of examples exist of systems where steering is thought unlikely to account for the dynamic adsorption channel. One such system is hydrogen adsorption on the Pt(533) surface [47,48] where hydrogen would be required to translate along the

4-atom wide (111) terraces in order to reach the dissociation site. CO and O pre-adsorption studies (where the CO or O is adsorbed purely onto the step) proved the step to be the site where desorption occurs, the blocking of the step site by CO or O causing the dynamic channel to disappear and leaving only the accommodated channel at very low E_i.

Debate surrounds the form of the dynamic channel of hydrogen on these various surfaces, for example, although PES calculations suggest steering to be responsible on W(100) [17,19,45,49] evidence has also been put forward to suggest that dynamic trapping is the channel responsible. A very precisely cut and well ordered W(100) crystal [11] was seen to exhibit an indirect channel considerably smaller in magnitude than a previous study of a W(100) surface [10], the differences being ascribed to the reduced defect site density, implying that a dynamic precursor dissociating at defect sites, as opposed to steering, is responsible for the channel. Studies of hydrogen adsorption upon the Cu alloyed W(100) surface observed S_0 to remain constant up to θ_{Cu}=0.5ML despite the corresponding TPD's showing a clear change in the surface and chemical adsorption potential. If the low energy channel of H_2/W(100) were of a direct type character such as dynamic steering it was thought that a change in adsorption potential would be accompanied by a change in S_0. S_0 was observed to remain constant with increasing Cu coverage for θ_{Cu}<0.5ML at E_i=35meV (this E_i being firmly inside the region where the dynamic channel is expected to dominate the dissociative sticking), the implication being drawn that adsorption took place via a dynamic precursor dissociating at defect sites which, unlike a steering channel, would not be significantly altered with Cu adsorption.

Although a dynamic channel does appear to be present, the shape of the $S_0(E_i)$ plot of H_2 on Mo(100) gives, as yet, no indication as to the character of the dynamic channel, both dynamic steering and dynamic trapping having been suggested to produce this long range low E_i channel extending to E_i far above that which is accountable by means of a fully accommodated precursor.

IV.4.2 Dependence of S_0 on Surface Temperature

From the data reported in section IV.3 three channels were identified for H_2 adsorption on Mo(100), occurring at low, intermediate and high E_i. The low energy channel demonstrated a clear T_S dependence, S_0 increasing with decreasing T_S, and this was attributed to a physisorbed fully accommodated precursor. The high energy channel was observed as being approximately T_S independent and was attributed to direct dissociation. The dominant channel at intermediate E_i was observed to display little or no T_S dependence, it being unclear whether S_0 remained independent of E_i or exhibited a slight decline with increasing E_i, this channel being attributed to a dynamic mechanism. Hard cube model calculations were performed and these strongly suggested that any T_S dependence associated with a precursor channel was due to the precursor's partition between dissociation and desorption rather than a temperature dependence of the initial trapping event.

The hard cube calculations were performed assuming the trapping to take place only via a physisorption well (~30meV), this falling well short of the >300meV required by the hard cube for the predicted T_S dependence of the trapping event to correspond to the observed T_S dependence at E_i=16meV. However, the implications drawn from the data analysis of $S_0(E_i)$ and $S_0(T_S)$ are that a physisorption channel coexists with a dynamic channel, this channel possibly being a dynamic precursor where the molecule may experience a dynamic trapping well. Given the possible contribution to the sticking of a dynamic precursor channel it seems pertinent to examine the possible contribution of such a dynamic channel to the cube calculations. Muller predicts a dynamic well (due to vibrational softening) of ~110meV as H_2 approaches a metal surface (in the case considered by Muller this is a Pt(111) surface, the (111) terraces of the Pt(533) surface have been demonstrated to be an active surface for dynamic trapping to take place and to display an almost identical temperature dependence to that observed here for Mo(100)). This potential well, although still falling some way short, is much closer to the depth required in order for the hard cube model to account for the T_S dependence of S_0 via the initial trapping event. However making cube calculations for a dynamic precursor well is not as simple as for a physisorption well. Physisorption is a relatively long range force, not dependent on the molecular

orientation or its position over the surface, whereas the dynamic well is dependent on the intra-molecular bond being weakened and this depends strongly upon molecular orientation and position, meaning that only some trajectories will provide full access to the dynamic well, hydrogen molecules on less favoured trajectories seeing only a reduced or negligible well. To estimate the true contribution full trajectory PES calculations should be performed in order to determine which trajectories contribute and to what extent. Without going this far it remains clear that the averaged dynamic potential well value experienced by the H_2 would be well below that calculated by Muller for the most favoured trajectory (molecular axis parallel to the surface above the bridge site) on Pt(111). It appears likely that the optimum dynamic well value will fall well short of that required by the hard cube model to account for the T_S dependence via trapping. Therefore, even with the inclusion of a dynamic well contribution to the hard cube model, the picture remains that of a T_S dependence being based on the partition between desorption and dissociation of the precursor rather than on the initial trapping event.

Even when taking into account a dynamic precursor well contribution calculations still predict little T_S dependence of the initial trapping event over the temperature range measured. The T_S dependence can therefore be considered as being accounted for almost entirely by the partition of the precursor channel between desorption and dissociation of the trapped precursor molecule. The partition function, as described by equation IV.11, can be rearranged to produce a y=mx+c type relation where $\upsilon_{des}/\upsilon_{diss}$ and ΔE can be determined from the y intercept and the gradient (respectively) of a plot of $\ln(\zeta/S_0-1)$ as a function of $1/T_S$.

$$\frac{\zeta}{S_0}-1=\frac{k_{des}}{k_{diss}} \qquad \textbf{(IV.12)}$$

$$\frac{\zeta}{S_0}-1=\frac{\upsilon_{des}}{\upsilon_{diss}}e^{-\frac{\Delta E}{RT_S}} \qquad \textbf{(IV.13)}$$

$$\ln\left(\frac{\zeta}{S_0}-1\right)=\ln\left(\frac{\upsilon_{des}}{\upsilon_{diss}}\right)-\frac{\Delta E}{RT_S} \qquad \textbf{(IV.14)}$$

As well as measuring the gradient and y intercept it is necessary to make an estimate of the trapping probability. According to the hard cube model, hydrogen adsorption on the Mo(100) surface is only expected to vary very slightly with temperature at 16meV (the hard cube plot exhibiting an increase in S_0 of only 0.012 over the range of temperatures recorded $167<T_S(K)<567$), therefore the estimate of the trapping probability can be expected to remain approximately constant within the temperature range covered by the data.

The partition function only describes the dissociative sticking probability taking place via an indirect accommodated channel, labelled here as $S_{0(accom)}$. Because the direct channel is predicted to be non-activated, and therefore still contribute to the sticking probability even at low E_i, the direct channel contribution must first be deducted from the data and a plot describing $S_{0(accom)}(T_S)$ produced. $S_{0(direct)}$ is estimated as being ~0.15 at E_i=16meV, and ~0.25 at E_i=32meV (see figure 18). In the case of the 16meV neon seeded beam, where a systematic error is present, the results are corrected further, increasing the S_0 value by 0.05 brings the values in line with those observed when having recorded $S_0(E_i)$ (see figure 9a).

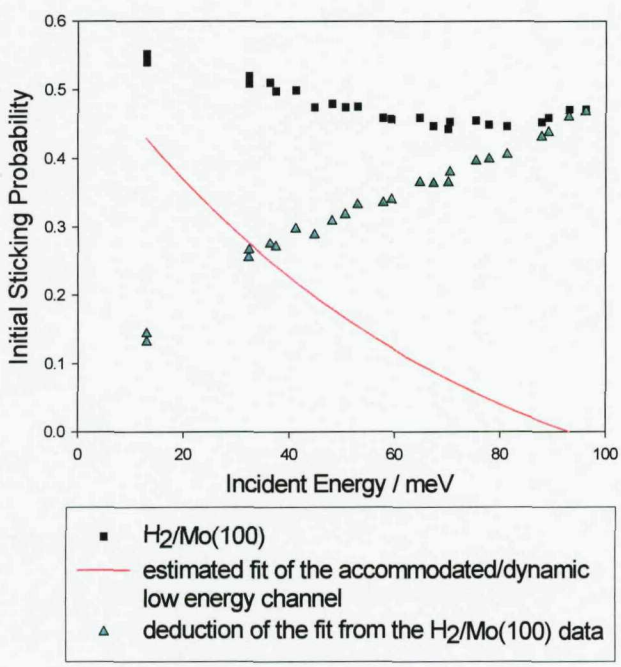

Figure 18: A "by sight" estimation of the accommodated/dynamic channel using a simple exponential decay and assuming a fit which converges with the data points as $E_i \rightarrow 0$, and falls away to a sticking probability of 0 when E_i=93meV. It should be noted that, according to accommodated/dynamic channel model predicted to be responsible for the decay in S_0 with increasing E_i, the true curve will not be a simple exponential decay, but the sum of 2 decays corresponding to sum of the accommodated and dynamic channels.

Figure 20 shows a plot of $S_{0(accom)}(T_S)$ at 16meV with the appropriate corrections. This plot is used to make an estimate of ζ, $S_{0(accom)} \rightarrow \zeta$ as $T_S \rightarrow 0$, provided $E_{des} > E_{diss}$. It is estimated that at 16meV $\zeta \approx 0.47$. Initially this estimate is based upon a simple linear regression and it should be noted that the equation defining the change in ζ with E_i does not result in a linear relationship (as illustrated by the computer generated fit shown in figure 20). It is therefore important to note that the value assigned to ζ is merely a best estimate given the available data and temperature range over which it has been recorded. By substituting in this value for ζ and plotting $\ln((\zeta/S_{0(accom)})-1)$ against $1/T_S$ figure 19 is produced.

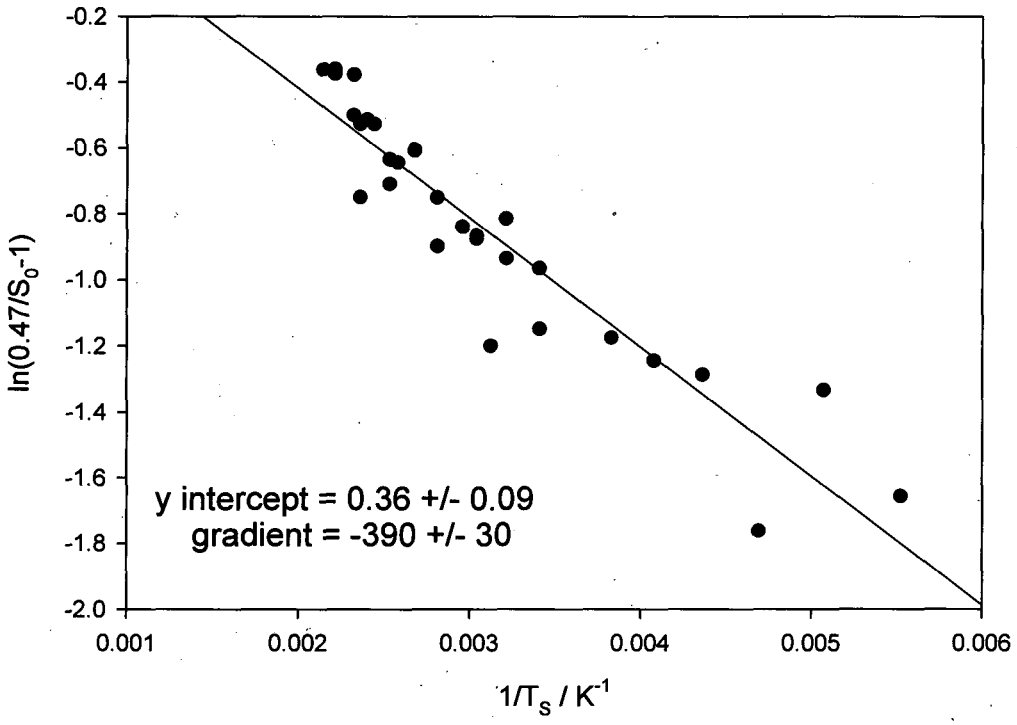

Figure 19: $\ln(\zeta/S_0-1)$ versus $1/T_S$, at E_i=16meV, $\theta=0^0$, for $180<T_S(K)<460$. The errors are calculated from the deviation of the data points from the linear regression

Measuring the gradient of the plot as being -390 +/- 30 K a value for E_{des}-E_{diss} is determined:

$$\Delta E = 3.2 \pm 0.2 \text{ kJmol}^{-1}$$

Similarly after measuring the y-intercept as being 0.36 +/- 0.09 a value for $\upsilon_{des}/\upsilon_{diss}$ is determined:

$$\frac{\upsilon_{des}}{\upsilon_{diss}} = 1.4 \quad +/- \ 0.4$$

The errors described here for ΔE and $\upsilon_{des}/\upsilon_{diss}$ are derived only from those described in figure 19 relating to the deviation of the data points from the linear regression. The true errors may be considerably larger, relating also to the estimation of ζ, and the estimation of the relative size of the direct channel as well as the size and nature of any contribution from a dynamic channel at the specific E_i.

Substituting the calculated values for ΔE, $\upsilon_{des}/\upsilon_{diss}$, and the estimated trapping probability, into equation IV.11 allows for the production of a plot of $S_{0(accom)}(T_S)$ which should fit well to the data. This can be seen in figure 20 (black line).

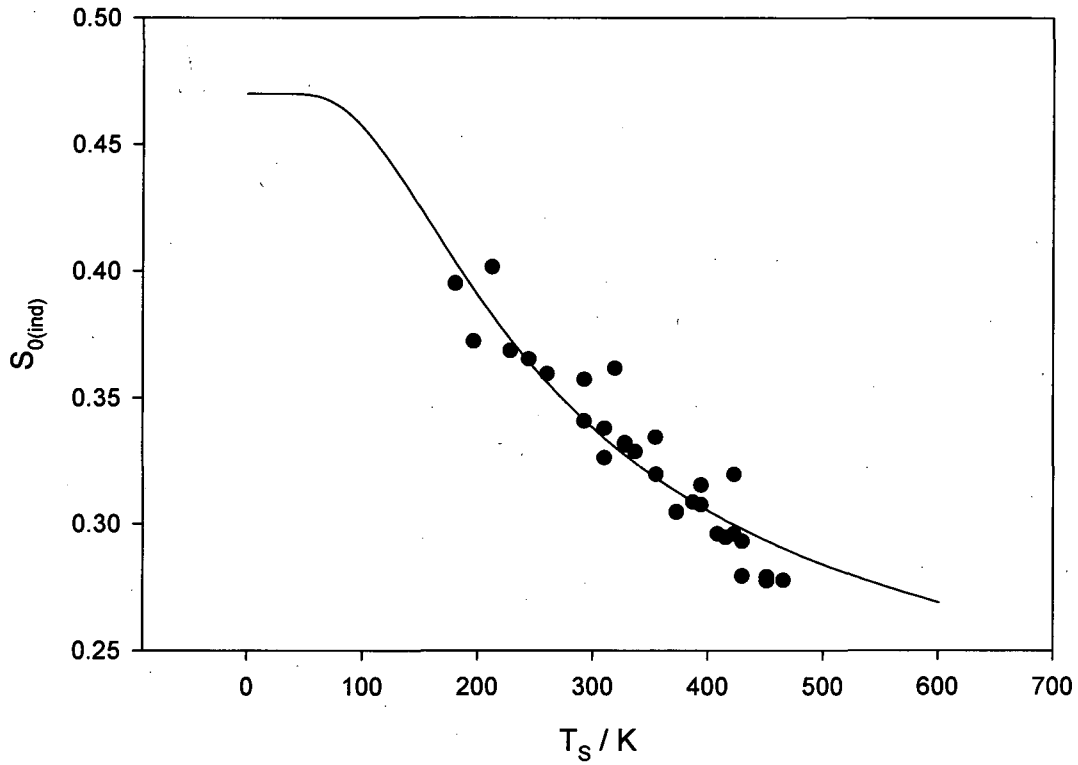

Figure 20: The indirect initial sticking probability, with the direct channel removed, plotted as a function of surface temperature, E_i=16meV, $\varphi=0^0$ *(black circles).*

Black line is $S_0 = \zeta\left(1+\frac{\upsilon_{des}}{\upsilon_{diss}}e^{\left(-\frac{\Delta E}{RT_S}\right)}\right)^{-1}$ with ζ=0.47, $\upsilon_{des}/\upsilon_{diss}$=1.4 and ΔE=3.2 kJmol^{-1}, plotted as a function of surface temperature.

A value of ΔE=3.2 +/- 0.2 kJmol^{-1} is equivalent to 33 +/- 3meV. E_{des} from a physisorbed precursor well, where no barrier to the trapping well is expected, should be equal to the potential well depth and this is predicted as being ~30meV for H_2 physisorbing on a transition metal surface. This implies that the contribution from E_{diss} is 0. This lack of a barrier to dissociation of the precursor would fit well with the picture already presented of a surface at which non-activated direct dissociation may take place, the implication being that little barrier exists to dissociation into the bridge site whether via direct or precursor mediated channels.

It must be noted that the error on ΔE may be considerably underestimated. The ΔE calculation relies on a value of ζ obtained via a linear regression to obtain a y-intercept, however (as described by equation IV.11 and illustrated by figure 20) a linear regression is only a rough estimation and not a true fit. Any error on ζ would be a

systematic error and therefore would not manifest itself in the errors calculated by determining the deviation of the data points from the linear fit of figure 19.

Additional errors originate from the assumption made in the partition function of equation IV.11, that all dissociative adsorption takes place via a typical accommodated precursor channel, $S_{0(accom)}$. Modifications to this have already been discussed in terms of deducting the direct channel contribution, $S_{0(direct)}$, which, due to the non-activated nature of the channel, will contribute to $S_{0(total)}$ even at low E_i. This estimation of the direct channel may also carry with it a constant systematic error.

Even after taking account of the direct channel contribution, there may still remain a contribution from a "dynamic channel", $S_{0(dynamic)}$, to the total initial sticking probability.

$$S_{0(total)} = S_{0(accom)} + S_{0(dynamic)} + S_{0(direct)} \qquad \textbf{(IV.15)}$$

The partition function of equation IV.11 in reality only describes the fully accommodated precursor channel, $S_{0(accom)}$, therefore deductions should be made from the total initial sticking probability to account for the presence of the direct and dynamic channel contributions, as described by equation IV.16 below:

$$S_{0(accom)} = S_{0(total)} - S_{0(dynamic)} - S_{0(direct)} \qquad \textbf{(IV.16)}$$

The uncertainty in the size and even the nature of the dynamic channel make it impossible to include a correction for this value, with the assumption having been made that $S_{0(dynamic)}=0$ at E_i=16meV. The contribution from a dynamic channel may introduce a further error to the calculation of ΔE and $\upsilon_{des}/\upsilon_{diss}$.
The uncertainty in the nature of the dynamic channel, being either dynamic steering or a dynamic precursor, makes it unclear whether the dynamic channel itself may contribute to the T_S dependence observed. If dynamic steering is responsible for the channel it could be considered to behave as a direct channel, remaining virtually unaffected by T_S. The dynamic precursor channel on the other hand may, like the physisorbed precursor, be governed by a partition function. However, even in the case

of a T_S dependent dynamic precursor channel the partition function of equation 11 may not provide an accurate description of the T_S dependence of the partition between dissociation and desorption of the dynamic precursor.

The typical picture of the dynamic precursor is of a molecule which accommodates energy to other molecular DOF as opposed to the surface, allowing trapping to take place for considerably higher E_i than would be possible for a typical physisorbing precursor. Whether, once trapped, the multiple rebounds predicted to take place with the surface [27,28,30] would allow accommodation of the energy of the precursor with the surface is a matter for debate. Recent theoretical calculations have suggested that the enhanced interaction time of the dynamically trapped hydrogen on Pd surfaces may result in the dissociation probability of the dynamic precursor exhibiting a significant T_S dependence [30]. At the very least it seems likely that a partition function describing the fraction of dynamically trapped molecules going on to dissociate, as opposed to desorbing, should include a modified partition function, the modification being represented here as χ, describing the extent to which the molecule is able to accommodate with the surface temperature (see equation IV.17).

$$S_{0(accom.)} = \zeta\left(1+\frac{\upsilon_{des}}{\upsilon_{diss}}e^{\left(-\frac{\Delta E}{RT_S}(\chi)\right)}\right)^{-1} \qquad \textbf{(IV.17)}$$

Where $\chi \rightarrow 1$ when the dynamic precursor always fully accommodates with the surface temperature,

And $\chi \rightarrow 0$ when no energy exchange takes place between the dynamic precursor and surface.

An identical gradient to that recorded here for the lowest E_i regime is also observed for hydrogen adsorption on the Pt(533) surface at similar E_i ($dS_0/dTS=-4\times10^{-4}$ K^{-1}) [47,48]. As has already been mentioned, the Pt(533) surface is made up of 4 atom wide terraces of (111) separated by (100) steps, and exhibits a dynamic channel to dissociative adsorption very similar to that of the Mo(100). On Pt(533) adsorption of sufficient CO to block all step sites was seen to remove the dynamic adsorption

channel while leaving the direct and accommodated precursor channels intact. This removal of the dynamic channel was not seen to correspond to any change in the T_S dependence with dS_0/dT_S also recorded as being -4×10^{-4} K^{-1} on CO/Pt(533) at the corresponding E_i [48]. The implication here is that this temperature dependence is associated entirely with the accommodated physisorption channel and that the dynamic channel is T_S independent. Given the identical T_S dependence of the Pt(533) and Mo(100) surfaces it seems not unreasonable to draw parallels. By E_i=32meV, where the accommodated physisorption channel of Mo(100) is predicted to make close to negligible contribution to the sticking probability, the T_S dependence of S_0 is seen to diminish from that observed at 16meV to just $dS_{0(ind)}/dT_S=-1.4\times10^{-4}$ +/- 0.2×10^{-4} K^{-1} (see figure 13), clearly suggesting that the main contributor to the T_S dependence at 16meV is the physisorption channel. It is not clear however whether the small T_S dependence at 32meV is merely due to the remnants of the physisorption channel, or due to a weakly T_S dependent dynamic channel.

If the T_S dependence at 32meV is considered to be associated almost entirely with the accommodated physisorption channel then the dynamic channel should be pictured as having very little or no T_S dependence, i.e. that $\chi\approx0$ in equation IV.17, as is suggested to be the case on Pt(533) [47,48]. . A weak or non-existent T_S dependence of the dynamic channel would agree with either the picture of a dynamic precursor, where normal translational energy is converted to other molecular DOF in order to allow trapping to take place with little or no accommodation of energy to the surface, or dynamic steering where adsorption takes place via an essentially direct type mechanism which requires no energy exchange with the surface to take place. The picture of a dynamic precursor exchanging little or no energy with the surface upon a collision can be understood in terms of a poor mass match and short interaction time of the H_2 with the surface causing energy exchange to be unusually inefficient.

Although this picture of the combination of fully accommodated and dynamic precursor would offer good agreement with that which has been suggested as being responsible for the H_2/Pt(533) system [47,48], the hard cube model predictions estimate the physisorption channel contribution to S_0 to drop to negligible levels already at ~25meV. The picture of a temperature independent dynamic channel would require the physisorption channel to still make a significant contribution to S_0 at

32meV in order to account for the T_S dependence present at this energy, which, although small, still produces a gradient ¼ the size of that seen at 16meV. However, over such a small energy range the hard cube model is not recognised as an accurate measure and should be viewed more as a rough guide, tending to provide only qualitative rather than quantitative agreement with actual observations. If the contribution of the physisorption channel at 32meV were viewed as being negligible, and the T_S dependence to be entirely due to the dynamic channel, this small but significant dependence of S_0 on T_S would favour the dynamic precursor picture over that of steering, with the energy exchange of the precursor with the surface possibly being enhanced by the multiple rebounds predicted to take place once trapping has occurred [27,28,30], enhancing the interaction time of the molecule and surface.

IV.4.3 Dependence of S on Hydrogen Coverage (θ_H)

The results from the $S(\theta_H)$ plots have been interpreted as being indicative of an indirect channel to dissociation being replaced by a direct dissociation channel as E_i is increased. This is in agreement with the picture presented by the data describing $S_0(E_i)$ and $S_0(T_S)$.

At E_i=32meV the shape of the $S(\theta_H)$ curve did not change in character with T_S (see figure 17). This lack of T_S dependence suggests that, if trapping takes place at this E_i, then increasing the surface temperature of the crystal does not reduce the ability of the hydrogen molecules to trap, or of the trapped precursor to go on to dissociate. Particularly when considered in conjunction with the much reduced T_S dependence of S_0 at 32meV with respect to that observed at 16meV (see figures 11 and 13), this lack of T_S dependence on $S(\theta_H)$ supports the idea that the dominant channel at 32meV is influenced very little by changes in T_S of the sample, and that a separate (T_S dependent) precursor channel must operate at lower incident energies to account for the T_S dependence observed at the lowest E_i, i.e. two low energy channels are present, one accommodated (dominant at the lowest E_i) and one dynamic and independent of T_S (dominating the intermediate E_i region). This is consistent with a typical accommodated physisorbing precursor making a large contribution to the dissociative

sticking probability at 16meV, but a dynamic mechanism, either dynamic steering within a direct channel, or a dynamic precursor within an indirect channel, coming to prominence by 32meV, before both being dominated by a typical direct channel at the high end of the incident energy spectrum (<80meV). Such an explanation would account well for the hard cube predictions which suggest a significant contribution to sticking (~25%) via a physisorbing precursor channel at 16meV, becoming insignificant (falling to <5% contribution to the total sticking probability) by 32meV (see figure 9b). By accounting for the temperature dependencies observed for H_2 on Mo(100) via a physisorbing precursor channel the uncertainty returns as to whether the dynamic contribution is via steering or an indirect precursor mechanism, both equally able to account for the drop in S_0 with increasing E_i and the reach of the low energy channel to unusually high incident energies with respect to what is predicted for a physisorbing accommodated precursor.

IV.4.4 Comparison Of H_2/Mo(100) and W(100) Adsorption Dynamics

The considerable similarity between Mo(100) and W(100) (the bcc bulk structure, the lattice spacing, the electronic structure, and the low temperature reconstruction), and the kinetics of hydrogen adsorption upon the two (hydrogen bridge bonding on both, the H causing the bridge site to form a dimer reconstruction, and both having a saturation coverage of 2ML), have already been considered in some detail (see sections IV.2.2).

Given these similarities it is perhaps unsurprising to find that the adsorption dynamics of the H_2/W(100) system in particular [10-12] shares many characteristics with those observed here for the H_2/Mo(100) adsorption system. Among them the large and heavily overlapping direct channel common in both, this being accompanied on both surfaces by a low energy channel decaying over an unusually large energy range, and sticking probabilities commonly within ~0.1 of those observed here for the Mo(100) surface (see figure 21).

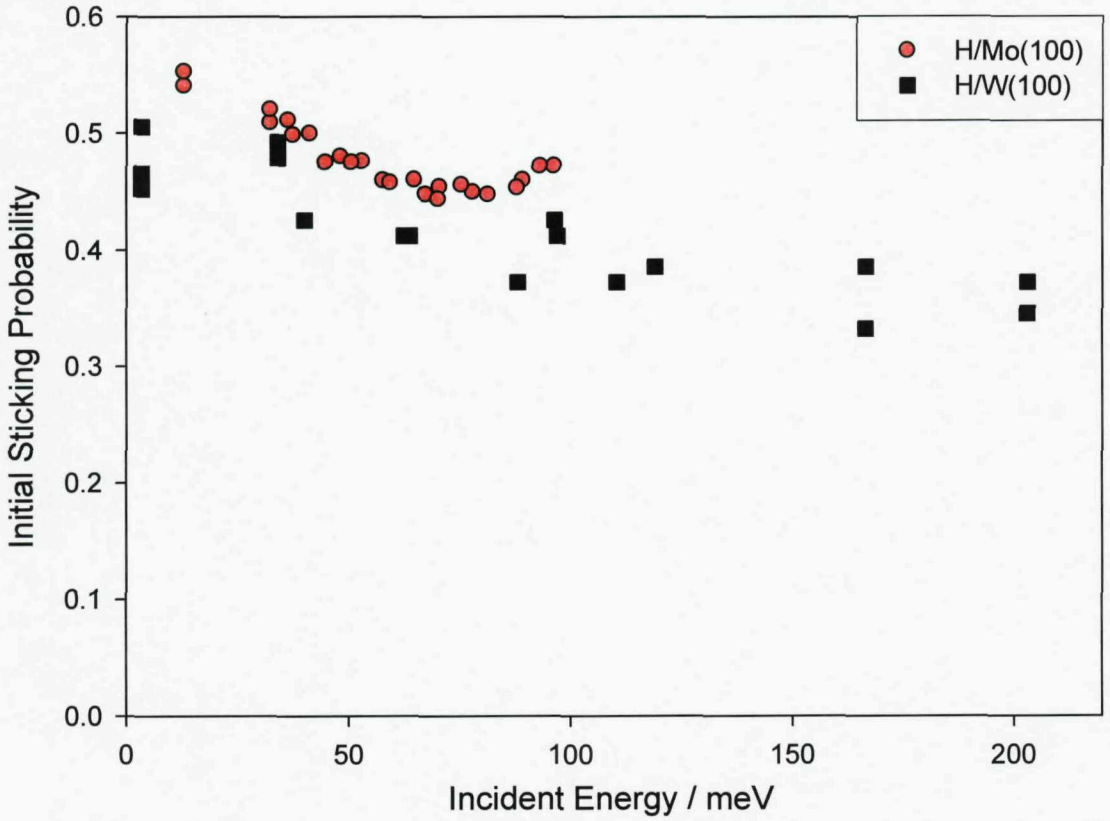

Figure 21: $S_0(E_i)$ of H_2 on Mo(100) at T_S=165K (red circles), and on W(100) (black squares) at T_S=300K (S_0 shown to be T_S independent on W(100)) . Both beams are directed perpendicular to the surface ($\varphi=0^0$)

The influence of the direct channel appears to be somewhat larger on the Mo(100) surface. Ab initio PES calculations of the H_2/W(100) system have revealed a surface with routes to direct dissociation where no barrier is encountered [19,46]. This is supported by calculations performed on dynamics data indicating a non-activated direct channel to be present on W(100) [14]. The non-activated direct channel for H_2 dissociation on W(100) implies that, with its larger direct channel, this is also the case for Mo(100). The greater contribution to S_0 of the direct channel on the Mo(100) surface implies that the barrier to direct dissociation on this surface is in general lower for a given trajectory, allowing a greater range of non-optimized trajectory barriers to be overcome at a given E_i.

Whereas the direct channel appears to be more dominant upon the Mo(100) this does not appear to be true of the indirect channel. The extension of the low E_i channel above that which can be understood in terms of an accommodated physisorbing precursor

channel has already been identified on W(100) [11,14] and Mo(100) (figure 9b) and attributed as strong evidence of the presence of a dynamic channel to dissociative adsorption. The reach of the low E_i channel of H_2 adsorption on the W(100) surface extends to higher still E_i values than were observed for Mo(100), with the channel making a significant contribution to S_0 up to ~150meV, double the E_i to which it appears to extend on Mo(100) and far above those predicted by the hard cube model of a fully accommodated physisorbed precursor channel. The extension of this channel to greater E_i on the W(100) surface might be indicative of differing dynamic channels upon the two surfaces, or a symptom of the differing adsorbate-adsorbate interactions and corresponding surface structures, as will be described shortly when comparing the behaviour of H_2 adsorption on the two surfaces with increasing hydrogen coverage. Alternatively it might imply that:

a) If a dynamic precursor is responsible for the channel, the greater radial extension of the 5d wave function of the W over the 4d of the Mo could result in more interaction of the electron density of the substrate with the anti-bonding orbitals of the H_2, causing a greater degree of vibrational softening to take place and creating a deeper dynamic precursor well on the W, better capable of trapping the H_2 molecules than the more shallow well of the Mo substrate.
b) If steering is the mechanism responsible then the curvature of the PES on W(100) may be more suited to the steering of energetic H_2 molecules than that of the Mo(100) surface.

The S_0 values appear in general slightly lower on W(100) (see figure 21), although there are conflicting reports within the literature as to the magnitude of the indirect channel on the W(100) surface, with other work showing a steeper increase in S_0 with decreasing E_i [10]. In this case S_0 does not entirely follow the trend displayed by the Mo(100) surface with S_0 values rising well above those of Mo(100) at low E_i, but this is explained in the literature as being most likely due to a relatively large concentration of defect sites on the surface used by the particular study enhancing the indirect channel to dissociation [11,12].

At low E_i hydrogen adsorption onto the W(100) surface exhibits a complex coverage dependence. S exhibits a coverage independence or even increases with coverage (for high and low surface temperatures respectively), this increase peaking at ~0.3ML. The complex coverage dependence persists up until a coverage of ~0.5ML, thereafter changing to a linear type $S = a(1-\theta)$ relationship, as illustrated in figure 22b and 22c (below).

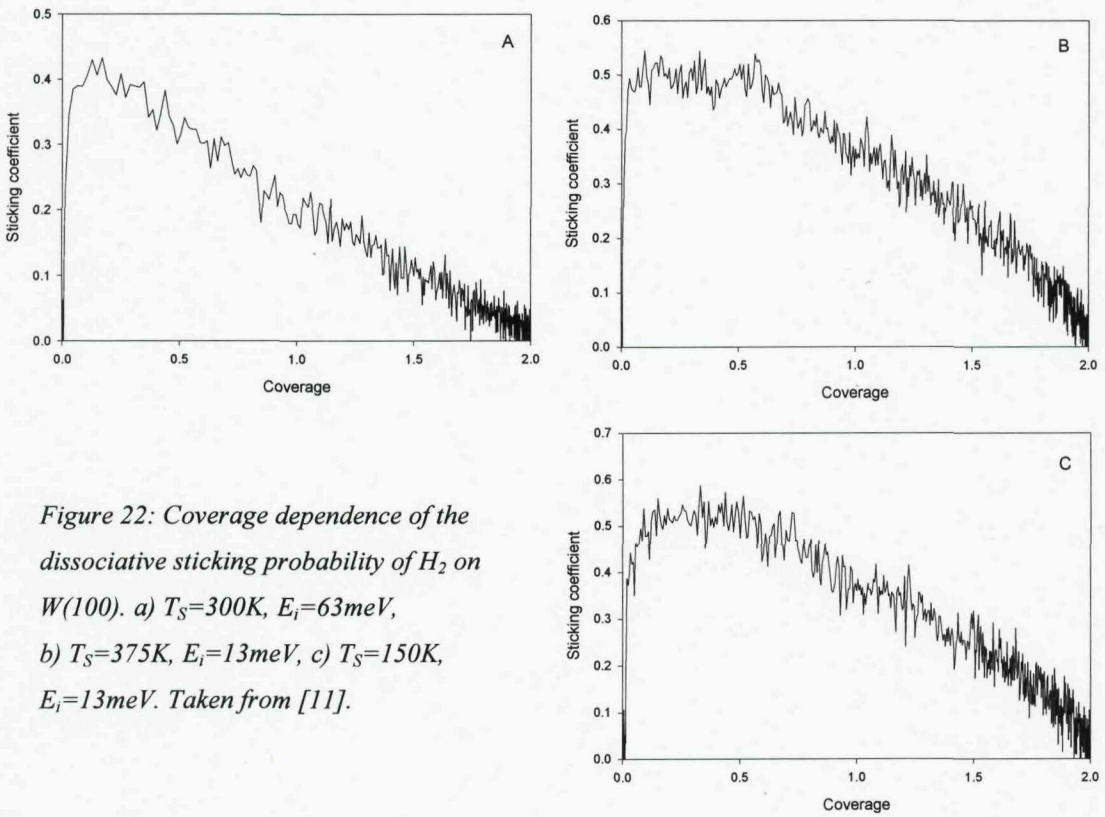

Figure 22: Coverage dependence of the dissociative sticking probability of H_2 on W(100). a) T_S=300K, E_i=63meV, b) T_S=375K, E_i=13meV, c) T_S=150K, E_i=13meV. Taken from [11].

Initially attempts were made to explain this behaviour within the framework of an accommodated indirect precursor channel. The suggestion was made that co-existing intrinsic and extrinsic precursors might account for the complex coverage dependence [11] (it being postulated that the adsorbed H producing a much better mass match for the incoming H_2 molecule might be sufficient to allow it to lose sufficient energy in a collision to be able to trap into the precursor state compared to a collision with a W substrate atom).

Interestingly it was noted that the maximum sticking probability (S_{max}), caused by the initial rise in sticking from the S_0 value as the coverage increased, exhibited a T_S dependence. It was suggested that the lack of T_S dependence of S_0 and the relative T_S dependence of S_{max} might be accounted for by the intrinsic and extrinsic channels respectively, with the intrinsic channel accounting for S_0 and being T_S independent, and the extrinsic channel having a T_S dependence and being responsible for S_{max}. The better mass match within the extrinsic channel of H_2 colliding with a hydrogen adatom, as opposed to that of the intrinsic channel where H_2 collides with a W atom of the substrate, might enhance the accommodation of energy to the surface and allow a T_S dependence to manifest itself.

However, this picture of intrinsic and extrinsic precursors did not satisfactorily account for all observations, with no evidence existing for precursor type trapping upon the saturated W(100)-(1×1)H surface, scattering data revealing the collision of the H_2 with this surface to be dominated almost entirely by an elastic event [11]. Furthermore, recent work using a surface oscillator model [30] casts some doubt as to whether mass match is the defining factor in determining the energy exchange between incident molecule and surface, suggesting that it is almost entirely dependent only upon the mass of the incident molecule.

An alternative suggestion was that the complex coverage dependence displayed by W(100) was largely due to surface structure changes induced by H adsorption. Evidence has been presented suggesting that the complex coverage dependence is associated specifically with adsorption into the β_2 state. Using a thermal source hydrogen has been adsorbed separately into the β_1 and β_2 states on the W(100) surface, with adsorption into β_1 observed to display a linear coverage dependence and β_2 a clear coverage independence [50]. Adsorption into the β_2 state corresponds to the creation of the c(2×2) structure and adsorption into β_1 its destruction [16,50], with 0.5ML being the coverage at which the c(2×2) structure disappears [6,16,51] and this corresponding also to the disappearance of the complex, and onset of the linear, coverage dependence.

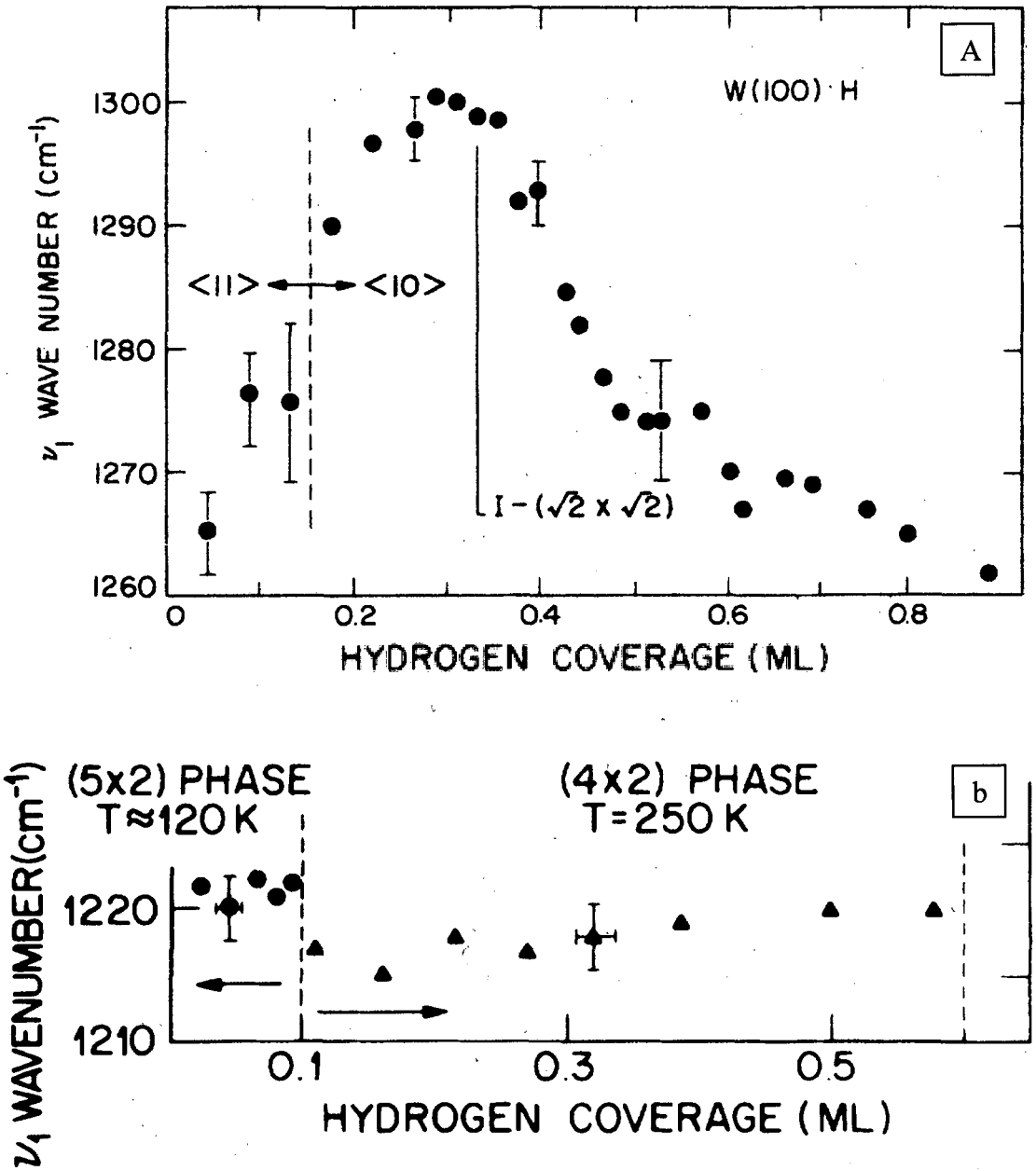

Figure 23: The wavenumber of the symmetric stretch mode (υ_1) as a function of hydrogen coverage for a) W(100) and b) Mo(100). υ_1 depends on the local substrate arrangement (i.e. the Mo-Mo or W-W dimer length), with larger symmetric stretch frequency indicative of shorter dimer length.. Both (a) and (b) are taken from [6]. The smallest dimer lengths for these reconstructed surfaces has been estimated as being 2.74 Å and 2.73Å for the W and Mo hydrogen induced reconstructed surfaces, respectively [6].

The wavenumber of the symmetric stretch mode is a measure of the degree of surface reconstruction, a larger stretch frequency indicating a more contracted dimer and hence

a greater degree of surface reconstruction around the hydrogen adsorption site. There is a correlation between the change in υ_1 and S as a function of θ_H for the H_2/W(100) system, with S_{max} occurring at ~0.3ML, the same value at which the surface reconstructed (as measured by υ_1) is greatest (figure 23a). In this respect W(100) should differ from the H_2/Mo(100) system which produces the most highly reconstructed bridge site already at the very lowest coverages (figure 23b). The reconstruction of the Mo(100) surface for $0<\theta_H(ML)<0.5$, sees little change in the bridge adsorption site, a fairly consistent Mo-Mo dimer length being maintained (as illustrated in figure 23b), the υ_1 wavenumber varying by as much as 40cm^{-1} on the W surface but by only ~5cm^{-1} on Mo. This is coupled with Mo(100) lacking the increase in S with θ_H seen for H_2 adsorption onto W(100) (figure 24).

The plot of $S(\theta_H)$ for the Mo(100) system displays a maximum sticking probability at lowest coverage (i.e. $S_{max}=S_0$) and exhibits an increasingly large negative gradient with increasing coverage (see figure 24a), with no sign of the boundary that defines the H/W(100) system, where at a particular θ_H the complex coverage dependence switches off to be replaced by a linear decrease in sticking probability with increasing coverage.

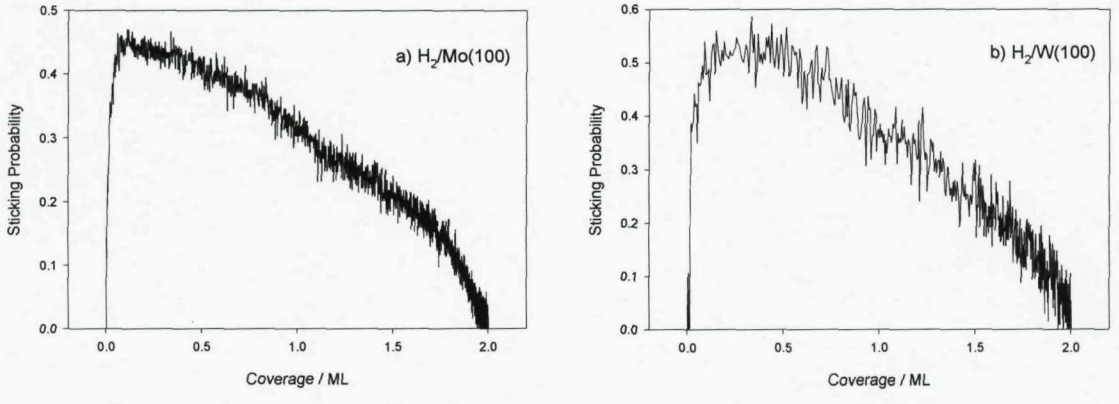

Figure 24: Sticking probability of H_2 on a) Mo(100), and b) W(100), as a function of coverage at low incident energy, E_i=13meV, and low surface temperature (Mo(100) T_S=165K, W(100) T_S=150K)

It seems unlikely that this correlation between the reconstruction of the adsorption site and behaviour of $S(\theta)$ for the two surfaces is merely coincidental. Instead it appears that changes in the sticking probability associated with the indirect channel are

determined by the degree of reconstruction of the favoured bridge adsorption site and the dissociation of the H_2 precursor at this site.

The production of a larger substrate atom displacement around the bridge site, as the favoured c(2×2) reconstruction is approached (analysis of IR frequency shifts putting the smallest dimer length at 2.74Å and 2.73Å for W and Mo respectively [6]), might indeed produce a site where H is more tightly bound and cause a subsequent drop in the barrier to dissociation encountered by the precursor. Figure 25 is a simplistic 1D representation of how this might be envisaged as taking place. It was estimated that an energy of 7meV was associated with the change in the local distortion around an isolated hydrogen (θ_H<0.1) on the W substrate from that experienced at ~0.3ML when the c(2×2) reconstruction is complete [16].

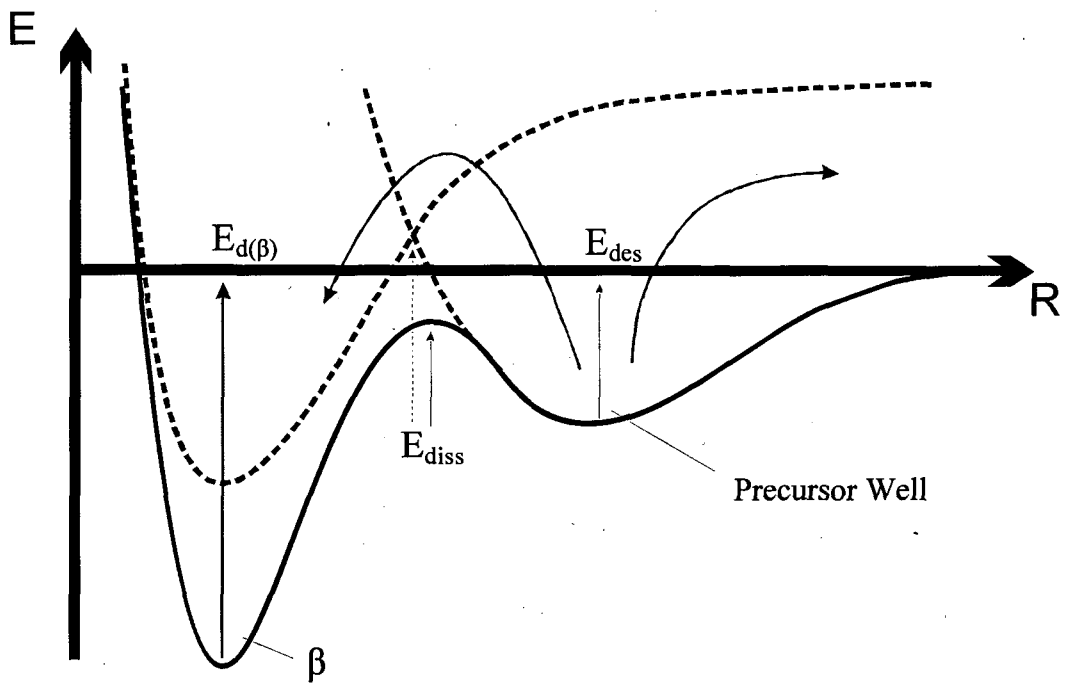

Figure 25: A simplistic 1D PES representation of hydrogen dissociative chemisorption via a dynamic precursor trapping well, where the potential energy is plotted as a function of the molecules perpendicular distance from the surface, R. The dotted line represents the hydrogen atom dissociating into a less tightly bound adsorption site and how this might result in an increase in the barrier to dissociation experienced by the precursor (E_{diss}). The precursor well and dissociative adsorption well (β) are labelled. $E_{d(\beta)}$ denotes desorption from the atomically adsorbed state, E_{des} indicates desorption from the dynamic precursor state and E_{dess} dissociation adsorption of the precursor. This type behaviour is the basis of the Bronstead Evans Polonyai relationship (used to produce volcano type plots defining a catalysts relative activity).

The evidence presented here has strongly suggested that the coverage dependence of the indirect channel to H_2 dissociative adsorption on Mo(100) and W(100) is heavily dependent on the surface reconstructions that take place as the hydrogen coverage of the surface increases. This difference in $S(\theta_H)$ behaviour for Mo(100) and W(100) is therefore likely to be due to the different mechanisms by which the 2 surfaces reconstruct. The island structure of H/Mo(100) allows immediate access to the most reconstructed dimer site, with first order phase transitions seeing islands of fully reconstructed surface growing in size as hydrogen coverage increases, whereas the 2nd order phase transition occurring across the entire W(100) surface sees the surface only gradually reconstructing with θ_H, reaching maximum bridge site substrate atom displacement only after substantial hydrogen adsorption has already taken place (~0.3ML). The difference can be traced to differing adsorbate-adsorbate interactions on the two surfaces, leading to 1st order island formation on Mo(100) but a gradual 2nd order phase transition across the entire surface on W(100) (as discussed in detail in section V.2.2).

The S_0 of H_2 on the Mo(100) surface displays a negative T_S dependence at low E_i (dS_0/dT_S=-4.1×10^{-4} K^{-1} at E_i=13meV). No such dependence is observed on the W(100) surface with S_0 recorded as being T_S independent at this energy [11]. However precisely this relationship is observed on W(100) for $S_{max}(T_S)$, with dS_{max}/dT_S=-4.1×10^{-4} K^{-1} at E_i=13meV. This similarity is not surprising since S_{max} on W(100) refers to adsorption into the fully reconstructed bridge site, equivalent to S_0 on Mo(100). In fact in the case of Mo(100) S_0=S_{max}.

For H_2 dissociation on both W(100) and Mo(100) S_{max} only displays a T_S dependence at very low E_i (this having been already examined earlier in this chapter where $-dS_0/dT_S$ was seen to drop by ¼ between E_i of 13meV and 32meV). In the case of Mo(100) this was presented as evidence of a fully accommodated physisorbing precursor channel dominating hydrogen adsorption at low E_i. It seems reasonable for the same conclusion to be drawn here for the channel responsible for adsorption into the fully reconstructed bridge site of W(100), i.e. that at E_i=13meV, S_{max} of H_2 on W(100) is determined primarily by an indirect adsorption channel where dissociative adsorption takes place via a fully accommodated physisorbing precursor.

It is difficult to imagine how the degree of bridge site reconstruction could significantly affect the initial trapping probability of the physisorbing H_2 molecule. Therefore it seems reasonable to conclude that the change in T_S dependence from the independence of S_0, to the $dS_0/dT_S=-4.1\times10^{-4}$ K^{-1} of S_{max} on the W(100) surface, is due to a change in the partition between dissociation and desorption of the precursor.

Assuming the T_S dependence of the sticking probability into the reconstructed or unreconstructed bridge site is determined by the partition function then the lack of T_S dependence of S_0 implies that in the case of adsorption of the precursor into the unreconstructed bridge site $E_{des}\approx E_{diss}$. The ability of the bridge site reconstruction to produce a more tightly bound H adatom and the related drop in barrier to dissociation this might produce has been described above (illustrated by figure 25) and would fit well with this picture, with the negative T_S dependence of S_{max} (according to equation IV.11) implying that $E_{des}>E_{diss}$ for H_2 adsorbing into the reconstructed bridge site.

In the past the lack of T_S dependence of H_2 adsorption on W(100) even at low E_i has been offered as evidence of dynamic steering [18,52,53] or of a dynamic precursor with virtually no energy exchange taking place between the precursor and surface [14]. However the comparison of the H_2/W(100) with H_2/Mo(100) and the above analysis of the two has lead to the conclusion that a fully accommodated channel contributes significantly to the dissociative adsorption probability of hydrogen on W(100) at $E_i\leq16$meV and that the lack of T_S dependence is due predominantly to $E_{des}\approx E_{diss}$ within the context of the partition equation (equation IV.11) describing the dissociation or desorption of the fully accommodated physisorbed H_2 precursor.

Whether the degree of reconstruction of the bridge site affects the dissociative adsorption probability via the dynamic channel might be interesting to examine. This would be done by comparing $S_0(E_i)$ with $S_{max}(E_i)$ over the intermediate energy range (roughly $32<E_i(meV)<150$) at which the dynamic channel of H_2/W(100) is thought to dominate. The currently favoured picture is of a dynamic precursor dissociating at defect sites [14]. Such a channel might be expected to remain unaffected by changes in the substrate lattice, with defects sites likely to remain unaffected by a hydrogen induced reconstruction of the bridge site.

IV.5 Conclusions

The dissociative adsorption of hydrogen has been studied on the Mo(100) surface using molecular beam techniques [54] to monitor the dependence of the dissociative sticking probability as a function of incident energy of the H_2 molecules, temperature of the Mo(100) substrate, and hydrogen coverage.

The initial sticking probability of H_2 varies non-monotonously with incident energy. This is typical of coexisting direct and indirect channels (e.g. N_2 adsorption on W(100) [39,41,42]), with a channel spanning the low incident energies, typically associated with indirect adsorption, seeing sticking probability drop with increasing incident energy as it becomes more difficult for the surface to accommodate sufficient energy for the initial trapping event to take place, and a channel coming to prominence only at higher incident energies, associated with direct dissociative adsorption, seeing sticking probability increase with increasing incident energy as the additional energy allows the molecule to access non-optimised dissociation trajectories. Using the W(100) system as a guide [14], the direct channel was determined to be non-activated, i.e. molecules with preferential trajectories adsorb without encountering a barrier to dissociation.

A fully accommodated indirect channel exists for the dissociative adsorption of H_2 molecules with low incident energy. This channel exhibits a complex coverage dependence and substrate surface temperature dependence characteristic of a fully accommodated indirect channel to dissociation of H_2 on other transition metal surfaces [14,48]. The surface temperature dependence is due predominantly to the partition between desorption and dissociation of the trapped precursor.

The low energy channel extends to incident energies far above those which a collision between the light and poorly mass matched H_2 molecule and Mo surface could be expected to accommodate via energy exchange between molecule and surface (whether through excitation of surface phonons or the creation of electron-hole pairs). Beyond the range of the accommodated precursor hydrogen adsorption within this low energy channel takes place instead via a "dynamic adsorption mechanism", either dynamic steering or a dynamic precursor. This "dynamic" channel exhibits only a very small, or

possibly no temperature dependence. Such behaviour would be consistent with both the picture of dynamic steering, where the channel is essentially a direct one in which slow moving molecules are strongly steered into orientations and sites favourable to dissociation [49], increasing molecular velocities reducing the effectiveness of the steering forces produced by the PES of the H_2/Mo(100) system, and is also consistent with the picture of a dynamic precursor where trapping occurs predominantly via loss of energy to other molecular degrees of freedom (thought to be mainly rotational [26]) and loss of energy to the surface is not a requirement for trapping to take place.

When the molecular beam incident upon the Mo(100) surface is of considerably smaller diameter than that of the face of the sample the gradual rise in background pressure, associated with a greater fraction of H_2 molecules incident upon the surface being reflected and contributing to the overall chamber pressure, levels off and remains relatively constant over a prolonged time period, indicating that the sticking probability also remains constant. This behaviour, along with its dependence on beam diameter, is offered as evidence supporting the picture of the adsorbed hydrogen being highly mobile. This behaviour takes place at high beam energies where trapping is not possible, as well as at low, meaning the phenomena is not associated merely with a mobile precursor but also atomic, dissociatively adsorbed, hydrogen. The explanation proposed is of mobile atomic hydrogen migrating across the Mo(100) surface, vacating adsorption sites within the beams incident area, thereby allowing additional hydrogen adsorption to take place at these sites, a steady state eventually being reached when the rates of hydrogen migration and adsorption become equal.

A comparison of the H_2/Mo(100) and H2/W(100) [10,11,12] adsorption systems leads to the conclusion that the degree of hydrogen induced surface reconstruction plays a crucial role in determining the fate of the accommodated precursors. The bridge site is responsible for atomic hydrogen adsorption on both surfaces and this bridge site reconstructs with changing hydrogen coverage. A greater degree of reconstruction (as measured by the decrease in substrate atom separation around the bridge site [6]) leads to a swing in the partition between desorption and dissociation of the precursor in favour of dissociation.

IV.6 References

[1] Han H. R., Schmidt L. D., J. Phys. Chem. 75(1971)227

[2] Zaera F., Kollin E. B., Gland J. L., Surf. Sci., 166(1986)L149

[3] Bafrali R., Bell A. T., Surf. Sci., 278(1992)353

[4] Prybyla J. A., Estrup P. J., Chabal Y. J., J. Chem. Phys. 94(1991)6274

[5] Chabal Y. J., Surf. Sci. Rep., 8(1988)211

[6] Chabal Y. J., Christman S. B., Arrecis J. J., Prybyla J. A., Estrup P. J., J. Electron Spec.and Rel. Phenom., 44(1987)17

[7] Prybyla J. A., Estrup P. J., Ying S. C., Chabal Y. J., Christman S. B., Phys. Rev. Lett., 58(1987)1877

[8] Prybyla A., Estrup P. J., Surf. Sci., 290(1993)413

[9] Prybyla J. A., Estrup P. J., Chabal Y. J., J., J. Vac. Sci. Technol., 5(1987)791

[10] Berger H. F., Resch Ch., Grosslinger G., Eilmsteiner G., Winkler A., Rendulic K. D., Surf. Sci. Lett., 275(1992)L627

[11] Butler D. A., Hayden B. E., Jones J. D., Chem. Phys. Lett., 217(1993)423

[12] Butler D. A., Hayden B. E., Topics in Catal., 1(1994)343

[13] Butler D. A., Hayden B. E., Chem. Phys. Lett., 232(1995)542

[14] Butler D. A., Hayden B. E., Surf. Sci., 337(1995)67

[15] Felter J.E., Barker R.A., Estrup P.J., Phys. Rev. Lett. 38(1977)1138

[16] Arrecis J. J., Chabal Y. J., Christman S. B., Phys. Rev. B, 33(1986)7906

[17] Kay M., Darling G. R., Holloway S., White J. A., Bird D. M., Chem. Phys. Lett., 245(1995)311

[18] Gross A., Surf. Sci., 363(1996)1

[19] White J. A., Bird D. M., Payne M. C., Phys. Rev. B, 53(1996)1667

[20] Beutl M., Lesnik J., Rendulic K. D., Hirschl R., Eichler A., Kresse G., Hafner J., Chem. Phys. Lett., 342(2001)473

[21] Jackson B., Metiu M., J.Chem.Phys., 86(1987)1026

[22] Muller J. E., Phys. Rev. Lett., 59(1987)2943

[23] Halstead D., Holloway S., J. Chem. Phys., 93(1990)2859

[24] Neumark D. M., Wodtke A. M., Robinson G. N., Hayden C. C., Lee Y. T., J. Chem. Phys. 82(1984)3045

[25] Darling G. R., Holloway S., J. Chem. Phys., 93(1990)9145

[26] Crespo C., Busnengo H. F., Dong W., Salin A., J. Chem. Phys., 114(2001)10954
[27] Busnengo H. F., Crespo C., Dong W., Rayez J. C., Salin A., J. Chem. Phys., 116(2002)9005
[28] Di Cesare A. Busnengo H. F., Dong W., Salin A., J. Chem. Phys., 118(2003)11226
[29] Diaz C., Martin F., Busnengo H. F., Salin A., J. Chem. Phys., 120(2004)321
[30] Busnengo H. F., Di Cesare M. A., Dong W., Salin A., Phys. Rev. B, 72(2005)125411
[31] Busnengo H. F., Dong W., Salin A., Phys. Rev. Lett., 93(2004)236103
[32] Barredo D., Laurent G., Diaz C., Nieto P., Busnengo H. F., Salin A., Farias D., Martin F., 125(2006)051101
[33] Davenport J. W., Estrup P. J., "The chemical physics of solid surfaces and heterogeneous catalysis", Elsevier Science Publishers B. V., chap.1, p.2, 1990
[34] Montoya A., Schlunke A., S. Haynes B. S., J. Phys. Chem. B, 110(2006)17145
[35] Panczyk T., Szabelski P., Rudzinski W., J. Phys. Chem. B, 109(2005)10986
[36] Daniels E. A., Gomer R., Surf. Sci., 336(1995)245
[37] Altshuler E. S., Mills D. L., Gerber R. B., Surf. Sci., 452(2000)95-107
[38] Butler D. A., PhD. Thesis, University of Southampton, 1994
[39] Rettner C.T., Stein H., Schweizer E. K., J. Chem. Phys., 89(1988)3337
[40] Rettner C.T., Schweizer E. K., Stein H., Auerbach D.J., Phys. Rev. Lett., 61(1988)986
[41] Rettner C.T., Schweizer E. K., Stein H., Auerbach D.J., J. Vac. Sci. Technol. A, 7(1989)1863
[42] Rettner C.T., Schweizer E. K., Stein H., J. Chem. Phys., 93(1990)1442
[43] Andersson S., Persson M., Harris J., Surf. Sci., 360(1996)L499
[44] Hoinkes H., Rev. Mod. Phys., 52(1980)934
[45] Hammer B., Scheffler M., Jacobsen K. W., Norskov J. K., Phys. Rev. Lett., 73(1994)1400
[46] Holloway S., Kay M., Darling G. R., Faraday Discuss. Chem. Soc., 105(1996)209
[47] Gee A. T., Hayden B. E., Mormiche C., Nunney T. S., J. Chem. Phys., 112(2000)7660
[48] Mormiche C., PhD. Thesis, University of Southampton, 2002
[49] Darling G. R., Kay M., Holloway S., Surf. Sci., 400(1998)314
[50] Tam P. W., Schmidt L. D., J. Chem. Phys., 52(1970)1150

[51] Horlacher Smith A., Barker R. A., Estrup P. J., Surf. Sci., 136(1984)327

[52] Alnot P., Cassuto A., King D. A., Surf. Sci., 215(1989)29

[53] Dixon-Warren St. J., Pasteur A. T., King D. A., Surf. Sci. Rev. and Lett. 1(1994)593

[54] King D. A., Wells M. G., Surf. Sci., 29(1972)454

Chapter V: Hydrogen adsorption on Mo(100)-c(2×2)N

V.1 Introduction

H_2 adsorption on the Mo(100) surface exhibits 3 differing channels to dissociation. Analysis of these channels is made difficult by the considerable overlap of the three, with a dynamic channel extending to relatively high E_i, and what appears to be a non-activated direct dissociation channel contributing to S_0 even at the lowest E_i.

The Mo(100)-c(2×2)N surface is well documented and relatively simple to recreate. This surface is seen to shift the direct dissociation channel present on Mo(100) up considerably in energy while appearing to leave the accommodated/dynamic low energy channel (which extends to E_i>60meV on Mo(100)) intact. This increase in the barrier to direct dissociation allows the low energy channel to be studied in detail without the results being clouded by the presence of the direct channel.

Mo(100)-c(2×2)N is also a good model for the Mo_2N catalyst.

V.2 Literature Analysis

V.2.1 Creation and Characterisation of the Mo(100)-c(2×2)N Surface

The Mo(100)-c(2×2)N surface is well documented in the literature [1-3] and has been shown to be a good model surface for the principal (200) surface exposed by the real Mo_2N catalyst in which half of the octahedral voids are filled by nitrogen atoms [1], with Mo_2N having been shown to display excellent catalytic activity in a wide variety of reactions, including NH_3 synthesis [4], hydrotreating [5], and CO hydrogenation [6]. The Mo(100)-c(2×2)N surface is associated with nitrogen bonding in half of all four fold hollow sites producing a nitrogen coverage of 0.5ML [1,2].

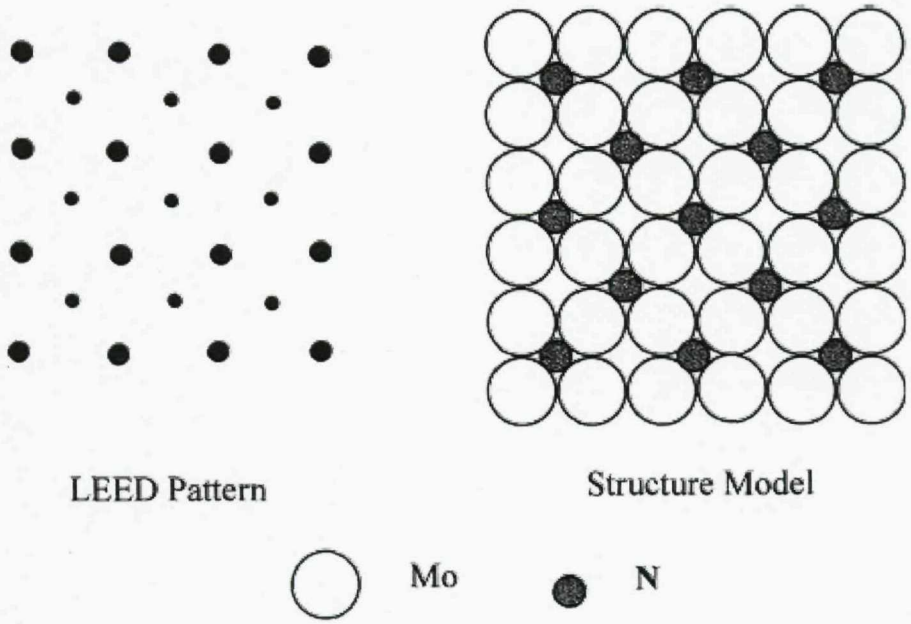

Figure 1: The ideal LEED pattern produced upon formation of a complete Mo(100)-c(2×2)N surface, and the structural model that this corresponds to with the filled circles corresponding to nitrogen adatoms having adsorbed into half of all four fold hollow sites. Taken from [2]

The Mo(100)-c(2×2)N surface is generally reported as being produced by first dosing >2L [3] nitrogen at low temperature (~160K) to saturate the surface, followed by annealing to between 1100K and 1170K [2,3], this treatment resulting in a sharp c(2×2) LEED pattern characteristic of the structure.

Initially, saturating the surface with nitrogen is reported to result in a (1×1) LEED pattern which persists up to a surface temperature of 1000K, with the clear c(2×2) pattern becoming visible between 1100K and 1300K, reverting back to a (1×1) structure above 1300K [3]. This behaviour was interpreted as the creation of a disordered surface upon initial nitrogen adsorption, the attainment of a c(2×2) ordered structure with heating, in which half of all four-fold hollow sites are occupied by nitrogen atoms (see figure 1), and finally the return to the clean surface Mo(100) structure as T_S is raised above the point at which associative recombination of all the four-fold hollow bonded N atoms takes place and the nitrogen is completely desorbed from the molybdenum surface.

A TPD study of the Mo(100)-c(2×2)N surface reveals a β desorption peak at 1310K (figure 2). This agrees well with the observed destruction of the c(2×2) LEED pattern above 1300K.

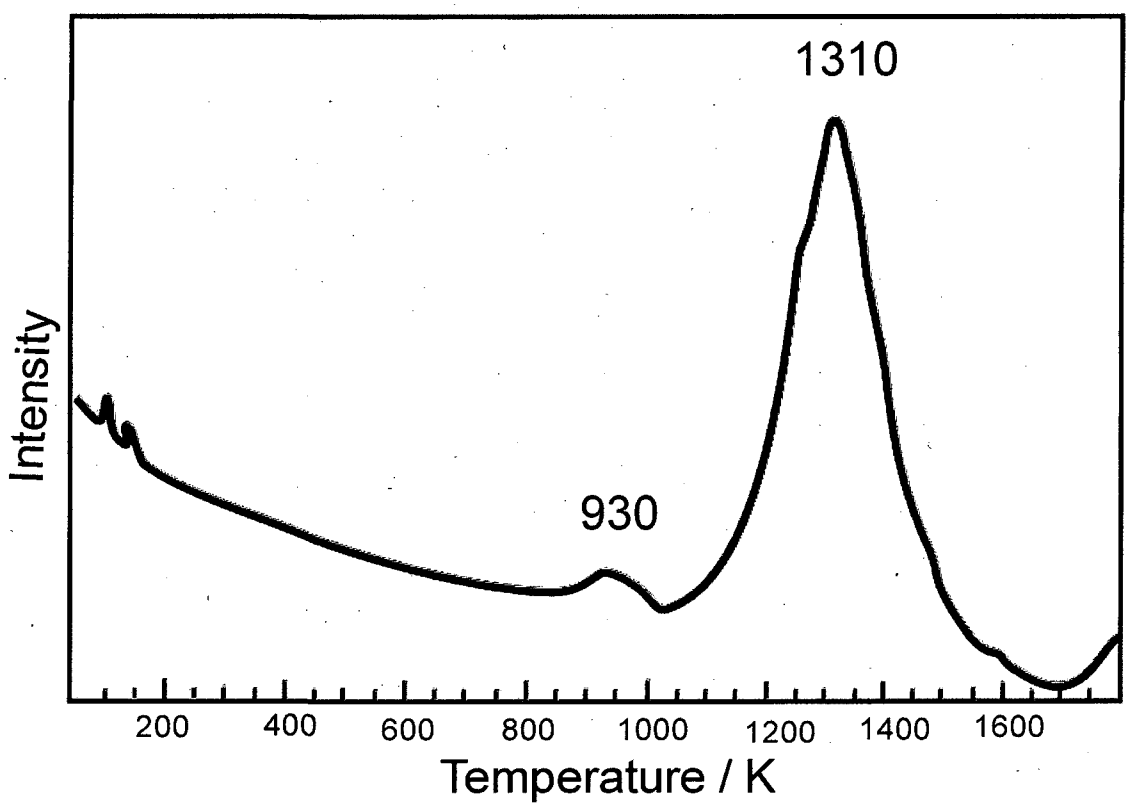

Figure 2: A thermal desorption spectrum of nitrogen from a prepared Mo(100)-c(2×2)N surface. The small desorption peak at 930K is attributed to N desorbing from areas where residual oxygen is present at the surface (taken from [3]).

V.2.2 H_2 Adsorption Studies on the Mo(100)-c(2×2)N Surface

Although Mo(100)-c(2×2)N has been well characterised as a surface it has yet to be the subject of any dynamics studies. What investigations there have been have centred on the adsorption/desorption kinetics of the system.

Zhu et al. studied the adsorption of CO and NO by use of HREELS, concluding that both adsorb not only on the top of Mo sites, but also react with the surface N sites [2]. More interesting to this study is the work of Bafrali and Bell and their use of TPD to

elucidate the sticking coefficients and maximum adsorption capacities of H_2 and NH_3 on the Mo(100)-c(2×2)N surface [1]. Their comparison of TPD studies of hydrogen adsorption on the clean Mo(100) and the Mo(100)-c(2×2)N surfaces shows a reduction in the hydrogen adsorption peaks associated with the bonding at bridge sites upon the Mo(100) surface (figure 3), indicating that nitrogen adsorption induces blocking of these adsorption sites.

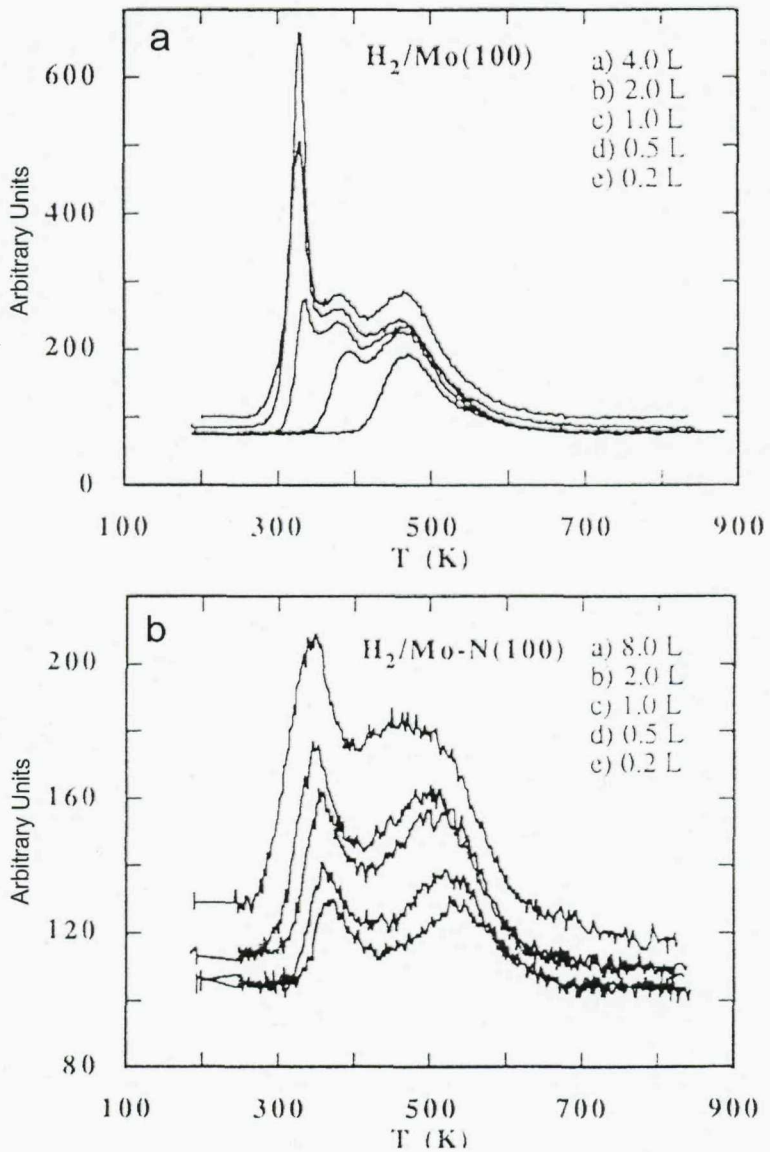

FIGURE 3: a TPD of hydrogen desorption for varying doses of hydrogen (given in langmuirs, L) from a) the Mo(100) surface, and b) the Mo(100)-c(2×2)N surface (taken from [1]). Note all Mo(100) peaks observed here by Bafrali and Bell are ~50K lower than those observed by myself (chapter IV.3.2) and others [7].

Bafrali and Bell observe a drop in saturation hydrogen coverage from 2.0ML on clean Mo(100) to approximately 0.5ML on Mo(100)-c(2×2)N [1]. It is hard to envisage bridge site bonding resulting in $\theta_{H(sat)}$=0.5ML while nitrogen occupies half of all four-fold hollow sites since if the presence of a nitrogen atom in an adjacent four-fold hollow does not affect the ability of a bridge site to accommodate adsorbed hydrogen then the surface should saturate at θ_H=2.0ML, and if the presence of an adjacent nitrogen does then the saturation coverage should be expected to be 0ML. Applying this argument to the atop site also would result in a saturation coverage of either 0 or 1.0ML. The simplest adsorption site to envisage providing saturation coverage of 0.5ML would be for hydrogen to adsorb in the remaining vacant four-fold hollow sites, those unoccupied by nitrogen atoms.

The similarity of the β hydrogen desorption peaks, reported by Bafrali and Bell [1], from Mo(100)-c(2×2)N with those of Mo(100) is not in accord with a change in adsorption site. It is therefore possible that the peaks observed in their TPD study are only the remnants of the clean surface bridge adsorption sites, perhaps due to an incomplete c(2×2) structure with some areas of the molybdenum surface remaining clean of nitrogen and allowing hydrogen bridge bonding to take place, or that they are due to hydrogen desorbing from residual defect sites at which relatively unperturbed molybdenum sites might be exposed. A TPD examining hydrogen desorption from the W(100)-c(2×2)N surface, where the same change in adsorption site is reported (from the bridge of the clean W(100) [8,9] to the four fold hollow of W(100)-c(2×2)N [10]), reveals a new desorption peak occurring at ~150K [10], associated with hydrogen desorbing from the c(2×2)N structure, this peak being considerably lower than the $400<T_S(K)<600$ peak range reported for desorption from the W(100) surface [11]. The TPD of Bafrali and Bell for H_2 desorption from Mo(100)-c(2×2)N [1] is only recorded for T_S>200K and would not have registered a new desorption peak should it have occurred at a similarly low temperature on the Mo(100)-c(2×2)N surface as was seen for the W(100)-c(2×2)N.

V.2.3 A Comparison of the Mo(100)-c(2×2)N and W(100)-c(2×2)N Surfaces

Nitrogen adsorption on the W(100) surface at room temperature results in a stable β_2 state associated with the c(2×2) structure and a less stable β_1 state above 0.5ML. The c(2×2) pattern is most clearly identified at θ_H=0.5ML and, similar to the Mo(100)-c(2×2)N surface, corresponds to nitrogen occupying half of all four-fold hollow sites. The origin of the β_1 state is, however, somewhat unclear.

The specific W(100)-c(2×2)N surface is produced in a very similar manner to that already described for the production of an Mo(100)-c(2×2)N surface; a prolonged N_2 dose, followed by annealing the surface to a temperature just below that at which the principal β peak (in this case the β_2) begins to desorb, producing a sharp c(2×2) LEED pattern [12]. On the tungsten surface this anneal corresponds to removal of the β_1 adsorbed nitrogen.

No equivalent β_1 state has yet been observed on the molybdenum surface. Ren and Zhai [3] did observe a small peak to appear at 930K, a few hundred K lower than the β peak responsible for the c(2×2) structure of Mo(100)-c(2×2)N (see figure 2), but suggested instead that this peak might be related to nitrogen desorbing from residual oxygen contaminants on the surface. The peaks observed were positioned at 930K and 1310K, and interestingly the relative position of one peak with respect to the other is much the same as was seen to be the case for the β_1 and β_2 nitrogen desorption peaks from the W(100) surface, these being observed at 1080K and 1450K respectively. It remains unclear whether the small peak observed by Ren and Zhai on Mo(100) is merely due to oxygen contamination or whether it might relate to the β_1 peak of N/W(100) and be characteristic of desorption from uncontaminated Mo(100)-N surface. However, it is clear that many similarities exist between the Mo(100) and W(100) nitrogen adsorption systems, including each having two low temperature physisorption (γ) peaks (corresponding to the normal and parallel orientations with respect to the surface) [2,13], the position of the principal β peak and therefore the strength with which the nitrogen is bound to the surface, the four-fold hollow adsorption site occupied by nitrogen at $\theta_N \leq 0.5$ML, and the c(2×2) LEED pattern

associated with the nitrogen layer at θ_N=0.5ML coverage, so it might perhaps be surprising if a state equivalent to the β_1 of N/W(100) did not also exist for the N/Mo(100) system. The β_1 state of nitrogen on W(100) is reported to become occupied only after high nitrogen exposure [14] and perhaps for this reason it has not yet been observed on molybdenum during studies directed at producing only the Mo(100)-c(2×2)N surface, this structure requiring just a 0.5ML nitrogen coverage.

Whereas no study of the dynamics of hydrogen adsorption onto the Mo(100)-c(2×2)N has previously been made, a brief dynamics study of adsorption onto the W(100)-c(2×2)N surface does exist, with a supersonic molecular beam having been used to probe the behaviour of the initial sticking probability of the H_2 as a function of its incidence energy [10]. As has already been shown to be the case on Mo(100) (chapter IV), on W(100) the overlap of the direct channel with the accommodated and dynamic channels for hydrogen adsorption made the precise contribution of the low energy channels difficult to determine [11], but, upon adsorption of nitrogen to create the W(100)-c(2×2)N surface, the barrier to direct dissociation of H_2 was shifted to sufficiently high E_i so as to be well removed from the accommodated and dynamic channels, apparently without significantly diminishing the size of the lower energy channel. No evidence of a direct channel to hydrogen dissociation on W(100)-c(2×2)N was observed even at incident energies as high as 200meV.

Hydrogen adsorption onto the W(100)-c(2×2)N surface was seen to result in a saturation coverage of ~0.5ML [10], the same value as was observed for the molybdenum equivalent [1], suggesting the same adsorption site to be responsible on both surfaces. Ab initio calculations of the PES of H/W(100) determined the bridge to be the most favourable site for atomic hydrogen adsorption, with a calculated adsorption energy of 1.9eV / molecule [15], in agreement with experiment, and with non activated routes to desorption existing for this site. The next most favourable site, just 0.4eV higher in energy, was calculated as being the four-fold hollow [15]. As has already been suggested regarding hydrogen adsorption onto a Mo(100)-c(2×2)N (chapter V.2.2), a saturation coverage of 0.5ML would appear to make the four-fold hollow the obvious candidate for the adsorption site, with hydrogen adsorbing into the fourfold hollows unoccupied by N atoms producing exactly this coverage.

A TPD study of H/W(100)-c(2×2)N was seen to exhibit an almost complete suppression of the desorption peaks associated with hydrogen desorption from the clean W(100), accompanied by a new desorption peak at a much lower T_S (~150K) [10] (as has already been mentioned). There is a correspondence here between the decrease in activation energy for desorption (associated with the desorption temperature seen in the TPD) and the increase in the minimum potential energy barrier to direct dissociation between W(100) and W(100)-c(2×2)N (associated with the incident energy at which the direct channel first begins to manifest itself), a trend observed also for the H_2/W(100)-c(2×2)Cu adsorption system [16]. There appears to be a proportional relationship between the activation energy for desorption and the activation energy for direct dissociation, with the W(100)-c(2×2)N surface exhibiting the lowest temperature desorption peak and greatest barrier to direct dissociation, the W(100)-c(2×2)Cu a desorption peak at a higher temperature and lower direct dissociation barrier, and the clean W(100) the highest temperature desorption peaks while only exhibiting a very small (or possibly non-existent) barrier to direct dissociation (figure 25 of chapter IV presents a simplistic picture of how this might be envisaged as taking place).

No such lower temperature absorption peak was observed by Bafrali and Bell in their study of the H/Mo(100)-c(2×2)N system [1], however, it is possible that they were unable to search to low enough temperatures, with the TPD beginning only at ~200K (the hydrogen desorption peak of the H/W(100)-c(2×2)N system being observed to appear at ~150K [10]). Given that the barrier to direct dissociative adsorption of H_2 on the Mo(100)-c(2×2)N surface appears to be shifted upwards in energy from that experienced by hydrogen adsorbing on the clean Mo(100) (this shift being examined shortly), in a manner similar to that observed for the equivalent W surfaces, it seems reasonable to expect a corresponding fall in the activation energy for hydrogen desorption, as is observed to take place between the equivalent W surfaces. It therefore seems reasonable to expect that a desorption peak should be present at lower temperatures than those observed for hydrogen desorption from the Mo(100).

V.3 Results

V.3.1 Summary

The method for the production of the Mo(100)-c(2×2)N surface is detailed. During the creation of this surface a new nitrogen adsorption site labelled β_1 is observed. Comparisons are drawn between this state and the β_1 of the N/W(100) system.

Hydrogen adsorption on to the Mo(100)-c(2×2)N surface is monitored as a function of incident energy, surface temperature and hydrogen coverage, and comparisons are drawn between this data and the equivalent data from hydrogen adsorption on the clean Mo(100) and the W(100)-c(2×2)N surfaces.

V.3.2 Creation of the Mo(100)-c(2×2)N surface

The Mo(100)-c(2×2)N structure was produced by first dosing nitrogen on to the surface at low temperature (~160K) to produce θ_N>0.5ML. This was followed by a 1170K anneal, this being observed to produce a c(2×2) LEED pattern, this pattern being characteristic of the Mo(100)-c(2×2)N structure. This method is the same as that followed by Ren and Zhai [3] and Zhu et al. [2].

High purity nitrogen (99.999% pure N_2) was introduced to the chamber either from a pure nitrogen beam or via gas doser a few centimetres from the crystal pointed directly at its front face. When using the beam the large aperture was used to ensure a beam diameter equal to that of the molybdenum sample. Subsequent desorption of nitrogen from the Mo(100) surface has been monitored via TPD analysis, the results of which are shown in figure 4 for a variety of coverages.

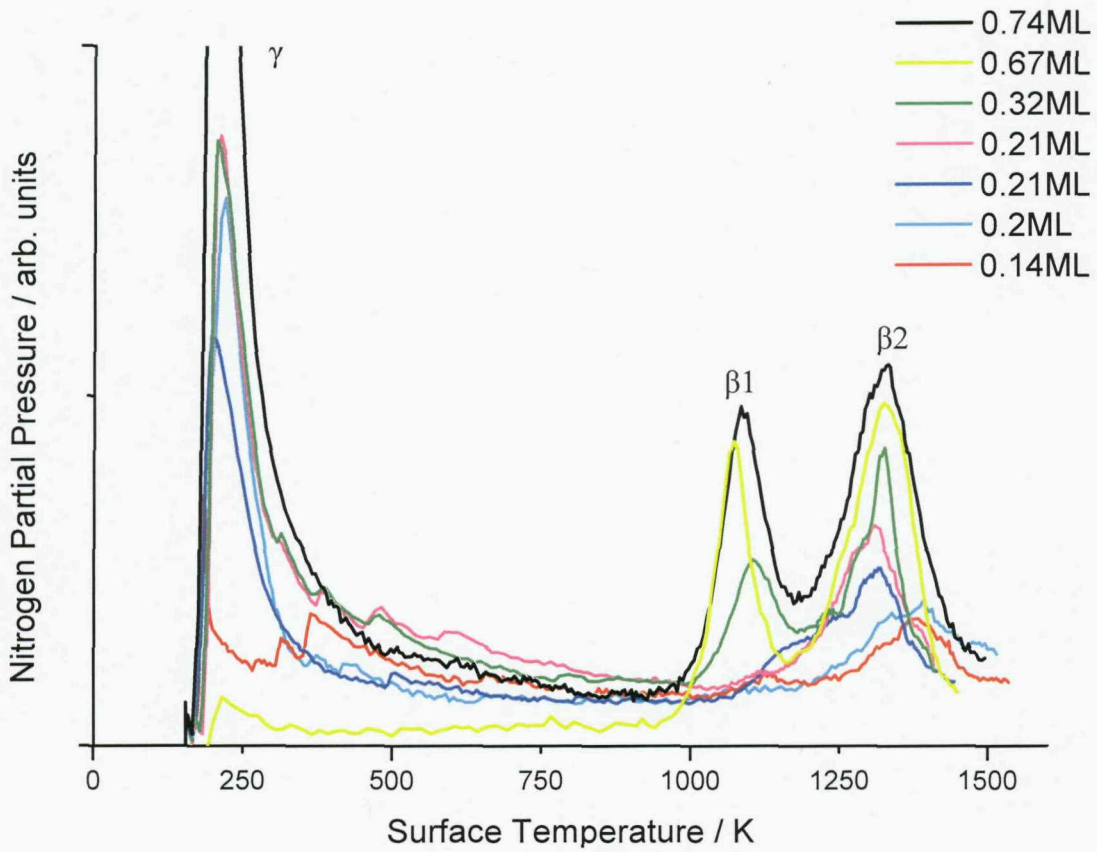

Figure 4: TPD of N_2 from the Mo(100) nitrogen covered surface taken at a range of coverages (recorded in ML). The surface displays 3 peaks, one γ peak at ~205K and two β peaks, β_1 at ~1080K and β_2 at ~1320K. The coverage values listed refer to atomically adsorbed nitrogen only, the presence (or lack) of the γ peak being clouded by the inaccuracy of the temperature recording at the lowest T_S,, the W3 type thermocouple being tailored to measuring high temperatures and not sub 0^0C values, and the close proximity of the peak to any contribution to desorption from the heating wires (desorption from the heating wires occurring due to the use of EB heating, where a spiral filament behind the sample is heated in order to eject electrons with which to bombard, and thus heat, the sample, this heating method also being tailored to producing the high temperatures required to clean the surface rather than producing the gradual rise from low temperatures required for the production of an accurate TPD).

Two atomically adsorbed states of nitrogen are present on the Mo(100) surface, labelled β_1 and β_2, corresponding to desorption peaks observed at ~1080K and ~1320K, and one molecularly chemisorbed state labelled γ, corresponding to the desorption peak at ~205K. This is the first time (to the best knowledge of this author) clear evidence for the β_1 state has been presented. The β_2 peak observed here has been

previously characterized in the literature [3] and is associated with a c(2×2) structure with nitrogen bonding in half of all four fold hollow sites giving a saturation coverage of 0.5ML [2,17]. The position of the β_2 peak, observed here as being at 1320K, is in good agreement with that reported in the literature of 1310K [3]. Table 1 makes a comparison between the various temperatures recorded for nitrogen desorption peaks from W(100) and Mo(100).

The ratio between β_1 and β_2 for the W(100) surface was reported as being 2:3 (although this measurement was made while noting that it was limited by the maximum dose possible without introducing surface contamination and not necessarily a saturation value) [14], and this is close to the saturation ratio of ~1:1 recorded here for the Mo(100) surface. In fact the structure model proposed by Sellidj and Erskine [13] for the saturated W(100)-N surface, based on EELS and LEED measurements, does predict a 1:2 ratio (i.e. 50%) between the β_1 and β_2 states. This ratio equates to a 0.75ML saturation coverage of atomic nitrogen on the Mo(100) surface (based on the saturation of β_1 being known to equate to a coverage of 0.5ML [2,17]).

The Mo(100)-c(2×2)N structure has in the past been reported as being produced after N_2 adsorption and subsequent anneal to 1100K or 1150K ([3] and [2] respectively). The TPD of figure 4 indicates that heating to around these temperatures will tend to remove the β_1 peak while leaving the β_2 nitrogen untouched. Indeed, by heating the crystal surface to 1170K the β_1 peak was seen to be completely removed while leaving the β_2 peak entirely intact (see figure 5). This was confirmed by examining the ratio of the integral of the β_1 state (figure 5b) and the β_2 state, with the β_1 state being initially desorbed, followed by a TPD, performed after re-cooling the surface, that removed the β_2 peak (figure 5c). Comparison of the TPD finds the β peaks to retain very close to a 1:2 ratio. It is also noted that after annealing to 1170K for a few seconds the β_1 peak does not return. This indicates there is no transfer from the β_2 to β_1 state during heating as was also noted to be the case for nitrogen adsorbed upon the W(100) surface [12].

previously characterized in the literature [3] and is associated with a c(2×2) structure with nitrogen bonding in half of all four fold hollow sites giving a saturation coverage of 0.5ML [2,17]. The position of the β_2 peak, observed here as being at 1320K, is in good agreement with that reported in the literature of 1310K [3]. Table 1 makes a comparison between the various temperatures recorded for nitrogen desorption peaks from W(100) and Mo(100).

The ratio between β_1 and β_2 for the W(100) surface was reported as being 2:3 (although this measurement was made while noting that it was limited by the maximum dose possible without introducing surface contamination and not necessarily a saturation value) [14], and this is close to the saturation ratio of ~1:1 recorded here for the Mo(100) surface. In fact the structure model proposed by Sellidj and Erskine [13] for the saturated W(100)-N surface, based on EELS and LEED measurements, does predict a 1:2 ratio (i.e. 50%) between the β_1 and β_2 states. This ratio equates to a 0.75ML saturation coverage of atomic nitrogen on the Mo(100) surface (based on the saturation of β_1 being known to equate to a coverage of 0.5ML [2,17]).

The Mo(100)-c(2×2)N structure has in the past been reported as being produced after N_2 adsorption and subsequent anneal to 1100K or 1150K ([3] and [2] respectively). The TPD of figure 4 indicates that heating to around these temperatures will tend to remove the β_1 peak while leaving the β_2 nitrogen untouched. Indeed, by heating the crystal surface to 1170K the β_1 peak was seen to be completely removed while leaving the β_2 peak entirely intact (see figure 5). This was confirmed by examining the ratio of the integral of the β_1 state (figure 5b) and the β_2 state, with the β_1 state being initially desorbed, followed by a TPD, performed after re-cooling the surface, that removed the β_2 peak (figure 5c). Comparison of the TPD finds the β peaks to retain very close to a 1:2 ratio. It is also noted that after annealing to 1170K for a few seconds the β_1 peak does not return. This indicates there is no transfer from the β_2 to β_1 state during heating as was also noted to be the case for nitrogen adsorbed upon the W(100) surface [12].

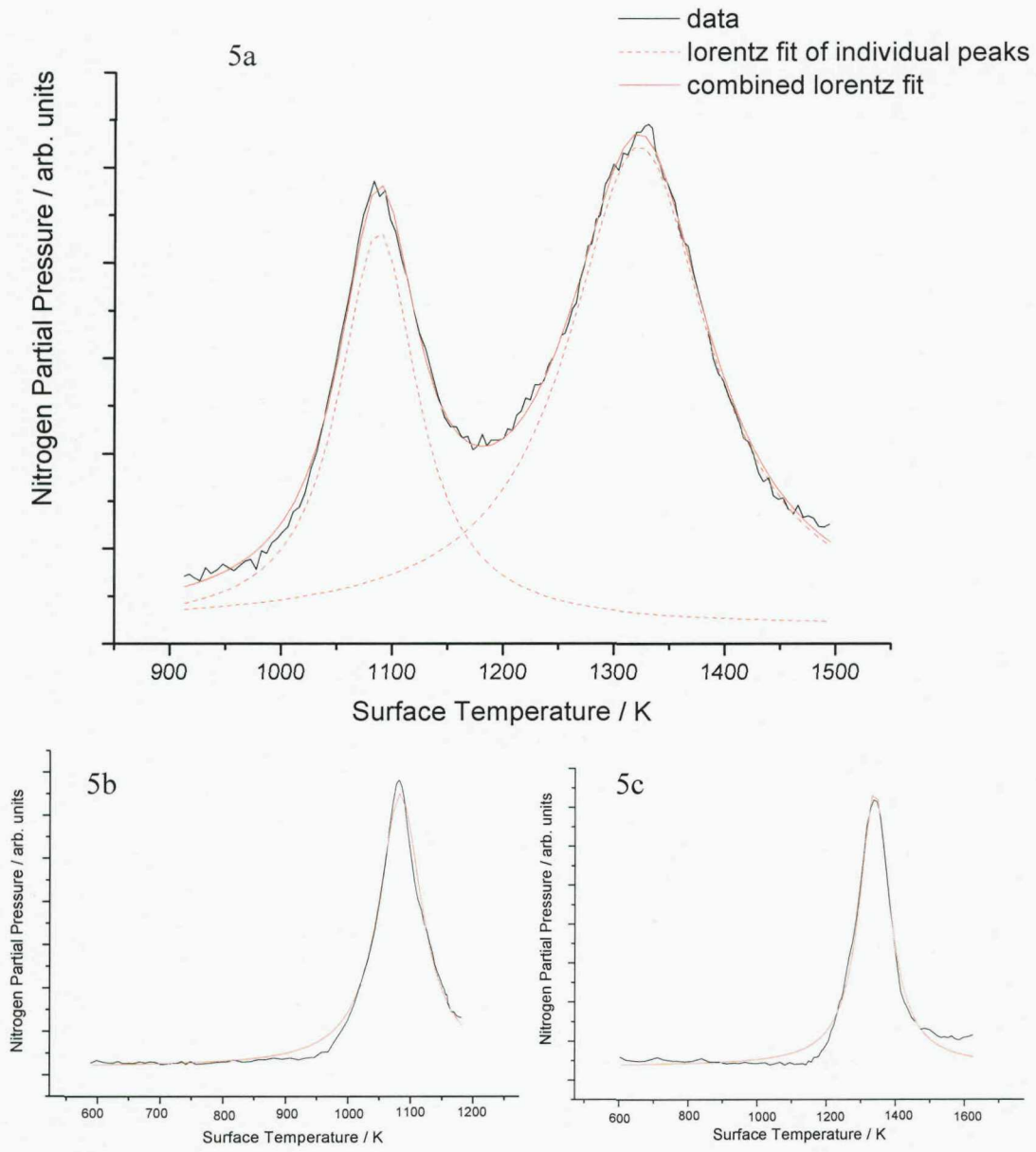

Figure 5: Calculation of the area encompassed by β_1 and β_2 after a saturating dose of N_2 (~240L). In figure (a) a multiple lorentzian peak fit finds β_1 to be 0.46 of the size of β_2. Figures (b) and (c) use a Lorentz peak fit area calculation to determine the areas of the β_1 and β_2 desorption peaks respectively, the TPD plotted in (c) being performed directly after the TPD shown in (b) has removed β_1. The ratio remains approximately constant with the isolated β_1 peak having an area 0.49 that of the isolated β_2.

In the case of W(100) the c(2×2) structure has also been associated with the removal of a β_1 state[12]. In the case of a W(100) substrate, annealing the nitrogen covered surface to temperatures just above the β_1 desorption peak was noted to result in the formation

of large domains of the perfect c(2×2) structure via inter-island coalescence eliminating out-of-phase boundaries.

As reported in the literature, saturating the Mo(100) surface with nitrogen was seen to result in a (1×1) LEED pattern. Removing the physisorbed nitrogen by anneal to 650K was seen to leave this (1×1) pattern intact, while an anneal to 1170K was seen to result in the production of a c(2×2) structure. This also compares well with the literature, where Ren and Zhai [3] observe a (1×1) pattern upon saturation at low temperatures, and the (1×1) pattern persisting up to a surface temperature of 1000K, with a clear c(2×2) pattern then becoming visible between 1100K and 1300K, this c(2×2) reverting back to a (1×1) structure above 1300K, presumably corresponding to the associative desorption of the nitrogen from the β_2 state on the surface at around this temperature.

Substrate	γ / K	β_1 / K	B_2 / K	Anneal temp. to produce c(2×2)N / K	Reference
Mo(100)		1080	1320	1170	This thesis
Mo(100)	~155 (2 states)			1150	[2]
Mo(100)		930?	1310	1100-1200	[3]
Mo(100)				1173	[1]
W(100)	170 & 180	860	1300 – 1450 *	900	[13]
W(100)		1080	1450	1020	[12]

Table 1: Comparison of data currently available examining nitrogen desorption temperatures from the Mo(100) and W(100) surface. (temperature of desorption peak maximum is dependent on coverage)*

Although the β_1 peak has not been previously reported, its existence is hardly surprising given the observation of a β_1 state appearing on W(100) after high nitrogen doses [12, 18] and taking account of the various other similarities observed to be present between the two surfaces [19] (as discussed above in section V.2.3).

The saturation of the β_2 peak associated with the c(2×2) surface, and the creation of the complete Mo(100)-c(2×2)N surface, was determined by calculating the amount of nitrogen desorbed during a TPD following an anneal to 1170K to remove all nitrogen from the surface not involved in the c(2×2) structure (see figure 6).

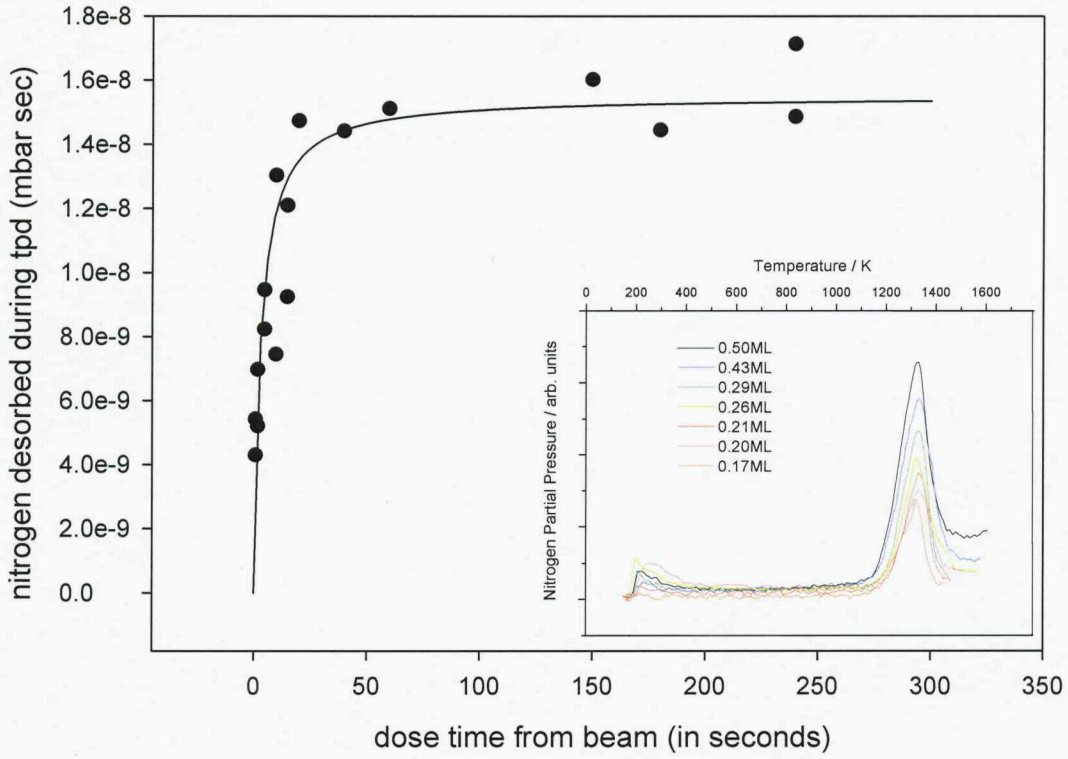

Figure 6: Nitrogen desorbed from β_2 peak during a TPD as a function of the dose time. Nitrogen is dosed using a pure N_2 beam, the beam diameter being set to approximately the same of that of the crystal, and the crystal then annealed to 1170K to remove the β_1 peak and produce the c(2×2)N surface structure. The data is fitted with an exponential rise to illustrate the dose required to produce the complete c(2×2)N structure.

Zhu et al. report saturation to take place after a >2L dose of nitrogen at low surface temperatures [2]. Saturation of the β_2 state, and subsequent creation of the complete Mo(100)-c(2×2)N surface by annealing, was seen to take place here after a 20 second dose of pure N_2 from the molecular beam. This is approximately equivalent to a 10L dose.

V.3.3 The adsorption site of Hydrogen on the Mo(100)-c(2×2)N surface

By integrating the area mapped out by the curve defining the hydrogen partial pressure as a function of time, from the point at which the flag is opened to the point at which the surface saturates, a measure is obtained, of the amount of hydrogen adsorbed in order to saturate the surface upon which the beam is incident. By using the large beam diameter on each surface and comparing the results a ratio of 0.23 is obtained between the hydrogen adsorbed to saturate the Mo(100)-c(2×2)N surface and that which saturates the clean Mo(100) surface. Taking the saturation value of hydrogen on Mo(100) as 2ML, as has already been well established in the literature [7,20], this gives a value of 0.46ML as the saturation coverage of hydrogen on the Mo(100)-c(2×2)N surface, a value within reasonable agreement with the approximate 0.5ML reported by Bafrali and Bell [1].

Arguments have already been put forward regarding the adsorption site of hydrogen on the Mo(100)-c(2×2)N surface (section V.2.2), with the four-fold hollow being expected to be the second most stable adsorption site on the Mo(100) surface (from comparison with theoretical calculations performed for the very similar H/W(100) system [15]) and nitrogen adsorption appearing to block adsorption into the more stable bridge site [1]. Also, unless a complicated restructuring of the surface takes place (something not observed by any studies), this saturation coverage of 0.5ML for hydrogen adsorption on a (100) surface, where nitrogen is present in half all four fold hollow sites, can only reasonably correspond to adsorption into the vacant four fold hollows.

As has also been discussed previously (section V.2.3), this change in adsorption site is expected to be accompanied by a drop in the strength of the hydrogen atoms' bond to the surface corresponding to a drop in the temperature required to desorb the atomically bound hydrogen from the surface. The temperature of this hydrogen desorption peak (from the Mo(100)-c(2×2)N surface) is somewhat uncertain. Bafrali and Bell [1] report two peaks at ~365K and ~535K, however it is suggested here that these peaks might correspond merely to hydrogen desorption from remaining areas of clean Mo(100), perhaps from defect/step sites, there being little shift in the peak

positions from those observed for H_2 desorbing from the clean Mo(100), and that the true peak(s) representing hydrogen desorbing from the Mo(100)-c(2×2)N might be out of the temperature range examined by their TPD (i.e. <200K), perhaps at a similar temperature to the ~150K reported for hydrogen desorption from the W(100)-c(2×2)N surface [10].

V.3.4 Dependence of S_0 on Incident Energy

The creation of the Mo(100)-c(2×2)N was seen to act to remove from the energy range examined (<80meV) the large direct channel to hydrogen dissociative adsorption which was observed to be present upon the clean Mo(100) surface (see chapter IV).

The removal of the direct channel to dissociation on the Mo(100)-c(2×2)N surface sees S_0 continuing to drop with increasing E_i, S_0 falling from ~0.4 at 13meV to <0.1 by ~70meV. The reach of this channel(s) appears to be close to equal that of the low energy channel on the Mo(100) surface (figure 18 chapter IV), S_0 on Mo(100) ceasing its decline and beginning to increase between 70 and 80meV indicative of the low energy channel disappearing at around this energy. The magnitude of $S_0(H_2)$ on Mo(100)-c(2×2)N across the given energy range also appears comparable to what might be expected upon the Mo(100) surface were the direct channel contribution to S_0 to be removed. It might appear that the S_0 values associated with the low energy channel(s) are slightly lower on the Mo(100)-c(2×2)N than on Mo(100), with S_0 at the lowest recorded E_i (13meV) measured as being ~0.55 on Mo(100), while only ~0.4 on Mo(100)-c(2×2)N, however the non-activated nature of the direct channel means that its contribution may still be sizeable at even this low E_i and might account for some or all of this difference in the S_0 values recorded for the two surfaces.

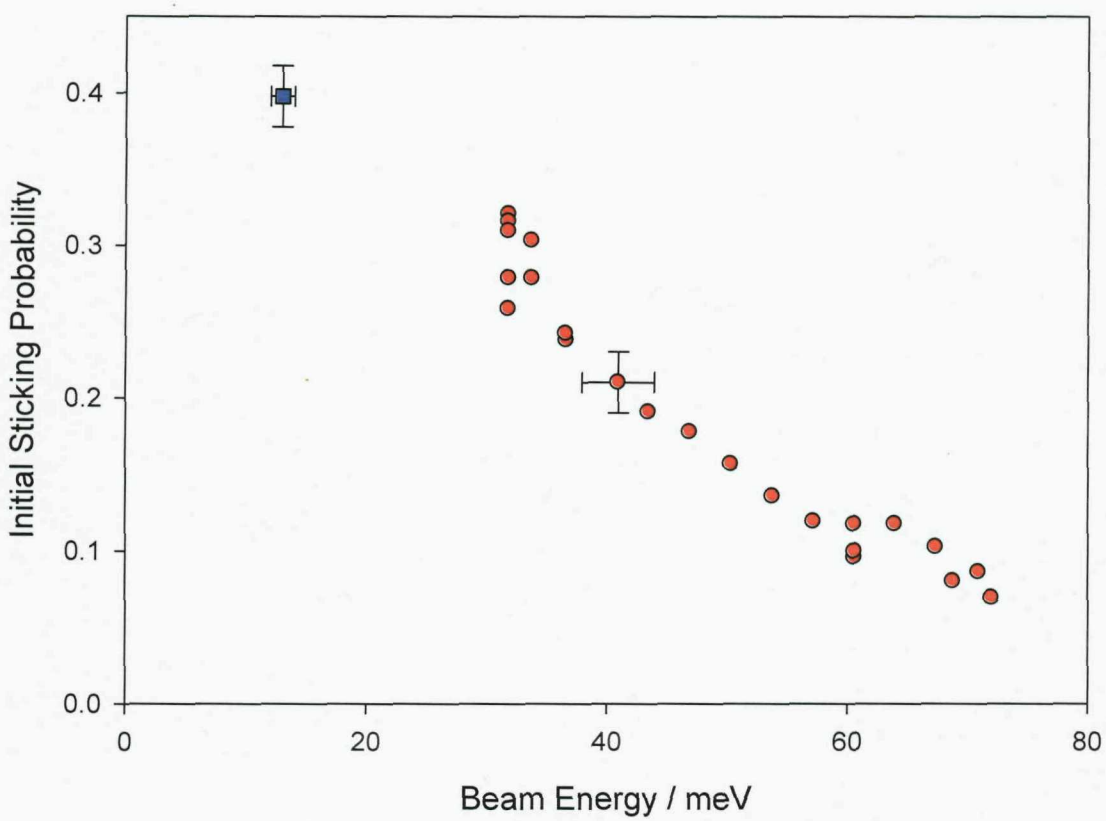

Figure 7: Initial sticking probability of H_2 on Mo(100)-c(2×2)N as a function of incident energy. T_S=165K, $\varphi=0^0$. The blue square represent data taken using an argon seeded beam, red circles represent data taken using a helium seeded beam.

Error calculations are made in the same manner as with the H_2/Mo(100) system (see chapter IV.3.4). The errors on S_0 are estimated to be +/- 0.02, double the size calculated for the H_2/Mo(100) surface. This is perhaps unsurprising since whereas the accuracy of the measurement upon Mo(100) was predominantly dependent upon achieving a clean surface, a contaminated surface tending to result in a reduced initial sticking probability, an accurate measurement of S_0 on Mo(100)-c(2×2)N not only requires the production of this initial clean Mo(100) surface before nitrogen dosing takes place, but also the subsequent removal of sufficient nitrogen to produce the perfect c(2×2) structure. If the surface is annealed to slightly too high a temperature loss of nitrogen from the β_2 adsorption state will tend to result in an increased S_0, whereas annealing to too low a temperature may fail to remove all the β_1 state nitrogen, and this was seen to tend to result in a decrease in the S_0 value.

The presence of nitrogen adatoms on the Mo(100) surface provides a better mass-match for the incident H_2 molecule than a substrate atom from the clean Mo(100). Typically this improved mass match is expected to enhance energy exchange between projectile and surface, and thereby increase the accommodated trapping probability at a given E_i.

V.3.5 Dependence of S_0 on Surface Temperature

On the Mo(100)-c(2×2)N surface, at E_i=32meV, an increase in T_S is seen to correspond to a decrease in S_0 of H_2 within the temperature range $165<T_S(K)<430$. The gradient is seen to vary somewhat across this temperature range, with S_0 beginning to drop less rapidly as T_S rises above 300K. Across the range $165<T_S(K)<300$ the gradient appears to remain relatively constant and is calculated as being $\sim 1.4\times10^{-3}$ K^{-1} an order of magnitude larger than the gradient recorded at the equivalent E_i for H_2 adsorption on the nitrogen free Mo(100) surface (1.4×10^{-4} K^{-1}, see chapter IV.3.5).

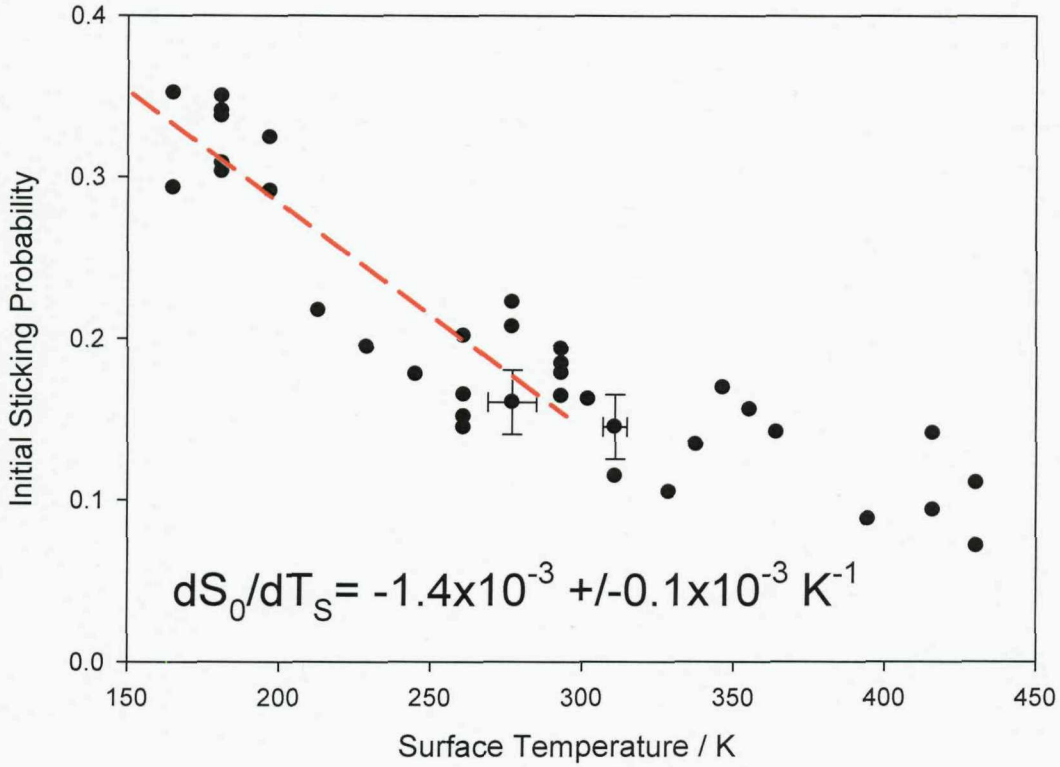

Figure 8: *Initial sticking probability of H_2 onMo(100)-c(2×2)N as a function of surface temperature, φ=0, E_i=32meV. T_S +/- 8K when <293K, T_S +/- 4K when ≥293K. Red dashed line shows the linear regression for 165<T_S(K)<300 data points only, where $dS_0/dT_S = -1.4\times10^{-3}$ K^{-1}.*

The route to dissociative adsorption of H_2 thought to be responsible for the decrease in S_0 with increasing E_i on various metal surfaces (including W(100) [11], W(100)-c(2×2)Cu [16,21], Pt(533) [22,23], Pd(111) [24,25]) is predicted to encompass a dynamic channel to accompany the classical accommodated precursor channel. The dynamic channel (whether steering or precursor) is typically described as having little or no T_S dependence (e.g. W(100) [11]). The removal of the direct channel to dissociation from the E_i range over which this dynamic and/or accommodated channel is seen to fall off might be expected to allow the identification of a temperature independent dynamic channel, if present, from the temperature dependent accommodated channel. This was searched for by comparing the variation of $S_0(E_i)$ on the Mo(100)-c(2×2)N surface of two temperatures at opposite extremes of the range over which the S_0 is seen to fall (i.e. at 165K and 302K, see figure 8). Upon the H_2/Mo(100) system two $S_0(E_i)$ plots taken at differing T_S were seen to converge (figure 10 chapter IV), but, due to the overlap of the direct channel, it was unclear whether this

convergence occurred because of the disappearance of merely the accommodated channel (indicating a temperature independent dynamic channel) or whether the disappearance of both the dynamic and accommodated channel was required for the convergence of the plots. No convergence of the two sets of $S_0(E_i)$ data points taken for H_2/Mo(100)-c(2×2)N system was seen to occur until $S_0 \rightarrow 0$.

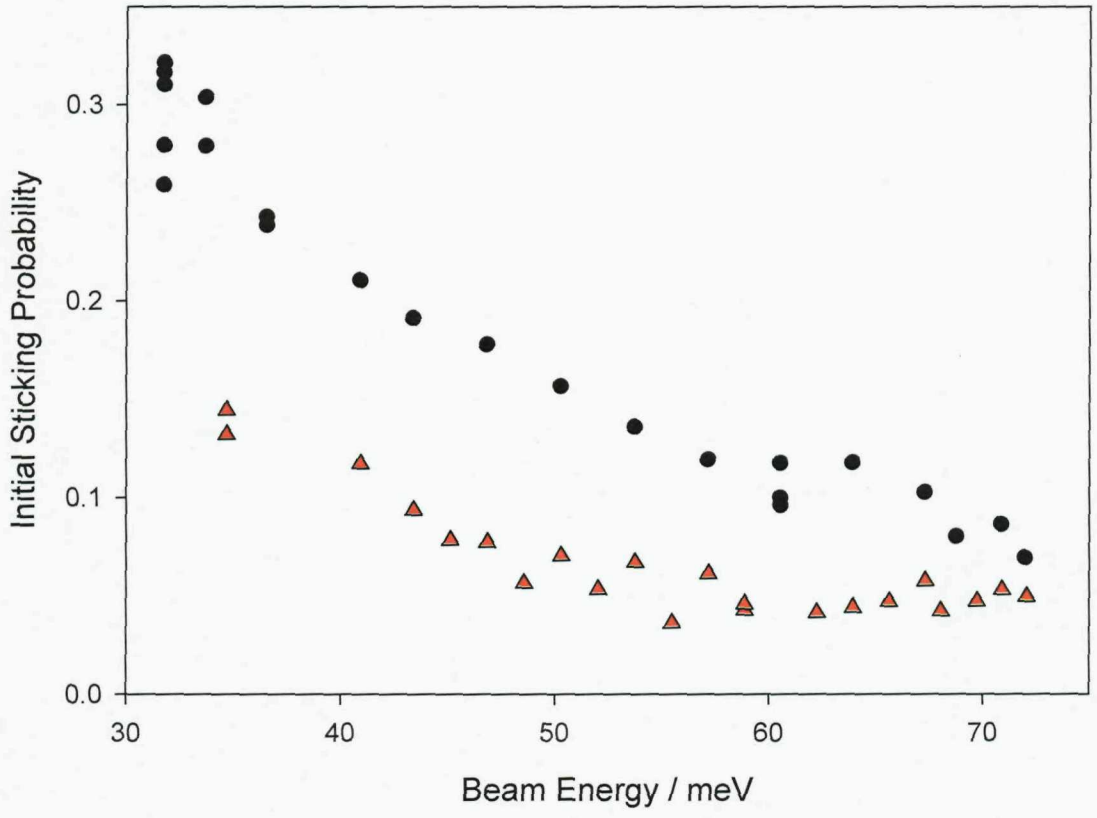

Figure 9: Initial sticking probability of H_2 on Mo(100)-c(2×2)N as a function of incident energy. T_S=160K (black circles), T_S=302K (red triangles). φ=0

At 72meV what little sticking remains was not seen to exhibit any more than the very most minimal of temperature dependencies. The small magnitude (S_0<0.1) and T_S independence of the initial sticking probability at this beam energy might imply direct sticking taking place on small areas of unperturbed Mo(100), perhaps at defect sites.

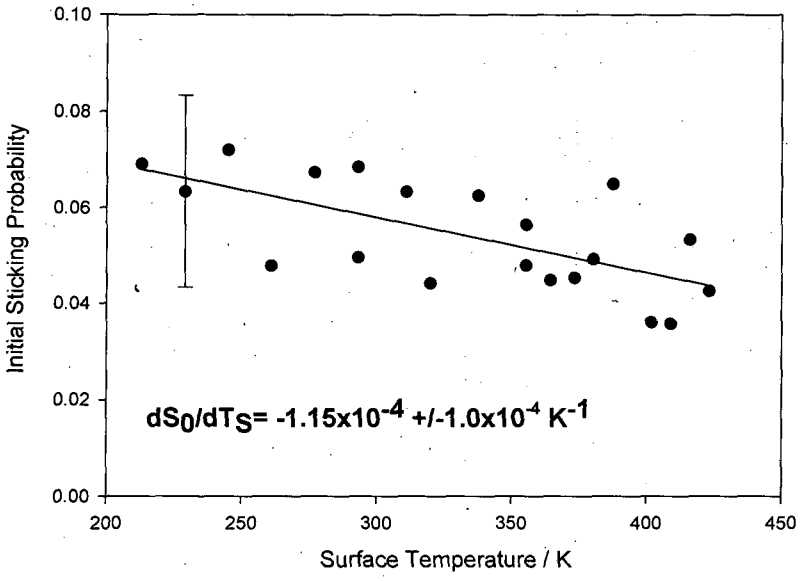

Figure 10: Initial sticking probability of H_2 on Mo(100)-c(2×2)N as a function of surface temperature, φ=0, E_i=72meV. Barely any T_S dependence is apparent given the size of the predicted errors.

V.3.6 Dependence of S on Hydrogen Coverage (θ_H)

At both E_i=13meV and 32meV a complex coverage dependence clearly exists. This is illustrated in figure 11 by the plots of $S(\theta_H)$, in both plots the sticking probability at first remaining relatively unaffected by changes in coverage, with the value of S then beginning to drop as θ_H increases, and this drop becoming more and more rapid as θ_H increases towards saturation coverage. This is consistent with an adsorption mechanism where the molecule does not require a vacant site for the initial trapping event to occur.

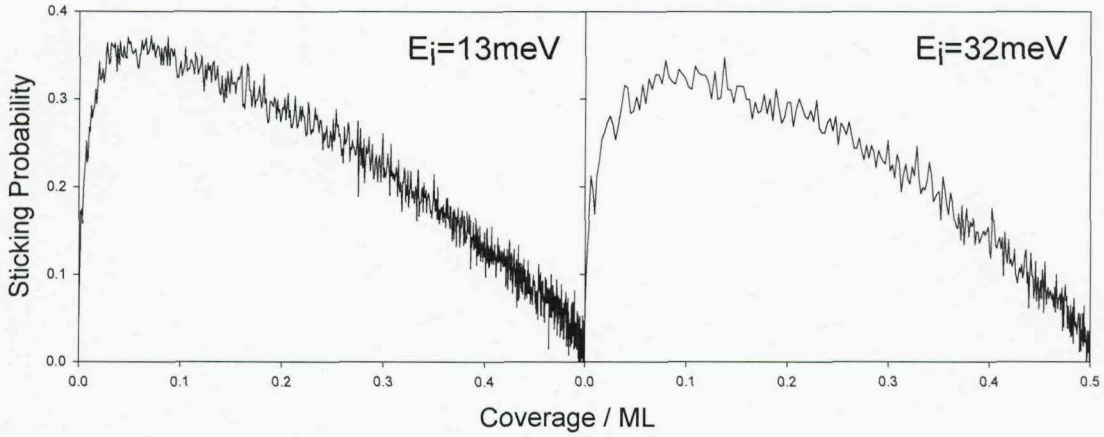

Figure 11: Sticking probability of H_2 on Mo(100)-c(2×2)N as a function of hydrogen coverage for E_i=13meV and E_i=32meV. T_S=165K, $\varphi=0^0$, and saturation coverage is 0.5ML.

V.4 Analysis

V.4.1 Dependence of S_0 on Incident Energy

The initial sticking probability of H_2 adsorbing on to the Mo(100)-c(2×2)N surface was observed to fall as E_i was increased from an initial value of 13meV, and to continue to decrease across the full range of measured incident energies (E_i<72meV). Such behaviour is consistent with the removal of the direct channel be present for the H_2/Mo(100) system across this range of E_i, i.e. the presence of nitrogen on the Mo(100) surface has shifted the barrier to direct dissociation upwards in energy, shifting the start point of the direct channel to E_i above the examined range where it no longer overlaps with the lower energy channel(s).

This removal of the direct channel overlap allows a more detailed examination of the lower energy channel(s). The expression "low energy channel" describing the decrease in S_0 with increasing E_i, seen to occur here between 0 and ~70meV, is used at present, in preference to referring to the indirect channel(s), to account for the possibility of a dynamic steering channel (an essentially direct type channel) making a contribution.

Upon Mo(100) this low energy channel, reaching to higher E_i than could be explained by a fully accommodated precursor channel, was interpreted in terms of a dynamic (either steering or precursor) channel (chapter IV.4.1) acting in conjunction with a classical indirect accommodated physisorption precursor channel. Such an interpretation has also been suggested for hydrogen adsorption onto the Pt(533) surface [22]. However, in the case of H_2 adsorption on Mo(100)-c(2×2)N the reach of the channel to high E_i cannot be automatically equated to the coexistence of a fully accommodated and a dynamic channel. The presence of nitrogen adatoms on the surface may considerably enhance the accommodated indirect channel, and whether this enhanced accommodated channel could account for significant sticking taking place up to almost 70meV must first be investigated.

A hard cube fit describing H_2 accommodated trapping upon a clean Mo substrate estimated the trapping probability to approach 0 by ~30meV (figure 9b chapter IV), this fell well short of what is required to account for the reach of the low energy channel of H_2 on the Mo(100)-c(2×2)N surface (up to ~70meV). Nitrogen adatoms, however, provide an enhanced mass-match for the light H_2 projectile from that provided by the considerably more massive molybdenum substrate atom and, incorporated into the hard cube calculation, results in an increased predicted trapping probability for a given E_i.

Figure 12 plots the $S_0(E_i)$ data measuring H_2 adsorption on the Mo(100)-c(2×2)N surface alongside hard cube trapping models for a variety of different effective surface masses. The effective surface mass allows the hard cube calculations to model the collision between incident particle and single surface atom, the atom often being allocated an increased mass to account for the collective response of the surface lattice during the collision. This scheme pictures the colliding particle as generating an impulse during the collision time, the impulse being a displacement of the crystal lattice positions propagating into the substrate lattice. It has been suggested [26] that the effective surface mass may be considered as being proportional to the distance which the impulse propagates into the lattice during the collision time, and hence proportional to the interaction time itself, which is in turn dependent upon the incident molecules velocity (a smaller velocity resulting in a longer interaction time). Typically the number of atoms expected to be involved might be between 1 and 5, with the

effective surface mass sampled converging towards 1 surface atom for very fast projectile molecules (i.e. very light or high energy molecules). Although the molecules here fall within the low energy regime hydrogen is a very light molecule and therefore will be expected to sample only a relatively small surface mass close to the value of a single surface atom.

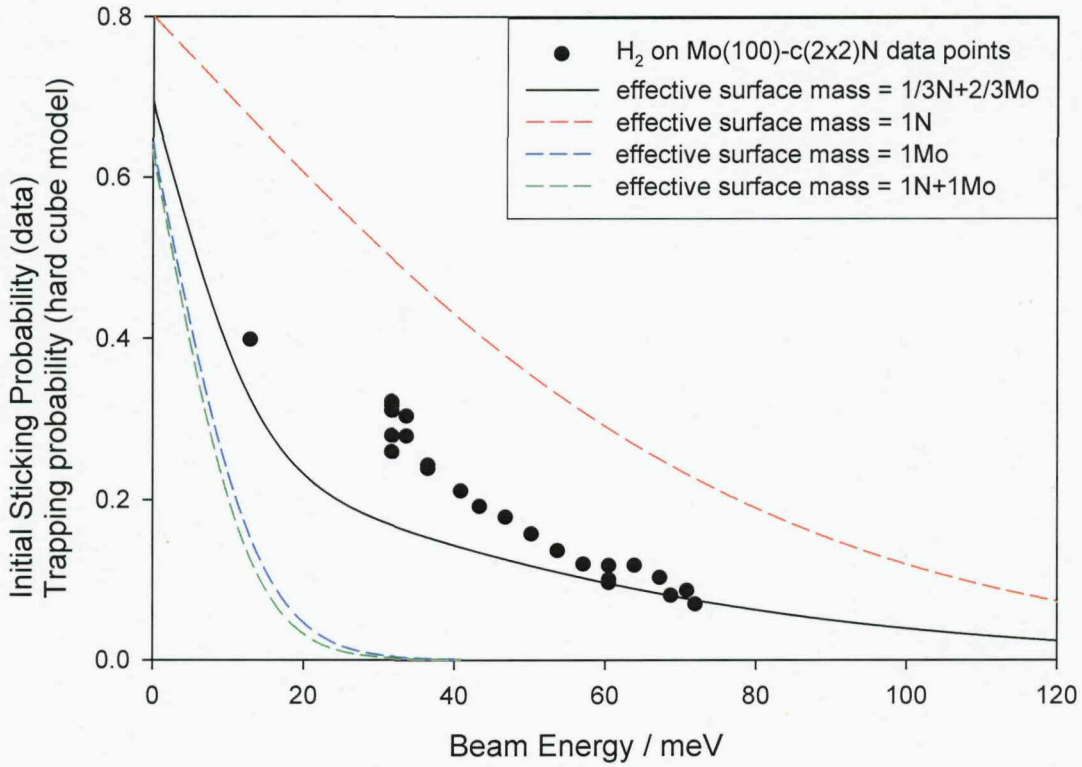

Figure 12: Comparison of the $S_0(E_i)$ values for T_S=165K, obtained via molecular beam K&W [27] type sticking, for H_2 adsorption on Mo(100)-c(2×2)N, and hard cube model trapping probability predictions for a variety of effective surface masses (with a well depth of 30meV, typical of a physisorption well for H_2 on a metal surface). The comparison is made with the proviso that the hard cube model only determines the trapping probability and that not all trapped molecules necessarily go on to dissociatively adsorb.

Initial indications are that the Mo(100)-c(2×2)N surface, as modelled by a hard cube calculation for the hydrogen interacting with a single N atom or a single Mo atom (the factor 1/3 and 2/3 accounting for the relative concentration of each at the surface), might well account for the low energy channel purely in terms of an accommodated precursor channel. This model is at the limit of the effective surface mass being equal

to the mass of a single surface atom, and the actual effective mass encountered by the H_2 is likely to be somewhat larger, resulting in lower trapping probabilities than those calculated here. It should also be noted that the hard cube model only accounts for the initial trapping event and any direct comparison between hard cube model and initial sticking probability data is making the assumption that all initially trapped molecules will go on to dissociate. The reality may be somewhat different, with a partition function (see equation V.5) defining the fraction of trapped molecules that go on to dissociatively adsorb. In the case of H_2 on both Mo(100) and Mo(100)-c(2×2)N the drop in S_0 with increasing T_S suggests the barrier to dissociation experienced by the precursor is smaller than the barrier to desorption, and in this case $S \rightarrow \zeta$ as $T_S \rightarrow 0$. However at 165K (the T_S for which the $S_0(E_i)$ data have been recorded) some fraction of the trapped molecule would still be expected to desorb as oppose to going on to dissociatively stick. Furthermore the presence of nitrogen is seen to alter the desorption site, the change in site from bridge to four fold hollow being accompanied by a reduction in bond strength (i.e. a shallower dissociative adsorption well). A more shallow dissociation well will tend to result in an increase in the barrier to dissociation, which, according to the partition function, would act to decrease the fraction of trapped molecules going on to dissociate. These considerations should emphasis the idea that although the hard cube model does serve as a good indicator, it cannot be relied upon here as definitive evidence of the accommodated channels ability to alone account entirely for the decrease in S_0, with increasing E_i, of H_2 on the Mo(100)-c(2×2)N surface occurring up to $E_i \approx 70$meV.

Alternatively to the hard cube model the improvement in energy exchange could also be envisaged in terms of an improved interaction time of the H_2 with the surface. The important role played by interaction time between projectile and surface was highlighted in a recent paper by Busnengo et al. [28] examining the interaction of H_2 with Pd surfaces using a surface oscillator model (as oppose to the rigid surface model commonly used to examine the PES of a H_2-metal system where energy exchange with the surface is neglected). The simulation changed the mass ratio either by increasing the mass of the projectile (from H_2 to D_2 or T_2) or by reducing the mass of the surface atom (while maintaining the surface oscillator vibrational frequency). If mass-match were to be the only defining factor in determining energy accommodation to the surface then a change in dissociation probability should be independent of whether it is

the surface mass or projectile mass which is altered. This was not found to be the case, with the calculations instead revealing little change when altering the surface mass value (which will alter the mass ratio while having little effect on the interaction time), but considerable change when changing the mass of the projectile molecule (a change that will alter considerably the evolution time of the molecule-surface collision and therefore change the overall interaction time of the molecule and surface). The conclusion drawn was that it was the time-scale of the interaction and not the mass ratio that was the main factor in determining the degree of energy exchange taking place between the molecule and surface.

The addition of nitrogen adatoms to the Mo(100) surface significantly alters the vibrational frequency (and therefore time period of vibration) of the surface atom which the H_2 projectile encounters. HREELS has been used to elucidate the surface phonon mode for a Mo surface (250 cm^{-1}) [29] and the stretching vibration mode of Mo-N (512 cm^{-1}) [2].

Equation V.1 defines the relationship between wavelength (and hence wavenumber) and vibrational frequency (υ_{freq}).

$$\upsilon_{freq} = \frac{c}{\lambda} \qquad \textbf{(V.1)}$$

The time period of a vibration being $1/\upsilon_{freq}$, thus giving a time period of vibration of 1.3×10^{-13} s for a Mo atom from the clean Mo(100) surface, and of 6.5×10^{-14} s for a N atom from the Mo(100)-c(2×2)N surface.

An estimate of the evolution time of the projectile molecule-surface collision is made assuming a distance of 0.5Å over which the interaction takes place (roughly equivalent to the repulsive portion of the PES encountered by an incoming molecule), with the evolution time (t) being equal to this interaction distance divided by the velocity of the projectile molecule (v). The velocity being calculated as follows:

$$E = 1/2 m v_{rms}^2 \qquad \textbf{(V.2)}$$

$$\therefore v_{rms} = \sqrt{\frac{2E}{m}} \qquad \textbf{(V.3)}$$

The interaction time for a 40meV beam thereby calculated as being $\sim 3\times10^{-14}$ s for H_2.

Figure 13 illustrates how the change in substrate from Mo(100) to Mo(100)-c(2×2)N can result in a time period of vibration much closer to the evolution time of the H_2 projectiles collision with the surface. This would result in an enhancement in the overall interaction time of the molecule and the surface and is therefore predicted to enhance the energy exchange taking place between molecule and surface. In figure 13 the evolution time for an N_2 molecule has been included to illustrate how the increased mass of the projectile acts to greatly increase the evolution time.

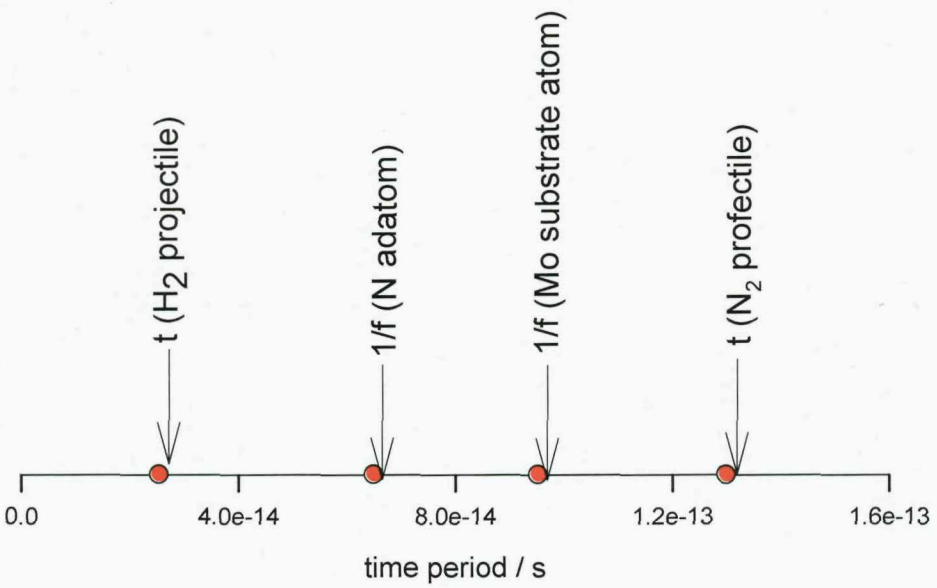

Figure 13: The evolution time of the molecule surface collision for a H_2 and N_2 projectile are plotted alongside the time period of vibration of an Mo substrate atom of the clean Mo surface and a N adatom of the Mo(100)-c(2×2)N surface.

Were a classical accommodated channel to account entirely for the low energy channel observed <70meV for H_2 adsorption upon the Mo(100)-c(2×2)N surface it would also be necessary for the presence of the c(2×2)N structure on the Mo(100) surface to account for the disappearance of the dynamic channel.

Two possible dynamic channels were suggested for H_2/Mo(100), dynamic steering or a dynamic precursor. A steering channel is typically thought to require a non-activated path to dissociation to be present and, although such a path appears to be present on the H_2/Mo(100) PES, it is clearly not for H_2/Mo(100)-c(2×2)N where the initiation of the direct channel is seen to shift to E_i>70meV. Because of this the disappearance of a dynamic steering channel is easy to account for and would, in fact, be expected. The disappearance of a dynamic precursor channel is somewhat more complicated to account for, with PES requirements of a dynamic precursor channel being somewhat more subtle. Generally the dynamic precursor is thought to require a substantial dynamic well due to a lowering of E^0_{vib} as the molecule approaches the surface, a late barrier (to allow access to this dynamic well), and a PES which encourages the molecules momentum normal to the surface to be converted into other molecular DOF. No detailed study of the PES of the H_2/Mo(100)-c(2×2)N has been performed, however the presence of the dynamic well formed by the lowering of E^0_{vib} requires a significant softening of the intra-molecular bond to take place. This softening occurs as the antibonding orbitals of the H_2 molecule shift downwards in energy as the surface is approached and the metals d-band electrons begin to interact with them as the bond with the surface begins to form [30]. The presence of nitrogen at the surface is likely to act to reduce the d-band electron density at the surface and hence might reduce the size of the dynamic well.

The alternative to the picture of a greatly enhanced accommodated channel being responsible for the reach and magnitude of the low energy channel observed on the Mo(100)-c(2×2)N surface, is of a low energy channel relatively unaffected by the presence of the nitrogen adatoms within the c(2×2) structure. The similarities in the magnitude of the S_0, and the energy range encompassed, by the low energy channels of H_2/Mo(100) and H_2/Mo(100)-c(2×2)N has already been noted (section V.3.4), and could be interpreted as a good indication that the presence of nitrogen adatoms on the Mo(100) surface acts only to move the activation of the direct channel upwards in energy to E_i above the energy range examined here, and that the low energy channel is left intact and relatively unaltered. The uncertainty in the hard cube models predictions of a large accommodated precursor channel have already been highlighted, and although the shift in the barrier to direct dissociative adsorption (resulting in the loss of the non-activated paths to dissociation) makes the presence of a dynamic steering

channel unlikely, it is by no means certain whether the dynamic channel present for the H_2/Mo(100) system is governed by a steering mechanism (a dynamic precursor also being a reasonable interpretation of the results). It remains a possibility that the increase in the accommodated channel caused by the presence of nitrogen adatoms is only small, and that a dynamic precursor channel remains largely responsible for the low energy channel of the H_2/Mo(100)-c(2×2)N system.

V.4.2 Dependence of S_0 on Surface Temperature

A plot of $S_0(T_S)$ taken at 32meV for H_2 dissociative adsorption on the Mo(100)-c(2×2)N was seen to exhibit a gradient far greater than that recorded for the nitrogen free Mo(100) surface (an entire order of magnitude greater).

On the Mo(100) surface a reduction in the T_S dependence (manifested by a decrease in the $S_0(T_S)$ gradient) between E_i of 13meV and 32meV was explained in terms of the disappearance of the accommodated channel and the relative T_S independence of the dynamic and direct channels which become more prominent with this jump in E_i. Section V.4.1 described how the presence of nitrogen adatoms on the Mo(100) surface will act to improve the ability of the surface to accommodate the E_i of the H_2 projectile improving the chances of the initial accommodated trapping event taking place, thereby enhancing the accommodated indirect channel to H_2 dissociation. Because of this it is reasonable to expect that, applying the same principals as have been used to explain the fall in T_S dependence between 32meV and 13meV on Mo(100) (i.e. the change in contribution from the T_S dependent accommodated channel acting to alter the observed T_S dependence), the T_S dependence at 32meV will be larger on the Mo(100)-c(2×2)N surface than on the Mo(100), with the nitrogen adatoms resulting in a more substantial contribution from the accommodated channel.

What does seem unusual is the magnitude of the gradient of $S_0(T_S)$ on Mo(100)-c(2×2)N, it being slightly more than double that observed even at E_i=13meV, the lower energy (where the accommodated channel is expected to be more prominent and hence the temperature dependence larger), upon the Mo(100) surface. The

explanation may lie in the trapping probability still being considerably larger on Mo(100)-c(2×2)N at 32meV than on Mo(100) at 13meV, according to the partition function (equation V.5) a greater trapping probability resulting in a steeper $S_0(T_S)$ gradient. The hard cube model predicts a trapping probability of only 0.15 for Mo(100) while a sticking probability roughly double this is recorded on Mo(100)-c(2×2)N. If this sticking probability is due entirely to an accommodated channel (unlike Mo(100) where S_0 is derived from a combination of direct, dynamic as well as the accommodated channels) the increase in accommodated trapping probability may be sufficient to account for the steeper gradient.

Another factor to affect the T_S dependence will be the difference in the barrier to desorption and dissociation, ΔE, of the accommodated precursor. According to the partition function (equation V.5) a drop in ΔE would also result in a greater dependence of the dissociative sticking probability on T_S over the recorded range. The shift in dissociative adsorption site from the bridge of the clean Mo(100) to the less energetically favourable four fold hollow on the Mo(100)-c(2×2)N would be expected to be accompanied by just such a drop in ΔE.

$$S_0 = \alpha\left(1+\frac{\upsilon_{des}}{\upsilon_{diss}}e^{\left(-\frac{\Delta E}{RT_S}\right)}\right)^{-1} \qquad \textbf{(V.5)}$$

The large dependence of S_0 on T_S at E_i=32meV displayed by the H_2/Mo(100)-c(2×2)N system adds support to the picture of a greatly enhanced accommodated channel with respect to that of the Mo(100). The gradient, $dS_0/dT_S=1.4\times10^{-3}$ K^{-1}, can be accounted for if the low energy channel of the H_2/Mo(100)-c(2×2)N system is considered as being due entirely, or almost entirely, to an accommodated precursor channel where trapping takes place via the accommodation of the projectile molecules energy to the surface, with little or no contribution to the low energy channel from a T_S independent dynamic adsorption mechanism.

A caveat to this proposition is the possibility that the large T_S dependence might instead be due to the temperature range over which the gradient is measured coinciding

with the temperature at which all hydrogen will desorb from the Mo(100)-c(2×2)N surface.

Bafrali and Bell [1] reported two desorption peaks of hydrogen from the Mo(100)-c(2×2)N surface, occurring at 325K and 550K, well above the 165-300K temperature range over which dS_0/dT_S was measured. However doubt has already been cast over the validity of these peaks in describing desorption from the pure Mo(100)-c(2×2)N surface (see section V.2.2), with the true desorption peak postulated to be below the temperature range over which Bafrali and Bell recorded their TPD.

V.4.3 Dependence of S on Hydrogen Coverage (θ_H)

In chapter IV a comparison between the θ_H dependence of H_2 adsorption upon the Mo(100) and W(100) surfaces illustrated the importance of the bridge bonding site reconstruction in determining the sticking probability, with changes in θ_H determining the degree of bridge site reconstruction. This dependence on bridge site reconstruction made the behaviour of S with respect to θ_H somewhat complicated to analyse, with uncertainty surrounding the degree to which any coverage dependence was due to adsorption site reconstructions and the degree to which the coverage dependence was reflective of an extrinsic indirect adsorption channel. The change in adsorption site, from bridge to four fold hollow, caused by the creation of the c(2×2)N structure upon the molybdenum surface, removes this uncertainty. What remains is a complex coverage dependence whose behaviour can be clearly assigned to the influence of an indirect channel to dissociative adsorption. The sticking probability of H_2 on the Mo(100)-c(2×2)N surface initially appears relatively insensitive to θ_H. As θ_H increases S falls more and more rapidly. This can be understood in terms of a precursor which does not require a vacant surface site over which to accommodate accounting for the initial θ_H independence, and the ability of the precursor to find a vacant site at which to dissociate becoming a limiting factor, and causing a drop in S, as the surface begins to saturate.

The strong similarity between the $S(\theta_H)$ plots taken at 13meV and 32meV is also worthy of note. Figure 14 superimposes the plot taken for 32meV onto that of 13meV, illustrating an almost perfect match between the two. This implies that adsorption at 32meV takes place via the same adsorption channel(s) as at 13meV. Due to the good mass match provided by the N adatoms an accommodated precursor channel is predicted to dominate at very low energies. The similarity of $S(\theta_H)$ at 13 and 32meV implies that the dominance of this accommodated channel stretches comfortably to incident energies as high as 32meV, supporting the picture of an enhanced accommodated precursor channel accounting fully for the drop in S_0 of H_2 with increasing E_i over the entire energy range on the Mo(100)-c(2×2)N surface.

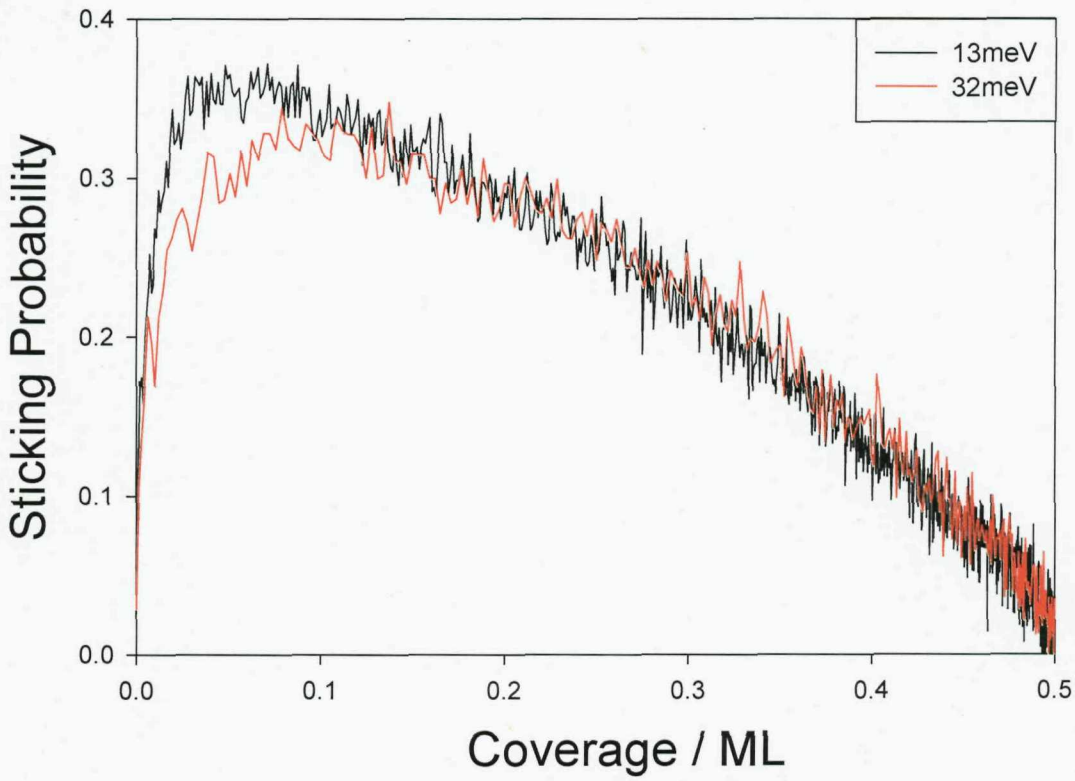

Figure 14: Sticking probability of H_2 on Mo(100)-c(2×2)N as a function of hydrogen coverage at T_S=165K and $\varphi=0^0$. Results from the E_i=32meV beam (red) have been superimposed on top of those from the 13meV beam.

There is a slight increase in initial sticking probability apparent at 32meV, occurring as hydrogen first begins to be adsorbed upon the Mo(100)-c(2×2)N. This increase in sticking takes place up to ~0.1ML and is not seen when using an E_i=13meV beam,

where S instead exhibits a coverage independence. Perhaps this indicates intrinsic and extrinsic accommodated precursor channels acting in tandem, with the extrinsic channel initially acting to increase S with increasing θ_H as the already adsorbed hydrogen provides a better mass match than the molybdenum atoms of the substrate for the trapping of subsequent H_2 molecules (before the lack of vacant sites for dissociation itself becomes limiting), and the intrinsic channel always acting to decrease S with θ_H as the concentration of vacant sites drops. The importance of the extrinsic channel might be expected to become more evident at higher E_i (i.e. at 32meV as opposed to 13meV), where accommodation of a larger quantity of E_i is required to allow the trapping event to take place and collision with the poorly mass matched molybdenum substrate atoms may begin to become insufficient. This might well be expected to result in an increase in S with θ_H occurring for E_i=32meV which is hidden by the more prominent contribution of the intrinsic channel at 13meV.

V.4 Conclusion

During the creation of the Mo(100)-c(2×2)N surface, a prolonged period of nitrogen adsorption was seen to result in the presence of two atomic adsorption states. Upon annealing the nitrogen saturated Mo(100) surface presented two nitrogen desorption peaks, labelled β_1 and β_2, occurring at ~325K and ~550K respectively, and with a ratio of 1:2. This is the first time the β_1 peak has been identified, but its presence should be expected given the presence of the 2 β, atomic nitrogen, peaks observed to be present for the N/W(100) system and taking into account the numerous other similarities between the two systems. The creation of the c(2×2)N structure on the Mo(100) surface is identified with the removal of the β_1 state.

The Mo(100)-c(2×2)N surface saturates with a hydrogen coverage of 0.5ML, corresponding to hydrogen occupying half all four fold hollow sites (with nitrogen adatoms already present in the other half of these sites).

Molecular beam King and Wells [27] type sticking experiments examining H_2 dissociative adsorption on the Mo(100)c(2×2)N surface revealed an initial sticking

probability which dropped with increasing incident energy up to an energy of 70meV. This corresponds to the removal of the large non-activated direct channel displayed by H_2 adsorption upon the clean Mo(100) surface. The loss of the non-activated direct channel is associated with the change in hydrogen dissociative adsorption site from bridge to four fold hollow, accompanied by a shift in barrier to direct dissociation, induced by the presence of the c(2×2)N structure.

The low energy adsorption channel of H_2 on Mo(100)-c(2×2)N is characterised by a falling initial sticking probability with increasing H_2 incident energy, and is due predominantly to an indirect accommodated precursor channel greatly enhanced from that presented by the nitrogen free Mo(100) surface, with either a small or no contribution from a dynamic precursor channel, and no dynamic steering channel contribution possible due to the removal of the non-activated direct dissociation channel. Hard cube model calculations clearly illustrate the greater reach and magnitude of the Mo(100)-c(2×2)N accommodated precursor channel over that of the Mo(100). The hard cube predictions are supported by a considerable T_S dependence indicative of a large accommodated trapping contribution to the initial sticking probability. Furthermore, the sticking probability at low incident energies exhibits complex coverage dependence indicative of an indirect adsorption channel dominating the sticking.

V.5 References

1) Bafrali R., Bell A. T., Surf. Sci., 278(1992)353

2) Zhu J. F., Guo J. C., Zhai R.S., Bao X>, Zhang X. Y., Zhuang S., Applied Surf. Sci., 161(200)86

3) Ren S. Z., Zhai R.S., Chinese J. Catal. 22(2001)297

4) Volpe L., Boudart M., J. Phys. Chem., 90(1986)4878

5) Schlatter J.C., Oyama S. T., Metcalf J. E., Lambert J. M., Ind. Eng. Chem. Res., 27(1988)1648

6) Oyama S. T., Sajkowski D. J., Prepr. Am. Chem. Soc., Div. Pet. Chem. 35(1990)233

7) Zaera F., Kollin E. B., Gland J. L., Surf. Sci., 166(1986)L149

8) Arrecis J. J., Chabal Y. J., Christman S. B., Phys. Rev. B, 33(1986)7906

9) Chabal Y. J., Christman S. B., Arrecis J. J., Prybyla J. A., Estrup P. J., J. Electron Spec.and Rel. Phenom., 44(1987)17

10) Butler D. A., Hayden B. E., Topics in Catal., 1(1994)343

11) Butler D. A., Hayden B. E., Jones J. D., Chem. Phys. Lett., 217(1993)423

12) Ota K., Tanaka M., Usami S., J. Electron Spec. and Rel. Phenom. 88-91(1998)571

13) Sellidj A., Erskine J.L., Surf. Sci., 220(1989)253

14) Clavenna L. R., Schmidt L. D., Surf. Sci., 22(1970)365

15) White J. A., Bird D. M., Payne M. C., Phys. Rev. B, 53(1996)1667

16) Butler D. A., Hayden B. E., Surf. Sci., 337(1995)67

17) Guo J. Ch., Zhu J. F., Luo H. B., J Mol. Catal. (China) 13(1998)259

18) Kanama D., Tanaka M., Matsuoka H., Shudo K. I., Fukutani K., Koide T., Japanese J. Applied Phys. 1, 43(2004)1551

19) Han H. R., Schmidt L. D., J. Phys. Chem., 75(1971)227

20) Prybyla J. A., Estrup P. J., Ying S. C., Chabal Y. J., Christman S. B., Phys. Rev. Lett., 58(1987)1877

21) Butler D. A., Hayden B. E., Chem. Phys. Lett., 232(1995)542

22) Mormiche C., PhD. Thesis, University of Southampton, 2002

23) Gee A. T., Hayden B. E., Mormiche C., Nunney T. S., J. Chem. Phys., 112(2000)7660

24) Busnengo H. F., Crespo C., Dong W., Rayez J. C., Salin A., J. Chem. Phys., 116(2002)9005

25) Crespo C., Busnengo H. F., Dong W., Salin A., J. Chem. Phys., 114(2001)10954

26) Grimmelmann E.K., Tully *T.C.*, Cardillo M.J., J. Chem. Phys. 72(1980)1039

27) King D. A., Wells M. G., Surf. Sci., 29(1972)454

28) Busnengo H. F., Di Cesare M. A., Dong W., Salin A., Phys. Rev. B, 72(2005)125411

29) Chen J. G., Chem. Rev. 96(1996)1477

30) Lundqvist B. I., Gunnarsson O., Hjelmberg H., Norskov J. K., Surf, Sci., 89(1979)196

31) Harris J., Surf. Sci., 221(1989)335

Chapter VI: Nitrogen adsorption on Mo(100)

VI.1 Introduction

Although the kinetics and surface structure of the N/Mo(100) system has been the subject of a handful of studies (including those of this thesis recorded in chapter V) the dynamics of the N_2/Mo(100) adsorption system has remained almost entirely untouched. The dynamics of the N_2/W(100) adsorption system, on the other hand, has been the subject of extensive experimental and theoretical investigation and is considered a model adsorption system, and since the kinetics and surface structures resulting from the adsorption of nitrogen upon the Mo(100) and W(100) surfaces show many close similarities, a comparison of the dynamics of the two is performed to help shed light on the mechanisms responsible. This chapter examines how the sticking probability of N_2 on Mo(100) varies with the incident energy of the N_2 molecule, the temperature of the Mo(100) surface, and its level of nitrogen pre-coverage.

VI.2 Literature Analysis

This section deals almost entirely with dynamical studies on the adsorption of nitrogen on Mo(100) (and comparisons with the equivalent W(100) adsorption system). For a description and analysis of the structure and kinetics of this system please refer back to chapter V.

VI.2.1 The kinetics and structure of the N/Mo(100) system

The kinetics and surface structure of nitrogen adsorbing onto the Mo(100) surface has already been examined in some detail in chapter V. The important aspects noted are as follows:

a) Two atomically chemisorbed, β, states exist, one (β_2) relating to the formation of the c(2×2) structure, and the other (β_1) only occurring after large doses of N_2.

b) β_2 saturation occurs at 0.5ML.

c) Complete β saturation (of β_1 and β_2) occurs at 0.75ML.

d) Atomic nitrogen tends to bond into the fourfold hollow sites.

e) The two β desorption peaks occur at 1080K and 1320K (for β_1 and β_2, respectively).

f) Two molecularly chemisorbed states exist, labelled γ^+ and γ^-, these are thought to correspond to molecular chemisorption with the molecule bonded perpendicular and parallel to the surface respectively [1].

g) The strong similarity between the adsorption states nitrogen forms upon the Mo(100) and W(100) is noted: both displaying β_1 and β_2 peaks at similar temperatures, both bonding into the fourfold hollow sites, with similar saturation coverage values, both surfaces also forming the c(2×2) structure with N bonded in half all fourfold hollow sites at 0.5ML. Also two molecularly chemisorbed states are observed upon both surfaces [1,2] labelled γ^+ and γ^-, these correspond to N_2 bonding perpendicular and parallel to the surface with King et al. having first identified the γ^+ and γ^- as having different bonding geometries [3]. Desorption from these states was observed to take place at very low surface temperatures, well below room temperature, observed on the W(100) surface at 170K and 180K respectively [2] and observed in this study to both occur at around 205K on Mo(100) (although a lack of accuracy in the low temperature readings meant that no observation of peak separation was possible here).

VI.2.2 Comparison of the kinetics and structure with N/W(100)

Given the similarity between nitrogen adsorption upon the Mo(100) and W(100) surfaces and the lack of data regarding, in particular, the dynamics for the Mo system, it seems pertinent to carry out an analysis of the dynamics of nitrogen adsorption on W(100), this system having received extensive attention and being considered to be a model adsorption system.

To add to the description of the kinetics and structure of nitrogen adsorption on W(100) described in the above comparison of the two it is also worth noting the studies of Grunze et al. [3] in identifying a mobile extrinsic physisorbed precursor to the chemisorbed γ state, this condensed phase physisorbed state being observed when T_S is held at 20K and areas of γ already exist on the surface. No intrinsic physisorbing precursor was observed, the potential energy surface therefore being thought to lead smoothly into the potential minimum of the linearly bonded configuration without any appreciable activation barriers between physisorption on the bare metal and chemisorption [3].

The overall suggested picture for N_2 adsorption on W(100) is of molecules going through a number of precursor states on the way to dissociation [4]. The initial step is suggested to be the steering of the molecule into the γ^+ state at the atop site, followed by subsequent migration to the bridge site, reorientation of the molecule to lie flat along the surface aligned parallel to plane two atoms making up the bridge site, and then a further reorientation of the molecule perpendicular to the bridge site (but still in the plane of the surface) to allow the molecule to dissociate into adjacent hollow sites [4], this being found to be the most exothermic dissociation site [4,5,6]. There was calculated to be a barrier to dissociation of the molecule in the bridge-hollow configuration [4], so the dissociation at the lowest energies from the precursor states may well be dominated by surface defects, as, for example, is suggested for the N_2/Fe system [7].

For the N_2 precursor bonding perpendicular to the surface at an atop site the picture which has been presented is that of 5σ and 2π orbitals of the molecule being localised

on the outer atom and the 4σ localised more on the inner, and the 1π having components on both atoms, with rehybridization of the 1π and 2π orbitals giving a lone pair on the outer atom (π_{out}) and metal-N bonding through the 2π component (π_{in}) on the inner atom. This picture was first suggested by Nilsen et al. for N_2 on Ni(100) [8], being found to be accurate also for the $N_2/W\gamma^+$ state [4].

VI.2.3 Dynamics of the N_2/W(100) adsorption system

The initial sticking probability of nitrogen on the W(100) surface displays non-monotonous behaviour, initially decreasing with increasing incident energy up to about 450meV, thereafter displaying a more gradual increase in S_0 with increasing E_i [9-11]. This is indicative of at least two channels to adsorption being present.

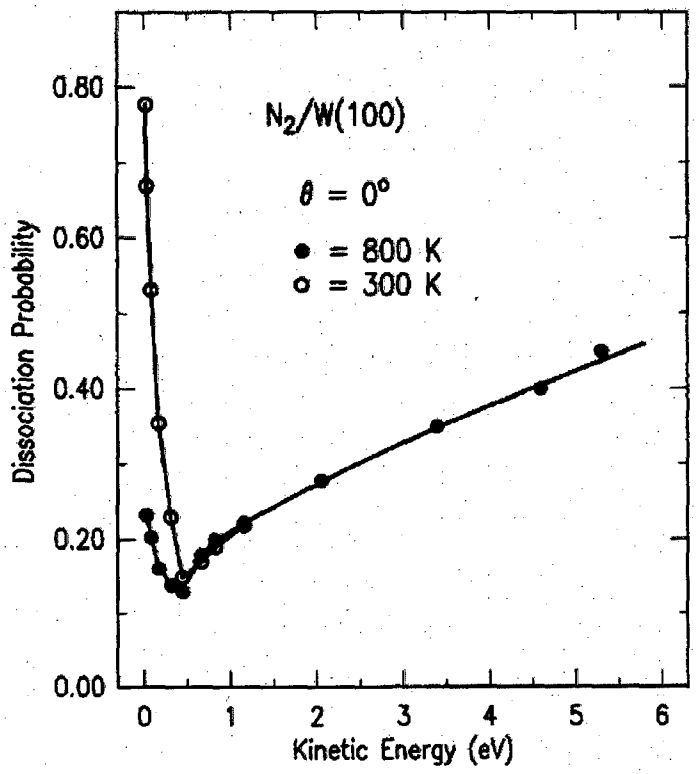

Figure 1: Reproduction of plot of $S_0(E_i)$ for N_2 adsorption on a W(100) surface, $\varphi=0^0$, taken for surface temperatures of 300K and 800K as indicated. This plot is taken from [11]

i) The Precursor Channel

a) Incident energy dependence

The initial decrease in S_0 is fairly rapid, with the sticking probability dropping from ~0.8 at 26meV to ~0.15 by 450meV [9]. This is behaviour typical of a precursor type channel, where the sticking probability decreases as the initial trapping event becomes less probable as a greater fraction of E_i must be accommodated in order for the molecule to trap.

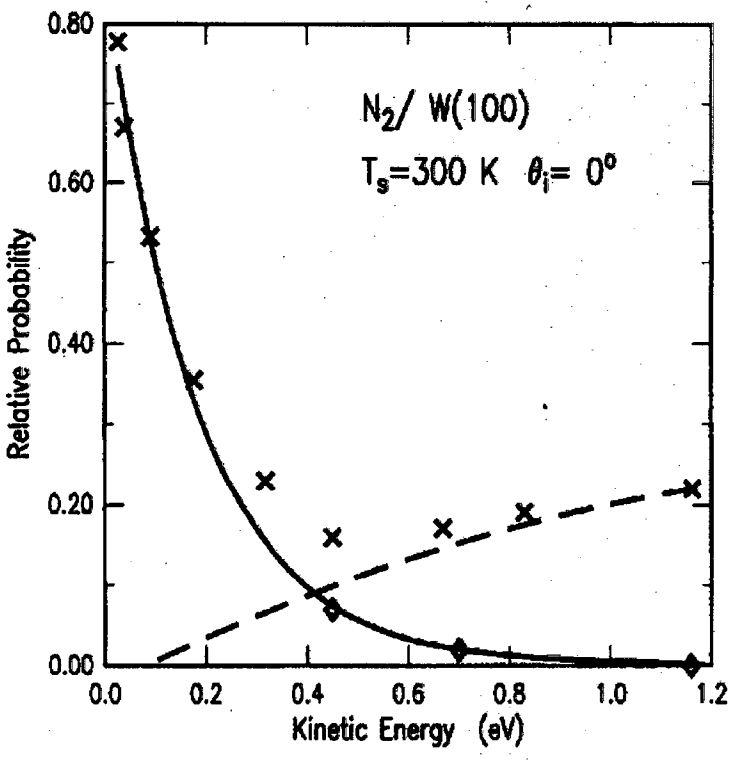

Figure 2: Reproduction of plot of $S_0(E_i)$ for N_2 adsorption on a W(100), $\varphi=0^0$, T_S=300K. The crosses indicate the overall S_0 values obtained directly from measurements. The diamonds represent an estimation of the indirect channel contribution to S_0 and this indirect channel has been provided with a fit of the form $S_{0(indirect)}=(a)\exp(-E_i/b)$. The dashed line is a fit to the difference between the solid curve and the crosses and is a prediction of the direct dissociation channel. This plot is taken from [11]

This behaviour is supported by a strong T_S dependence, a complex coverage dependence (with the sticking probability remaining constant over a large coverage range), and a large cosine scatter component, all of which are indicators of a precursor channel being in operation and being the dominant factor in determining the sticking probability.

b) Surface temperature dependence

The T_S dependence within the precursor channel sees the initial sticking probability fall for a 30meV beam from ~0.8 at 300K to <0.2 at 1000K [9], and from ~0.6 at 200K to ~0.1 by 1000K for a 88meV beam [10]. By plotting $\ln((\zeta/S_{0(accom)})-1)$ against $1/T_S$, (this relationship originating from the Arrhenius type relationship reproduced here in equation VI.1), and by assuming a trapping probability which remains constant with T_S, a linear regression fit allowed ΔE and $\upsilon_{des}/\upsilon_{diss}$ to be calculated [9], the values determined as being 0.16±0.01eV and 18±3 respectively. The ratio of $\upsilon_{des}/\upsilon_{diss}=18$ provided a rough guide to the relative steric constraints for desorption and dissociation. From this value it was concluded that the steric requirements for dissociation are considerably more stringent than for desorption [11].

A slight deviation from linearity was noted. This was shown to be associated with the trapping probability exhibiting a slight temperature dependence, with ζ recorded by monitoring the fraction of scattered flux not accounted for in the direct elastic scattering channel, the plot of ζ as a function of T_S was seen to display a slight curvature, varying by as much as 20% over the range $150<T_S(K)<1500$ [12], this was further supported by hard cube calculations predicting a very similar behaviour. By including the variation in ζ in the Arrhenius type plot the slight curvature was eliminated, with no significant change seen to take place in the gradient estimation and therefore the calculated ΔE and $\upsilon_{des}/\upsilon_{diss}$ values [11]. This weak dependence of ζ on T_S confirmed the strong T_S dependence as being predominantly due to changes in the fraction of trapped species desorbing (as oppose to the degree of trapping able to take place), i.e. T_S primarily served to reduce the number of molecules that went on to dissociate, by biasing the kinetics in favour of desorption..

$$S_0 = \zeta\left(1+\frac{\upsilon_{des}}{\upsilon_{diss}}e^{\left(-\frac{\Delta E}{RT_S}\right)}\right)^{-1} \qquad \text{VI.1}$$

As well as examining the variation of trapping probability with T_S, a hard cube fit is also able to provide close agreement with the disappearance of the trapping channel by 0.5eV observed by experiment [11] (using a cube mass, m, of between 1 and 1.8 surface atoms and a well depth, U, of 0.27eV, this value based on the estimated well depth for the N_2/W(110) system [13]). Good agreement with the hard cube model is indicative of an accommodated precursor channel, where sticking takes place via energy loss to the surface during an initial collision at which the molecule traps or rebounds back into the vacuum, the fate of the molecule within the hard cube model depending upon whether or not sufficient momentum normal to the surface is retained after the collision to allow the molecule to escape the attractive potential well created by the surface. In a simple picture of this, trapping will occur when the fraction of incident energy that is lost to translation exceeds $E_i/(E_i+U)$.

c) Coverage dependence

The sticking probability of N_2 on W(100) was found to be initially independent of the level of nitrogen coverage (within the low energy region in which the precursor adsorption channel is expected to be dominant), with the sticking probability remaining steady up to a coverage of 0.3ML then dropping steadily up to the point at which the surface saturates (at ~0.6ML) [9,10]. A lack of coverage dependence is typical behaviour for a mobile extrinsic precursor, where the initial trapping event does not require a vacant surface site over which to take place, the sticking only beginning to fall once the availability of vacant surface sites becomes limiting. The coverage dependent behaviour of the sticking probability appeared to be relatively independent of T_S within the energy range at which the precursor channel dominates, with the exception that at very low T_S (85K) the coverage curve actually extends to >1.5ML , (while only reaching to 0.6 ML at 200K and 800K) with the plot remaining flat virtually all the way up to 1.5ML [10]. Subsequent heating of this saturated surface was seen to produce a desorption peak in the region of 180K corresponding to desorption from the γ molecular state, indicating that at low surface temperature population of both the atomic and molecularly chemisorbed states is possible and that almost all trapped molecules go on to dissociate (since no visible change in the sticking probability occurred with the saturation of the atomic state at ~0.6ML, and subsequent population of the purely molecular). This proposal was supported by scattering

experiments which failed to detect a trapping desorption component for the clean surface under these conditions, indicating that all trapped species did indeed stay on the surface [10].

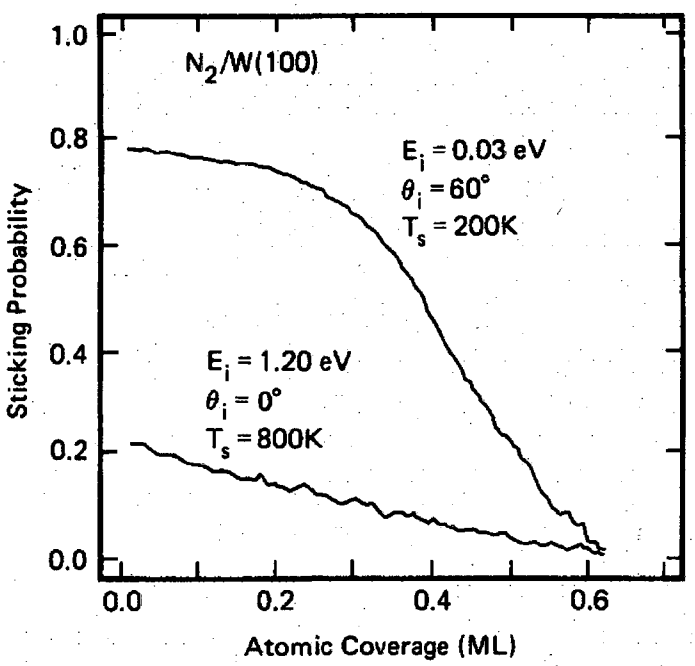

Figure 3: Reproduction of a plot of $S(\theta_N)$ of N_2 adsorption on a W(100) surface for E_i=0.03eV, incident angle (denoted in figure as θ, not to be confused with coverage) $\varphi=60^0$, T_S=200K (upper curve), and for E_i=1.2eV, $\varphi=0^0$, T_S=800K (lower curve). This plot is taken from [9]

The flatness of the sticking coverage plot suggests that the trapping probabilities into the extrinsic and intrinsic precursor states are virtually identical at low energies and surface temperatures. This might be considered rather surprising since the adsorbed nitrogen either in the β, atomic form, or γ, molecular form, would be expected to modify the interaction potential and the effective surface mass. An explanation offered was that trapping occurs at distances well beyond the plane containing the adsorbates. Such a picture being supported by the fact that the sticking probability was seen to become more dependent on the coverage as the E_i is increased (within the realms of the indirect channel, i.e. E_i<400meV) [10], with the flat region of plots taken at 0.03, 0.088 and 0.26eV becoming increasingly less flat. The sticking probability of a 0.03eV plot (T_S=85K) was seen to remain essentially constant (at S=0.88±0.03) with increasing coverage, whereas a plot of S(θ) at 0.26eV and 85K saw the sticking probability initially fall slightly up to ~0.6ML before rising again up until a coverage of 1.5 after which S quickly drops to 0. A higher collision energy is likely to be associated with a closer approach of the molecule to the surface, and based on this, an explanation for the phenomenon was offered in terms of a smaller trapping probability for a site

containing an atomic β species (due to the change in the potential), but a larger trapping probability for a site containing the molecular γ species (perhaps due to the improved mass match between the projectile molecule and surface species).

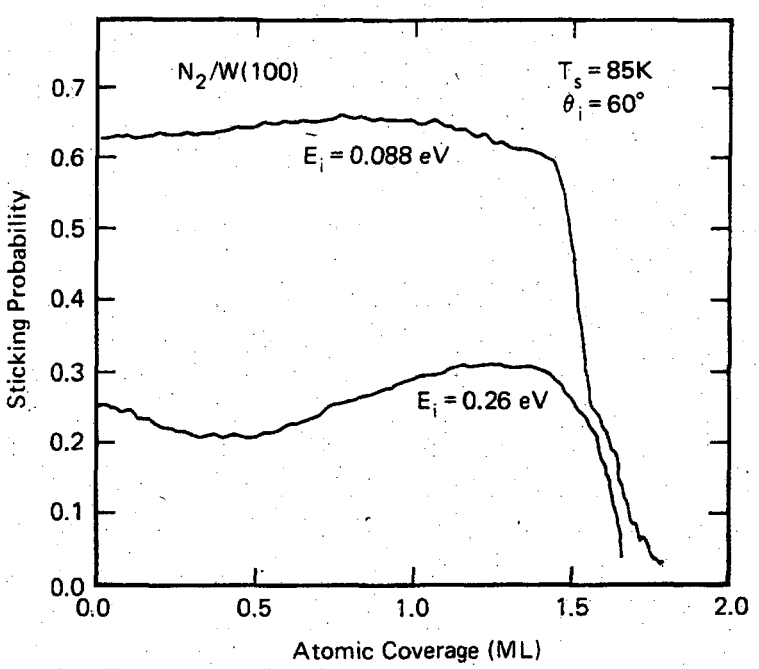

Figure 4: Reproduction of a plot of $S(\theta_N)$ of N_2 adsorption on a W(100) surface for T_S=85K, $\varphi=60^0$, and E_i of 0.088eV (upper curve) and 0.26eV (lower curve). This plot is taken from [10]

d) Theoretical investigations

Most of the experimental data regarding the N_2/W(100) adsorption system has now stood for well over 10 years, allowing the system to be considered as a model system for typical accommodated precursor mediated dissociative adsorption. However, a recent theoretical study, using ab initio calculations at the DFT/GGA level to construct a 6D PES for the interaction of the N_2 with the frozen W(100) surface, has suggested that, as has already been demonstrated to be the case for hydrogen adsorption systems [14-19], dynamic trapping might play a crucial role in the precursor mediated adsorption of nitrogen on the W(100) metal surface.

Most molecules were predicted to follow a complex route to dissociation, undergoing multiple encounters with the surface, the average number of rebounds before dissociation being 21 at 0meV, 7.7 at 200meV and 3.1 at 1eV [6]. Such behaviour might correspond to dynamic trapping, with multiple collisions occurring before

dissociation takes place typically corresponding to a dynamically trapped molecule. The dynamic trapping behaviour postulated [6] is explained in terms of a bow net effect: the molecule, once it has reached a distance of ~2.3Å from the surface, finding itself below a potential roof with the only way back to vacuum being through the top-vertical configuration, thereby causing a bottleneck in phase space. This dynamic precursor might be expected to trap more readily than the typical accommodated type.

Whereas the form of dynamic trapping responsible for the dynamic precursor of hydrogen allowed molecules to trap without the need for accommodation of energy to the surface, with the initial incident energy instead being dissipated to other molecular degrees of freedom, resulting in the prediction of trapping taking place with little or no dependence on T_S, accommodation of the much heavier N_2 projectile is not a problem, energy being exchanged readily with the surface, particularly after multiple encounters. The result of this is a dynamic precursor channel to dissociative adsorption that is likely to display the same strong T_S dependence exhibited for the typical accommodated precursor equivalent.

In the case of hydrogen a dynamic precursor is traditionally associated with a weakening of the intra-molecular bond and corresponding drop in the vibrational ground state of the molecule creating a potential well in the exit channel [20,21]. Such behaviour could struggle to account for the variation of the coverage dependent behaviour of the sticking probability with E_i described above, the suggested explanation for which relied upon a picture of trapping at low E_i taking place at a distance well beyond the plane of the adsorbates [10]. To cause the weakening of the intra-molecular bond the molecule is required to make a relatively close approach to the surface in order to begin to experience a bonding interaction with the surface. However, in the case of N_2, where the suggested mechanism is instead associated with the standard physisorption/chemisorption potential wells and the requirement that the molecule be in a specific orientation in order to penetrate a potential roof and return to the vacuum, the dynamic mechanism is fully compatible with the suggested explanation regarding the variations in coverage dependence.

It begins to become clear that from this analysis that the behaviour of this form of the dynamic precursor might be harder to identify from that of the typical accommodated

precursor than is the case for the H_2 dynamic precursor mediated adsorption system. The main observable effect of the N_2 dynamic trapping channel is likely to be a somewhat greater degree of successful trapping for a given incident energy and thereby a precursor dissociation channel reaching across a greater range of E_i, (and correspondingly small trapping desorption component in the scatter as most trapped molecules will tend to go on to dissociate even at high T_S) than might be predicted by typical precursor dynamics.

Although the peculiar energy dependence of the coverage within the precursor dominated E_i region is shown to be consistent with the suggested N_2 dynamic precursor mechanism, the lack of any large discrepancy between the actual data and hard cube model (as was observed for the H_2/W(100) and H_2/Mo(100) systems), the hard cube model trajectory studies providing semiquantitative agreement with the behaviour of the N_2/W(100) system recorded by the molecular beam studies [10], and the strong temperature dependence, are both factors counting against the dynamic precursor picture. Clearly the existence of a dynamic precursor to nitrogen adsorption might therefore merit further investigation.

ii) The Direct Channel

a) Incidence energy dependence

Above 0.5eV S_0 is seen to gradually rise with increasing E_i. This behaviour is common among systems where a direct channel dominates dissociation (e.g. N_2 on W(110) [13], N_2 on W(100)-c(2×2)Cu [22]), with the initial sticking probability increasing as the increase in E_i allows the molecule greater access to non-optimised trajectories to dissociative adsorption. Theoretical investigation of the N_2/W(100) system predicted a lowest barrier to direct dissociation of 0.5eV [4], although the results of molecular beam experiments appear to predict a somewhat lower value (approximately 0.1eV [11]), this value being somewhat more difficult to pinpoint than is typically the case for a purely direct dissociative adsorption system, such as N_2/W(100)-c(2×2)Cu (where the

threshold to direct dissociative adsorption is recorded at 0.6±0.1eV [22]), because of the overlap of the indirect precursor mediated channel to adsorption present here.

b) Surface temperature dependence

Little or no temperature dependence is reported within the E_i range (>0.5eV) thought to be dominated by the direct adsorption channel, with S_0 remaining constant (within the predicted error limits) over the temperature range $300<T_S(K)<1000$ [11]. This behaviour is as expected for a direct channel, with no accommodation of energy with the surface required in order for dissociation to take place via a direct sticking event.

c) Coverage dependence

Saturation coverage is reported to be ~0.6ML from the direct beam, consistent with saturation of the β atomic chemisorption states but not the γ molecular chemisorption states. Within the direct channel (>500meV) the sticking probability is seen to fall almost linearly with coverage [10], as is typical of a direct channel where the incoming molecule requires a single vacant adsorption site for dissociation to successfully take place (the "spare" adatom then being able to migrate across the surface in search of an additional vacant site at which to adsorb). The saturation coverage, however, remains constant at around the 0.6ML mark.

VI.3 Results and Analysis

VI.3.1 Summary

After obtaining a clean Mo(100) surface (as described in chapter III), a range of K&W type experiments (also described in chapter III) were performed examining the sticking of N_2 on Mo(100) for a range of incident energies, E_i, and Mo(100) surface temperatures, T_S. The initial sticking probability, S_0, on a cold Mo surface has been recorded and analysed. The variation of S_0 has also been recorded and analysed for a range of T_S for a low, intermediate and high energy beam. In addition to these, plots

have been produced examining in detail how the sticking, S, varies with nitrogen coverage, θ_H, over the range of conditions and the saturation coverage of nitrogen on the surface has been recorded using a range of surface temperatures and a range of beam energies.

Data relating to the structure and kinetics of the N/Mo(100) system has already been presented in chapter V. This includes:

a) a calculation of the coverage required to saturate the surface with atomically chemisorbed nitrogen, this being calculated as being 0.75ML,

b) a TPD study of the system in which two atomically chemisorbed states β_1 and β_2 at 1080K and 1320K, respectively, are identified, these exhibiting a saturation ratio of 1:2, as well as what appears to be a molecularly chemisorbed γ state occurring at ~205K,

c) and the corresponding surface structures observed using LEED, where the saturation of the β_2 state was associated with a progression from the initial (1×1) pattern to a c(2×2) pattern, reflecting a structure where nitrogen is bonded in half all the fourfold hollow sites, and where the subsequent filling of the β_1 state resulted in a return to the (1×1) pattern.

VI.3.2 Dependence of S_0 on Incidence Energy

The plot of $S_0(E_i)$ taken for a cooled surface (T_S=181K) demonstrates non-monotonous behaviour, with two clearly identifiable channels, one at low energy and another dominating above ~400meV. Below 400meV S_0 exhibits a sharp, exponential like, decay with increasing E_i, S_0 dropping from a value of ~0.75 at 70meV to <0.2 by 400meV.

There is a slightly greater delay in the response time of the QMS for N_2 than was the case for H_2 and this has been taken into account when determining P_1 in the calculation

of S_0 (see equation III.11) by tracing the trend of the plot back to the flag open value (labelled t_f in figure 13 chapter III).

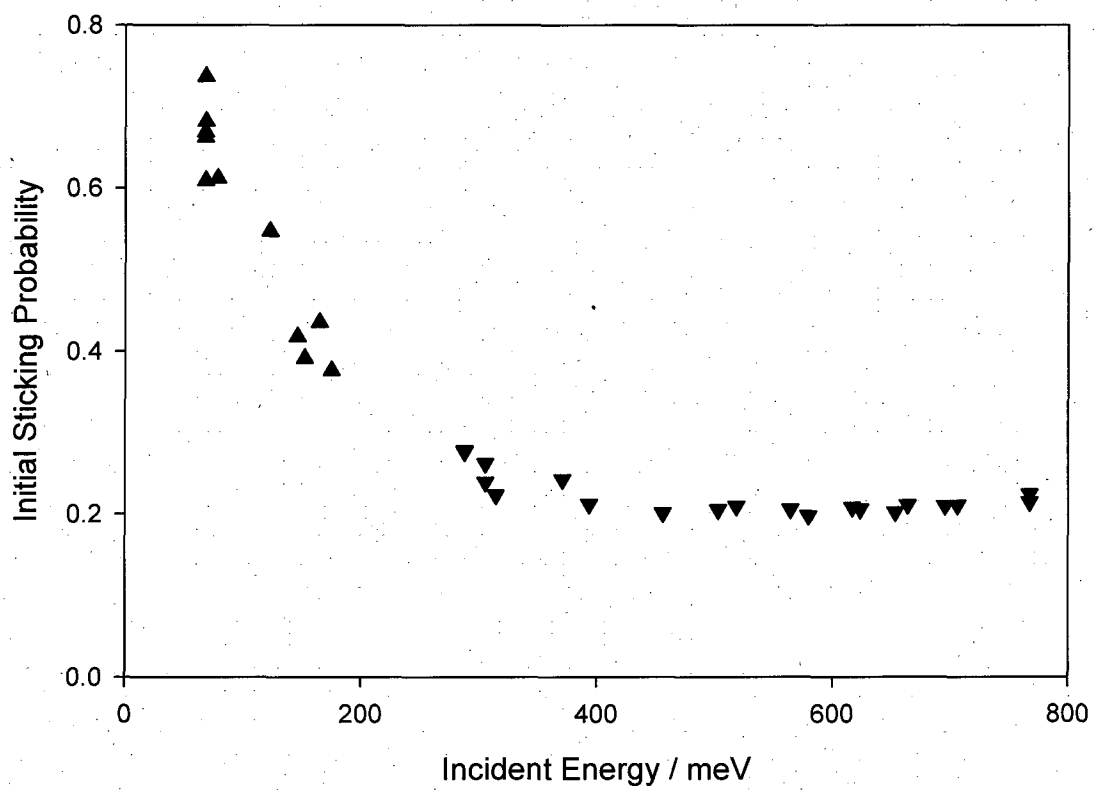

Figure 5: $S_0(E_i)$ of nitrogen on Mo(100). T_S=181K, $\varphi=0^0$. Data taken using an argon (upward pointing triangles) and helium (downward pointing triangles) seeded beam. A drift multiple of 1.4360 and 0.6860 was applied to equation II.54 for the argon seeded and helium seeded beams respectively to account for the deviation of the velocity from that predicted by equation II.51, large mass differences, requiring large changes in velocity, resulting in the real behaviour deviating significantly from the ideal. The drift multiples were calculated using previous TOF data recorded for 1%N_2/Ar and 1%N_2/He beams on this system [24].

This form of non-monotonous behaviour is often indicative of an indirect precursor mediated channel to dissociative adsorption dominating at low E_i where the sticking probability decreases as the initial trapping event becomes less probable since a greater fraction of E_i must be accommodated in order for the molecule to trap, and a direct channel to dissociation dominating in the higher E_i region where the sticking probability increases as the increase in E_i allows the molecule greater access to non-optimised trajectories to dissociative adsorption. Non-monotonous behaviour of this

form is observed and also explained in terms of a precursor mediated channel acting in conjunction with a direct channel for the N_2/W(100) system.

VI.3.3 Dependence of S_0 on Surface Temperature

The indirect and direct channels exhibit markedly different dependencies on surface temperature. Whereas the direct channel exhibits no T_S dependence the precursor mediated channel exhibits a strong T_S dependence. This is seen clearly in figure 6 where a plot of $S_0(E_i)$ is presented for a variety of T_S. At high incident energy the initial sticking probability appears to be the same for the range of surface temperatures measured ($181<T_S(K)<665$). This is consistent with a direct channel where no accommodation of energy with the surface is required in order for dissociation to take place via a direct sticking event. At intermediate energy (E_i=288meV) a temperature dependence already begins to manifest itself (see figure 6), becoming even more pronounced within the lower energy region (68meV), consistent here with a precursor experiencing a reduced trapping capability with increasing T_S and/or a change in the fraction of trapped species desorbing, with T_S acting to reduce the number of molecules that go on to dissociate by biasing the kinetics in favour of desorption.

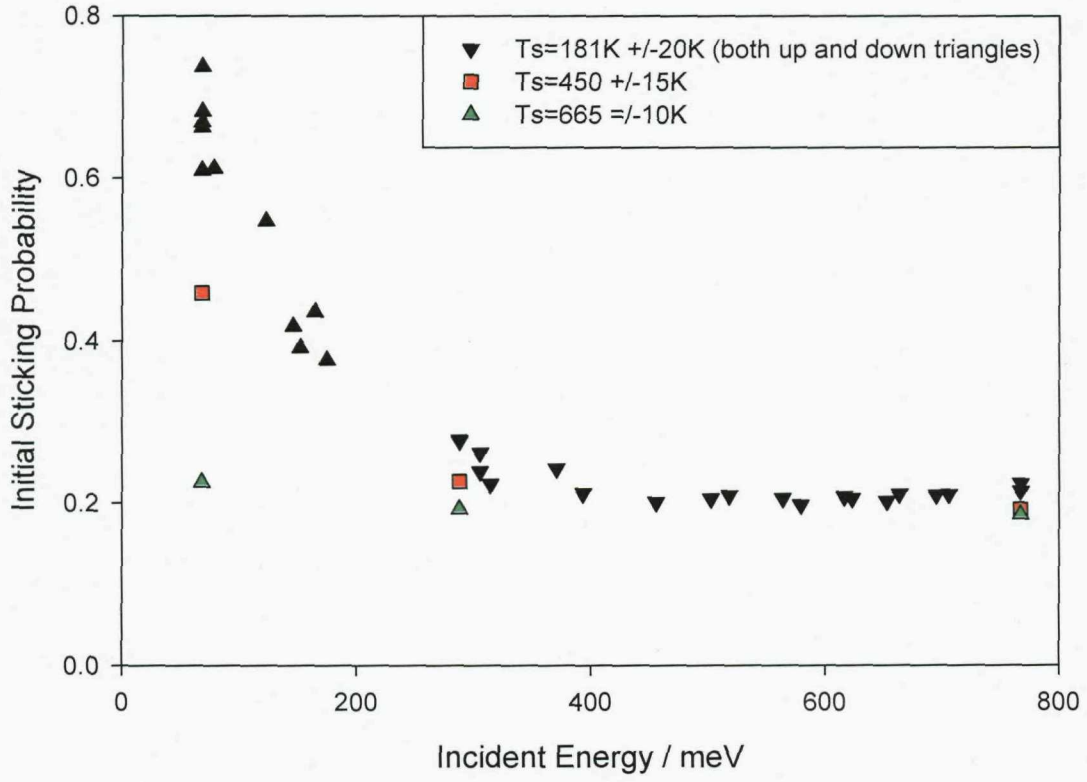

Figure 6: Initial sticking probability of N_2 on Mo(100) as a function of incident energy, taken with the surface held at a variety of temperatures (181, 450 and 665K), $\varphi=0^0$. The increase in the error on T_S, as the T_S value is reduced, is due to errors associated with the use of the W3-type thermocouple which is designed specifically for the accurate measurement of high temperatures.

Although at low E_i S_0 is seen to decline considerably when the surface temperature is elevated, the S_0 values recorded at these elevated T_S are still greater than what might be expected from a purely direct contribution. The direct channel, which appears to exist independently from the indirect channel for E_i>450meV, is typically seen to make a contribution to the initial sticking probability which declines either linearly, or, when approaching its threshold more rapidly still, in magnitude as E_i is reduced, and therefore a maximum sticking probability of about 0.16 might be reasonably expected at 68meV (although the true value is likely to be considerably lower as shall be examined shortly). The sticking probability of ~0.46 recorded for T_S=450K and even of ~0.23 recorded for T_S=665K are considerably higher than can be accounted for via this typical direct channel behaviour. The behaviour indicates instead a precursor mediated channel to dissociation, the molecularly chemisorbed state of N_2 on the

Mo(100) surface having been seen to desorb at 205K or lower (see figure 4, chapter V) and therefore adsorption into the molecular state being incapable of producing any contribution to the measured sticking probability at 450 and 665K unless the molecular state is able to act as a precursor to dissociative adsorption, atomic nitrogen being stable as a chemisorbed surface species at these temperatures.

$S_0(T_S)$ has been plotted for a range of incident energies, allowing the behaviour of the sticking probability as a function of surface temperature to be traced in more detail. These plots are shown in figures 7,8 and 9 for E_i of 68, 288 and 767meV respectively. It is clear that the plots taken at 68 and 288meV show a strong dependence on surface temperature. The fact that a strong temperature dependence is observed towards both ends of the E_i range over which the indirect channel is dominant, is an indicator that the mechanism responsible for the indirect channel remains the same throughout. This is as opposed to a typical accommodated precursor operating within the lower energy regime and some sort of dynamic channel superseding it at higher energies, such as is the case for H_2 adsorption upon Mo(100) (see chapter IV) and various other metal surfaces (e.g. W(100) [25], W(100)-c(2×2)Cu [16], Pd(110) [19], Pd(111) [26] etc.) where the initial reduction in S_0 with increasing E_i was explained in terms of two distinct channels, a typical accommodated precursor channel at the lowest energies and a dynamic channel (either trapping or steering) at higher energies, one of the main indicators of these two channels being the initial T_S dependence at low E_i disappearing while still remaining within the region where S_0 reduces with increasing E_i (i.e. not yet in the region where direct dissociation dominates).

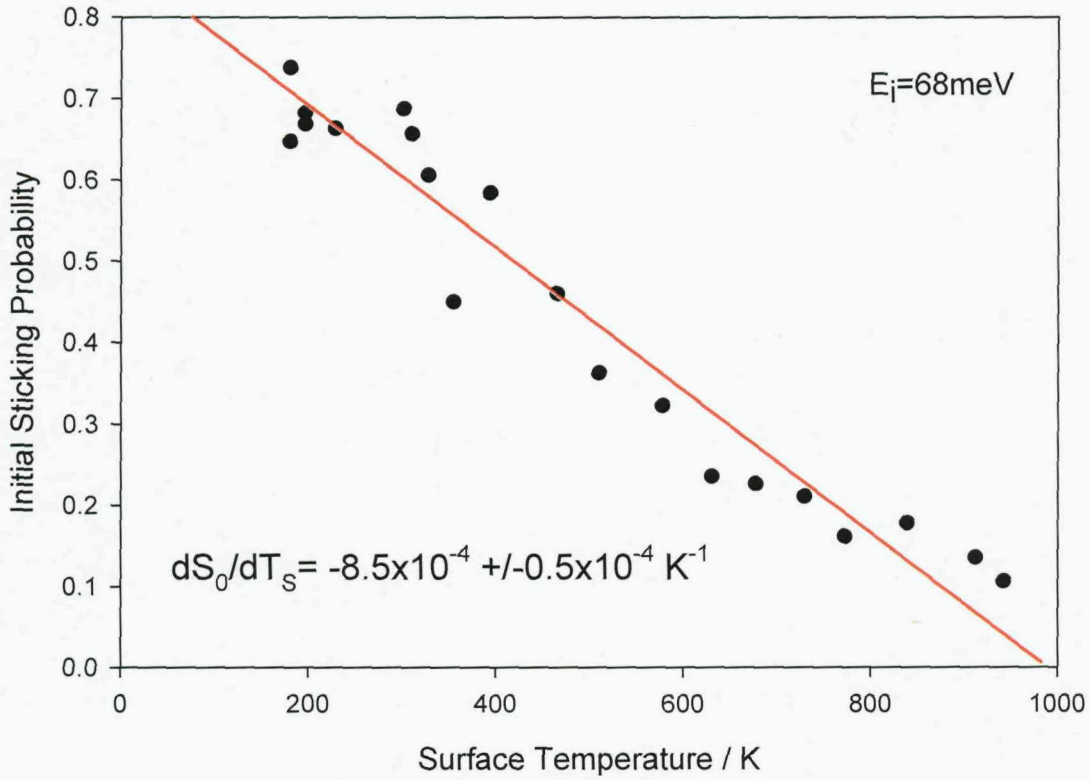

Figure 7: Initial sticking probability of N_2 on Mo(100) as a function of surface temperature, $\varphi=0$, $E_i=68meV$. Linear fit of the data produces a gradient of $-8.5\times10^{-4} \pm 0.5\times10^{-4} K^{-1}$.

The gradient of $S_0(T_S)$ produced at the lowest recorded E_i (68meV) is approximately double that seen for H_2 adsorption onto the Mo(100) surface, but almost identical (within the margins of error) to the gradient from the equivalent plot of N_2 adsorbing onto the W(100) surface ($dS_0/dT \approx -8\times10^{-4}$ for $E_i=88meV$ and $\varphi=0^0$ for the N_2/W(100) system) [10].

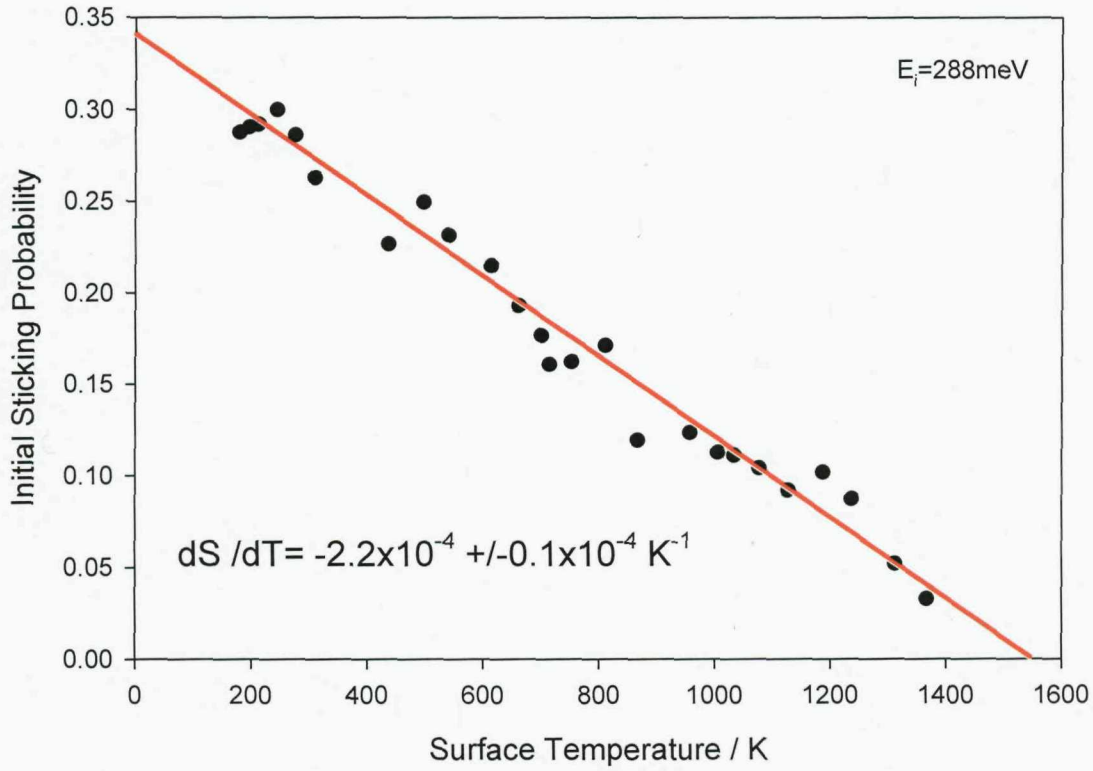

Figure 8: Initial sticking probability of N_2 on Mo(100) as a function of surface temperature, φ=0, E_i=288meV. Linear fit of the data produces a gradient of $-2.2\times10^{-4}\pm0.1\times10^{-4}K^{-1}$.

The gradient of the $S_0(T_S)$ plot at E_i=288meV (see figure 8) sees a decreased, though still considerable, gradient, consistent with a decreased overall contribution to the initial sticking probability from the indirect channel, with the larger incident energy (compared with that of figure 7) resulting in the surface having a much reduced trapping capability. By E_i=767meV, the temperature dependence is seen to all but disappear. The disappearance of any significant surface temperature dependence is typically associated with the lack of an indirect accommodated precursor channel to dissociation, and if a significant sticking probability still remains (here $S_0\approx0.2$) the presence of a direct dissociation channel.

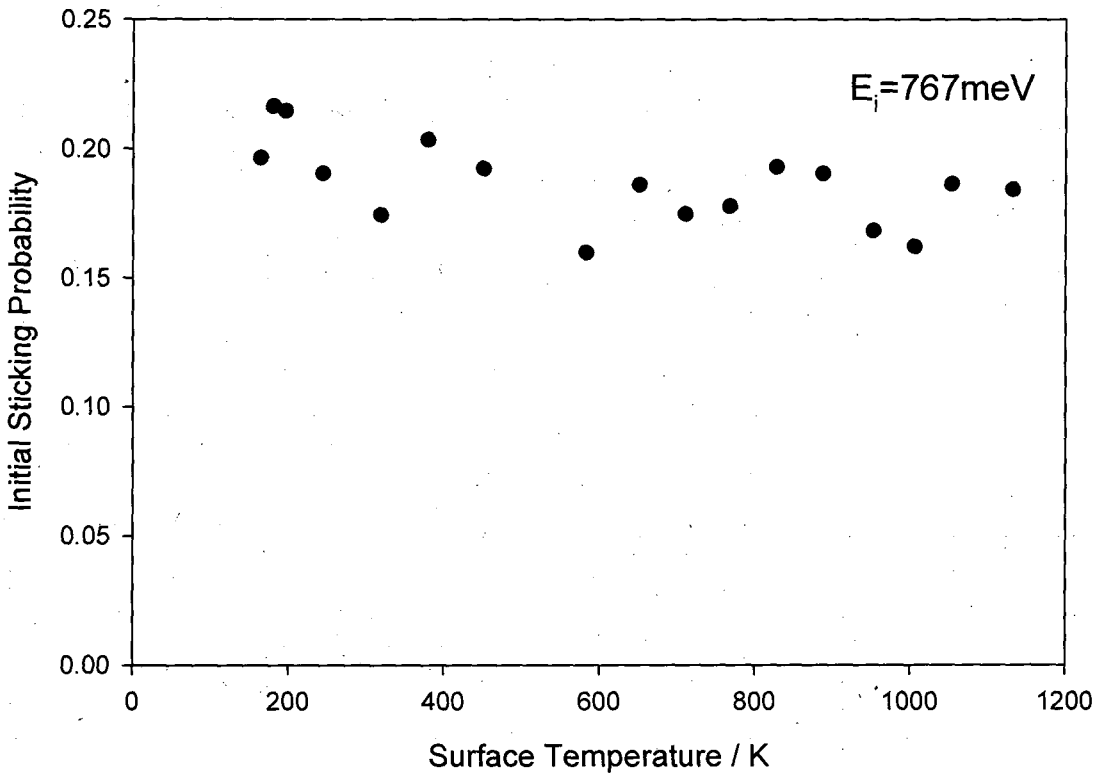

Figure 9: Initial sticking probability of N_2 on Mo(100) as a function of surface temperature, φ=0, E_i=767meV.

Rearranging equation VI.2 in the same manner as has already been performed in chapters IV and V, produces a y=mx+c type plot from which ΔE and $\upsilon_{des}/\upsilon_{diss}$ can be calculated from the gradient and the y-intercept respectively.

$$S_0 = \zeta\left(1+\frac{\upsilon_{des}}{\upsilon_{diss}}e^{\left(-\frac{\Delta E}{RT_S}\right)}\right)^{-1} \qquad \text{VI.2}$$

Rearranged into y=mx+c format where (assuming ζ to be constant with T_S) y=ln(ζ/S_0-1), m=gradient of the plot, x=1/T_S and c=y-intercept.

$$\ln\left(\frac{\zeta}{S_0}-1\right) = -\left(\frac{\Delta E}{R}\right)\left(\frac{1}{T_S}\right)+\ln\left(\frac{\upsilon_{des}}{\upsilon_{diss}}\right) \qquad \text{VI.3}$$

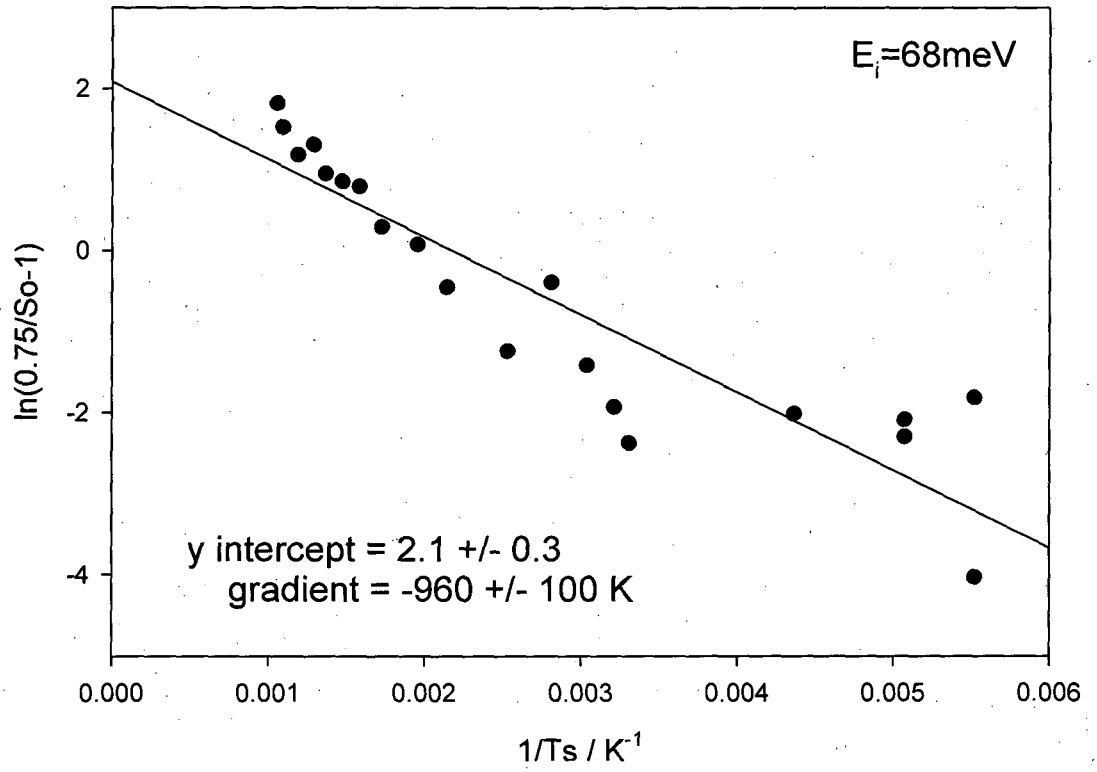

Figure 10: ln(ζ/S_0-1) versus 1/T_S, at E_i=68meV, φ=0^0, for 180<T_S(K)<950. A linear fit is performed in order to calculate the gradient and y-intercept values with the associated errors calculated from the deviation of the data points from the linear regression

By substituting the gradient and y-intercept values derived from the plot of figure 10 (for an E_i=68meV beam) into equation VI.3 and assuming a constant trapping probability values are derived for the difference between the barriers to desorption and dissociation experienced by the precursor and the ratio of frequency factors for desorption and dissociation. These are as follows,

For E_i=68meV:

$$\Delta E = 8.0 \pm 0.8 \text{ kJ/mol}$$

$$= 83 \pm 9 \text{meV}$$

$$\upsilon_{des}/\upsilon_{diss} = 8 \pm 1$$

It is worth noting that some of the data points deviate considerably from the linear fit, and that a fit with a very different gradient and y-intercept would be produced if the

data points at the highest, $1/T_S$, x-axis values were ignored. Often a considerable deviation from linearity of this form is associated with either a large direct channel contribution or a trapping probability which varies with surface temperature [11].

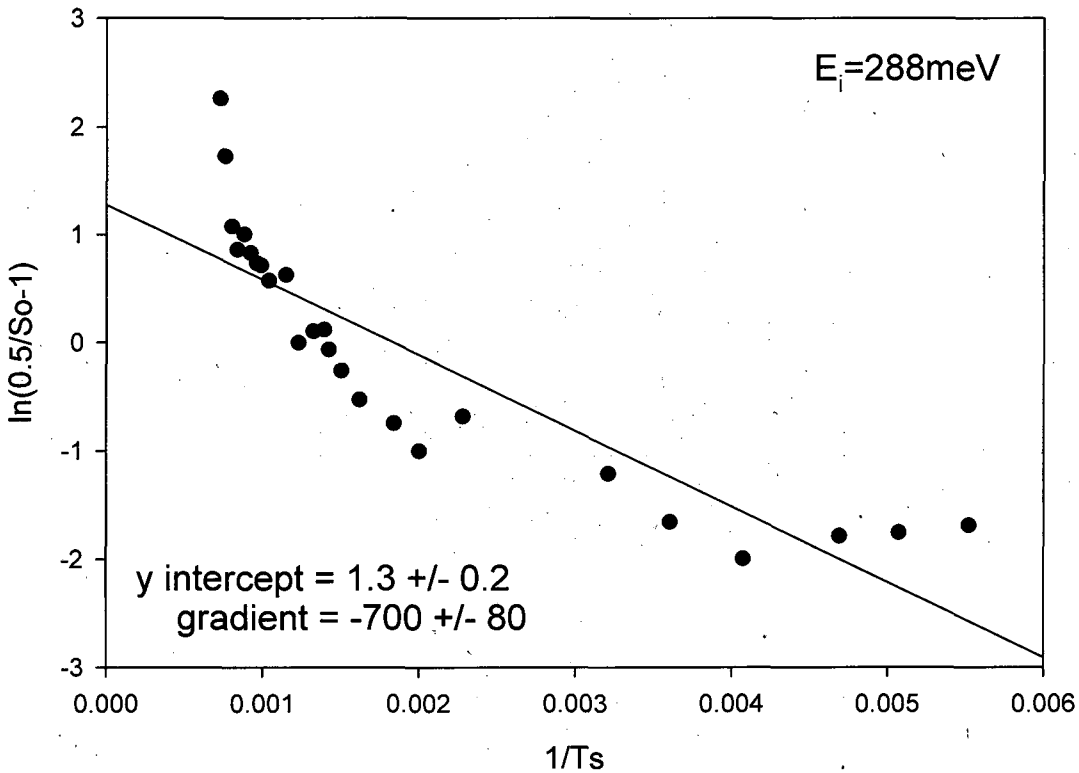

Figure 11: $\ln(\zeta/S_0-1)$ versus $1/T_S$, at E_i=288meV, $\varphi=0^0$, for $180<T_S(K)<1370$. A linear fit is performed in order to calculate the gradient and y-intercept values with the associated errors calculated from the deviation of the data points from the linear regression

Figure 11, illustrating the behaviour of a 288meV beam, exhibits even clearer deviation from linear behaviour than was observed from the equivalent plot for the 68meV beam (figure 10). As already noted this deviation from linearity is likely to be due to either a considerable direct channel contribution to the sticking probability, or a trapping probability that varies with T_S.

Applying equation VI.3 (in the same manner shown above for the E_i=68meV beam) to the data obtain from the linear fit shown in figure 11 results in the following values for ΔE and $\upsilon_{des}/\upsilon_{diss}$,

For E_i=288meV:

$$\Delta E = 60 \pm 7 meV$$
$$= 5.8 \pm 0.7 \text{ kJ/mol}$$
$$\upsilon_{des}/\upsilon_{diss} = 3.7 \pm 0.6$$

Many of the data points deviate considerably from the linear regression and therefore these values for ΔE and $\upsilon_{des}/\upsilon_{diss}$ are likely to be inaccurate. Indeed given that there is no reason why an increase in incident energy should affect the barriers to desorption and dissociation experienced by the precursor (the difference between which is represented by ΔE) it is assumed that an unaccounted for error is entering into the calculation. This will be examined further and the data re-evaluated in the analysis section (chapter VI.4.2).

VI.3.4 Dependence of S on Nitrogen Coverage (θ_N)

i) Saturation coverage

The variation in sticking probability with nitrogen surface coverage has been recorded for a range of surface temperatures and incident energies. From these plots of $S(\theta_N)$ it was also possible to make an estimate of the particular saturation coverages. By measuring the area encompassed by the K&W plot from the time of the flag being opened to the time at which the surface saturated a calculation of the saturation coverage of the surface can be produced (see figure 12).

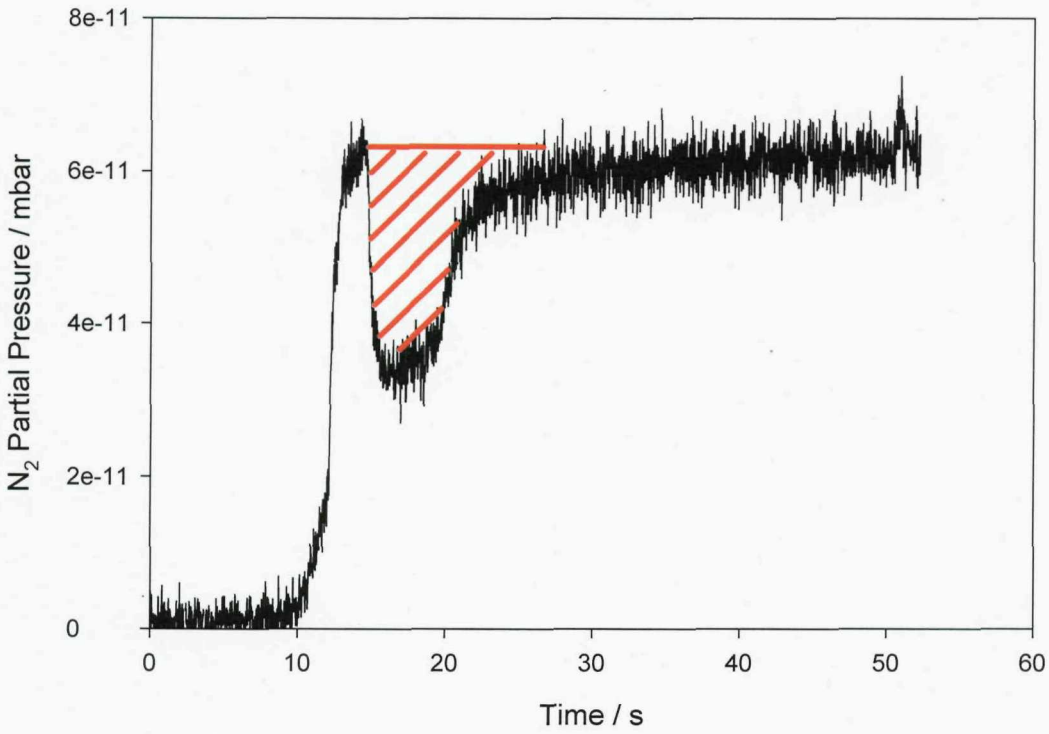

Figure 12: Example of a K&W [27] plot for nitrogen adsorption onto the Mo(100) sample surface (E_i=68meV, T_S=293K) . The red shaded area indicates the area from which the saturation coverage calculation is made.

When using a 68meV beam a ratio of ~2.6 was observed between the saturation of the Mo(100) surface held at 165K (~3.1×10^{-10} s.mbar) and its saturation at 197K≤T_S<700 (~1.1×10^{-10} s.mbar). This increase in the saturation coverage is taken to be indicative of an additional chemisorbed state of nitrogen being accessible and stable on the surface at this E_i and T_S. Given the low temperature at which the surface is required to be held in order to observe this additional chemisorption state, the molecularly chemisorbed, γ, state (thought to be a precursor to dissociative adsorption) is the likely candidate, both atomically adsorbed states remaining stable until T_S>1000K. The presence of this molecularly chemisorbed nitrogen will be in addition to the atomic, dissociatively chemisorbed, nitrogen present at both the lower and higher T_S (as evidenced by subsequent TPD spectrum). Saturation of the atomic (β_1 and β_2) states was recorded as taking place at 0.75ML (see chapter V.3.2), and therefore, applying the ratio of 2.6, this equates to a saturation coverage of ~1.43 ±0.13ML at 165K (remembering that

when in its molecular form 1ML of nitrogen will be the equivalent, in terms of quantity adsorbed, to 2ML of atomic nitrogen).

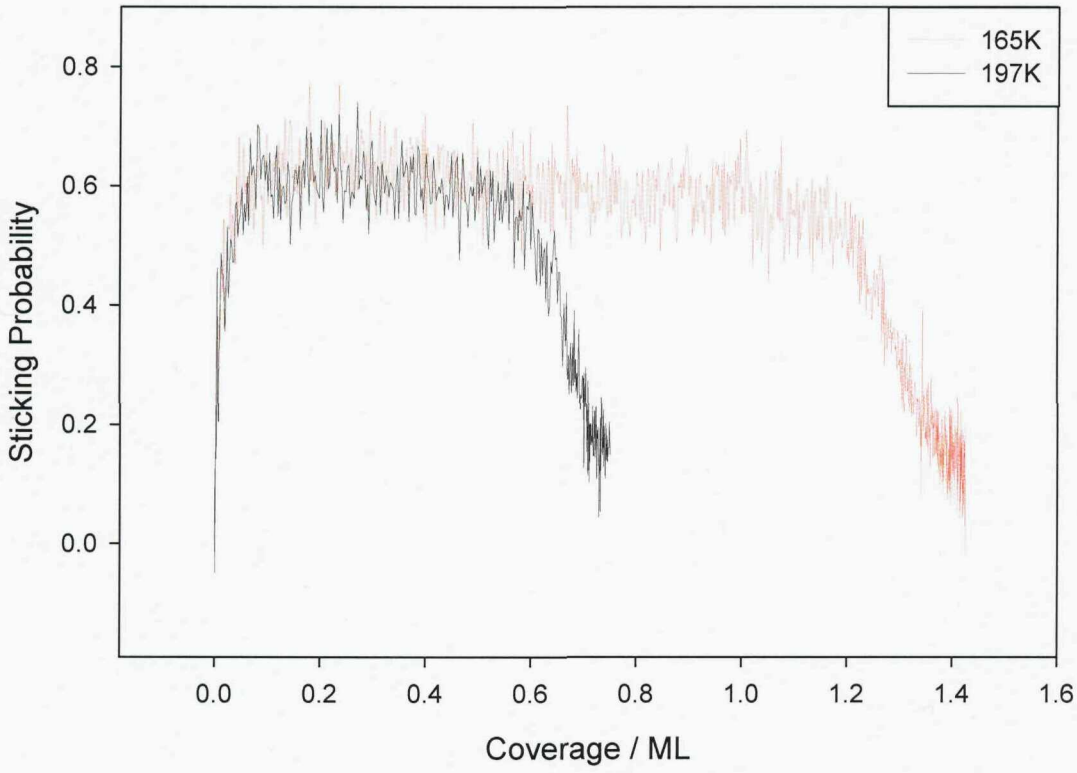

Figure 13: $S(\theta_N)$ for nitrogen adsorption onto an Mo(100) surface for E_i=68meV and $\varphi=0^0$ at T_S=165K (red) and 197K (black). At 197K nitrogen is retained at the surface in the dissociatively adsorbed atomic state only, whereas the greater saturation coverage recorded for the surface maintained at 165K indicates nitrogen is retained at the surface in both the atomic and molecular chemisorption states.

This increase in saturation coverage at the lowest T_S was not observed when using a high energy beam. At 659meV the saturation coverage remained at 0.75ML even when the surface temperature was held at 165K, implying that molecules with high incidence energy are not able to access the molecular adsorption states. This is consistent with the disappearance of the precursor channel at high incident energies (as illustrated by figure 6), where the large E_i of the molecules makes initial trapping into the molecularly bound states unlikely, the molecule being incapable of losing sufficient energy to allow it to remain bound in the molecular chemisorption, γ, potential well which acts as the precursor to dissociation. However, saturation of the γ, as well as β,

states, for the Mo(100) surface maintained at 165K, was observed to take place up to 300meV (with no further measurements of the saturation coverage being made until >600meV), this being close to the full range of E_i encompassed by the indirect channel, implying that within the entire indirect channel nitrogen dissociation is able to take place via adsorption into the γ precursor state (as opposed to dissociation occurring via a dynamic potential well created by a drop in the vibration ground state of the molecule as it approaches the surface [21] as was suggested might be the case for hydrogen adsorption upon the Mo(100) surface (see chapter IV)).

Similar behaviour was noted for nitrogen adsorption upon the W(100) surface [10], where, within the E_i region in which precursor mediated dissociation takes place, the saturation coverage was seen to grow from 0.6ML at $T_S \geq 200K$ to ~1.7ML at $T_S=85K$. This was also explained in terms of retention of nitrogen in the molecularly adsorbed, γ, state contributing to the saturating nitrogen coverage of the surface.

The loss of the ability of the surface to adsorb and retain molecular nitrogen by 197K agrees well with the observation of the γ desorption peak at 205K (see chapter V.3.2). However, it should be noted that the desorption of nitrogen from the γ state (on either W or Mo) at slightly elevated T_S does not preclude it from acting as a precursor to dissociative chemisorption at these temperatures, provided the lifetime of the state is sufficient for the nitrogen to find a path to dissociation.

ii) Coverage dependence at low and high Ei

At low E_i the plot of $S(\theta_N)$ exhibits a complex coverage dependence, the sticking probability remaining constant until close to saturation (apart from the abrupt initial increase in S associated with the response time of the QMS when the flag is opened and the pressure falls).

This behaviour is consistent with an extrinsic precursor channel where the initial trapping event does not require a vacant surface site and the sticking probability only falls when the surface nears saturation and the ability of the trapped molecule to locate a suitable vacant surface site at which dissociate becomes limiting.

In the case of T_S=165K (and also 181K), where the molecularly chemisorbed state is stable the sticking probability is seen to remain constant up until saturation coverage is virtually reached. In fact the form of the complex coverage exhibited within the E_i region in which the indirect channel is dominant was seen to remain relatively unaffected by changes in T_S, the sticking probability remaining virtually independent of changes in coverage, until saturated coverage is approached (see figure 14).

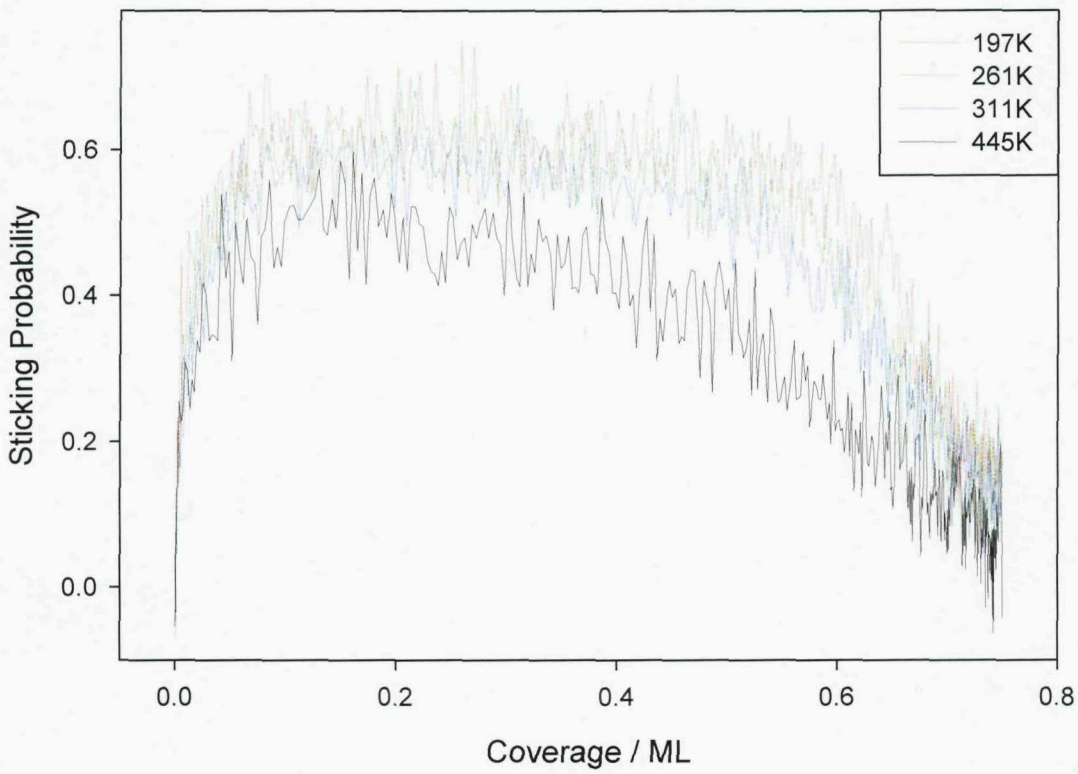

Figure 14: $S(\theta_N)$ for nitrogen adsorption onto an Mo(100) surface for E_i=68meV and $\varphi=0^0$ at T_S=197K (red), 261K (green), 311K (blue) and 445K (black).

At high E_i, outside the realm of the precursor mediated channel, the behaviour of the sticking probability as a function of coverage is very different. Figure 15a is a plot of $S(\theta_N)$ performed using an incidence energy of 637meV, and can be seen to exhibit very different behaviour to that seen at 300meV (figure 15b) and 68meV (figure 15c). The complex coverage behaviour observed at lower E_i is replaced by an almost linear decline in S with increasing θ_N. This behaviour is typical of a direct channel where the

sticking probability is limited by the need for a vacant surface site in order for the initial dissociative adsorption event to take place. That $S(\theta_N)$ displays a linear decline as oppose to a quadratic decay indicates that only a single vacant adsorption site is required for the initial direct dissociative adsorption to take place with the remaining nitrogen atom presumably able to migrate across the surface to locate a second adsorption site.

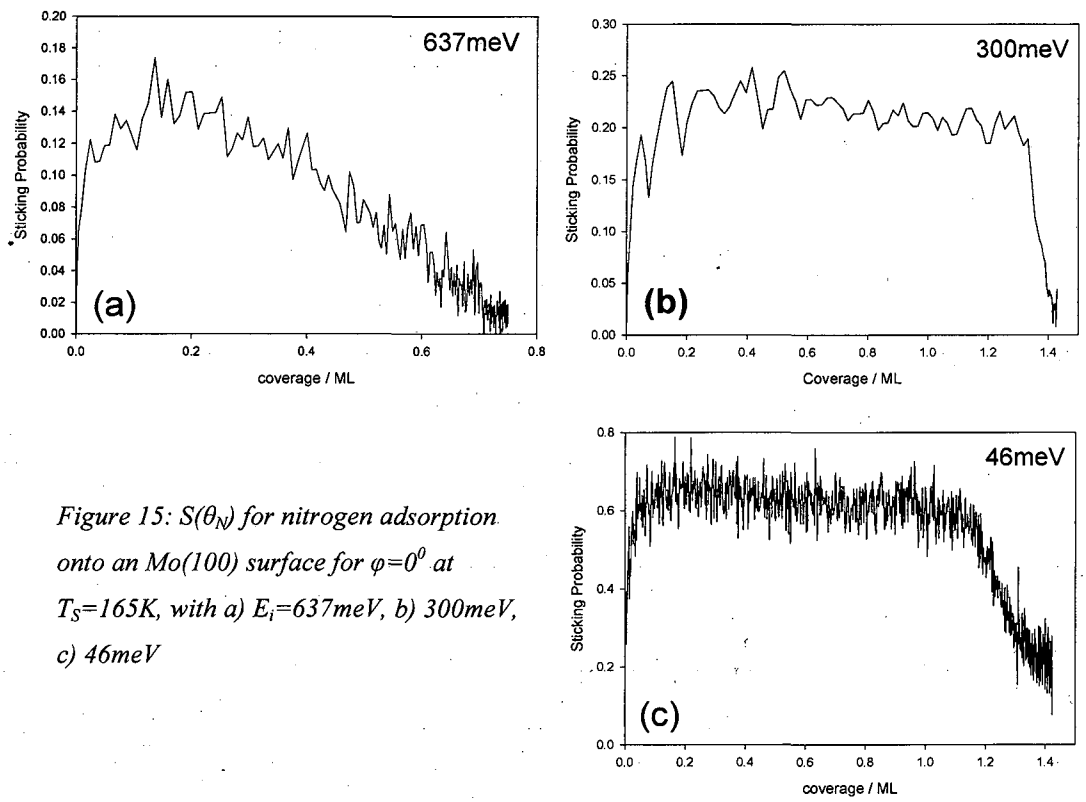

Figure 15: $S(\theta_N)$ for nitrogen adsorption onto an Mo(100) surface for $\varphi=0^0$ at $T_S=165K$, with a) $E_i=637meV$, b) 300meV, c) 46meV

VI.4 Discussion

VI.4.1 Dependence of S_0 on Incidence Energy

The implications of the non-monotonous behaviour of S_0 as a function of E_i for H_2 adsorption on the Mo(100) surface were discussed in the results section. The picture suggested was that of two channels to dissociative adsorption, a typical fully accommodated precursor mediated indirect channel resulting in an initial drop in S_0 with increasing E_i, and a direct dissociation channel becoming prevalent >400meV and

resulting in a steady incline in S_0 with increasing E_i, with a degree of overlap between the two channels occurring at the intermediate E_i (the overlap likely to be greatest between 300 and 400meV).

The hard cube model [28] should provide a good fit to data describing a typical accommodated precursor channel. The hard cube fit of the trapping probability as a function of incident energy is illustrated in figure 16, and, although the hard cube fit defines trapping probability rather than the dissociative adsorption probability recorded by the data, at low T_S these two values should be close to equal provided the barrier to desorption experienced by the trapped molecule is greater than the barrier to dissociation, since virtually all trapped molecules will proceed to the dissociated state. Indeed it was noted when observing the saturation coverage at low T_S, that the γ precursor state remains stable at T_S=181K, i.e. that all trapped molecules remain stuck at the surface whether or not they go on to dissociate. In this particular case the initial trapping probability, ζ, might be expected to be equal to S_0. In addition a data set for T_S=450K has been included to illustrate how the increase in temperature causes the results to deviate from the model provided by the hard cube.

The hard cube fit is performed for a data set where T_S=165K, and using a surface cube mass of 1Mo atom and potential well depth of 50meV an excellent fit to the data was obtained giving a strong indication that the channel is indeed that of a fully accommodated indirect precursor. It was, however, noted that a trapping potential well depth of 50meV seemed rather shallow given the value calculated for the difference in potential barrier height to desorption and dissociation experienced by the molecule, ΔE, based on an examination of the temperature dependence of the initial sticking probability, of roughly 140meV, and the lack of any evidence suggesting that access to the trapping well is activated. A possible solution is suggested within Volpilhac and Salin's [6] theoretical investigations of N_2 adsorption on W(100). Within their research they suggest that a particular orientation is required in order for the molecule to bypass the potential roof it experiences when trapped, blocking its path to desorption, and hence causing a bottle neck in phase space, and that this can be thought of as a form of dynamic trapping. Such circumstances might result in the trapped molecule experiencing a large barrier to desorption during most attempts to desorb and thereby resulting in a ΔE value larger than the depth of the trapping well encountered by the

molecule, with the molecule steered into the favourable orientations required to access this well without the need for overcoming a potential barrier. An alternative hard cube fit is also produced using a well depth of 170meV (and an effective surface cube mass value of 2Mo) which fits more intuitively with the calculated ΔE value and is closer to that used by Rettner et al. [11] in their use of the hard cube model to provide a fit to the N_2/W(100) system and also provides a reasonable (if slightly less well matched) fit to the data.

It should be noted that the ability of the hard cube model to generate a full curve describing reasonably accurately the precursor adsorption channel does not mean that the model is expected to be fully appropriate for the system. However it is an intuitively reasonable way of generating a curve describing a typical fully accommodated precursor channel to dissociation, and its good agreement with the data is a good indicator that a fully accommodated precursor channel is responsible for the initial decline in S_0 with increasing E_i. Compare this, for example, to the case of hydrogen adsorption onto the Mo(100) surface examined in chapter IV, where the hard cube model exhibits a huge deviation from the actual data or the even greater deviation from the hard cube trajectory calculations exhibited by hydrogen adsorption upon W(100) [29] (this type of behaviour being taken as a good indicator of a dynamic rather than fully accommodated adsorption channel for the H_2/Mo(100) system).

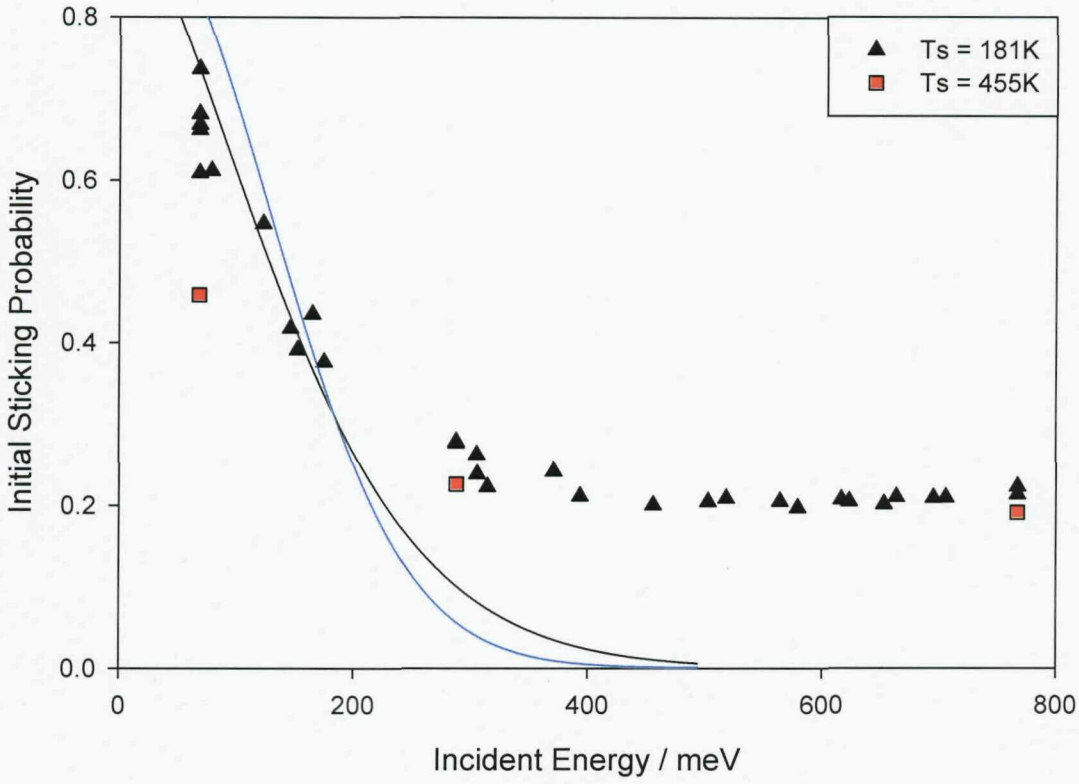

Figure 16: Plot of $S_0(E_i)$ of nitrogen on Mo(100). T_S=181K, $\varphi=0^0$. Two hard cube fits have been performed using an effective surface cube mass and trapping potential well of 1Mo atom and 50meV (black), and 2Mo atoms and 170meV (blue).

By assuming that the hard cube fit accurately accounts for the indirect sticking probability it is also possible, by deducting the hard cube fit from the initial sticking probability data, to illustrate the behaviour of the direct channel (see figure 17). This estimate of the direct channel suggests a minimum barrier to direct dissociation of between 50 and 100meV, with the direct channel being inactive at E_i<50meV.

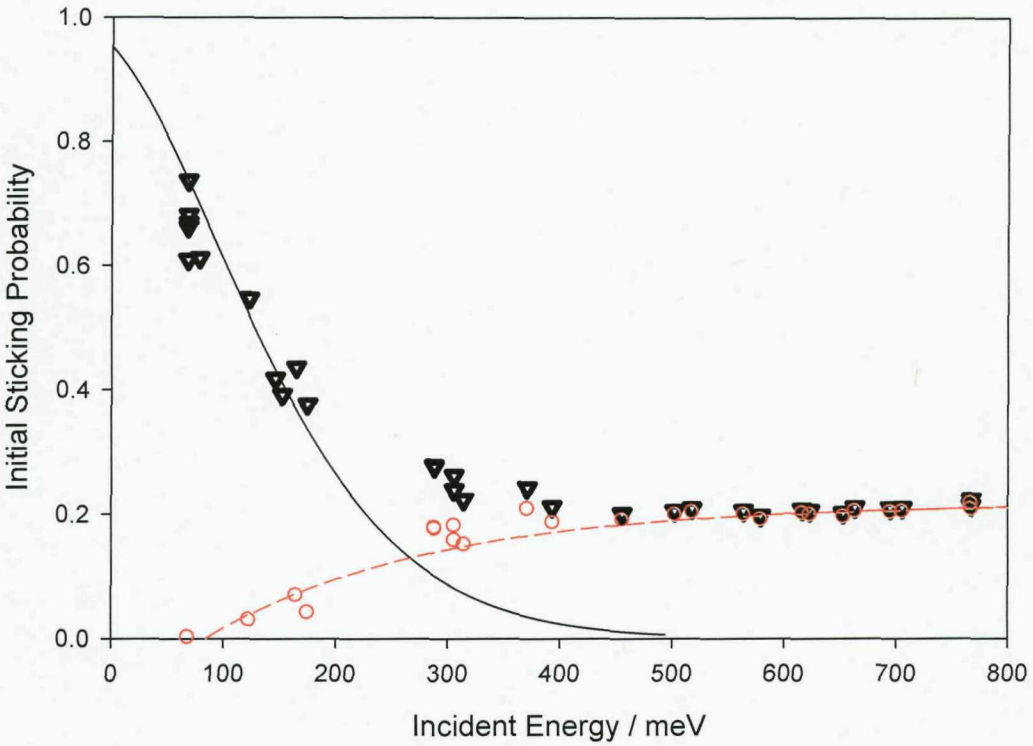

Figure 17: $S_0(E_i)$ data points (black triangles) with hard cube fit (effective surface cube mass of 1Mo and potential trapping well depth of 50meV) (solid black line). Based on the assumption that the hard cube fit provides a good description of the indirect channel the hard cube fit has been deducted from the data points to produce a prediction of the purely direct channel contribution (red circles) which is also provided with a curve fit to aid the reader (dashed red line).

Comparison of the predicted direct channel with that predicted for the same E_i range for the N_2/W(100) system reveals remarkably similar behaviour (see figure 2). Although the gradient appears shallow at first glance, on closer inspection it is realised that this is merely due to the limits of the energy range over which the data has been taken. The increase in S_0 with E_i typical of a direct channel is predicted to become clearer over a larger incident energy range following the manner in which this relationship progresses on the N_2/W(100) surface (see figure 1).

VI.4.2 Dependence of S_0 on Surface Temperature

Figures 10 and 11 show the plots for $\ln(\zeta/S_0-1)$ as a function of $1/T_S$ for E_i of 68meV and 288meV respectively. The linear fit to these plots produced rather different

gradients, and thereby also different values for ΔE and $\upsilon_{des}/\upsilon_{diss}$. As was already noted it is difficult to envisage why altering the incident energy of the molecule might alter the barriers to dissociation or desorption experienced by the precursor and hence why the ΔE value should differ beyond that predicted by the error estimations. As also mentioned previously, the commonly attributed sources of the deviation are either a large direct channel contribution (seemingly unlikely, particularly at 68meV where the direct channel contribution to the initial sticking probability is predicted to be either very small or completely absent), or that the assumption that the trapping probability, ζ, remains independent of surface temperature is incorrect. Indeed removal of the data points most clearly deviating from linear behaviour (as illustrated in figure 18) produces plots from which calculations based on the linear regression fit described above result in a ΔE value calculated from the E_i=68meV plot equal to that calculated from the E_i=288meV plot within the predicted error margins.

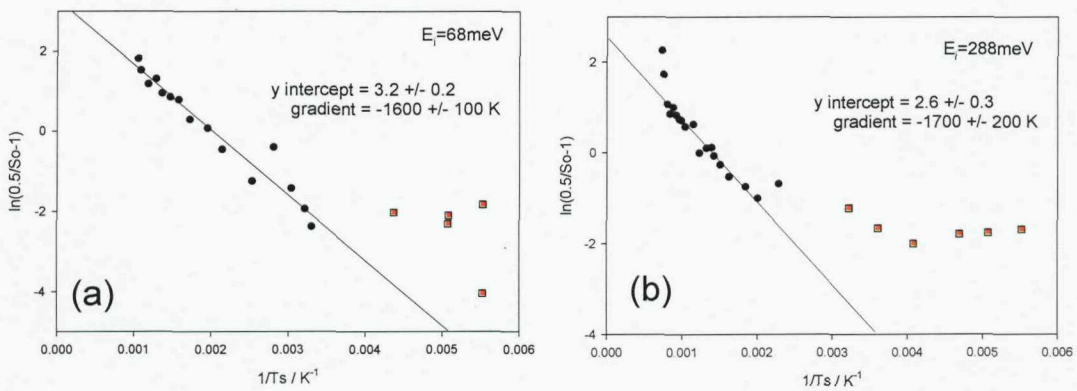

Figure 18: $\ln(\zeta/S_0-1)$ versus $1/T_S$ with linear fits recalculated ignoring the data points most clearly deviating from linear behaviour (denoted by red squares), for a) E_i=68meV and b) E_i=288meV, (based on the original plots of figures 10 and 11 respectively).

The alternative values for gradient, y-intercept, ΔE and $\upsilon_{des}/\upsilon_{diss}$ calculated while ignoring the most obviously non-linear points, originating from the low T_S data points, are as follows:

At 68meV:

Gradient = -1600 ±100K

y-intercept = 3.2 ±0.2

ΔE = 138 ±9meV

= 13.3 ±0.8 kJ/mol

$\upsilon_{des}/\upsilon_{diss}$ = 25 ±2

At 288meV:

Gradient = -1700 ±200K

Y-intercept = 2.6 ±0.3

ΔE = 146 ±17meV

= 14 ±2 kJ/mol

$\upsilon_{des}/\upsilon_{diss}$ = 13 ±2

Given that the E_i=68meV will have the smaller direct channel contribution, the ΔE value from this data set is taken as the more accurate measure, noting that 138meV, and its predicted error range of ±9meV, falls entirely within the range of errors predicted for the calculation of ΔE using the E_i=288meV data set.

A similar deviation from linearity, also for the data points originating from the S_0 measurements taken for low T_S, was noted on the N_2/W(100) system [9]. This deviation was ascribed to a temperature dependence of the trapping probability, it being possible to measure the trapping probability of this system independently using scattering data. The hard cube model was seen to provide a good fit to the trapping data, and by applying the hard cube fit to the ζ value for the plot of $\ln(\zeta/S_0-1)$ as a function of $1/T_S$, allowing ζ to vary with T_S, the data points were all seen to conform to the linear fit.

Unfortunately no such scattering data exists for the N_2/Mo(100) system. Variables for the effective surface cube mass, m, and trapping potential energy well, U, were chosen to produce a hard cube model showing a trapping probability with a similar temperature dependence to that observed for the N_2/W(100) system [11] (see figure 19), but, despite attempts to apply this and numerous other hard cube models, altering both the U and m parameters to alter the manner in which ζ varies with T_S, to the plots of figures 10 and 11, little improvement was seen in terms of producing data points which conformed to a good linear fit (those derived from the low T_S initial sticking data still deviating most significantly from the most obvious line of best fit).

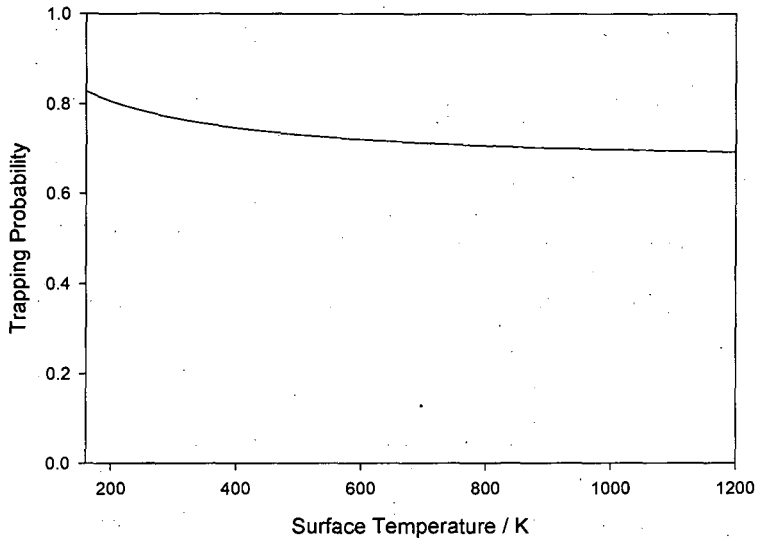

Figure 19: Plot of the hard cube model describing the trapping probability as a function of surface temperature with m=2Mo, U=50meV, these values corresponding to those which provided the best fit to the $S_0(E_i)$ data (see figure 16)

It has already been noted that the W3-type thermocouple used to record the temperature during these experiments is designed specifically to measure high temperatures and may struggle to measure low temperature correctly, particularly <273K. It is possible that this is the root cause of the deviation from linearity. However, without any data recording the scatter from the surface, which could be used to confirm the behaviour of the trapping probability with respect to surface temperature, it remains unclear as to whether this might be the factor responsible.

Perhaps the most likely cause of the deviation of the plot of $\ln(\zeta/S_0-1)$ as a function of $1/T_S$ from linearity is the presence of a stable molecularly chemisorbed, γ, state. The presence of this γ state could be expected to result in $\alpha=S_0$ below a certain critical temperature at which the γ state begins to desorb. This should result in $\ln(\zeta/S_0-1)\rightarrow-\infty$

if the sticking were entirely indirect. However, a small contribution to S_0 from a direct channel is still expected even at incident energies as low as 68meV, and therefore S_0 never approaches ∞. Because the direct channel is expected to be almost entirely temperature independent across the measured range this should result in an unchanging, but non-infinite, value for $\ln(\zeta/S_0-1)$ with decreasing T_S below a certain critical temperature at which the γ adsorption state becomes stable. Although this would seem to explain the above behaviour well some uncertainty remains, with initial estimates (based on changes in the saturation coverage value, see chapter VI.3.4) of the critical temperature, above which the γ state ceases to remain stable on the surface, putting the value at ~197K, but the plateau in the $\ln(\zeta/S_0-1)$ value occurring here at ~230K and ~310K for incident energies of 68meV and 288meV, respectively. However, this conflicts somewhat with the TPD plot measuring the desorption of nitrogen from the Mo(100) surface (see figure 4, chapter V) which does appear to indicate a γ state extending to sufficiently high T_S.

VI.4.3 Dependence of S on Nitrogen Coverage (θ_H)

As has been made clear when initially examining the results, the coverage dependence observed for nitrogen adsorbing onto the Mo(100) surface is entirely consistent with a precursor channel to dissociation dominating dissociative adsorption below 400meV and a direct channel being entirely responsible for dissociative adsorption at higher energies. The lower incident energy is shown to allow access to a molecularly chemisorbed state, labelled γ, which is thought to act as a precursor to dissociation.

Within the E_i range associated with the precursor channel (E_i<400meV) the lack of any initial increase or decrease in S with nitrogen adsorption upon the clean surface (excluding the initial jump in S as the flag is opened which is due to the response time of the QMS) suggests that the trapping probabilities into the intrinsic and extrinsic precursor states are virtually identical (see figures 15b and 15c). This is surprising since pre-adsorbed nitrogen might be expected to modify the interaction potential, however, such behaviour has already been observed for the N_2/W(100) system [10] and was explained in terms of the initial trapping taking place at distances well beyond

the plane of the adsorbates. Such an explanation could also account for the behaviour of the sticking probability of nitrogen as a function of coverage upon the Mo(100) surface.

VI.4.4 Comparison of Nitrogen adsorption on the Mo(100) and W(100) surfaces

During chapter V it was noted how similar the surface structure and kinetics of nitrogen adsorption onto Mo(100) and W(100) were. However, even taking this into account it is still surprising just how similar the dynamics of the two adsorption systems proved to be.

The indirect channel of N_2/Mo(100) was seen to be almost identical in size and reach to that experienced by the N_2/W(100) system [9,10,11] in terms of the variation in the initial sticking probability as a function of incident energy of the N_2 projectile. For both surfaces the channel exhibits a high S_0 at the low E_i (both exhibiting $S_0 \approx 0.6$ at E_i=80meV) falling with increasing energy and, according to the fits performed for both systems data sets, becoming negligible ($S_0 < 0.1$) by ~350meV and ~450meV on Mo(100) and W(100) [11] respectively. Both data require a fit to be performed due to the overlap of the direct and indirect channels, with S_0 gradually ceasing to decrease and beginning to increase with E_i as the direct channel comes to prominence. This crossover in dominance between the indirect and direct channels occurs within the energy range of between 400 and 500meV. Indeed, fits performed upon the direct channel contribution on each of the two systems predict very similar thresholds for the onset of the direct channel (determined to be ~100meV on W(100) [11] and within the energy range 50-100meV here on Mo(100) (see figure 17)). The gradient of $S_0(E_i)$ on Mo(100), within the region where the direct channel is predicted to be almost entirely responsible for sticking (E_i>500meV), is found to be almost identical to that on W(100) over a similar energy range, suggesting that the direct channel behaviour on Mo(100) is likely to cause S_0 to continue to rise with further increasing E_i beyond the range measured here in a monotonous manner very similar to that observed by experiment for the N_2/W(100) system.

Given the similarities between the dynamics of N_2/Mo(100) and N_2/W(100) illuminated by examination and comparison of the initial sticking probability as a function of the incident energy of the N_2 molecule, with both exhibiting very similar direct and indirect channels, it is perhaps unsurprising that both systems also exhibit a very similar T_S dependence, with the indirect channel on both being strongly dependent on T_S and the direct being T_S independent. It is interesting to note that, based on the $S_0(T_S)$ data from within the indirect channel, ΔE (the difference in barriers to desorption and dissociation experienced by the precursor) was calculated to be 160 ±10meV on W(100) [9,11]. This value is very similar to the value from the $S_0(T_S)$ data obtained during the current study, when the calculation was made while ignoring the apparently poorly fitting low T_S data points, where ΔE was calculated as being 138 ±9meV.

A comparison has already been drawn between the coverage dependence of the sticking probabilities for the indirect channels of the two systems, these having been noted as exhibiting a coverage independence extending until saturation is virtually complete. Both also exhibit a linear decrease in S_0 with θ within the direct channel energy region as is typical of a direct channel.

VI.5 Conclusion

The adsorption dynamics of nitrogen has been studied on the Mo(100) surface. Molecular beam techniques have been used to monitor the dependence of the sticking probability as a function of the incident energy of the N_2 molecule, or the surface temperature of the Mo(100) substrate, and of the degree of nitrogen coverage on the substrate surface.

The initial sticking probability of N_2 on Mo(100) varies non-monotonously with incidence energy as is typical of overlapping indirect and direct channels to dissociation. The indirect channel is most likely due to a fully accommodated precursor, this assumption being supported by the strong temperature dependence and the coverage independence of the sticking probability displayed by the indirect channel and the good fit to the indirect channel $S_0(E_i)$ data points provided by the hard cube

model. The direct channel is predicted to be activated, with a threshold for the incident energy of the N_2 molecule predicted as being somewhere between 50-100meV, thereafter the sticking probability increasing with increasing incident energy as a greater number of non-optimised trajectories to direct dissociation become accessible.

The similarities in the kinetics and surface structures of the N/Mo(100) and N/W(100) systems have already been noted in chapter V. In addition it has now been possible to draw comparisons between the dynamics of the two systems. Both the N_2/Mo(100) and N_2/W(100) systems display a similar threshold energy to activation of the direct channel and both display indirect channels of similar magnitude and with a reach stretching across a similar energy range. Dissociative adsorption of N_2 taking place via the precursor channel exhibits similar coverage independence on each surface, this coverage independence stretching almost to the point of saturation (implying an intrinsic precursor dominating sticking on both). It also exhibits a similar surface temperature dependence on each surface and calculations performed examining this temperature dependence reveals the precursors on both systems to experience very similar conditions, the difference between the barriers to desorption and dissociation experienced by the N_2 precursor being almost identical on each surface.

VI.6 References

[1] Zhu J. F., Guo J. C., Zhai R.S., Bao X>, Zhang X. Y., Zhuang S., Applied Surf. Sci., 161(200)86

[2] Sellidj A., Erskine J.L., Surf. Sci., 220(1989)253

[3] Grunze M. J., Fuhler J., Neumann M., Brundle C. R., Auerbach D. J., Behm J., Surf. Sci., 139(1984)109

[4] Serrano M., Darling G. R., Surf. Sci., 532-535(2003)206

[5] Volpilhac G., Busnengo H. F., Dong W., Salin A., Surf. Sci., 544(2003)329

[6] Volpilhac G., Salin A., Surf. Sci., 556(2004)129

[7] Egberg R.C., Dahl S., Logadottir A., Larsen J. H., Norskov J. K., Chorkendorff I., Surf. Sci., 491(2001)183

[8] Nilsson A., Weinelt M., Wiell T., Bennich P., Karis O., Wassdahl N., Stöhr J., Samant M. G., Phys. Rev. Lett., 78(1997)2847

[9] Rettner C. T., Stein H., Schweizer E. K., J. Chem. Phys., 89(1988)3337

[10] Rettner C. T., Schweizer E. K., Stein H., Auerbach D. J., J. Vac. Sci. Technol. 7(1989)1863

[11] Rettner C. T., Scheizer E. K., Stein H., J. Chem. Phys., 93(1990)1442

[12] Rettner C. T., Schweizer E. K., Stein H., Auerbach D. J., Am. Phys. Soc. 61(1988)986

[13] Yates J. T. Jr., Klein R., Madey T. E., Surf. Sci., 58(1976)469

[14] Muller J. E., Phys. Rev. Lett., 59(1987)2943

[15] Butler D. A., Hayden B. E., Chem. Phys. Lett., 232(1995)542

[16] Butler D. A., Hayden B. E., Surf. Sci., 337(1995)67

[17] Di Cesare A. Busnengo H. F., Dong W., Salin A., J. Chem. Phys., 118(2003)11226

[18] Busnengo H. F., Di Cesare M. A., Dong W., Salin A., Phys. Rev. B, 72(2005)125411

[19] Barredo D., Laurent G., Diaz C., Nieto P., Busnengo H. F., Salin A., Farias D., Martin F., 125(2006)051101

[20] Muller J. E., Applied Phys. A, 49(1989)681

[21] Muller J. E., Phys. Rev. Lett., 59(1987)2943

[22] Butler D. A., Hayden B. E., Surf. Sci., 342(1995)21

[23] Serrano M., Darling G. R., Surf. Sci., 532-535(2003)206

[24] Butler D. A., PhD . Thesis, University of Southampton, 1994

[25] Gee. A., PhD. Thesis, University of Southampton, 2000

[26] Crespo C., Busnengo H. F., Dong W., Salin A., J. Chem. Phys., 114(2001)10954

[27] King D. A., Wells M. G., Surf. Sci., 29(1972)454

[28] Logan R. M., Stickney R. E., J. Chem. Phys., 44(1966)195

[29] Butler D. A., Hayden B. E., Jones J. D., Chem. Phys. Lett., 217(1993)423

Conclusion

A detailed knowledge of the underlying reaction mechanisms can be useful in the design of better catalysts. The dynamic, kinetic and surface structure UHV studies detailed within this thesis provide valuable insight into just such underlying reaction mechanisms. This thesis concentrates mainly upon the dynamics of H_2 and N_2 adsorption upon the Mo(100) surface.

Analysis of the hydrogen adsorption dynamics of the system indicates 3 distinct channels to dissociation. These were: a classical accommodated channel, where the initial sticking probability reduces rapidly with increasing molecular incident energy and is dependent on surface temperature (an increase in surface temperature resulting in a reduced sticking probability), a dynamic channel, which exhibits a much slower decay in its contribution to the dissociative sticking probability with increasing incident energy and little or no temperature dependence, and a non-activated direct channel, which sees the sticking probability increase with incident energy and exhibit a very small positive temperature dependence. The accommodated and dynamic channels exhibited complex hydrogen coverage dependence, whereas the sticking probability appears to exhibit a more linear like decrease with increasing coverage within the energy range where the direct channel is seen to dominate, the detail of this relationship being clouded somewhat by the migration of adsorbed atomic hydrogen across the surface.

The addition of nitrogen to form an Mo(100)-c(2×2)N surface structure acts to completely remove the dynamic channel and the non-activated direct channel, the presence of nitrogen adatoms resulting in the minimum barrier to direct dissociation being shifted to a value above 70meV. However, the presence of nitrogen did act to considerably enhance the accommodated channel.

Examination of the dynamics of nitrogen adsorption upon the Mo(100) surface shows no sign of a dynamic channel, but a strongly temperature dependent accommodated channel is identified, this channel overlapping with a direct channel to dissociative adsorption, the direct channel exhibiting only a small potential barrier (~50meV) for

N_2 molecules approaching the surface with trajectories favourable to direct dissociation taking place. Within the energy range in which the indirect channel is dominant the sticking probability falls rapidly with increasing incident energy but remains relatively unaffected by increasing nitrogen coverage until complete saturation of the surface is approached. This indicates a mobile extrinsic precursor, able to trap upon areas of surface already pre-covered by nitrogen adatoms and to then locate a suitable site for dissociation. The direct channel, on the other hand, exhibits no apparent surface temperature dependence and a gradual rise in the initial sticking probability with increasing incident energy is observed within the energy range in which the direct channel is dominant. This is interpreted in terms of the increase in incident energy allowing the molecule greater access to non-optimised direct dissociation trajectories.

In terms of the application of these findings one such application could be in relation to the recent theoretical studies of Norskov et al. [1] into the potential for improving the longstanding Iron-based ammonia synthesis catalyst commonly used in industry. They examined the possibility of engineering a bimetallic alloy to provide a higher ammonia synthesis catalytic activity than is provided by the current mulit-promoted Fe catalyst. Their theoretical investigations led them to suggest a number of Mo based bimetallic alloys as being excellent candidates, a supposition confirmed experimentally by Jacobsen who produced a CoMoN catalyst with a higher activity than that of the commercially multi-promoted iron catalyst [2]. It is hoped that the data and analysis provided here regarding the dynamics of hydrogen and nitrogen

780-980 K and, by comparing this with various similar studies on the W(100) surface [4-9], as well as performing theoretical calculations demonstrating that a substitutional alloy (with Pd atoms replacing half of all Mo atoms in the upper most layer of the surface) is energetically favoured in comparison to an over layer structure at half monolayer coverage, they identified this c(2×2) diffraction pattern as being due to a substitutional surface structure. Due to the proximity of Ni and Pd in the periodic table, it seems reasonable to expect that a NiMo substitutional alloy would form in a similar manner and, since this bimetallic alloy has already been identified as being an active and stable ammonia synthesis catalyst at industrially relevant conditions [2], it is suggested that this might be a good candidate to which to initially extend these studies. It is hoped that these dynamical studies of H_2 and N_2 adsorption upon Mo(100) might be used as a platform to stimulate further studies into the viability of bimetallic Mo alloys as ammonia synthesis catalysts.

A second application of the findings presented in this study is to compliment the numerous studies already in existence providing comparison between the H_2/Mo(100) and H_2/W(100) adsorption systems [10-15]. With all current studies relating to the kinetics and surface structures, and with the H_2/W(100) system being a model adsorption system with extensive dynamical studies having already been undertaken [16-21], the contribution of a study into the dynamics of the H_2/Mo(100) system to this field acts, in some ways, as the final piece in the picture of this comparison.

By comparing the H_2 sticking probability upon the two surfaces as a function of the hydrogen coverage the degree of bridge site reconstruction (induced by hydrogen adsorption) is identified as an important factor in defining the adsorption dynamics. The contribution made by the low energy channel (assigned to a combination of dynamic and classical accommodated channels) to the sticking probability is observed to be particularly susceptible to changes in the bridge site, this manifesting itself in terms of a reduction in the surface temperature dependence of the initial sticking probability when adsorbing into the less reconstructed bridge sites.

In most other respects the dynamics of the two adsorption systems is found to be very similar. The Mo(100) surface did however exhibit a slightly larger direct channel to

hydrogen dissociative adsorption, direct dissociation appearing to be non-activated for both systems, but the barrier to direct dissociation being seen to be generally lower for a given trajectory on Mo(100) thereby allowing a greater range of non-optimised trajectory barriers to be successfully overcome for a given molecular incident energy. The dynamic channel on the other hand appears to be more prominent for the H_2/W(100) system, with this channel (defined by a fall in initial sticking probability with increasing incident energy) extending to 150meV on W(100) [18,21], roughly double the incident energy to which it is observed to extend to for the H_2/Mo(100) system. The initial sticking probabilities do generally appear to be larger on Mo(100) even at the low incident energies where the accommodated/dynamic channel is expected to dominate, however this is put down to two factors, the first being the greater size of direct channel on Mo(100) and its non-activated nature resulting in an overlap with the accommodated/dynamic channel, and the second being the difference in the hydrogen induced surface structure changes of the two surfaces, with hydrogen adsorption upon Mo(100) immediately causing the bridge site to change to its most strongly reconstructed form, but the W(100) surface only achieving this after adsorption of roughly 0.3ML of hydrogen [12]. It is suggested that whereas on Mo(100) the initial sticking probability, S_0, is also the maximum sticking probability (as a function of hydrogen coverage), $S_{max(\theta)}$, this is not the case on W(100). An area of interest for future investigation might be the comparison of $S_{max(\theta)}$ for the two adsorption systems as oppose to a comparison of S_0.

A comparison of the nitrogen adsorption dynamics upon the two surfaces was also carried out with the two found to be remarkably similar in all respects. When comparing the variation of the initial sticking probability with respect to molecule incident energy, surface temperature and nitrogen coverage the two systems were seen to behave almost identically [22-24], with only small quantitative disparities observed between the two.

It can be concluded therefore, that the major aim of the thesis, as outlined in chapter I, which was to study the dynamics of the dissociative adsorption of H_2 and N_2 upon molybdenum (100), has been achieved.

References

[1] Jacobsen C J H, Dahl S, Bjerne S, Clausen S B, Logadottir A, Norskov J K, J. Am. Chem. Soc., 123(2001)8404

[2] C.J.H. Jacobsen, Chem. Commun. (2000) 1057

[3] Wu D., Lau W. K., He Q., Feng Y. J., Altman M. S., Chan C. T., Phys. Rev. B, 62(2000)8366

[4] Attard G. A., King D. A., Surf. Sci., 188(1987)589

[5] Attard G. A., King D. A., Surf. Sci., 222(1989)351

[6] Attard G. A., King D. A., Surf. Sci., 222(1989)360

[7] Attard G. A., King D. A., Surf. Sci., 223(1989)1

[8] Hu P., Wander A., Morales de la Garza L., Bessent M. P., King D. A., Surf. Sci., 286(1993)L542

[9] Judd R. W., Reichelt M. A., Scott E. G., Lambert R. M., Surf. Sci., 185(1987)515

[10] Han H. R., Schmidt L. D., J. Phys. Chem. 75(1971)227

[11] Zaera F., Kollin E. B., Gland J. L., Surf. Sci., 166(1986)L149

[12] Chabal Y. J., Christman S. B., Arrecis J. J., Prybyla J. A., Estrup P. J., J. Electron Spec.and Rel. Phenom., 44(1987)17

[13] Prybyla J. A., Estrup P. J., Ying S. C., Chabal Y. J., Christman S. B., Phys. Rev. Lett., 58(1987)1877

[14] Felter J.E., Barker R.A., Estrup P.J., Phys. Rev. Lett. 38(1977)1138

[15] Reutte J. E., Chabal Y. J., Christman S. B., J Electron Spec. Rel. Phenom., 44(1987)325

[16] Butler D. A., Hayden B. E., Surf. Sci., 337(1995)67

[17] Butler D. A., PhD . Thesis, University of Southampton, 1994

[18] Butler D. A., Hayden B. E., Jones J. D., Chem. Phys. Lett., 217(1993)423

[19] Butler D. A., Hayden B. E., Topics in Catal., 1(1994)343

[20] Butler D. A., Hayden B. E., Chem. Phys. Lett., 232(1995)542

[21] Berger H. F., Resch Ch., Grosslinger G., Eilmsteiner G., Winkler A., Rendulic K. D., Surf. Sci. Lett., 275(1992)L627

[22] Rettner C. T., Stein H., Schweizer E. K., J. Chem. Phys., 89(1988)3337

[23] Rettner C. T., Schweizer E. K., Stein H., Auerbach D. J., J. Vac. Sci. Technol. 7(1989)1863

[24] Rettner C. T., Scheizer E. K., Stein H., J. Chem. Phys., 93(1990)1442

Appendix A

Derivation of the hard cube trapping probability

The hard-cube model describes the trapping of a molecule at a surface. It predicts the probability of sufficient normal momentum being transferred from the molecule to the surface to allow successful trapping to take place. This is a classical model and neglects any contribution to trapping from transfer of normal momentum to other molecular degrees of freedom.

The hard cube model was originally developed by Goodman [1], Trilling [2] and Oman [3], but these neglected the thermal motion of the surface during the collision and could not account for the net energy transfer from the gas to the surface. Logan and Stickney [4] proposed a model to address this shortcoming, basing it on the following assumptions:

i) The interaction of gas atom and surface is represented by an impulsive force of repulsion, i.e. both the gas and surface particles can be considered as rigid elastic particles.

ii) The surface is perfectly smooth. This allows the potential energy well for a gas-surface interaction to be considered as uniform across the surface, and hence the interaction does not alter the tangential velocity of the gas particle (i.e. there are no forces acting parallel to the surface).

These two assumptions are combined by considering the surfaces atoms as individual cubes orientated with one face parallel to the surface plane, moving only in the direction normal to the surface plane. Each gas particle (spherical, rigid and elastic) is pictured as interacting with only one of these cubes. This allows the tangential velocity component to remain unchanged, while the normal component changes according to Newton's laws.

iii) The surface atoms are represented by independent particles (cubes) confined by square well potentials (rigid boxes). A gas particle interacts with a single surface atom by entering the "box", colliding with the cube then departing.

iv) A temperature dependent distribution of velocities (normal to the plane of the surface) is assigned to the surface atoms. A 1D Maxwell distribution is chosen with this seen to satisfy certain equilibrium conditions.

A restriction occurring as a consequence of this approach is that, for only a single collision to occur, the mass ratio of the gas to the surface particles must be less than 1/3. This is not much of a restriction since, practically, this is often the case.

The Molecular Velocity in the Potential Well (v_{well})

The velocity of the molecule (v_{vac}) before entering the square potential well (of depth U), will be accelerated by v_{add} as a result of the well:-

$$v_{vac} = -\sqrt{\frac{2E_i}{m}} \qquad \text{A.1}$$

$$U = \frac{m v_{add}^2}{2} \qquad \text{A.2}$$

m is the mass of the incident molecule.

Note that the velocities are taken to be positive when moving away from the surface and negative when impinging.

The resulting velocity of the particle upon impact with the surface is:-

$$v_{well} = -\sqrt{\left(v^2 + \frac{2U}{m}\right)} \qquad \text{A.3}$$

The Molecular Velocity after Collision with the Surface (v'_{well})

From conservation of momentum:-

$$m v_{well} + M_{eff} v_{cube} = m v'_{well} + M_{eff} v'_{cube} \quad \text{A.4}$$

v_{cube} is the velocity of the surface cube before impact, v'_{cube} the velocity after impact, and M the mass of the surface cube.

From Newton's Law for elastic collisions:-

$$v'_{well} - v'_{cube} = v_{cube} - v_{well} \quad \text{A.5}$$

$$v'_{cube} = v'_{well} - v_{cube} + v_{well} \quad \text{A.6}$$

By combining equations A.4 and A.6 the following equation can be produced:-

$$m v_{well} + M_{eff} v_{cube} = m v'_{well} + M_{eff} (v'_{well} - v_{cube} + v_{well}) \quad \text{A.7}$$

$$m v'_{well} + M_{eff} v'_{well} = m v_{well} - M_{eff} v_{well} + 2 M_{eff} v_{cube} \quad \text{A.8}$$

Dividing by M_{eff} gives:-

$$\mu v'_{well} + v'_{well} = \mu v_{well} - v_{well} + 2 v_{cube} \quad \text{A.9}$$

$$v'_{well} (\mu + 1) = v_{well} (\mu - 1) + 2 v_{cube} \quad \text{A.10}$$

Hence:-

$$v'_{well} = \frac{v_{well}(\mu - 1) + v_{cube}}{(\mu + 1)} \qquad \text{A.11}$$

μ is the reduced mass.

Velocity of the Cube below Which the Impinging Molecule Will Trap

The energy required to escape the potential well after collision is U. Therefore the minimum velocity required is:-

$$v_{escape} = \sqrt{\frac{2U}{m}} \qquad \text{A.12}$$

To remain trapped in the well the following condition must be true,

$v'_{well} < v_{escape}$

Therefore:-

$$\frac{v_{well}(\mu - 1) + v_{cube}}{(\mu + 1)} < \sqrt{\frac{2U}{m}} \qquad \text{A.13}$$

$$v_{cube} < \frac{(\mu + 1)}{2}\sqrt{\frac{2U}{m}} + \frac{(\mu - 1)}{2}\sqrt{\left(v_{vac}^2 + \frac{2U}{m}\right)} \qquad \text{A.14}$$

If it is stated that:-

$$v_{limit} = \frac{(\mu + 1)}{2}\sqrt{\frac{2U}{m}} + \frac{(\mu - 1)}{2}\sqrt{\left(v_{vac}^2 + \frac{2U}{m}\right)} \qquad \text{A.15}$$

Then for trapping to occur:-

$$v_{cube} < v_{limit} \qquad \text{A.16}$$

Fraction of Surface Cubes Capable of Collision and of trapping a Particle (i.e. verifying equation A.16): $P_c(v)$

The probability of a surface cube having a velocity v, P(v), is dependent on the energy of the 'state', E, and the surface temperature, T_S. The probability of occupying a particular state is determined using the Boltzmann distribution.

The probability of a surface cube being capable of collision and having a velocity below V_{limit} is shown by equation A.17, with $P_c(v)$ being the probability of colliding with a surface site of velocity v, hence:-

$$P_c(v) = \int_{-\infty}^{V_{limit}} P_c(v).P(v)dv \qquad \text{A.17}$$

The probability of a surface cube having velocity v(P(v)) is:-

$$P(v) = \frac{e^{\left(-\frac{M_{eff}v^2}{2kT}\right)}}{Q} \qquad \text{A.18}$$

Where Q is the partition function:-

$$Q = \int_{-\infty}^{+\infty} e^{\left(-\frac{M_{eff}v^2}{2kT}\right)} dv \qquad \text{A.19}$$

Using the standard integral:-

$$\int_0^{+\infty} e^{(-bv^2)} dv = \frac{1}{2}\sqrt{\frac{\pi}{b}} \qquad \text{A.20}$$

And substituting in equation A.19:-

$$a^2 = \frac{M_{eff}}{2kT} \qquad \text{A.21}$$

Hence:-

$$\int_0^{+\infty} e^{\left(-a^2v^2\right)} dv = \frac{1}{2}\sqrt{\frac{\pi}{a^2}} \qquad \text{A.22}$$

Therefore:-

$$Q = 2\left(\int_{-\infty}^{+\infty} e^{\left(\frac{M_{eff}v^2}{2kT}\right)} dv\right) = \frac{\sqrt{\pi}}{a} \qquad \text{A.23}$$

Finally resulting in:-

$$P(v) = \frac{a}{\sqrt{\pi}} e^{\left(-a^2 v^2\right)} \qquad \text{A.24}$$

If the surface is receding from the impinging molecule the probability of colliding with a surface site of velocity v ($P_c(v)$) will be small, falling to zero when the surface is moving away with the same velocity as the incident molecule (V_{well}). The maximum probability will be when the surface and molecule are moving in opposite directions.
Hence:-

$$P_c(v) = \frac{v_{well} - v}{v_{well}} = 1 - \frac{v}{v_{well}} \qquad \text{A.25}$$

Now substituting equations A.24 and A.25 into A.17:-

$$P_c(v) = \int_{-\infty}^{v_{limit}} \left(1 - \frac{v}{v_{well}}\right)\left(\frac{a}{\sqrt{\pi}} e^{\left(-a^2 v^2\right)}\right) dv$$

$$= \int_{-\infty}^{v_{limit}} \left(\frac{a}{\sqrt{\pi}} e^{\left(-a^2 v^2\right)}\right) dv - \int_{-\infty}^{v_{limit}} \frac{v}{v_{well}} \left(\frac{a}{\sqrt{\pi}} e^{\left(-a^2 v^2\right)}\right) dv \qquad \text{A.26}$$

Then using the identity:-

$$\int_{-\infty}^{z} dv = \int_{-\infty}^{0} dv + \int_{0}^{z} dv \qquad \text{A.27}$$

$$\int_{-\infty}^{v_{limit}} \left(\frac{a}{\sqrt{\pi}} e^{\left(-a^2 v^2\right)}\right) dv = \frac{a}{\sqrt{\pi}} \left(\int_{-\infty}^{0} e^{\left(-a^2 v^2\right)} dv + \int_{0}^{v_{limit}} e^{\left(-a^2 v^2\right)} dv\right) \qquad \text{A.28}$$

$e^{(-x^2)}\{0,\infty\}$ is a reflection of $e^{(-x^2)}$ $\{0,-\infty\}$, and therefore:-

$$\int_{-\infty}^{0} e^{(-a^2v^2)}dv = \int_{0}^{-\infty} e^{(-a^2v^2)}dv = \frac{1}{2}\frac{\sqrt{\pi}}{a^2} \qquad \text{A.29}$$

And hence:-

$$\int_{-\infty}^{0} \frac{a}{\sqrt{\pi}} e^{(-a^2v^2)}dv = \frac{1}{2} \qquad \text{A.30}$$

Using the identity:-

$$erf(z) = \frac{2}{\sqrt{\pi}} \int_{0}^{z} e^{(-x^2)}dx \qquad \text{A.31}$$

and by substituting in u=av:-

$$\int_{0}^{z} e^{(-x)}dx = \int_{0}^{av} e^{(-u^2)}\frac{dv}{du}du \qquad \text{A.32}$$

Therefore:-

$$\int_{0}^{v_{limit}} e^{(-a^2v^2)}dv = \frac{\sqrt{\pi}}{2a} erf\left(av_{limit}\right) \qquad \text{A.33}$$

Using equations A.29 and A.33, equation A.28 becomes:-

$$\int_{-\infty}^{v_{limit}} \left(\frac{a}{\sqrt{\pi}} e^{\left(-a^2 v^2\right)} \right) dv = \frac{a}{\sqrt{\pi}} \left(\frac{1}{2} \frac{\pi}{\sqrt{a^2}} + \frac{\sqrt{\pi}}{2a} erf\left(a v_{limit}\right) \right)$$

$$= \frac{1}{2} + \frac{1}{2} erf\left(a v_{limit}\right) \qquad \text{A.34}$$

$$\int_{-\infty}^{v_{limit}} \frac{v}{v_{well}} \left(\frac{a}{\sqrt{\pi}} e^{\left(-a^2 v^2\right)} \right) dv = \frac{a}{\sqrt{\pi} v_{well}} \int_{-\infty}^{v_{limit}} \left(v e^{\left(-a^2 v^2\right)} \right) dv \qquad \text{A.35}$$

By substituting $u=-a^2v^2$ and $\frac{dv}{du} = -2a^2 v$

$$\frac{a}{\sqrt{\pi} v_{well}} \int_{-\infty}^{v_{limit}} \left(v e^{\left(-a^2 v^2\right)} \right) dv = \frac{a}{\sqrt{\pi} v_{well}} \int_{-\infty}^{v_{limit}} v e^u \frac{dv}{du} du$$

$$= \frac{a}{\sqrt{\pi} v_{well}} \int_{-\infty}^{-a^2 v_{limit}} \frac{v}{-2a^2 v} e^u du$$

$$= \frac{1}{2a\sqrt{\pi} v_{well}} \int_{-\infty}^{-a^2 v_{limit}} e^u du$$

$$= \frac{1}{2a\sqrt{\pi} v_{well}} e^{\left(-a^2 v_{limit}^2\right)} \qquad \text{A.36}$$

By substituting equations A.34 and A.36 into equation A.26, the trapping probability can be written as:-

$$P_c(v) = \frac{1}{2} + \frac{erf\left(a v_{\lim it}\right)}{2} + \frac{e^{\left(-a^2 v_{\lim it}^2\right)}}{2a\sqrt{\pi} v_{\lim it}} \qquad \text{A.37}$$

The hard-cube simulations used within this thesis were modeled using an excel spreadsheet.

References

[1] Goodman F. O., Proc. Intern. Symp. Rarefied Gas Dyn. (4th Toronto 1964), 2(1965)366

[2] Trilling L., J. de Mecanique, 3(1964)215

[3] Oman R. A., Bogan A., Li C. H., Proc. Intern. Symp. Rarefied Gas Dyn. (4th Toronto 1964), 2(1965)396

[4] Logan R. M., Stickney R. E., J. Chem. Phys., 44(1966)195

Appendix B

Calculation of the drift in the incident energy of the reactant molecules from the ideal value

At large mass differences between seed and reactant particles, requiring large changes in the velocity of the reactant particles, the real behaviour of the molecules will deviate significantly from the ideal behaviour defined by equation B.1.

$$E_{i(react)} = \frac{5}{2}\frac{m_{(react)}}{\sum x_i m_i} k_B T_n \qquad \textbf{(B.1)}$$

This drift from the ideal behaviour is recorded in table.1 where the values calculated using equation A.1 are compared with values calculated from time of flight (TOF) profiles recorded by Butler for this system [1].

TOF profiles are for the indicated beam mixtures with T_{nozzle}=312K. The period between pulses was 4500μs and the pulse width 22.5μs (0.5% duty cycle chopper disk). The flight path from the chopper to mass spectrometer was 0.303m.

Beam Composition	$E_{i(react)}$ (calculated using equ A.1, T_n=312K)	Time of Flight(μs) taken from [1]	$E_{i(react)}$ (calculated from TOF data, T_n=312K)	Drift in E_i from ideal values
1%H_2/He	34	133±5	35±3	+0.03
1%H_2/Ar	3	239±10	13±1	+3.33
1%N_2/He	444	185±10	288±16	-0.35
1%N_2/Ar	47	409±10	67±2	+0.43

The drift multiple must be included when using equation A.1 to calculate the incident energy of the reactant particles within the beam line.

References

[1] Butler D. A., PhD . Thesis, University of Southampton, 1994

Appendix C

Calibration of the W3 type thermocouple <273K

The W3-type thermocouple is designed to accurately measure high temperatures. To use this thermocouple to measure temperatures below 273K it was necessary to calibrate the thermocouple against a K-type thermocouple, this being commonly used to record low temperatures.

W3-type thermocouple / mV	K-type thermocouple / mV	Temperature / K
0	798	293
-100	-157	277
-200	-662	261
-300	-1600	245
-400	-2347	229
-500	-2821	213
-600	-2920	197
-700	-3461	181
-800	-3997	165
-900	-4330	147
-1000	-4669	134
-1100	-4889	125

Appendix D

The Mo vapour pressure produced as a function of the anneal temperature

The following is the vapour pressure of molybdenum associated with heating the sample to a range of temperatures. This data is taken from the MISTA-DCA INSTRUMENTS Materials Source Selection Table For MBE. The melting point of molybdenum is at 2617^0C.

Temperature to which Mo sample is heated / K	1592	1822	2177	2527
Vapour pressure produced / torr	10^{-8}	10^{-6}	10^{-4}	10^{-2}